Design of Reinforced Concrete Frames of Limited Ductility

A Thesis
Presented for the Degree
of
Doctor of Philosophy in Civil Engineering
at the
University of Canterbury
Christchurch
New Zealand

by

Soesianawati Watson

January, 1989

To my husband, Neville

Abstract

An experimental programme was carried out to investigate the flexural strength and ductility of reinforced concrete columns under simulated earthquake loading. The main variable examined was the quantity of transverse reinforcement for concrete confinement. The experimental results were described and compared with theoretical studies. It was found that to achieve adequate ductility in columns, the current New Zealand concrete design code NZS3101:1982 equations for concrete confinement need to be refined. Using design charts for ductility, which were previously derived from a theory for cyclic moment-curvature behaviour, a refined design equation to replace the current code equations is proposed.

The inelastic dynamic response of frames of limited ductility was examined, and compared with the response of ductile frames. The analysis indicated that non-capacity designed frames, designed for seismic forces corresponding to a limited ductility demand, performed reasonably well. Although some plastic hinges did develop in the columns, the ductility demand was acceptable and can be achieved by appropriate detailing. As a result, some suggestions for the seismic design requirements of frames of limited ductility are presented.

Acknowledgements

The research reported in this thesis was undertaken at the Department of Civil Engineering, University of Canterbury, under the overall guidance of its Head, Professor R. Park.

I wish to sincerely thank Prof. R. Park, the supervisor of this project, for his invaluable help and constant encouragement. The helpful advice given by Prof. T. Paulay, and the assistance given by Dr. A.J. Carr in the computer work are also gratefully acknowledged. Prof. M.J.N. Priestley is thanked for the fruitful discussions at the early stage of this project.

Thanks are extended to the technical staff of the Department of Civil Engineering, for their assistance and advice in the experimental programme. In particular, thanks are due to Messrs N.W. Prebble (now retired), G.E. Hill, G.H. Clarke, S. Pasa, R. Allen, P. Yellowance. Mr. L. Gardner is thanked for developing the photographs, and Mrs. V. Grey is thanked for her drafting assistance.

I am also grateful for the permission to use the computer facilities in the Department of Electrical and Electronic Engineering, University of Canterbury, during the preparation of this thesis.

The financial assistance provided by the Ministry of Works and Development and the University of Canterbury, and the materials supplied by the Pacific Steel Limited, Auckland and the Fletcher Steel Limited, Christchurch, are greatly appreciated.

Finally, I wish to express my sincere gratitude to my and my husband's families for their constant encouragement and understanding.

Notation

a_1, a_2	=	Mass and stiffness participation factors, respectively
A_b	=	Area of reinforcing bar
A_c	=	Area of core concrete of column section
A_g	=	Gross area of column section
A_{sh}	=	Area of hoop bars and supplementary cross-tie confining reinforcement in one principal direction of column section
A_{sx}	=	Total area of x-direction transverse bars
A_{sy}	=	Total area of y-direction transverse bars
A_v	=	Area of effective hoop legs in resisting shear
b	=	Overall width of rectangular column section
b_c	=	Width of concrete core, measured to the centre-line of perimeter hoop
b_w	=	Width of web of concrete section
c	=	Concrete cover thickness, measured to the centre-line of perimeter hoop
C_μ	=	Basic seismic coefficient, given in DZ4203:1986 [39]
d	=	Effective depth of concrete section
d_b	=	Diameter of reinforcing bar
d_c	=	Diameter of confined concrete core of circular column section, measured to the centre-line of spiral or circular hoop
D	=	Overall diameter of circular column section
	or	Dead load
E	=	Earthquake load
E_c	=	Young's modulus of elasticity for concrete
E_s	=	Young's modulus of elasticity for for steel in tension
E_{sc}	=	Young's modulus of elasticity for for steel in compression
E_{sec}	=	Secant modulus of confined concrete at maximum strength
E_{sh}	=	Strain hardening modulus for steel in tension
E_{shc}	=	Strain hardening modulus for steel in compression
f	=	Section type factor
f_c	=	Concrete stress
f'_c	=	Specified concrete compressive strength
f_{co}	=	In-situ unconfined concrete compressive strength
f_l	=	Transverse confining stress
f'_l	=	Effective transverse confining stress [3]

f_r	=	Effective transverse confining stress [4]
f_s	=	Steel stress
f_{su}	=	Ultimate tensile strength of steel
f_{suc}	=	Ultimate compressive strength of steel
f'_t	=	Tensile strength of concrete
f_y	=	Yield strength of steel in tension
f_{yc}	=	Yield strength of steel in compression
f_{yh}	=	Yield strength of transverse reinforcing steel
F_i	=	Horizontal static load at level i
F_t	=	Horizontal static load at top storey
g	=	Acceleration of gravity
g'	=	Ratio of distance between the centres of the longitudinal bars in the extreme faces to the width of concrete core
G	=	Shear modulus
h	=	Overall height of rectangular column section
	or	Storey height
h"	=	Dimension of concrete core of section measured to outside of peripheral hoop
h_b	=	Overall beam depth
h_c	=	Concrete core dimension, measured to the centre-line of perimeter hoop
	or	Overall column depth
H	=	Lateral applied load
H_{ACI}	=	Lateral applied load, corresponding to M_{ACI}
H_{max}	=	Maximum experimental lateral load
I	=	Second moment of area of section
I_e	=	Effective second moment of area of section
I_g	=	Second moment of area of gross section
jd	=	Lever arm between the centroid of the tension reinforcement and the centre of the compression stress block of a reinforced concrete section
k_{cc}	=	Strength enhancement factor for confined concrete
k_e	=	Confinement effectiveness coefficient, based on area ratio
k_e^*	=	Confinement effectiveness coefficient, based on ratio of first moments of area
K	=	Stiffness matrix
l	=	Length of cantilever column, measured from the point of maximum moment to point of contraflexure
l_c	=	Length of confined region of column
ℓ	=	Length of cantilever column, measured from the face of central stub to point of contraflexure
	or	Clear storey height
ℓ_p	=	Equivalent plastic hinge length
L	=	Live load
L_r	=	Reduced live load
L_s	=	Live load at serviceability

m	=	Mass per unit length
	or	$f_y/0.85f'_c$
M	=	Bending moment
	or	Structural material factor
	or	Mass matrix
M_{ACI}	=	Theoretical flexural strength, calculated using the code [2] approach
M_{code}	=	Column bending moment at the centre-line of a beam, derived from the code specified lateral seismic loading
M_{col}	=	Design moment at critical section of column
$M_{col,red}$	=	Reduced design moment at critical section of column
M_i	=	Ideal flexural strength, defined as maximum moment reached before the curvature ductility factor φ_u/φ_y exceeds 5.0
M_{max}	=	Maximum bending moment
M_o	=	Pure bending moment
M'_y	=	Moment calculated at the first yield of longitudinal reinforcement, or when the extreme compressive fibre strain reaches 0.002, whichever is smaller
M_{1b}	=	Flexural strength from moment-axial force interaction diagram with applied axial load of $2P_b/3$
M_{2b}	=	Flexural strength from moment-axial force interaction diagram with applied axial load of $P_b/3$
P_b	=	Axial load at balance failure point
P_e	=	Axial compression load on column due to design gravity and seismic loading
P_{yc}	=	Ultimate axial force in compression
P_{yt}	=	Ultimate axial force in tension
P_{eq}	=	Design axial load of column due to earthquake load only
r	=	$E_c/(E_c - E_{sec})$ in Popovics' equation
	or	Bilinear factor
R	=	Ratio of strain increase to stress increase at the peak strength of confined concrete
	or	Risk factor
R_l	=	Reduction factor for live load
R_m	=	Bending moment reduction factor
R_v	=	Axial force reduction factor
s'	=	Clear spacing between spiral or hoop bars in which arching action of concrete develops
s_h	=	Centre-to-centre spacing of spiral or hoop sets
S	=	Structural type factor
S_{cc}	=	First moment of total core area of concrete
S_{ce}	=	First moment of effectively confined core area
t	=	Time
T	=	Natural period of vibration
U	=	Required ultimate load capacity
v_b	=	Basic shear stress carried by concrete

v_c	=	Ideal shear stress carried by concrete
V	=	Total horizontal seismic shear force at base
V_c	=	Shear resistance of concrete member provided by concrete mechanisms
V_{code}	=	Column shear force derived from code specified seismic loading
V_{col}	=	Column design shear force
V_i	=	$V_c + V_s$
	=	Total ideal shear strength of column
V_{oe}	=	Maximum earthquake induced beam shear force at the development of beam flexural overstrength
V_s	=	Shear resistance of concrete member provided by shear reinforcement mechanisms
V_u^o	=	Shear force associated with flexural overstrength of member
w_i'	=	Clear transverse spacing between longitudinal bars in which arching action of concrete develops
W_t	=	Total seismic weight of structure
x	=	ϵ_c/ϵ_{cc} in Popovics' equation
X_{eff}	=	Effective number of transverse bars with area A_b in x direction
Y_{eff}	=	Effective number of transverse bars with area A_b in y direction
Z	=	Zone factor
α	=	s'/d_c or s'/h_c
	or	Modification factor for the cover thickness of square section to be used for the rectangular section, depends on the section side ratio b/h
β	=	b_c/h_c
γ	=	Unit weight of concrete
$\gamma f_c'$	=	Curvature ductility modification factor to allow for the influence of f_c'
γf_y	=	Curvature ductility modification factor to allow for the influence of f_y
γf_{yh}	=	Curvature ductility modification factor to allow for the influence of f_{yh}
Δ	=	Lateral displacement of column
Δ_y	=	Lateral displacement of column at yield
Δ_p	=	Lateral displacement of column due to plastic deformations along the member
ϵ_c	=	Concrete compressive strain
ϵ_{cc}	=	Strain at maximum confined strength of concrete f_{cc}'
ϵ_{cmax}	=	Maximum concrete compressive strain
ϵ_{cu}	=	Ultimate concrete compressive strain
ϵ_{co}	=	Compressive strain at maximum in-situ unconfined concrete strength f_{co}'
ϵ_{sh}	=	Steel strain at the commencement of strain hardening of steel in tension
ϵ_{shc}	=	Steel strain at the commencement of strain hardening of steel in compression
ϵ_{spall}	=	Compressive strain at which unconfined cover concrete spalls
ϵ_{su}	=	Ultimate tensile strain of steel
ϵ_{suc}	=	Ultimate compressive strain of steel
ϵ_y	=	Yield strain of steel

θ_p	=	Equivalent plastic hinge rotation
κ	=	$X_{eff}/h_c + Y_{eff}/b_c$
λ	=	Parameter in CEB [22] equation for concrete confinement
	or	Fraction of critical damping
μ	=	Displacement ductility factor
μ_n	=	Nominal displacement ductility factor
μ_r	=	Real displacement ductility factor
ρ	=	Area of longitudinal tension reinforcement divided by effective area of beam section
ρ_{cc}	=	Volumetric ratio of longitudinal reinforcement in the confined core concrete
ρ_s	=	Volumetric ratio of confining reinforcement
$\rho_{s,code}$	=	Volumetric ratio of confining reinforcement required by the code [2]
ρ_t	=	Area of longitudinal reinforcement divided by gross area of column section
$\rho_t m$	=	Mechanical reinforcing ratio
ρ_w	=	Volumetric ratio of tension reinforcement
ϕ	=	Strength reduction factor
ϕ_o	=	Flexural overstrength factor
φ	=	Curvature
φ_y	=	Yield curvature
φ'_y	=	Curvature calculated at the first yield of longitudinal tension steel, or when the extreme compressive fibre strain of concrete reaches 0.002, whichever is smaller
φ_{max}	=	Maximum curvature
φ_{peak}	=	Curvature at peak of moment-curvature hysteresis loops
ω	=	Dynamic magnification factor
	or	Frequency of vibration

Contents

Chapter 1

INTRODUCTION

The performance of structures under seismic excitations has been investigated widely in New Zealand and overseas. The basic criteria that have to be satisfied in designing an earthquake resistant structure are: to provide adequate stiffness and strength to ensure that structural damage can be prevented under moderate earthquakes, and to provide sufficient stiffness and adequate ductility to dissipate energy during major earthquakes so that collapse does not occur.

Adequate ductility in a reinforced concrete structure can be achieved by means of providing appropriate longitudinal reinforcement and sufficient transverse reinforcement in potential plastic hinge regions of structural members where the energy dissipation is expected to take place.

One role of transverse reinforcement in potential plastic hinge regions of columns is to provide confinement to compressed concrete in the core of the section.

Seismic codes of various countries have formulated recommendations for confining reinforcement, in terms of design equations for the quantities, and limitation of the spacings of confining reinforcement, length of confined regions etc. to ensure that the required ductility demand can be achieved. The development of code provisions together with previous studies regarding the role of confining reinforcement in columns is summarized in Chapter 2.

Some structures, however, due to the configuration of structural components or functional requirements, may possess strengths which are greater than needed for full ductility. The seismic performance of this type of structure, which need only limited ductility, is of interest to structural engineers in New Zealand. This was shown by the establishment of a study group by the Management Committee of the New Zealand National Society for Earthquake Engineering (NZNSEE) in late 1985 to examine the behaviour of structures of limited ductility [1].

The main object of the NZNSEE study group of structures of limited ductility was to compile information to enable the engineers to:

- Economically design structures which fall between full ductility and elastic, that is, structures with strengths greater than required by code seismic loading for fully ductile behaviour, or less important structures which do not warrant detailing for full ductility.

Chapter 1

INTRODUCTION

The performance of structures under seismic excitations has been investigated widely in New Zealand and overseas. The basic criteria that have to be satisfied in designing an earthquake resistant structure are: to provide adequate stiffness and strength to ensure that structural damage can be prevented under moderate earthquakes, and to provide sufficient stiffness and adequate ductility to dissipate energy during major earthquakes so that collapse does not occur.

Adequate ductility in a reinforced concrete structure can be achieved by means of providing appropriate longitudinal reinforcement and sufficient transverse reinforcement in potential plastic hinge regions of structural members where the energy dissipation is expected to take place.

One role of transverse reinforcement in potential plastic hinge regions of columns is to provide confinement to compressed concrete in the core of the section.

Seismic codes of various countries have formulated recommendations for confining reinforcement, in terms of design equations for the quantities, and limitation of the spacings of confining reinforcement, length of confined regions etc. to ensure that the required ductility demand can be achieved. The development of code provisions together with previous studies regarding the role of confining reinforcement in columns is summarized in Chapter 2.

Some structures, however, due to the configuration of structural components or functional requirements, may possess strengths which are greater than needed for full ductility. The seismic performance of this type of structure, which need only limited ductility, is of interest to structural engineers in New Zealand. This was shown by the establishment of a study group by the Management Committee of the New Zealand National Society for Earthquake Engineering (NZNSEE) in late 1985 to examine the behaviour of structures of limited ductility [1].

The main object of the NZNSEE study group of structures of limited ductility was to compile information to enable the engineers to:

- Economically design structures which fall between full ductility and elastic, that is, structures with strengths greater than required by code seismic loading for fully ductile behaviour, or less important structures which do not warrant detailing for full ductility.

- Evaluate existing structures that do not possess the ductility detailing required by modern codes nor possess adequate strength to respond elastically to design earthquake loads.

For this type of structure, less ductility demand can be expected and therefore the required quantities of confining reinforcement can be reduced.

One of the aims of the present study is to investigate the behaviour of columns under simulated earthquake loading, containing various quantities of confining reinforcement, particularly columns with less confining reinforcement than that recommended by the New Zealand code [2]. The test results of this type of column are described and compared with recent theoretical studies [3,4] in Chapter 3.

The theoretical studies, confirmed by experimental results [5], indicate that the New Zealand code [2] design equations for concrete confinement need to be refined to achieve satisfactory performance of columns under seismic disturbances. Chapter 4 describes the theoretical predictions of flexural ductility of columns. A refined design equation for the quantities of confining reinforcement to replace the existing code equations is proposed.

To ensure that the energy dissipation occurs in the chosen structural members as expected, a capacity design approach has been developed in New Zealand [6]. In this approach, the chosen energy-dissipating members are suitably designed and detailed, and sufficient reserve strengths are given to the other members. Since a large ductility demand can be more easily achieved in beams than in columns, a strong column-weak beam concept was adopted. This means that columns must be stronger than beams to ensure that beam sidesway mechanisms will develop. In structures of limited ductility, column sidesway mechanisms may be acceptable, provided that the required ductility is not so great and the other brittle failure can be prevented. In such structures, the capacity design procedure becomes less important and a simplified design procedure can be applied. Chapter 5 compares the inelastic dynamic response of capacity designed ductile frames and non-capacity designed frames of limited ductility. A step-by-step design procedure for frames of limited ductility is outlined.

The existing code seismic requirements for ductile frames and frames of limited ductility are compared in Chapter 6. Some provisions to extend the existing seismic requirements of frames of limited ductility, as in Section 14 of the New Zealand code [2], are also proposed.

The major conclusions from the study undertaken, and some suggestions for future research are given in Chapter 7.

Chapter 2

SUMMARY OF PREVIOUS STUDIES AND CODE PROVISIONS FOR CONFINING REINFORCEMENT IN THE POTENTIAL PLASTIC HINGE REGIONS OF COLUMNS

2.1 Introduction

This chapter reviews briefly the experimental studies of columns with solid sections subjected to simulated earthquake loading, undertaken at the University of Canterbury over the past ten years. The results of these studies, together with the other studies as summarized by Priestley and Park [13,14], have greatly improved the understanding of the behaviour of columns under seismic attacks, and led to an improvement in the seismic design provisions used in New Zealand.

The New Zealand code provisions [2], with regard to the requirements of confining reinforcement in the potential plastic hinge regions of columns, are also discussed and compared with the overseas provisions in this chapter.

2.2 Previous Experimental Investigations of Strength and Ductility of Columns at the University of Canterbury

Since 1978, after the installation of a 10 MN DARTEC electro-hydraulic testing machine, much of the structural concrete research in the Department of Civil Engineering at the University of Canterbury has been directed towards the assessment of the strength and

ductility of reinforced concrete columns, bridge piers and piles, containing different quantities and configurations of longitudinal and transverse reinforcement, under simulated earthquake loading.

The experimental research of the behaviour of columns with solid sections, was initiated by Gill *et al.* [7] and Potangaroa *et al.* [8], who investigated the behaviour of squat columns with square and octagonal sections. Further tests of more slender columns were carried out by Ang *et al.* [9] and Zahn *et al.* [4].

The confining reinforcement in the columns tested, in the form of spirals or rectangular hoops, was generally designed to the requirements of versions of the New Zealand code [10,11,2]. The other variables investigated were the type of section, the level of axial compression, the aspect ratio L/D or L/h of columns, and the use of different grades of transverse reinforcement.

More recent experimental work was carried out by Soesianawati *et al.* [5] on the behaviour of square columns with low axial compression containing less quantities of confining reinforcement than recommended by the New Zealand code [2]. The test results indicated the necessity of further investigation into the behaviour of columns, with large axial compression. Tests of this type of column were then conducted. For convenience, the results of both studies are described together in Chapter 3.

Gill *et al.* [7]

Four column units with 550 mm square cross section, and with an aspect ratio of $L/h = 2.2$, were designed to the first draft DZ3101:1978 [10] requirements for confining reinforcement. The aim of the tests was to investigate the possible improvement of these provisions.

Potangaroa *et al.* [8]

In this project, a total of five octagonal columns of 600 mm cross section were tested. The aim of the tests was similar to that of the investigation by Gill *et al.* [7]. Four units were designed in accordance with the DZ3101 [10] recommended quantities of confining reinforcement. The fifth column was designed using the Ministry of Works and Development requirements CDP 810/A [12], for an axial load level of $P_e = 0.35 f'_c A_g$. Due to the over conservatism of CDP 810/A, this unit was re-tested with an axial compression of $P_e = 0.7 f'_c A_g$. For this level of axial load, the transverse reinforcement for this unit satisfied the DZ3101 recommended quantity. These squat columns have an aspect ratio of $L/D = 2.0$.

Ang *et al.* [9]

A further investigation was carried out to examine the ductility of columns with higher aspect ratio, designed as recommended by the revised draft DZ3101 [11]. Four column units, two with octagonal sections and two with square sections, were tested. The lateral dimension and the length of the units were 400 mm and 1600 mm, respectively, giving an aspect ratio of 4.

Zahn *et al.* [4]

Two square columns and two octagonal columns with the same dimensions as the specimens tested by Ang *et al.* [9], were designed using the NZS3101:1982 [2] requirements for confining reinforcement. The main objective was to investigate the behaviour of columns with high

strength transverse steel. It is known that the yield force of the confining reinforcement bar is the main parameter in determining the efficiency of confinement. The test, therefore examined the possibility of the replacement of larger quantities of Grade 275 steel with smaller quantities of Grade 380 steel.

Table 2.1 compares the properties of the column units tested [7,8,9,4], with the current New Zealand code requirements [2]. It is evident that the quantities of confining reinforcement ranged from 0.83 to 2.0 times the code recommended quantity. A comparison with the quantities required by the design charts derived by Zahn *et al.* [4] to achieve an available $\varphi_u/\varphi_y = 20$, is also made in Table 2.1.

It is obvious, that the quantities provided were generally sufficient, to provide that level of ductility, except for three columns, namely Ang *et al.* Oct. 2, and Potangaroa *et al.* Unit 3, and Zahn *et al.* Oct.6, which contained $\approx$ 80% of the design charts requirements. For some columns with low axial compression, such as those of Ang *et al.* Oct.1 and Zahn *et al.* Oct.5, the charts did not indicate the necessity for confining reinforcement.

In general, the other code requirements for concrete confinement, and for preventing premature buckling of longitudinal bars, were also satisfied.

The test results for the above columns are summarized in Table 2.2. A comparison with the theoretical predictions using the analytical procedures of Mander *et al.* [3] is also made. It can be seen that the theory predicts the experimental results reasonably well. The available curvature ductility in some columns was under-estimated by the theory, because of the larger confinement available in the units due to the central stub, which was not taken into account in the analysis. This resulted in more ductile behaviour, and therefore larger available curvature ductility. The moment enhancement above the code flexural strength predicted by an empirical equation [14] (see Chapter 3 for details) agreed well with the experimental values. Due to lack of information, some items are not listed in Table 2.2.

2.3 Code Provisions for Seismic Design of Confining Reinforcement in the Potential Plastic Hinge Regions of Columns

2.3.1 General

There are differences between code provisions in New Zealand and overseas for the amount and distribution of confining reinforcement in columns necessary to ensure adequate ductility. However, the basic idea of using transverse reinforcement to confine compressed concrete is generally similar.

Table 2.1: Properties of Column Units Tested by Previous Researchers at University of Canterbury

Researcher	Unit	$\frac{P_e}{\phi f'_c A_g}$	f'_c (MPa)	dia.-s_h (mm)	f_{yh} (MPa)	Transverse Reinforcement for Confinement			Transverse Reinforcement for Antibuckling	
						1	2	3	4	5
Gill *et al.* [7]	1	0.26	23.1	R10-80	297	0.95	3.04	0.15	3.3	1.56
	2	0.214	41.4	R12-75	316	0.92	3.08	0.14	3.1	2.38
	3	0.42	21.4	R10-75	297	1.03	1.62	0.14	3.1	2.21
	4	0.60	23.4	R12-62	294	1.32	1.30	0.11	2.6	3.14
Potangaroa *et al.* [8]	1	0.237	28.4	R10-75	300	0.83	1.88	0.13	3.1	-
	3	0.543	26.6	R10-50	300	0.89	0.77	0.08	2.1	-
	4	0.387	32.9	HD10-70	423	0.87	0.97	0.12	2.9	-
	5	0.35	32.5	R16-55	280	2.00	2.75	0.09	2.3	-
	5b(6)	0.70	32.5	R16-55	280	1.36	0.95	0.09	2.3	-
Ang *et al.* [9]	Oct.1	0.20	26.0	R6-40	308	1.00	-	0.1	2.5	-
	Oct.2	0.56	28.5	R10-55	280	1.04	0.85	0.14	3.4	-
	Sq.3	0.38	23.6	R12-100	320	1.47	1.41	0.25	6.3	6.7
	Sq.4	0.21	25.0	R10-90	280	1.22	4.95	0.23	5.6	4.1
Zahn *et al.* [4]	Oct.5	0.13	32.1	HD10-135	466	1.11	-	0.34	8.4	-
	Oct.6	0.67	23.5	HD10-75	466	1.35	0.80	0.19	4.7	-
	Sq.7	0.23	28.0	HD10-117	466	1.26	4.0	0.29	7.3	6.6
	Sq.8	0.42	37.2	HD10-92	466	0.93	1.12	0.23	5.8	6.6

Notes:

1. ratio of actual A_{sh} to A_{sh} required by New Zealand code [2]
2. ratio of actual A_{sh} to A_{sh} required by design charts [4] for curvature ductility factor $\varphi_u/\varphi_y = 20$
3. ratio of s_h to b (New Zealand code [2] requires $s_h/b \leq 0.2$)
4. ratio of s_h to d_b (New Zealand code [2] requires $s_h/d_b \leq 6$)
5. ratio of available tie force to New Zealand code [2] requirement of $\frac{1}{16}$ longitudinal bar force at 100 mm centres, applicable only for square sections
6. Unit 5 was re-tested with high axial compression
7. f'_c was measured at time of testing of column units
8. The strength reduction factor ϕ was assumed to be 1.0

Table 2.2: Comparison of Experimental Results and Theoretical Predictions for Column Units Tested by Previous Researchers at University of Canterbury

Researcher	Unit	φ_y(rad/m)		Δ_y(mm)		M_{ACI} (kNm)	M_{max}/M_{ACI}			φ_{max}(rad/m)		φ_{max}/φ_y	
		1	2	1	2	3	1	2(5)	4	1	2	1	2
Gill et al. [7]	1	0.007	0.0085	5.7	5.0	691	1.25	1.04	1.19	0.1470	0.120	21.0	14.1
	2	0.007	0.0083	4.2	4.5	905	1.12	1.03	1.16	0.140	0.0913	20.0	11.0
	3	0.007	0.0072	3.6	3.6	646	1.30	1.20	1.37	0.0980	0.0893	14.0	9.4
	4	0.006	0.005	2.5	2.4	598	1.52	1.42	1.72	0.0960	0.0720	16.0	8.5
Potangaroa et al. [8]	1	-	0.0061	5.2	5.6	723	1.23	1.10	1.17	-	0.1324	25.4	21.7
	3	-	0.0044	3.5	2.8	672	1.44	1.36	1.59	-	0.0352	8.5	8.0
	4	-	0.0052	4.0	3.9	803	1.30	1.20	1.32	-	0.0887	16.3	17.0
	5	-	0.0061	3.5	3.1	807	1.34	1.21	1.28	-	0.0878	16.1	14.4
	5b(6)	-	0.0034	3.5	1.8	564	2.26	1.90	1.98	-	0.0507	-	14.9
Ang et al. [9]	Oct.1	0.0088(7)	0.0093	7.5	9.6	216	1.23	1.04	1.15	0.2112	0.1776	24.0(8)	19.1
	Oct.2	0.0076	0.0064	6.5	5.3	215	1.44	1.32	1.63	0.0380	0.1286	50.0	15.8
	Sq.3	0.0077	0.0102	6.6	7.1	269	1.24	1.16	1.31	0.1463	0.1540	19.0	15.1
	Sq.4	0.0109	0.0113	9.3	8.8	258	1.17	1.05	1.16	0.2398	0.1413	22.0	12.5
Zahn et al. [4]	Oct.5	0.0094	0.0092	11.4	10.3	219	1.09	1.04	1.13	-	0.1555	-	16.9
	Oct.6	0.0083	0.0053	9.8	4.5	180	1.51	1.52	1.89	-	0.1002	-	18.9
	Sq.7	0.0105	0.0118	11.8	9.0	291	1.19	1.07	1.17	-	0.1758	-	14.9
	Sq.8	0.0086	0.0087	9.5	6.4	358	1.15	1.24	1.37	-	0.1296	-	14.9

Notes:

1. $\varphi_y, \Delta_y, M_{max}$ and φ_{max} from experiment
2. $\varphi_y, \Delta_y, M_{max}$ and φ_{max} from cyclic moment-curvature theory
3. From code theoretical approach [2] using measured f'_c and f_y, and assuming ϕ=1.0
4. From empirical equation [14]
5. Maximum moment from experiment measured at the first cycle of $\mu = 2$
6. Re-tested with $P_e = 0.7 f'_c A_g$
7. φ_y was calculated theoretically
8. φ_{max}/φ_y based on the theoretical φ_y.

2.3.2 Basic Principles Concerning the Role of Confining Reinforcement

In early studies in 1928, Richart, Brandtzaeg, and Brown [15] found that the strength and ductility of concrete were significantly increased during triaxial compression loading, compared with uniaxial loading, because the lateral pressure confined the concrete and reduced the tendency for internal cracking and volume increase just prior to failure.

In practice, concrete is generally confined by transverse reinforcement in the form of spirals or hoops. Richart *et al.* [16] found that the enhancement of strength and ductility of concrete confined by fluid pressure, was similar to that observed for concrete confined by transverse reinforcement.

ACI Committee 103 in 1933 [17] reported that the ultimate strength of concentrically loaded reinforced concrete columns confined by spirals could be expressed by a single formula as follows:

$$\frac{P}{A_c} = Cf'_c(1-\rho_{cc}) + f_y\rho_t + kf_{yh}\rho_s \tag{2.1}$$

where P=ultimate concentric load on column, A_c=cross-sectional area of core concrete, C=a constant, found to be 0.85, f'_c=compressive strength of concrete cylinders, ρ_{cc}=ratio of area of longitudinal reinforcement to A_c, f_y and f_{yh}=yield strengths of longitudinal reinforcement and spirals, respectively, k= a constant, ranged between 1.5 to 2.5 with an average of 2.0, and ρ_s=volumetric ratio of spirals to core concrete. Eq. 2.1 indicates that when spiral steel is used, transverse reinforcement is twice as efficient as longitudinal steel as far as increasing the load carrying capacity of the columns is concerned.

To achieve considerable enhancement of strength in columns, sufficient quantities of transverse reinforcement have to be provided. The increase in strength of concentrically loaded columns due to confining reinforcement should exceed the strength of cover concrete. This requirement is based on the assumption that the strength of confined columns after the spalling of concrete should be at least equal to the strength of unconfined columns before the concrete spalling, in order to prevent a sudden loss in load carrying capacity. If the strength of cover concrete is assumed to be $0.85f'_c$, the minimum required spiral reinforcement is then given by:

$$\begin{aligned} 2\rho_s f_{yh}A_c &= 0.85f'_c(A_g - A_c) \\ \rho_s &= \frac{0.43f'_c}{f_{yh}}\left(\frac{A_g}{A_c} - 1\right) \end{aligned} \tag{2.2}$$

2.3.3 ACI Building Code Requirements

Based on the above principle of maintaining the strength of concentrically loaded columns, the American Concrete Institute Building Code ACI 318-71 [18] recommended the quantities for spiral reinforcement in the potential plastic hinge regions of columns in seismic design as follows:

For columns with $P_e > 0.4P_b$,

$$\rho_s = \frac{0.45f'_c}{f_{yh}}(\frac{A_g}{A_c} - 1) \tag{2.3}$$

but not less than $0.12f'_c/f_y$. Tests indicated that considerable toughness and ductility was achieved in columns containing spirals as required by Eq. 2.3. The lower bound $0.12f'_c/f_y$ was applied to large columns with small cover thickness.

When $P_e < 0.4P_b$, columns were designed as flexural members.

These requirements were maintained in ACI 318-77 [19] and ACI 318-83 [20]. Except that the limitation of axial load of $0.4P_b$ was replaced by $0.1f'_cA_g$ in ACI 318-83. The following requirements for confining reinforcement in forms of rectangular hoops or cross ties were also specified:

$$A_{sh} = 0.3s_hh"\frac{f'_c}{f_{yh}}(\frac{A_g}{A_c} - 1) \tag{2.4}$$

or

$$A_{sh} = 0.12s_hh"\frac{f'_c}{f_{yh}} \tag{2.5}$$

whichever is greater.

Also, since 1971, the ACI 318 requirements for the length of the confined potential plastic hinge regions have been the greater of the overall thickness h, where h is the larger sectional dimension for rectangular columns or the diameter of circular columns, one-sixth of the clear height of column, or 18 in. (457 mm). However, the requirements for the spacings of confining reinforcement have been changed. In addition to the requirement of a spacing not exceeding 4 in. (102 mm), the ACI 318-83 also specified that the transverse reinforcement shall be spaced at distances not exceeding one quarter of the minimum member dimension.

The ACI 318 requirements as described above, became the basis of the seismic design provisions for concrete confinement in columns of many countries, including New Zealand [2] and Europe [22]. The SEAOC code [23] also used the provisions and the detailing specified by the ACI 318.

2.3.4 CEB Model Code Requirements for Seismic Design of Concrete Structures

General

The Comite Euro-International du Beton CEB Bulletin d'Information N^o 165, 1985 [22] specifies a set of seismic design provisions, which is known as the Model Code for Seismic Design of Concrete Structures.

According to the code [22], structural systems may possess different *ductility levels* as follows:

- *Ductility Level I (DL I).* This level of ductility is associated with relatively large design lateral forces, so that only a little inelastic response occurs even during the largest earthquake. Structures with ductility level I may be considered as elastic responding structures.
- *Ductility Level II (DL II).* This level of ductility will enable the structures to enter inelastic range under repeated cyclic loading, without premature brittle-type failure. Structures DL II may be considered as structures of limited ductility.
- *Ductility Level III (DL III).* For this level of ductility, special procedures for the evaluation of design actions, and for the proportioning and detailing of structural elements are to be adopted to ensure the development of selected mechanisms with large energy-dissipation capacities. Structures DL III may be considered as ductile structures.

With regard to the detailing of columns of structures DL II and DL III, the code specifies the following requirements. When the axial compression load $P_e \leq 0.1 f'_c A_g$, the columns are considered as flexural members. When $P_e > 0.1 f'_c A_g$, the requirements described in the following sections are applied.

Column Critical Regions

The critical regions of a column, which are denoted as potential plastic hinge regions in the New Zealand code [2], are considered to be the regions at each end of a column above and below connections over a length from the faces of the connection of not less than the larger of the longer column cross-section dimension in the case of a rectangular column, or the diameter of the section in the case of a circular column, one-sixth of the clear height of column, or 450 mm.

Quantities of Confining Reinforcement in the Column Critical Regions

For structures DL II, a minimum diameter of 8 mm in the form of spiral or hoop reinforcement shall be provided, with the maximum spacings of the smaller of eight times the

minimum diameter of longitudinal bars, one half the least cross-sectional dimension of the section, or 200 mm. These quantities shall be continued throughout the length of the beam-column joint.

For structures DL III, the volumetric ratio of transverse reinforcement (spirals or hoops) shall not be less than the greater of:

$$\rho_s = \lambda_1 \frac{f'_c}{f_{yh}} \tag{2.6}$$

$$\rho_s = \lambda_2 (\frac{A_g}{A_c} - 1) \frac{f'_c}{f_{yh}} \tag{2.7}$$

The values of λ_1 and λ_2 are given in Table 2.3, as a function of the axial compression loads.

Table 2.3: Values of λ_1 and λ_2

P_e/f'_cA_g	0.10	0.20	0.30	0.40	0.50
λ_1	0.05	0.06	0.07	0.08	0.09
λ_2	0.18	0.22	0.26	0.30	0.34

It is obvious, that the values of λ_1 and λ_2 increase with the axial load levels, indicating that the higher the axial load, the more confinement is needed to confine the compressed concrete.

For rectangular sections, the volumetric ratio ρ_s is defined as

$$\rho_s = \frac{A_{sh}}{s_h h_c} \tag{2.8}$$

The minimum diameter of spirals or hoops shall be 8 mm. However, more stringent requirements for the hoop spacings are given for structures of DL III. That is, the maximum spacings shall not exceed the smaller of six times the minimum diameter of longitudinal bars, a quarter of the least cross-sectional dimension of section, or 150 mm.

2.3.5 New Zealand Concrete Design Code NZS3101 Seismic Design Provisions

In the first draft of the most recent New Zealand concrete design code, Draft Code DZ3101:1978 [10] the length of the confined potential plastic hinge regions was specified as in ACI 318-77.

However, based on theoretical moment-curvature studies conducted by Park *et al.* [24] for rectangular columns, using the stress-strain model for confined concrete derived by Kent and Park [25], and by Park *et al.* [26] for circular columns, the quantities of confining reinforcement in the potential plastic hinge regions specified by the ACI and SEAOC codes, were modified to account for the effect of axial compression in the columns.

For circular columns, it was required that

$$\rho_s = q\frac{f'_c}{f_{yh}}(0.375 + 1.25\frac{P_e}{f'_c A_g}) \tag{2.9}$$

where $q = 0.12$ or $q = 0.45(A_g/A_c - 1)$, whichever is greater, $P_e \geq 0.1 f'_c A_g$, and $\rho_s = 4A_b/(s_h d_s)$

The diameter of spiral or circular hoop bar was to be at least 10 mm, and the maximum centre-to-centre spacing of spirals or hoops was not to exceed the smaller of one-fifth of column diameter, six times the minimum diameter of longitudinal bars, or 125 mm.

For rectangular columns, it was required that

$$\rho_s = q\frac{f'_c}{f_{yh}}(0.33 + 1.67\frac{P_e}{f'_c A_g}) \tag{2.10}$$

where $q = 0.12$ or $q = 0.3(A_g/A_c - 1)$, whichever is greater, $P_e \geq 0.1 f'_c A_g$, and $\rho_s = A_{sh}/(s_h h")$

The minimum diameter and spacing of hoops was similar to that for spiral or circular hoop steel, except that the spacing of 125 mm was increased to 150 mm.

Comparing Eqs. 2.9 and 2.10, it is obvious that in a rectangular column, the required quantities of transverse reinforcement were more dependent on the axial load level than in a circular column. Due to their shape, spirals or circular hoops are capable of providing uniform confining pressure to concrete. This is not the case for rectangular hoops or cross-ties which because of their shape, can only apply confining pressure near the corners of the hoops and the ends of the cross-ties, therefore the concrete is only confined effectively in those areas, resulting in smaller area of effectively confined concrete. When the axial load is high, the strength of columns is more dependent on the strength of confined concrete. The smaller area of effectively confined concrete results in less strength and ductility of such columns, and therefore larger quantities of confining reinforcement are required for rectangular columns.

However, more experimental results [7,8] obtained from tests on a range of near full size reinforced concrete columns, and designed according to the draft code [10] requirements for concrete confinement, showed that displacement ductility factors of at least 6 and 8 were

achieved in square and circular columns, respectively. Moreover, at the end of the tests, the maximum inelastic deformation capacity of the columns was not fully reached, and the strength was still maintained, indicating that the columns could have reached much higher ductility factors than those available.

As a result of the above test results, the requirements for the quantities of confining reinforcement were modified to give the same level of dependency on the axial compression for both circular and rectangular columns. Also, the length of the confined potential plastic hinge regions was modified according to the axial load levels, since when the axial load level increased, failure could possibly occur outside the confined region unless the confined region was long enough.

The volumetric ratio for spirals or circular hoops, and for rectangular hoops, in the potential plastic hinge region was then given in the second draft of the code [11] as

$$\rho_s = q\frac{f'_c}{f_{yh}}(0.5 + 1.25\frac{P_e}{f'_c A_g}) \tag{2.11}$$

where $q = 0.12$ or $q = 0.30k(A_g/A_c - 1)$, whichever is greater, $\rho_s = 4A_b/(s_h d_s)$, and $k = 1.5$ for circular hoop arrangement, and $\rho_s = A_{sh}/(s_h h")$, and $k = 1.0$ for rectangular hoop arrangement.

It is also required that $P_e < \phi 0.7 f'_c A_g$ or $P_e < \phi 0.7 P_o$, where P_o=ideal axial load compressive strength when the load is applied with zero eccentricity.

The centre-to-centre spacing of both spirals and circular and rectangular hoops should not exceed the smaller of one-fifth of the least lateral dimension of the cross section, six longitudinal bar diameters, or 200 mm.

It is expected that columns with the quantities of confining reinforcement as given by Eq. 2.11 will be capable of reaching a curvature ductility factor φ_u/φ_y of at least 20, which should allow typical bridge piers or building columns in a storey to achieve a displacement ductility factor of at least 8 [21].

The length of potential plastic hinge region is recommended as follows. When $P_e \leq 0.3 f'_c A_g$, not less than the larger column section, or where the moment exceeds 0.8 of the maximum moment at that end of the member. When $P_e > 0.3 f'_c A_g$, the length is increased by 50%.

The above recommendations were confirmed by research work carried out by Ang *et al.* [9]. The design provisions in the New Zealand concrete design code NZS3101:1982 [2] follow these recommendations.

2.4 Comparison of the Code Provisions for Quantities of Confining Reinforcement in the Potential Plastic Hinge Regions of Columns

The code provisions discussed above indicated the necessity for confining reinforcement to provide adequate ductility in columns. They were initiated by the ACI building code, and followed by the New Zealand and CEB codes with some modifications, particularly with regards to the effects of axial compression in columns on the available ductility (see Ref. [27]).

Although the modifications made by the CEB code were not as obvious as those made by the New Zealand code, both provisions indicate that more confining reinforcement is necessary to maintain the strength and ductility of columns with large axial compression. Fig. 2.1 compares the quantities of confining reinforcement required by the codes for a typical column section.

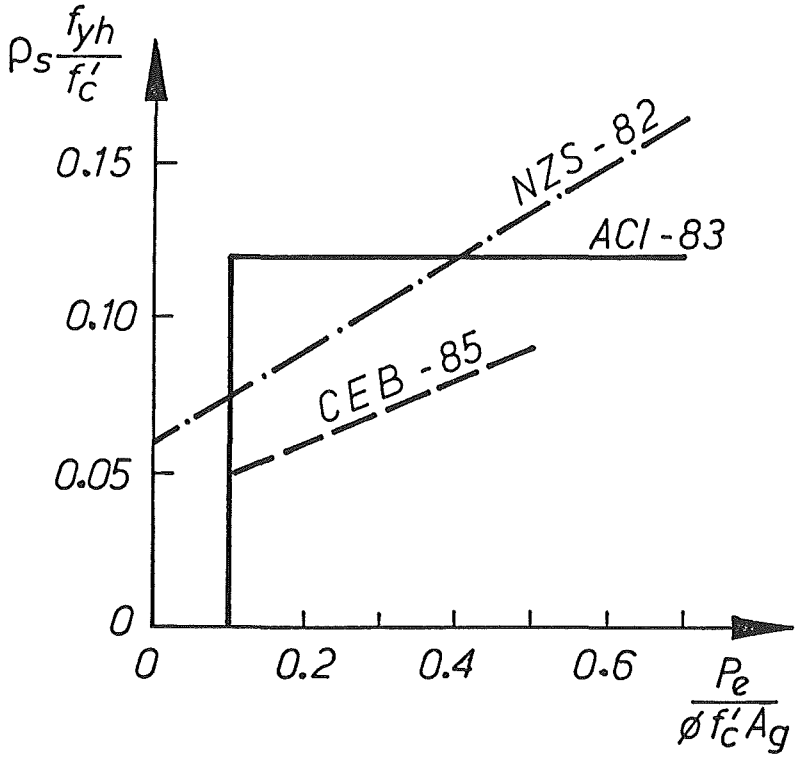

Figure 2.1: Comparison of Code Quantities of Confining Reinforcement for a Column

The step change in the ACI requirements which occurs at $P_e = 0.1 f'_c A_g$, does not give a rational amount of confining reinforcement needed when the axial load ratio is slightly less than $0.1 f'_c A_g$.

Although the CEB code went a step further by linearly increasing the quantities with the axial load level as in the New Zealand code, the quantities are much less than recommended by both the ACI and New Zealand codes.

Fig. 2.1 shows clearly that there is still considerable disagreement between the codes. The basic difference between the ACI and New Zealand codes arise because the ACI code provisions are based on preserving the concentric load capacity of columns whereas the New Zealand code provisions are based on attaining adequate curvature ductility capacity.

Although the New Zealand provisions recommend the greatest quantities of confining steel, it was found in recent theoretical studies [3,4] (see Chapter 4), that the New Zealand provisions need to be made even more dependent on the level of axial compression in columns if the requirement for adequate ductility is to be maintained.

Chapter 3

EXPERIMENTAL INVESTIGATION OF THE BEHAVIOUR OF SQUARE AND OCTAGONAL COLUMNS UNDER COMBINED FLEXURE AND AXIAL LOADS

3.1 Introduction

The current New Zealand concrete design code [2] specifies the following equation for the quantity of confining reinforcement required in potential plastic hinge regions of reinforced concrete columns of ductile structures:

$$\rho_s = q\frac{f'_c}{f_{yh}}(0.5 + 1.25\frac{P_e}{f'_c A_g}) \tag{3.1}$$

where $q = 0.12$ or $q = 0.30k(A_g/A_c - 1)$, whichever is greater.

For spirals or circular hoops, $\rho_s = 4A_b/(s_h d_s)$ and $k = 1.5$, and for rectangular hoop reinforcement with or without supplementary cross ties, $\rho_s = A_{sh}/(s_h h")$ and $k = 1.0$, where s_h is the centre-to-centre spacing of hoop sets, $h"$ or d is the dimension of concrete core of section measured to the outside of perimeter hoop or spiral, A_g is the gross area of column cross section, A_c is the area of concrete core of section measured to outside of peripheral hoop or spiral, f'_c is the concrete compressive strength, f_{yh} is the yield strength of transverse hoops, P_e is the axial compression load due to design gravity and seismic loading and ϕ is the strength reduction factor.

The centre-to-centre spacing of transverse reinforcement in potential plastic hinge regions should not exceed the smaller of one-fifth of the least lateral dimension of cross section, six longitudinal bar diameters,or 200 mm.

As mentioned in Chapter 2, the equation was based on the ACI [19] and SEAOC [23] equation, with an additional term to include the axial compression as a variable. This modification was resulted from theoretical and experimental studies carried out at the University of Canterbury [14], which showed that the level of axial compression in columns did affect the available ductility of the columns. Recent analytical studies [4] however, indicated that the above code equation might not be able to provide adequate ductility when the axial compression level is high, and therefore the equation may need to be made more dependent on the level of axial compression.

On the other hand, an experimental study carried out by Soesianawati *et al.* [5] showed that only one-half of the quantity of confining reinforcement recommended by the code [2] is sufficient to provide adequate ductility in columns with low axial compression levels.

In addition, significant tests have also been conducted in the United States. Johal *et al.* [31] examined the effect of axial load, and the amount, type and details of transverse reinforcement, on the strength and ductility of columns subjected to simulated seismic loading. Ten units with axial compression loads of 0.2 to $0.4f'_cA_g$ were tested. The results indicated that the flexural overstrength of columns, above the code calculated strengths increases with axial load level, but that the ductility decreases substantially. Also, a reduction in the amount of transverse reinforcement results in a lower available ductility.

Fafitis and Shah [32] investigated the behaviour of confined columns subjected to monotonic flexure and constant axial compression. The confining reinforcement was designed to the ACI 318-77 [19] requirements. The axial load levels were varied from 0.25 to $0.8f'_cA_g$. It was found that the degree of flexural overstrength depends on the axial load levels, the amount of confinement, the compressive strength of concrete and the shape of columns. It was also shown that the square columns exhibited higher flexural overstrength than the circular sections. However, the available ductility in the columns was not indicated.

Sheikh, Yeh and Menzies [33], and Yeh and Sheikh [34] tested fifteen column specimens subjected to concentric compressive loads, and sixteen column specimens subjected to combined flexure and constant axial compression. One of the aims of this study was to investigate the effects of distribution and quantities of transverse reinforcement on the strength and ductility of columns. As expected, an increase in the amount of confining reinforcement significantly enhanced the strength and ductility of the columns. The effect of axial load levels on the behaviour of columns was also examined. Surprisingly, it was found that for some columns with high axial compression, the flexural strength of the columns did not even reach the theoretical strength calculated using the code approach for unconfined concrete.

It is evident, although several experimental investigations of the behaviour of columns under simulated seismic loading have been conducted in New Zealand and overseas, there is still insufficient information regarding the available ductility of columns with large axial compression. More experimental work is required to examine the behaviour of this type of column in order to verify the analytical prediction [4], concerning with the dependency of quantities of confining reinforcement on the level of axial compression.

In this chapter, a description of an experimental investigation of seven reinforced concrete columns, with various quantities of transverse reinforcement, subjected to moderate and large axial compression, and reversible lateral load is presented. This includes the design,

construction and instrumentation of the column units, material properties used, and a brief explanation of the testing procedure. The experimental results are reported in the following form: General Performance, Hysteretic Behaviour, Measured Curvature Distribution, Available Curvature Ductility Factor, Equivalent Plastic Hinge Length and Plastic Rotation, and Measured Strain Profile. A comparison with theoretical predictions is also made.

3.2 Design of Column Units

3.2.1 Background

In 1985, four square reinforced concrete columns with low axial compression, which contained smaller quantities of confining reinforcement than recommended by the code [2] were tested [28], under constant axial compression and cyclic flexure to simulate earthquake loading. The details of these units are listed in Table 3.1, and the cross sections and dimensions are shown in Figs. 3.1a and b.

Table 3.1: Properties of Column Units with Low Axial Compression

Unit	$\frac{P_e}{\phi f'_c A_g}$	f'_c (MPa)	dia.-s_h (mm)	f_{yh} (MPa)	Transverse Reinforcement for					
					Confinement			Antibuckling		Shear
					1	2	3	4	5	6
1	0.1	46.5	R7-85	364	0.43	–	0.21	5.3	2.08	1.0
2	0.3	44	R8-78	360	0.46	1.12	0.20	4.9	2.93	2.01
3	0.3	44	R7-91	364	0.30	0.74	0.23	5.7	1.94	1.65
4	0.3	40	R6-94	255	0.17	0.41	0.24	5.9	0.97	1.34

Notes:

1. ratio of actual ρ_s to ρ_s required by code [2]
2. ratio of actual ρ_s to ρ_s required by design charts [4] for $\varphi_u/\varphi_y = 20$
3. ratio of s_h to b
4. ratio of s_h to d_b
5. ratio of tie force to $\frac{1}{16}$ longitudinal bar force at 100 mm centres
6. ratio of shear strength to design shear force
7. f'_c was measured at time of testing of column units
8. f_y was 446 MPa

The results of these column tests are summarized as follows: Units 1 and 2, which contained 43% and 46% of the code [2] recommended quantity of confining reinforcement, and with axial load levels of 0.1 or $0.3f'_cA_g$, respectively, achieved a displacement ductility factor of at least 8 without significant strength degradation. The longitudinal bars at the extreme fibre eventually fractured. Units 3 and 4, with 30% and 17% of the code recommended quantity of confining reinforcement, and with an axial load level of $0.3f'_cA_g$, achieved displacement ductility factors of at least 6 and 4, respectively. Fracture of an octagonal hoop was observed at the end of testing Unit 3, and a failure of hoop anchorage followed by buckling of longitudinal bars terminated the test of Unit 4.

The current experimental work is a continuation of the above study [28]. In this project, the flexural strength and ductility of columns with moderate to high axial compression loads are investigated, so that the behaviour of columns over a greater range of axial load levels can be explored in more detail.

3.2.2 Description of the Additional Column Units

Seven column units 3.9 m high were designed and constructed. Five of the units (Units 5 to 9) were of square cross section, and the other two (Units 10 and 11) were of octagonal cross section. The cross sections and the dimensions of the columns, and the arrangement of longitudinal and transverse reinforcement in the columns are shown in Fig. 3.1. Because the specimens were approximately one half scale, the concrete cover to the transverse reinforcement was made 13 mm whereas the New Zealand code [2] requires a minimum cover thickness of 25 mm for cast in situ beams and columns.

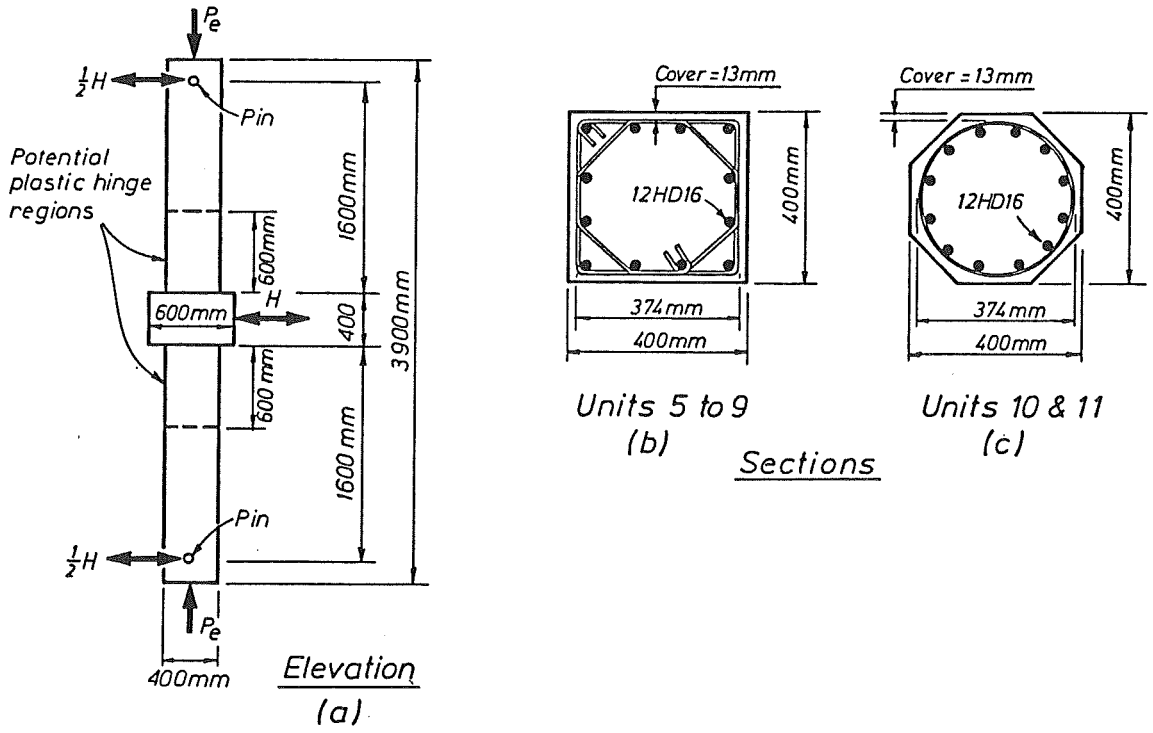

Figure 3.1: Cross Sections and Dimensions of Column Units

The critical plastic hinge regions of the columns where maximum moment occurs, and therefore damage is expected, are the regions above and below the central stub (see Fig. 3.1).

For Units 5 and 6 with square cross section, the axial load level was $0.5f'_cA_g$, and the transverse reinforcement was designed to be 4/9 and 2/9 times the quantities given by the code [2]. For Unit 10 with octagonal cross section, the axial load level was $0.5f'_cA_g$, and the transverse reinforcement was designed to be one-half of the code quantity. For Units 7 and 8 with square cross section, the axial load level was $0.7f'_cA_g$, and the transverse reinforcement was designed to be 2/3 and 4/9 of the code recommended quantity. Also, with an axial load level of $0.7f'_cA_g$, Unit 9 of square cross section was designed in accordance with the design charts for ductility [4] to achieve a curvature ductility factor of 20. Testing of this unit was aimed to confirm the analytical prediction [4] that the current code [2] equation for confinement might be unconservative for columns with high axial compression. This prediction was also examined by testing Unit 11 with an octagonal cross section, which was designed according to the code recommended quantity of confinement for ductile detailing. Table 3.2 summarizes the details of all column units tested.

Table 3.2: Details of Column Units with Moderate and Large Axial Compression

Unit	Column Cross Section	Design f'_c (MPa)	$\frac{P_e}{\phi f'_cA_g}$	Transverse Reinforcement			
				diameter (mm)	s_h (mm)	f_{yh} (MPa)	$\frac{\rho_s}{\rho_{s,code}}$
5	square	35	0.5	8	81	372	0.45
6	square	35	0.5	6	96	388	0.22
7	square	30	0.7	12	96	308	0.67
8	square	30	0.7	8	77	372	0.45
9	square	30	0.7	12	52	308	1.24
10	octagonal	35	0.5	8	84	372	0.50
11	octagonal	30	0.7	10	57	338	1.01

In order to keep the quantities of transverse reinforcement to the expected percentages of the code quantities as mentioned previously, different compressive strengths of concrete were used in design. Units 5, 6 and 10, which had an axial load level of $0.5f'_cA_g$, were designed using a compressive strength of 35 MPa. For Units 7, 8, 9 and 11 which had an axial load level of $0.7f'_cA_g$, a compressive strength of 30 MPa was used. The actual yield strengths of transverse reinforcing steel was used in the design calculations for transverse reinforcement.

The arrangements of reinforcement in typical square and octagonal column units, including close up views of the reinforcement in the central stub and at the end of the column, are shown in Fig. 3.2. It can be seen that outside plastic hinge regions, the spacings of transverse reinforcement was taken as twice those provided in the potential plastic hinge regions. Around the loading pins at the column ends, closer spacings of transverse reinforcement were placed to resist bursting stresses due to the concentration of high axial compression.

In designing the transverse reinforcement of the column units, the code [2] limitation of $6d_b$ for the spacing to prevent buckling of longitudinal reinforcement in the plastic hinge regions,

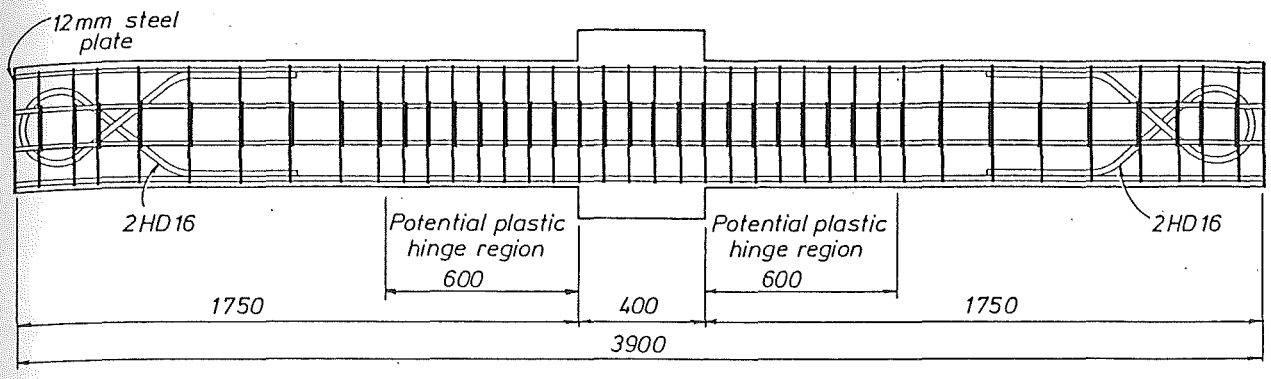

(a). Square Column Unit (Reinforcement in Central Stub Is Not Shown)

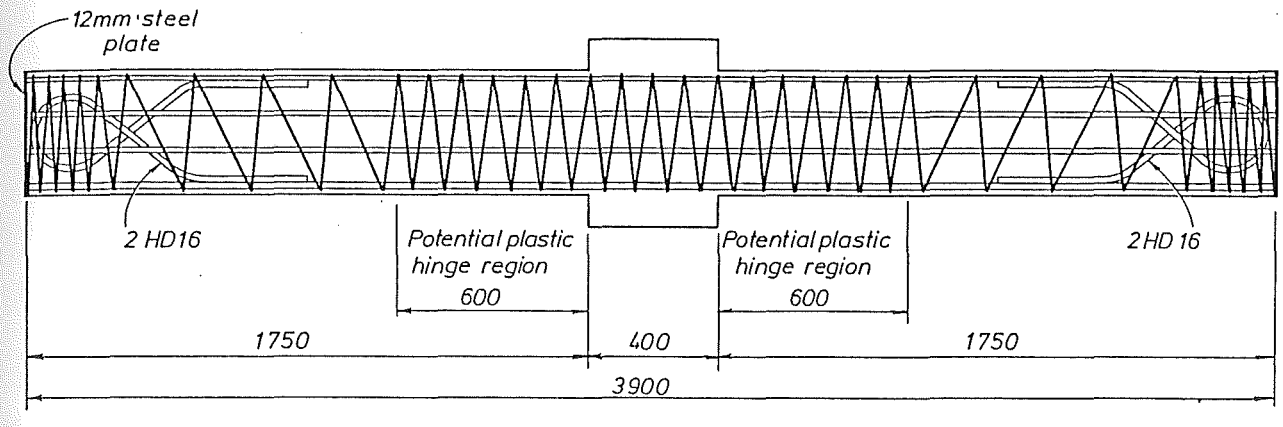

(b). Octagonal Column Unit (Reinforcement in Central Stub Is Not Shown)

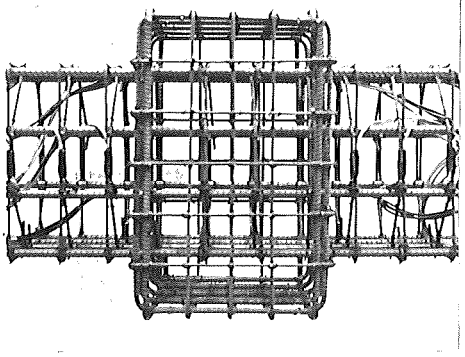

(c). Reinforcement in Central Stub

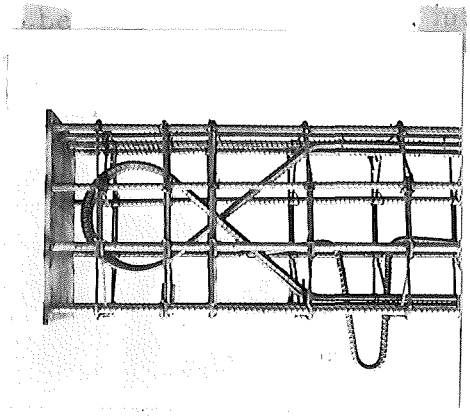

(d). Reinforcement at End Pin

Figure 3.2: The Arrangements of Reinforcement in Column Units

and $12d_b$ outside plastic hinge regions, was satisfied. The maximum permitted spacing in the plastic hinge regions was then 96 mm as used in Units 6 and 7. Smaller spacings were used in the other units.

3.3 Construction of Column Units

The reinforcing cage was first fabricated by tying the transverse bars to the longitudinal bars. The steel end plates of 12 mm thickness were welded to the longitudinal bars at each end of the cage. The reinforcing steel to form the central stub, was also placed. The stub was expected to behave elastically during the test. As shown in Fig. 3.2d, two $\propto$ shaped reinforcing bars surrounding each end pin were also located to control any cracking of concrete in this region. Fig. 3.3 shows the reinforcing cage of a typical column unit.

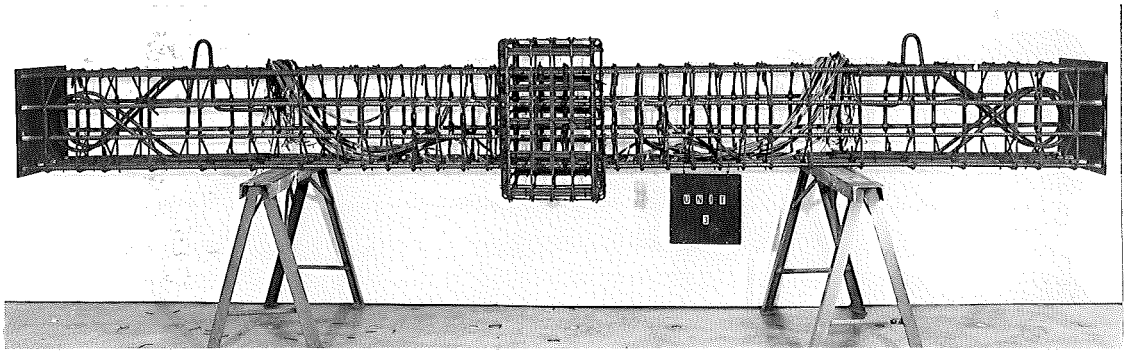

Figure 3.3: Reinforcing Cage of a Typical Column Unit

The cage was then placed in a plywood mould which had been painted and oiled to facilitate the removal of the unit after curing. The 55 mm diameter steel tubes were located at the position of the pins, and the 10 mm diameter steel rods for holding the potentiometers were also positioned and screwed to prevent any movement. These rods had polystyrene tips at both ends to ensure that the crushing of cover concrete during testing would not affect the measurements. Four 16 mm diameter anchor bars, to be used for lifting the unit into the DARTEC machine, and four 32 mm diameter plastic tubes to be used for the bolts of the lateral load jack assembly were placed. A complete reinforcing cage in the mould, ready for placing the concrete in a horizontal position, is shown in Fig. 3.4.

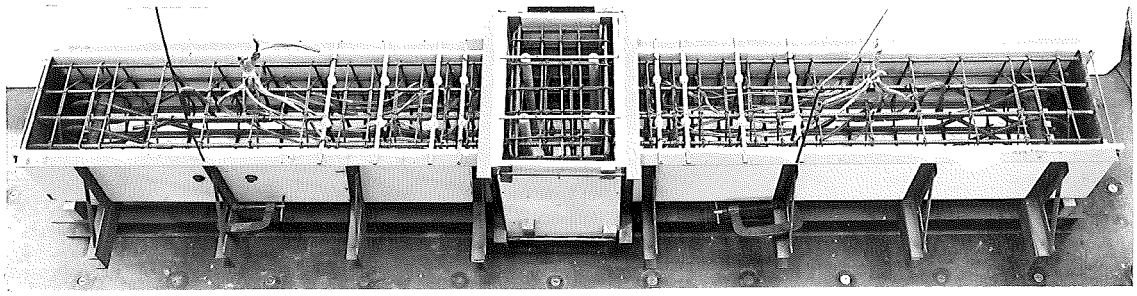

Figure 3.4: Reinforcing Cage in a Plywood Mould

Two batches of concrete were provided by a local ready-mix supplier with target mean compressive strengths of either 35 or 30 MPa. The cement content was 290 kg/m^3 and 330

kg/m^3, respectively. A graded aggregate with a maximum size of 12 mm was used. The concrete had a slump of 100 mm.

From the first batch of concrete, with a target strength of 35 MPa, three column units, namely Units 5, 6 and 10 were cast. Twelve 200 × 100 mm diameter concrete cylinders and three 120 mm square beams 400 mm long were also cast. From the second batch, with a target strength of 30 MPa, four column units, namely Units 7, 8, 9 and 11 were cast together with fifteen cylinders and three beams with the same dimensions as above.

The specimens were compacted by mechanical vibrators. The suface of the specimens was then trowelled smooth, covered with damp sacks and polythene, and kept moist for seven days. The cylinders and the beams were vibrated on a vibrating table and left to cure in a fog room at $20°C$ and 100% relative humidity until tested.

3.4 Instrumentation of Column Units

The instrumentation for measuring displacements is shown in Fig. 3.5. Three 300 mm travel SAKAE linear potentiometers were installed on the side of the stub to measure the horizontal displacement and to calculate the rotation of the stub. Ten pairs of linear potentiometers of either 50 mm travel or 30 mm travel, aligned vertically at five levels above and below the stub, were used to calculate the column curvatures and compressive strains in the core concrete. This calculation was carried out assuming that plane sections remain plane after bending.

The potentiometers measuring vertical deformations were mounted on the steel rods which passed horizontally through the columns and were cast in the columns. To ensure that these potentiometer measurements would not be effected by the deformations of the transverse and longitudinal reinforcing bars, different gauge lengths were used, depending on the spacings of the transverse reinforcement. Table 3.3 shows the distance of the potentiometer rods from the face of the stub for each column unit.

To measure the strains in the plastic hinge regions, SHOWA N11-FA-5-120-11 5 mm electrical resistance strain gauges with a gauge factor of 2.11 were attached on the hoops and spirals (see Fig. 3.6). For each position, the gauges were placed in pairs so that the axial stress could be obtained with effect of bar bending eliminated.

For the square columns, the electrical resistance strain gauges were placed on both the octagonal and square hoops and on the four sets of hoops above and below the central stub, except for Unit 9 where because of the small hoop spacing of 52 mm the gauges were placed on every second hoop at four levels above and below the stub. For the octagonal columns, they were placed on the five spiral turns above and below the central stub, except for Unit 11 where because of the small spiral spacing of 57 mm the gauges were placed on every second spiral turn at five levels above and below the stub.

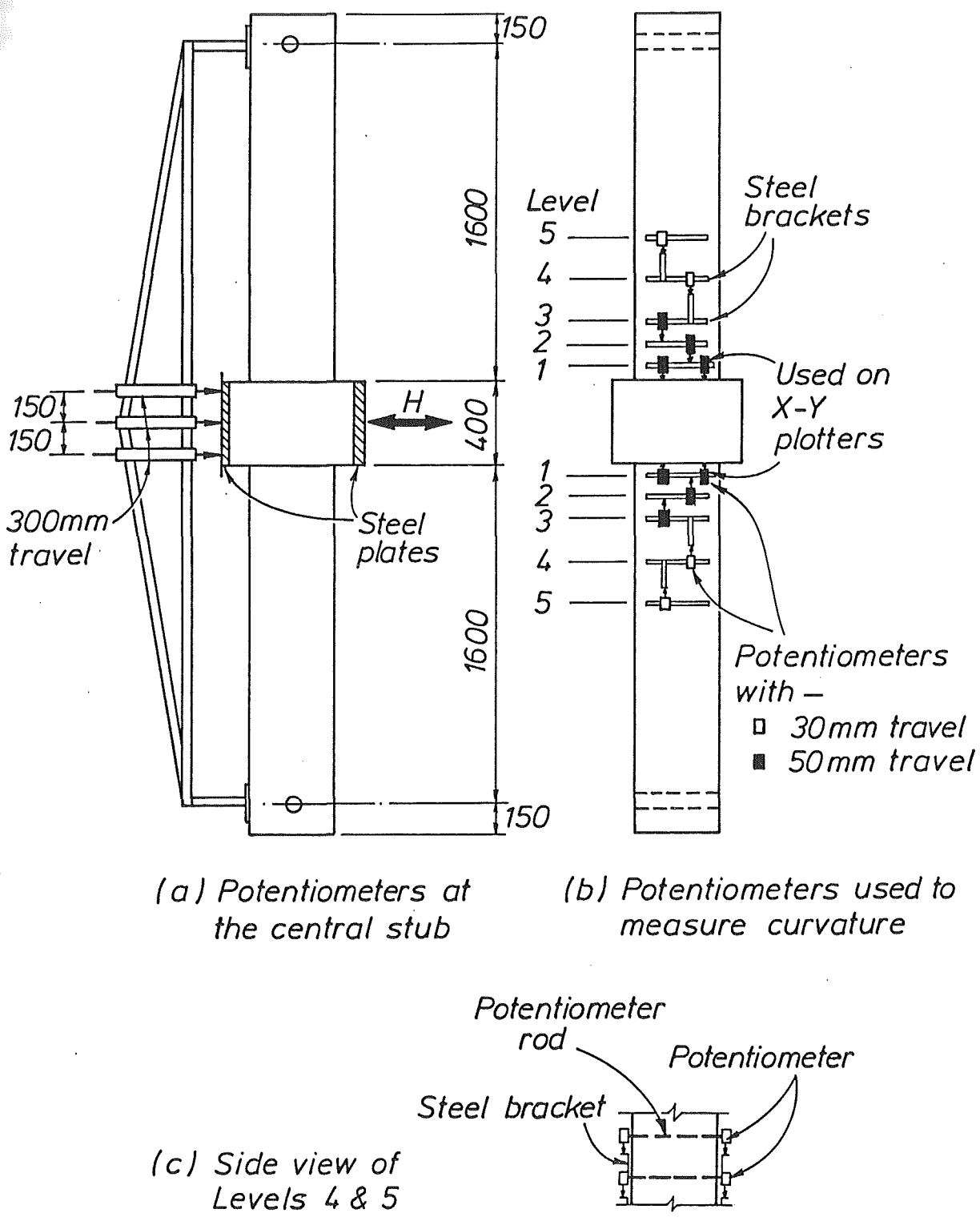

Figure 3.5: Positions of Potentiometers on the Column Units

Table 3.3: The Distance of Potentiometer Rods from the Face of the Central Stub for Each Column Unit, in mm

Unit	1st level	2nd level	3rd level	4th level	5th level
5	80	160	310	470	630
6	80	160	310	470	630
7	80	180	280	460	640
8	80	160	310	470	630
9	100	200	350	510	710
10	80	160	320	500	680
11	80	160	320	500	680

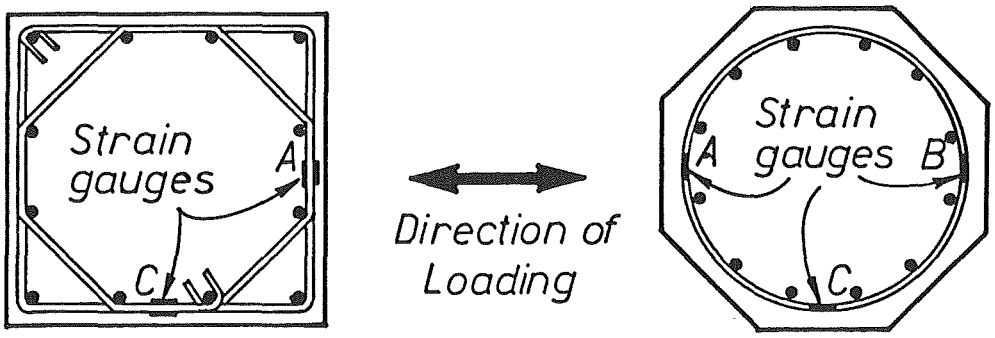

Figure 3.6: Positions of Electrical Resistance Strain Gauges on the Hoops and Spirals

The electrical resistance strain gauges in the square columns were placed prior to the fabrication of the reinforcing cages. The strain gauges in the octagonal columns, were attached to the spirals after fabricating the cages.

At selected stages during testing, the output voltages from the linear potentiometers and strain gauges were recorded by a SOLARTRON data logger. Using a data reduction program [35], the corresponding longitudinal and transverse strains were calculated.

Three X-Y plotters were used to plot the hysteresis loops of lateral load-displacement at the central stub, and lateral load–curvature at the top and bottom plastic hinge positions.

3.5 Material Properties

In order to predict the strength of the column units accurately, it is necessary to determine the properties of materials used. Tensile tests for both the longitudinal and transverse reinforcing steel, and compression and bending tests for the concrete, were carried out.

The tensile tests on the reinforcing steel were conducted in accordance with the British Standard BS18:Part 2:1971 specification [36].

The measured properties of the longitudinal reinforcing bar HD16 are shown in Fig. 3.7. It can be seen that the yield strength is much larger than the specified strength of 380 MPa. This steel in fact was micro-alloy high strength steel, which will be replacing the current high strength Grade 380 steel. It has a longer yield plateau and less significant strain hardening strength enhancement than the current Grade 380 steel.

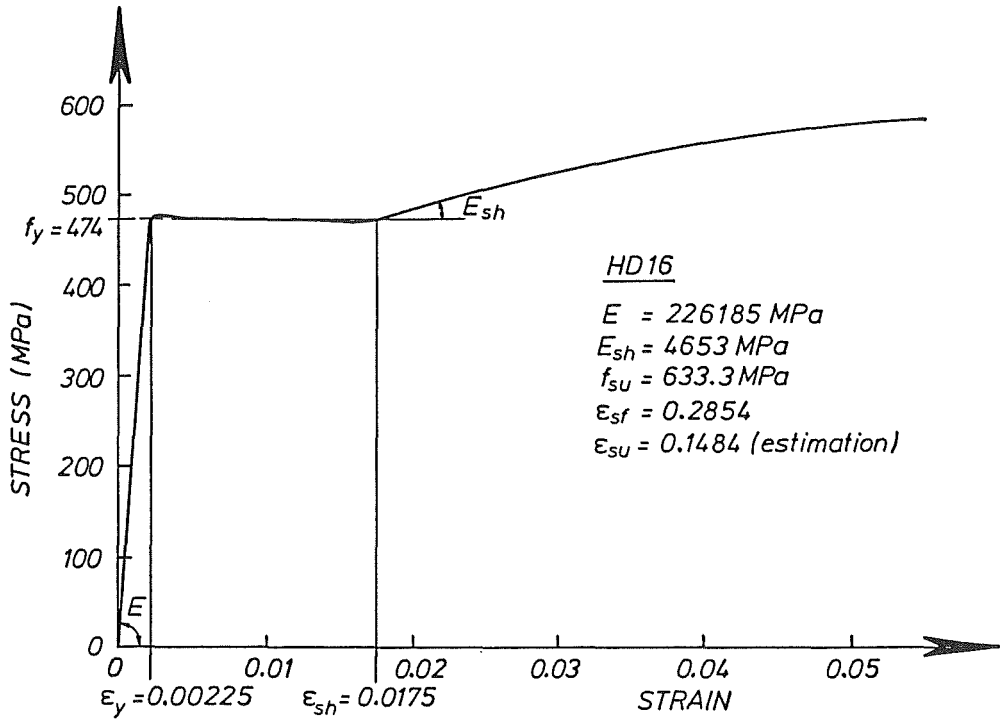

Figure 3.7: Stress-Strain Curve for Longitudinal Bar HD16

The transverse reinforcing steel used was of plain round bars of Grade 275, with diameters varying from 6 to 12 mm. For round bar R8, although the yield point was not as obvious as for the other bars, an approximate curve, which shows yield plateau and strain hardening, can still be plotted (see Fig. 3.9). Therefore, the yield strength and the yield strain for this bar were determined using the procedure similar to that used for the other bars which had well defined yield points. This procedure, is preferred to that specified in the BS 1971 [36] and ASTM 1973 [37], where the yield strength of steel lacking a well-defined yield point is defined as the stress corresponding to a strain of 0.005. Since the plain round bars R8 and R10 were used as spirals for Units 10 and 11, tensile testing of samples of straightened spirals was also carried out. The stress-strain curves of the bars obtained from the tests, are shown in Figs. 3.8, 3.9 and 3.10, respectively.

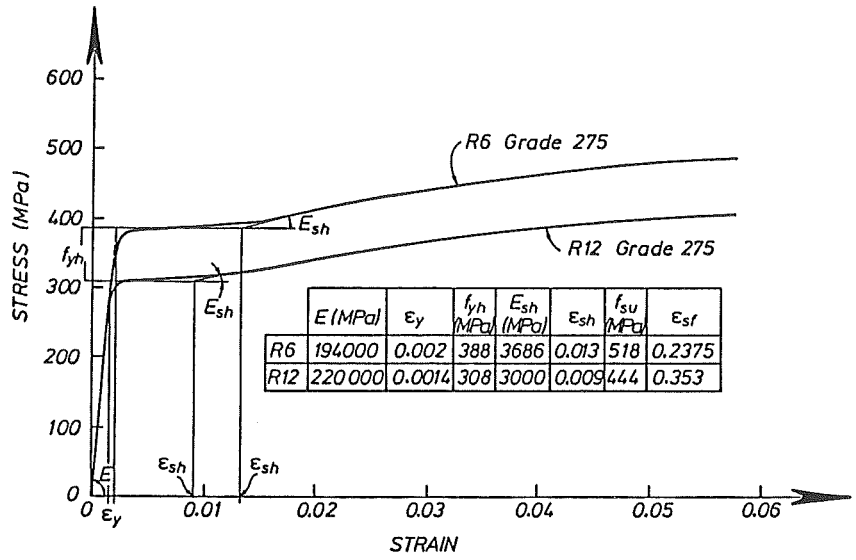

	E (MPa)	ε_y	f_{yh} (MPa)	E_{sh} (MPa)	ε_{sh}	f_{su} (MPa)	ε_{sf}
R6	194000	0.002	388	3686	0.013	518	0.2375
R12	220000	0.0014	308	3000	0.009	444	0.353

Figure 3.8: Stress-Strain Curves for Transverse Bars R6 and R12

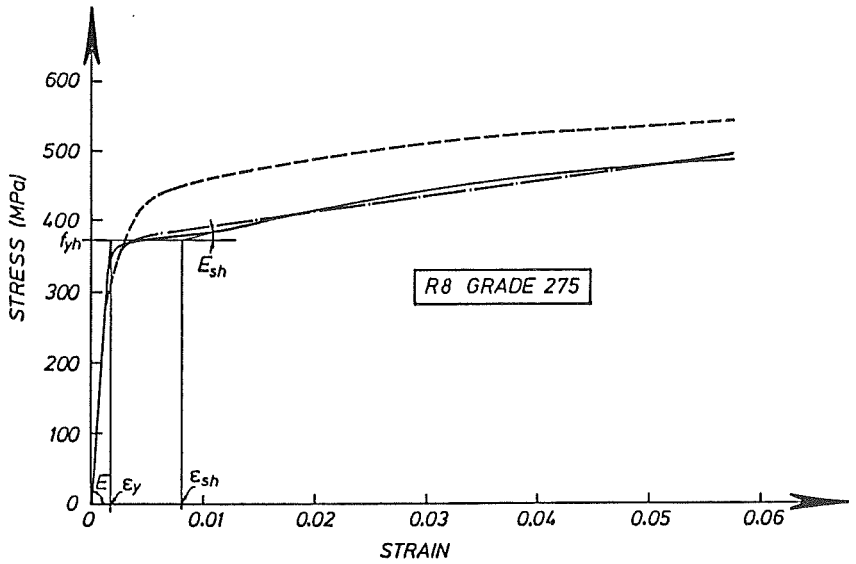

Figure 3.9: Stress-Strain Curves for Transverse Bar R8

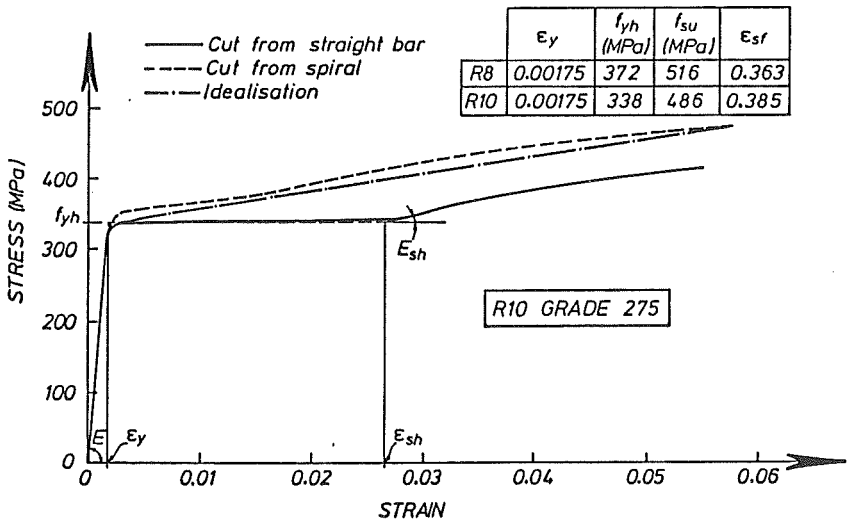

	ε_y	f_{yh} (MPa)	f_{su} (MPa)	ε_{sf}
R8	0.00175	372	516	0.363
R10	0.00175	338	486	0.385

Figure 3.10: Stress-Strain Curves for Transverse Bar R10

Meggegotto and Pinto [3] proposed a formula to determine an ideal stress-strain curve of straightend spirals (see Eq. 3.2). This theoretical curve, which generally lies between the measured curves for straight bar and straightened spirals, has been considered to be more reasonable for use in determining the properties of spiral reinforcement. The theoretical yield strength for the straightened spirals was found to be very close to that obtained from the straight bars, and therefore the yield strength of the straight bars was used in design.

$$f_s = E_s\epsilon_s \left[Q + \frac{1-Q}{(1+(E_s\epsilon_s/f_y)^R)^{1/R}} \right] \tag{3.2}$$

where $Q = 0.6E_{sh}/E_s$
$R = 0.1D/d_b, 1 \leq R \leq 20$
D = centre-to-centre diameter of the spiral
d_b = diameter of spiral bar

The compressive strengths of the concrete were obtained from 200 × 100 mm diameter concrete cylinders tested according to the procedure specified in the New Zealand Standard NZS 3112:Part 2:1980 [38]. The compressive strengths tested at 28 days for the first and second batches were found to be 36 and 31.5 MPa, respectively. Table 3.4 lists the concrete compressive strengths measured on the days of testing the column units. Each test result is the average strength obtained from three cylinders.

Table 3.4: Compressive Strength of Concrete at Stage of Testing the Column Units

Unit	Batch	Age of Concrete, Days	Compressive Strength, MPa
5	1	153	41
6	1	168	40
7	2	157	42
8	2	150	39
9	2	164	40
10	1	215	40
11	2	187	39

Bending tests on concrete beams with a 120 mm square cross section and 400 mm length, were also carried out in accordance with the NZS 3112:Part 2:1980 [38] specifications to evaluate the modulus of rupture of concrete. The values of modulus of rupture obtained at the age of 28 days for the two batches of concrete were both 4.8 MPa.

3.6 Comparison of the Quantities of Transverse Reinforcement in Column Units with Requirements Specified by the Code and by Design Charts for Ductility

3.6.1 Introduction

To ensure that the available ductility of a column exceeds the ductility demand during a severe earthquake, the New Zealand concrete design code [2] specifies quantities of transverse reinforcement in the potential plastic hinge regions of reinforced concrete columns of ductile moment-resisting frames. The transverse reinforcement is intended to adequately confine the concrete in the compression zone, to prevent buckling of compressed longitudinal bars, and to provide shear resistance.

In this section, the quantities of transverse reinforcement provided in the column units are compared with the code recommended quantities. A comparison of the quantities of confining reinforcement with those required by the design charts for ductility [4] to achieve a curvature ductility factor of 20 is also made.

3.6.2 Comparison of the Requirements of the Code and the Design Charts for Ductility with the Quantity of Transverse Reinforcement Provided in Column Units for Concrete Confinement

The New Zealand concrete design code [2] requires that in the potential plastic hinge regions of columns, the quantity of transverse reinforcement should not be less than those given by Eq. 3.1. The centre-to-centre spacings of transverse reinforcement should not exceed the smaller of: one-fifth of the least lateral dimension of cross section, or six times longitudinal bar diameter, or 200 mm.

Table 3.5 compares the actual quantity of transverse reinforcement provided in the column units with that required by the code [2], and by the design charts for ductility [4] for an available curvature ductility factor of φ_u/φ_y=20. The background of the design charts is described in Chapter 4. The calculation of the code and design chart quantities was conducted using the measured material strengths of steel and concrete. It can be seen that the actual transverse reinforcement for concrete confinement varied from 19% to 93% of the code recommended quantity, and from 21% to 70% of that required by the design charts for ductility.

The actual s_h/b or s_h/D ratios for Units 6, 7 and 10 exceeded the code limiting value of 0.20, but less than 0.25. It is worth noting that, based on the experimental results, a limitation of $s_h/b = 0.25$ has been proposed to replace the current code requirement of $s_h/b = 0.20$ [5]. The spacings used in the column units therefore, were within the proposed spacings of $s_h/b \leq 0.25$.

Table 3.5: Comparison of the Quantity of Transverse Reinforcement in the Column Units with the Requirements Specified by the Code and by the Design Charts for Ductility

Unit	$\frac{P_e}{\phi f'_c A_g}$	Transverse Reinforcement for					
		Confinement			Antibuckling		Shear
		1	2	3	4	5	6
5	0.5	0.38	0.42	0.20	5.1	2.74	2.04
6	0.5	0.19	0.21	0.24	6.0	1.36	1.51
7	0.7	0.48	0.38	0.24	6.0	4.31	2.79
8	0.7	0.34	0.25	0.19	4.8	2.88	2.29
9	0.7	0.93	0.70	0.13	3.3	7.95	3.61
10	0.5	0.44	0.33	0.21	5.3	N.A.	2.26
11	0.7	0.77	0.44	0.14	3.6	N.A.	3.38

Notes:

1. ratio of actual A_{sh} to A_{sh} required by code [2]
2. ratio of actual A_{sh} to A_{sh} required by design charts [4] for $\varphi_u/\varphi_y = 20$
3. ratio of s_h to b
4. ratio of s_h to d_b
5. ratio of tie force to $\frac{1}{16}$ longitudinal bar force at 100 mm centres
6. ratio of shear strength to design shear force V_i/V_u^o
7. f'_c was measured at time of testing of column units, and f_y=474 MPa

3.6.3 Comparison of the Code Requirements with the Quantities of Transverse Reinforcement Provided in Column Units for Maintaining Stability of Compressed Longitudinal Bars

The New Zealand concrete design code [2] requires that the yield force in the hoop or cross tie should at least equal one-sixteenth of the yield force of the longitudinal bar or bars it is to restrain at 100mm centres. This requirement may be written as:

$$A_{te} = \frac{\sum A_b f_y}{16 f_{yh}} \frac{s}{100} \tag{3.3}$$

where A_{te}=area of the leg hoop or cross tie, $\sum A_b$=sum of the areas of the longitudinal bars reliant on the tie, f_y=yield strength of longitudinal bars and f_{yh}=yield strength of hoops.

The code also requires that the centre-to-centre spacings of hoop sets should not exceed six times longitudinal bar diameter.

As can be seen from Table 3.5, the transverse reinforcement provided in the column units satisfied the code requirements for restraint of longitudinal bars from premature buckling.

3.6.4 Comparison of the Code Requirements with the Quantities of Transverse Reinforcement Provided in Column Units for Shear

In the capacity design approach, it is required that the ideal shear strength of a column V_i should at least equal to the column design shear force, V_u^o, which results from the flexural overstrength that can be developed in the plastic hinge regions of the column. In the design of the column units, the design shear force was taken as the shear force corresponding to a column flexural strength of 1.1 $\times$ ideal flexural strength.

The New Zealand concrete design code [2] calculates the ideal shear strength of column V_i as a summation of shear strength provided by concrete mechanisms V_c, and by shear reinforcement mechanisms V_s.

Shear Strength Provided by Concrete Mechanisms

The contribution of concrete to provide shear strength is given by:

$$V_c = v_c b_w d \tag{3.4}$$

where v_c is nominal shear stress carried by concrete, b_w is width of column and d is effective depth of column.

In the plastic hinge region:

For $P_e/(\phi f_c' A_g) \leq 0.1$,

$$v_c = 0 \tag{3.5}$$

For $P_e/(\phi f_c' A_g) > 0.1$,

$$v_c = 4v_b\sqrt{\frac{P_e}{\phi f_c' A_g} - 0.1} \tag{3.6}$$

Outside of the plastic hinge region:

$$v_c = (1 + \frac{3P_e}{\phi f_c' A_g})v_b \tag{3.7}$$

where $v_b = (0.07 + 10\rho_w)\sqrt{f'_c} \leq 0.2\sqrt{f'_c}$, $\rho_w = A_s/(b_w d)$, and A_s=area of tension reinforcement.

Shear Strength Provided by Shear Reinforcement Mechanisms

The contribution of shear reinforcement to the shear strength is given by:

$$V_s = \frac{A_v f_{yh} d}{s_h} \tag{3.8}$$

where A_v=total area of shear reinforcement parallel to the direction of shear force.

It is evident from Table 3.5, that shear was not critical in columns with moderate and high axial compression, due to the large contribution of concrete shear mechanisms. The shear strengths provided in the column units met the code requirements satisfactorily.

3.7 Testing Procedures for Column Units

The testing procedures for the column units were similar to the previous tests carried out at the University of Canterbury [14,5]. The 10 MN DARTEC universal testing machine was used to apply axial load to the column units which was kept constant throughout the tests. Reversible lateral loads were applied through a 1 MN hydraulic jack which had a capacity of 1120 kN in compression, 840 kN in tension and an available travel of 400 mm.

Preparation for testing, including the installation of the column units in the DARTEC machine and the loading frame, was described in detail in Refs. [9] and [28].

Fig. 3.11 illustrates a set-up of a column unit with the loading frame. The following sign convention for loading is used. When the unit is pushed, positive loading is applied, and when it is pulled, negative loading is applied.

The applied lateral loading also followed a pattern similar to previous tests at the University of Canterbury. First, the unit was loaded with an initial loading cycle to 75% of the theoretical ultimate load H_{ACI}, where H_{ACI} was calculated from the theoretical flexural strength of column M_{ACI}, using the code [2] approach, and based on the measured concrete and steel strengths. The experimental yield displacement Δ_y was then calculated by extrapolating a straight line from the origin through the peak load of $75\%H_{ACI}$ to the theoretical ultimate load $\pm H_{ACI}$ as shown in Fig. 3.12. Having established the Δ_y, the subsequent cycles were displacement controlled to various levels of nominal displacement ductility factors μ_n where $\mu_n = \Delta/\Delta_y$, and Δ=lateral displacement at the central stub.

The displacement history used for Units 9 and 11 consisted of two complete cycles to nominal displacement ductility factors $\mu_n = \pm 2, \pm 4, \pm 6, \pm 8$ etc. until complete failure of the column occurred or until the test had to be terminated for other reasons. For Units 5, 6, 7, 8 and 10, which were expected to have limited ductility, the displacement history consisted of two cycles to $\mu_n = \pm 1, \pm 2, \pm 3, \pm 4$ etc.

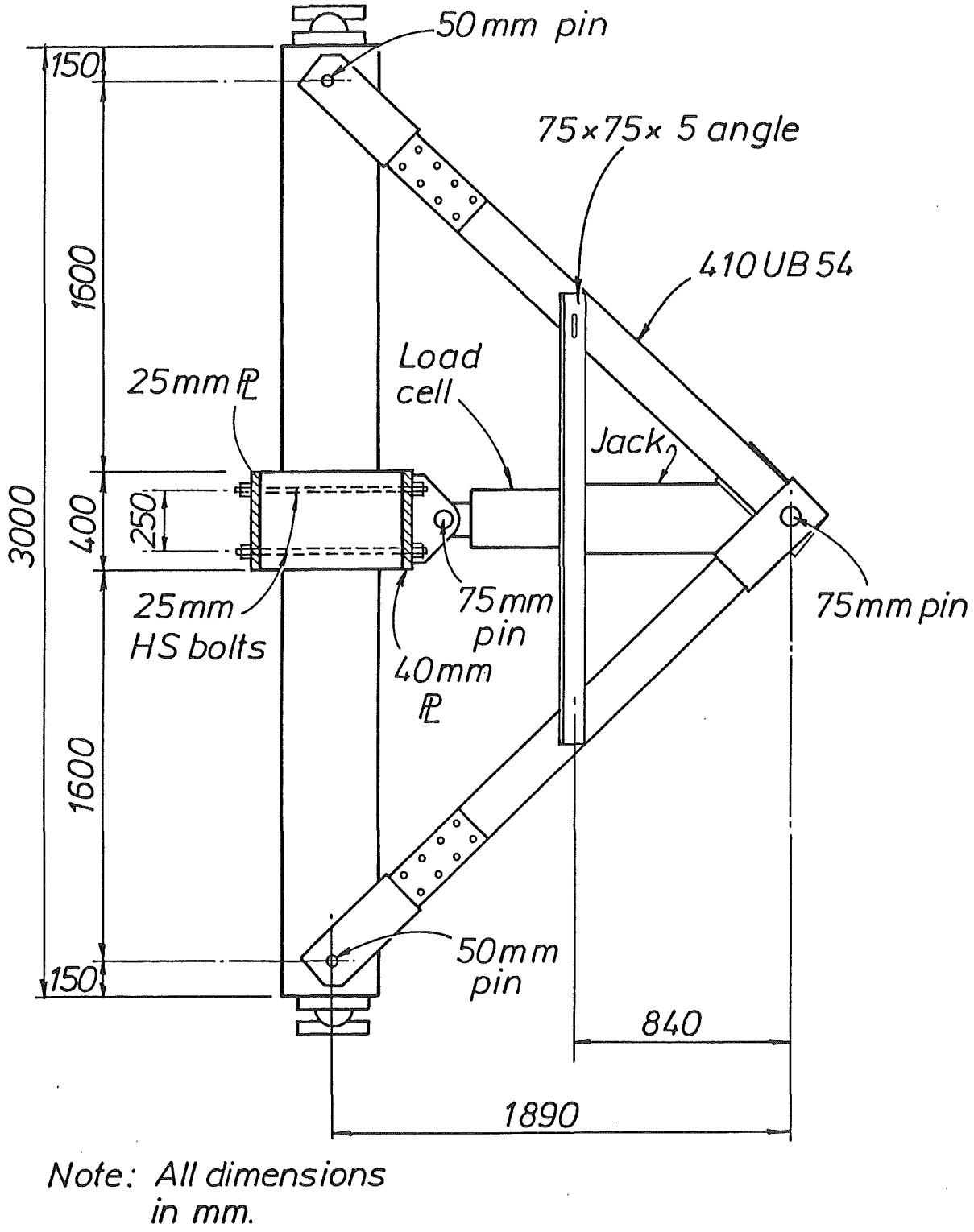

Figure 3.11: A Column Unit with the Loading Frame

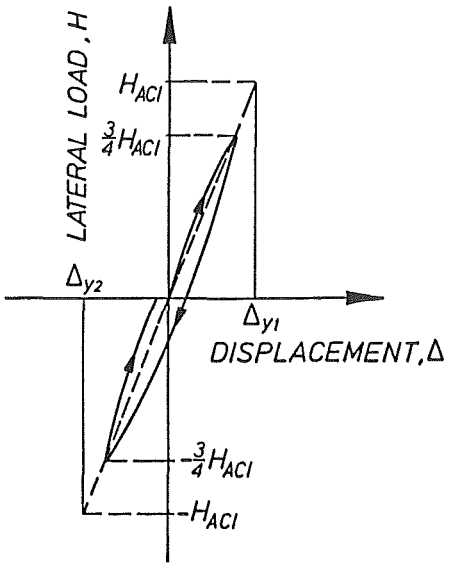

Figure 3.12: Determination of the Experimental Yield Displacement Δ_y

3.8 Experimental Results and Observations

The aspects of the experimental investigations of the column units are reported in the following sections:

3.8.1 General Performance

For Units 5,6 and 10, which had axial load levels of $0.5f'_cA_g$, first flexural cracks were observed in the column adjacent to the face of the stub when the lateral load was about 75% of the theoretical ultimate load. For Units 7,8,9 and 11, no flexural cracks were detected at this first stage of loading, since the predicted cracking load was higher than this peak load. After completing this first loading cycle, the experimental yield displacement was calculated, and the imposed displacements during the following loading cycles were determined.

Some fine vertical cracks were observed in the stub, although heavy reinforcement had been provided in this region. Similarly, some vertical cracks occurred in the regions surrounding the loading pins at each end of the column units. These cracks were more significant in Units 7, 8, 9 and 11 which had axial load levels of $0.7f'_cA_g$, due to the high bursting stresses resulting from the concentrated axial load applied to the columns at the pins. However, these cracks were far from the plastic hinge regions.

When the next excursion was applied, the existing flexural cracks in the plastic hinge regions became larger and some new cracks appeared. Vertical splitting of cover concrete also commenced.

Greater column strengths were observed for lateral loading in the positive direction. This was because when the applied load was in the negative direction, the units had already sufferred cracking and plastic deformations from the previous positive loading cycles.

When a nominal displacement ductility factor of μ_n=3 was applied to Units 5,6 and 10, the cover concrete at the top or bottom plastic hinge region started to spall. During the negative loading cycle, spalling of the cover concrete occurred at both plastic hinges. For the other units which had high axial loads, spalling of the cover concrete started at $\mu_n = 2$. The strains at first spalling ϵ_{spall} for all column units are given in Table 3.7.

With further increase in the imposed displacement, the transverse and longitudinal bars at the plastic hinge regions became visible, and most of the cover concrete spalled off. Eventually the longitudinal bars started to buckle. Further excursions resulted in the penetration of crushing into the core concrete, and significant strength degradation then occurred.

Units 5 and 11 exhibited similar behaviour during the last stage of testing. The lateral load capacity degraded markedly followed by buckling of the longitudinal bars which terminated the tests.

Units 6 and 8 indicated a sudden drop of lateral load carrying capacity at the end of testing. This type of behaviour is characteristic of columns with small quantities of transverse reinforcement, where the transverse reinforcement was not sufficient to provide adequate concrete confinement, or to maintain the stability of compressed longitudinal bars against buckling.

For Unit 7, buckling of the longitudinal bars occurred outside the bottom plastic hinge region over a length of 1200 mm from the face of the central stub. This damaged region was greater than the required confined length recommended by the code of 1.5 times the depth of column or equal to 600 mm. It is worth noting that the transverse bar spacings were under the code [2] limitation for anti-buckling requirements (i.e. $6d_b$ in the plastic hinge region, and $12d_b$ outside the plastic hinge region).

As expected by the theory [4], Unit 9 exhibited ductile behaviour. The unit still maintained its strength after completing two cycles of $\mu_n = 10$. It was decided to terminate the test of Unit 9 at this stage.

In the case of Unit 10, buckling of the longitudinal bars resulted in significant degradation in strength. Some spirals at the bottom plastic hinge eventually fractured at the end of testing.

Figs. 3.13 to 3.19 illustrate the visible damage to Units 5 to 11 at their succesive displacement peaks and at the end of testing.

3.8.2 Hysteretic Behaviour

The experimental hysteresis loops showing the lateral load-displacement at the central stub, and lateral load-column curvatures are given in Figs. 3.20a,c and d to 3.26a,c and d. For comparison, the lateral load-displacement hysteresis loops predicted by the cyclic moment-curvature theory [3] are also plotted in those figures (see Figs. 3.20b to 3.26b). The column curvatures were found from the potentiometers at the first level mounted at the top and bottom plastic hinges adjacent to the central stub over a 50 mm gauge length.

Figure 3.13: Visible Damage to Unit 5 During Testing

Figure 3.14: Visible Damage to Unit 6 During Testing

Figure 3.15: Visible Damage to Unit 7 During Testing

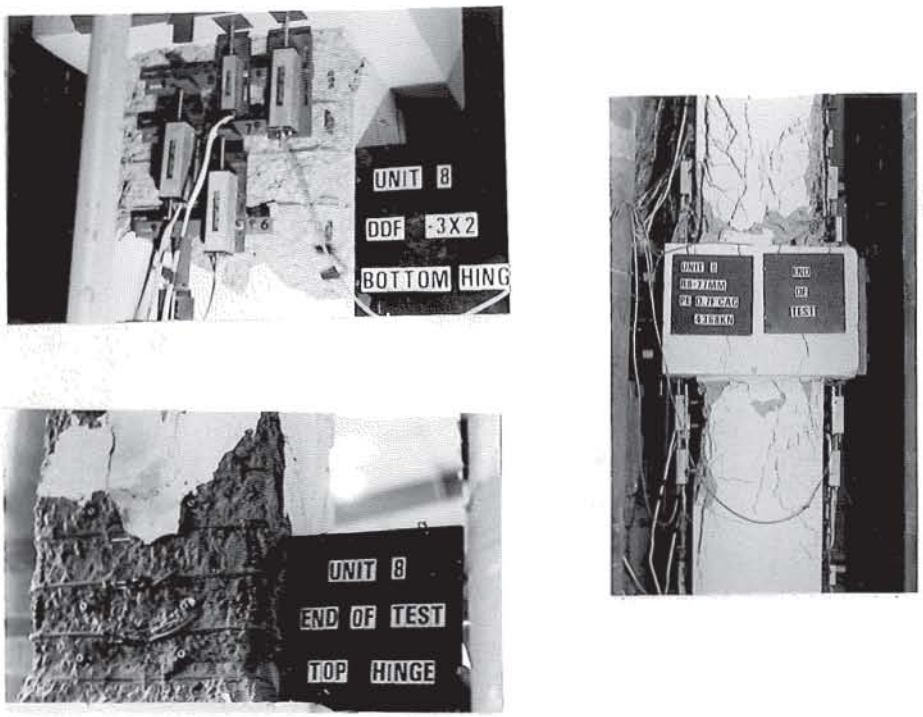

Figure 3.16: Visible Damage to Unit 8 During Testing

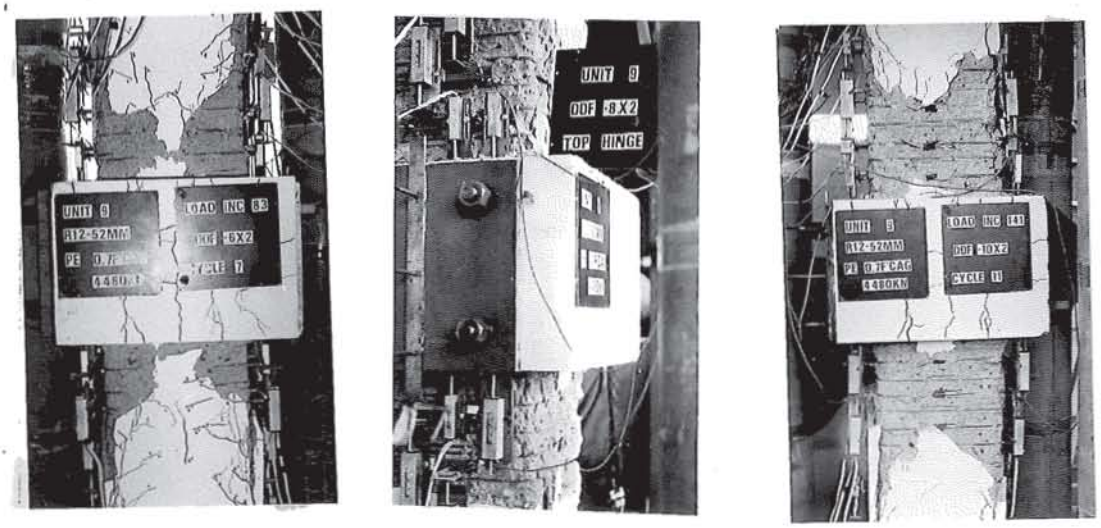

Figure 3.17: Visible Damage to Unit 9 During Testing

Figure 3.18: Visible Damage to Unit 10 During Testing

Figure 3.19: Visible Damage to Unit 11 During Testing

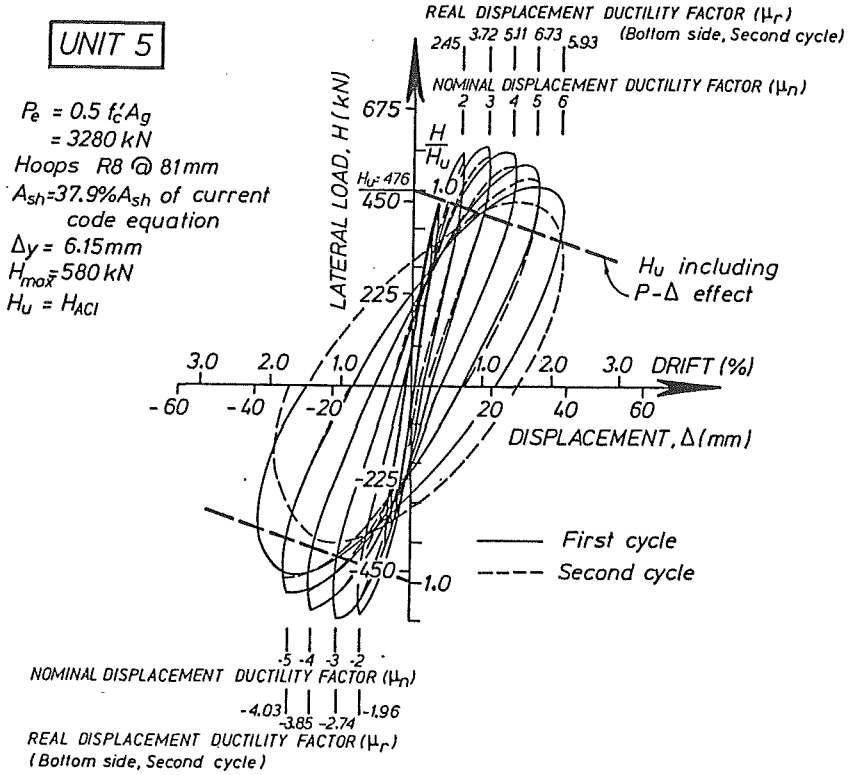

(a). Experimental Lateral Load-Displacement Hysteresis Loops for Unit 5

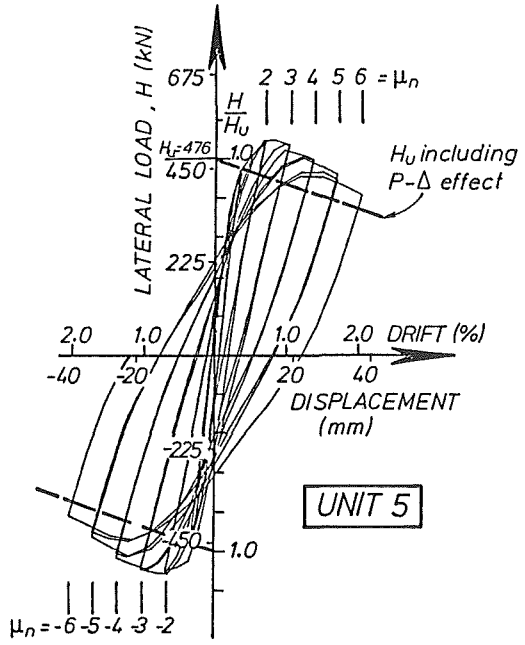

(b). Theoretical Lateral Load-Displacement Hysteresis Loops for Unit 5

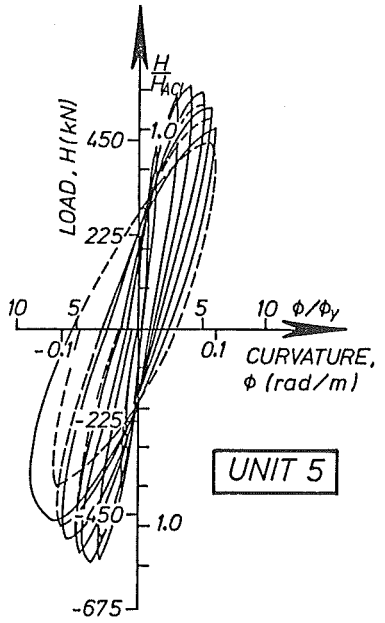

(c). Experimental Lateral Load-Top Column Curvature Hysteresis Loops for Unit 5

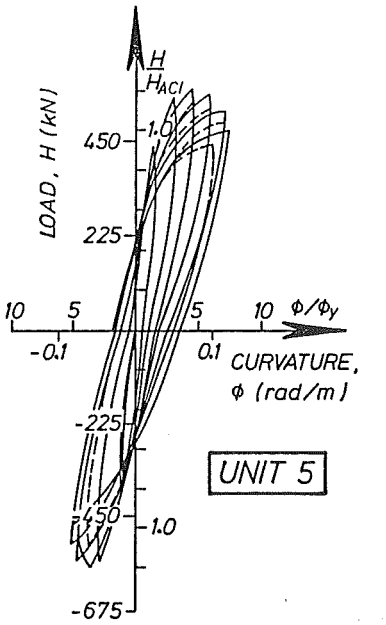

(d). Experimental Lateral Load-Bottom Column Curvature Hysteresis Loops for Unit 5

Figure 3.20: Lateral Load-Deformation Hysteresis Loops for Unit 5

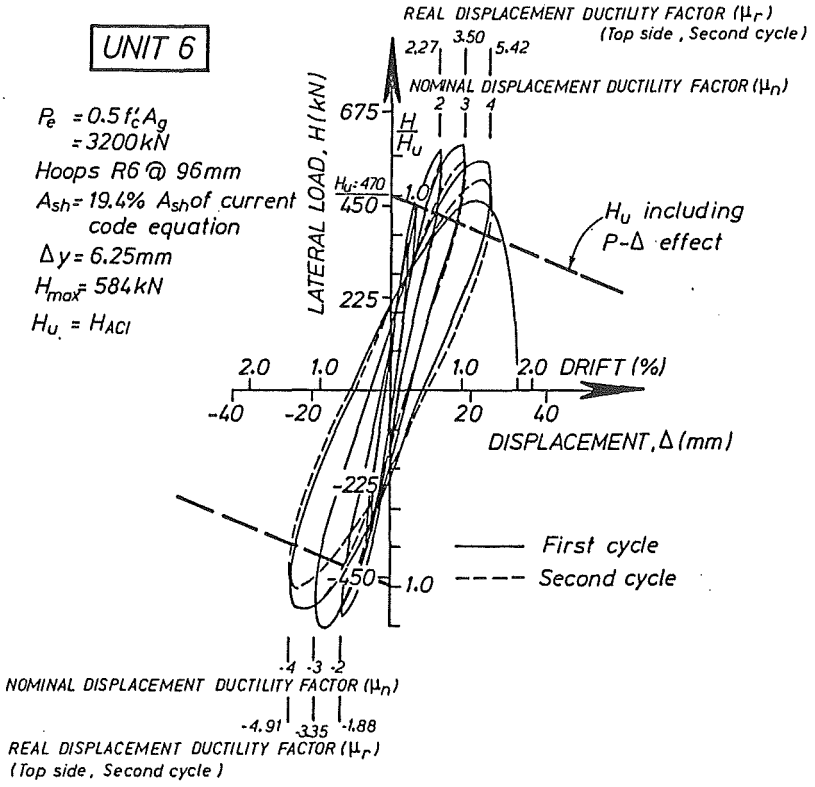

(a). Experimental Lateral Load-Displacement Hysteresis Loops for Unit 6

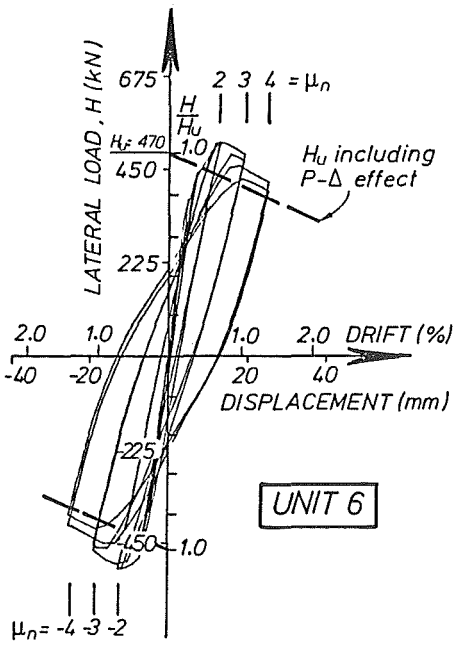

(b). Theoretical Lateral Load-Displacement Hysteresis Loops for Unit 6

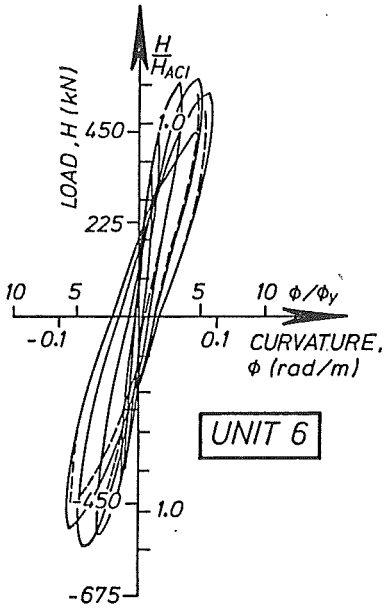

(c). Experimental Lateral Load-Top Column Curvature Hysteresis Loops for Unit 6

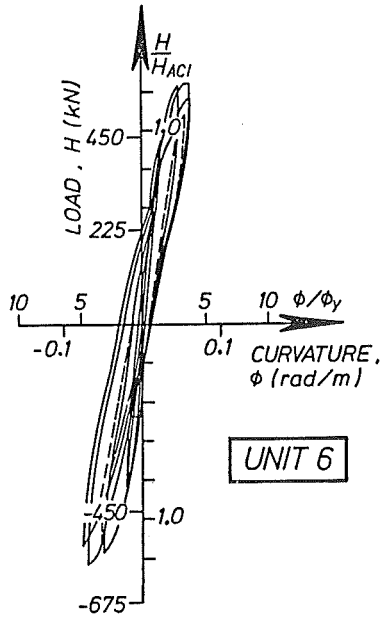

(d). Experimental Lateral Load-Bottom Column Curvature Hysteresis Loops for Unit 6

Figure 3.21: Lateral Load-Deformation Hysteresis Loops for Unit 6

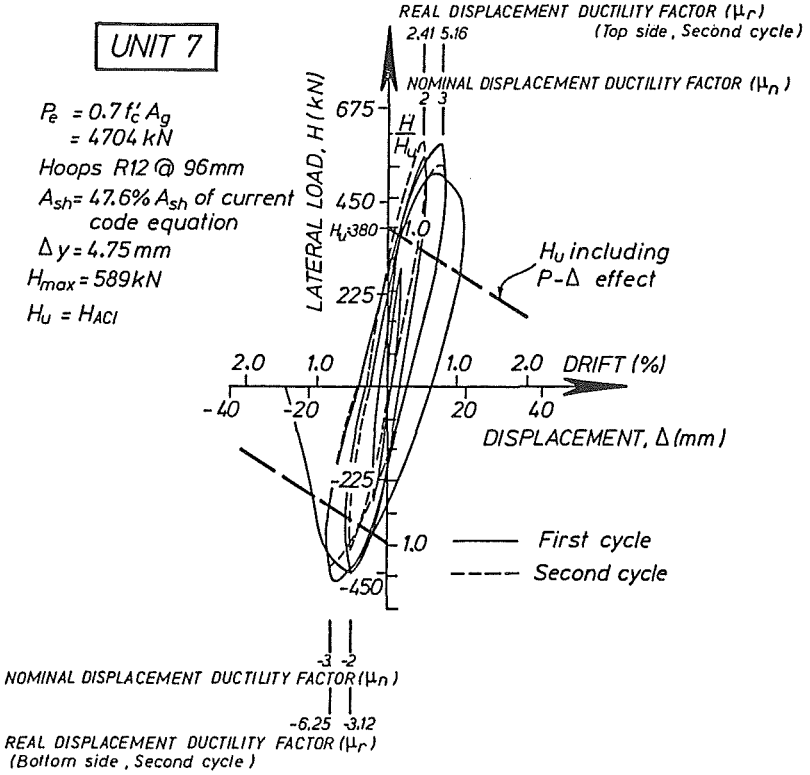

(a). Experimental Lateral Load-Displacement Hysteresis Loops for Unit 7

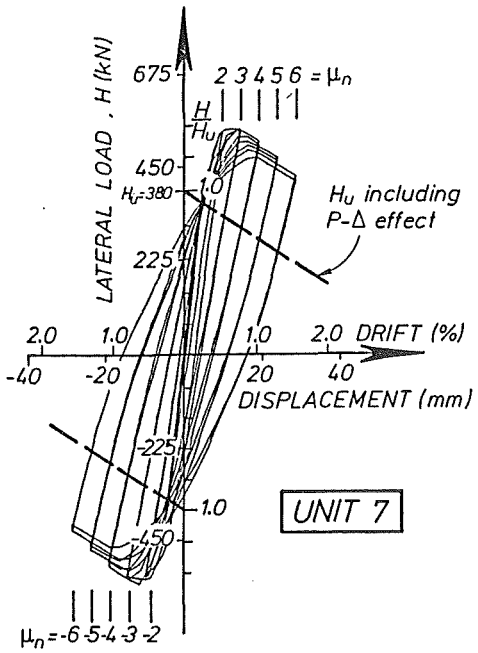

(b). Theoretical Lateral Load-Displacement Hysteresis Loops for Unit 7

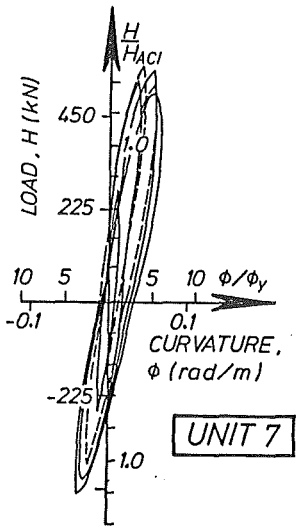

(c). Experimental Lateral Load-Top Column Curvature Hysteresis Loops for Unit 7

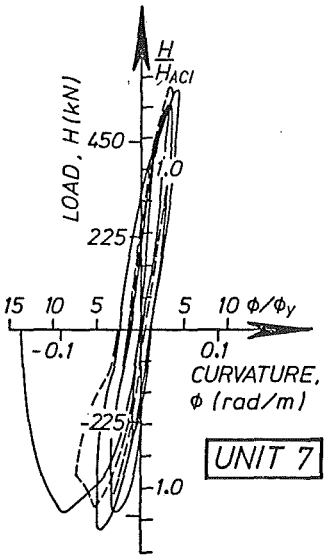

(d). Experimental Lateral Load-Bottom Column Curvature Hysteresis Loops for Unit 7

Figure 3.22: Lateral Load-Deformation Hysteresis Loops for Unit 7

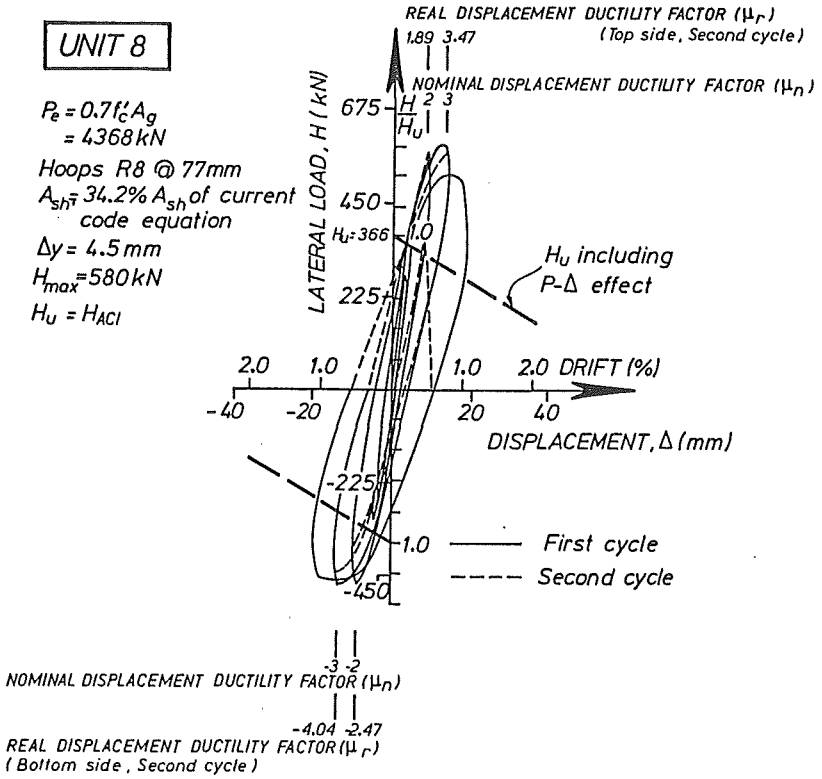

(a). Experimental Lateral Load-Displacement Hysteresis Loops for Unit 8

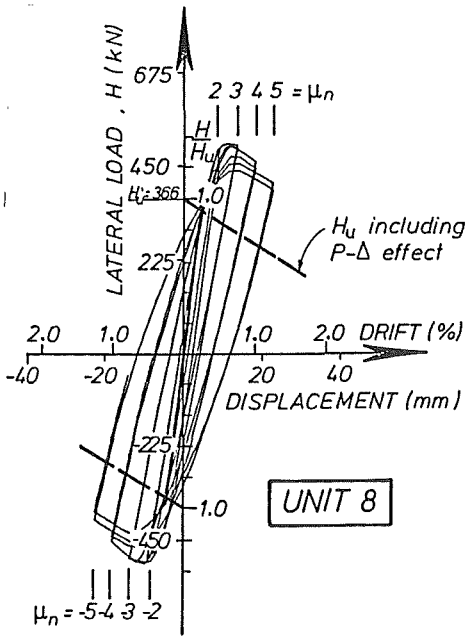

(b). Theoretical Lateral Load-Displacement Hysteresis Loops for Unit 8

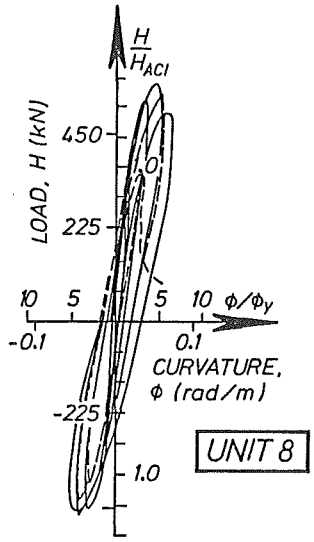

(c). Experimental Lateral Load-Top Column Curvature Hysteresis Loops for Unit 8

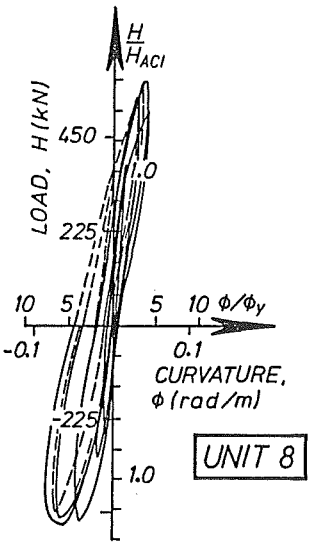

(d). Experimental Lateral Load-Bottom Column Curvature Hysteresis Loops for Unit 8

Figure 3.23: Lateral Load-Deformation Hysteresis Loops for Unit 8

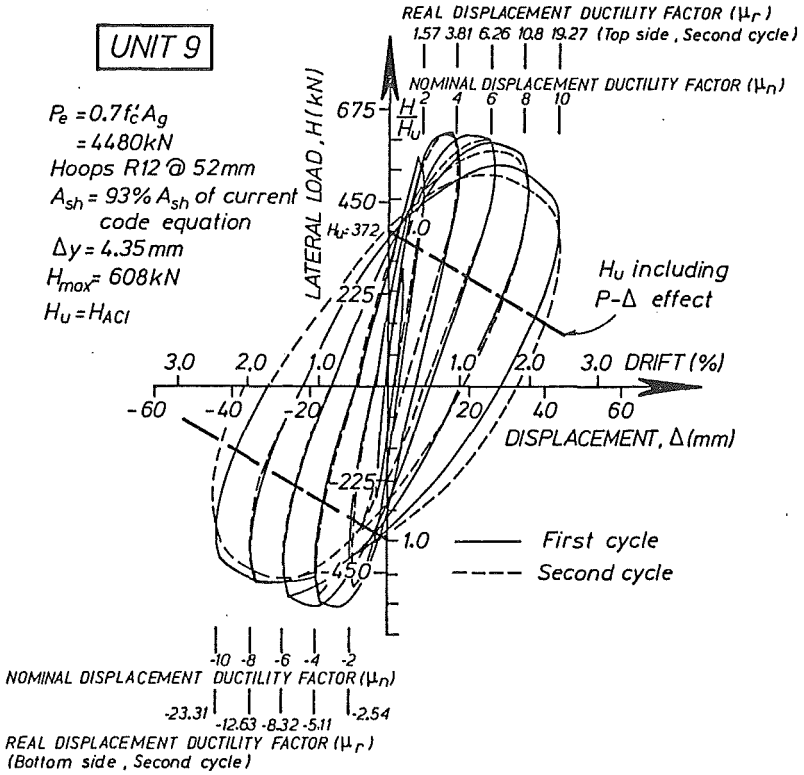

(a). Experimental Lateral Load-Displacement Hysteresis Loops for Unit 9

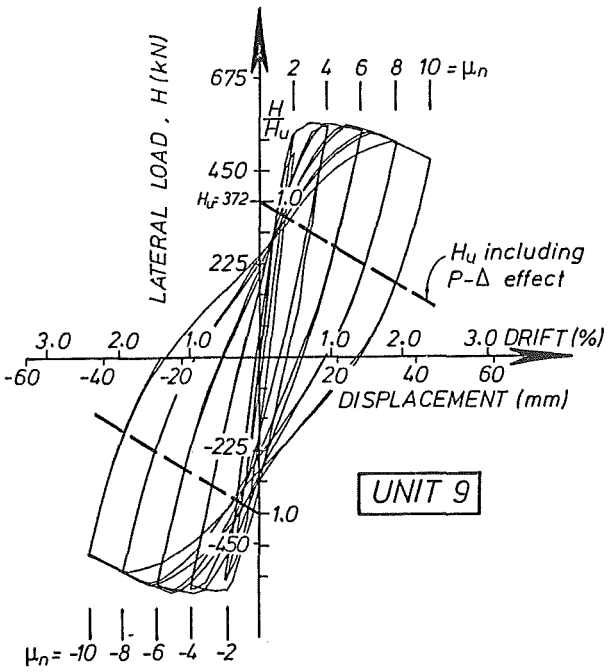

(b). Theoretical Lateral Load-Displacement Hysteresis Loops for Unit 9

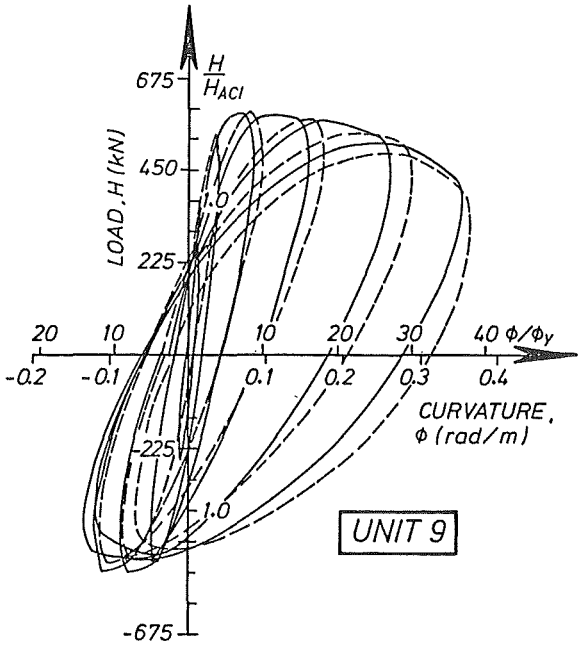

(c). Experimental Lateral Load-Top Column Curvature Hysteresis Loops for Unit 9

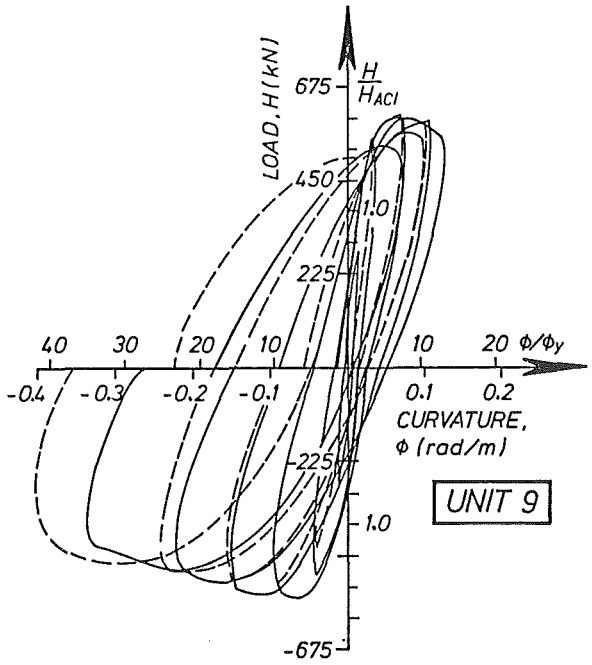

(d). Experimental Lateral Load-Bottom Column Curvature Hysteresis Loops for Unit 9

Figure 3.24: Lateral Load-Deformation Hysteresis Loops for Unit 9

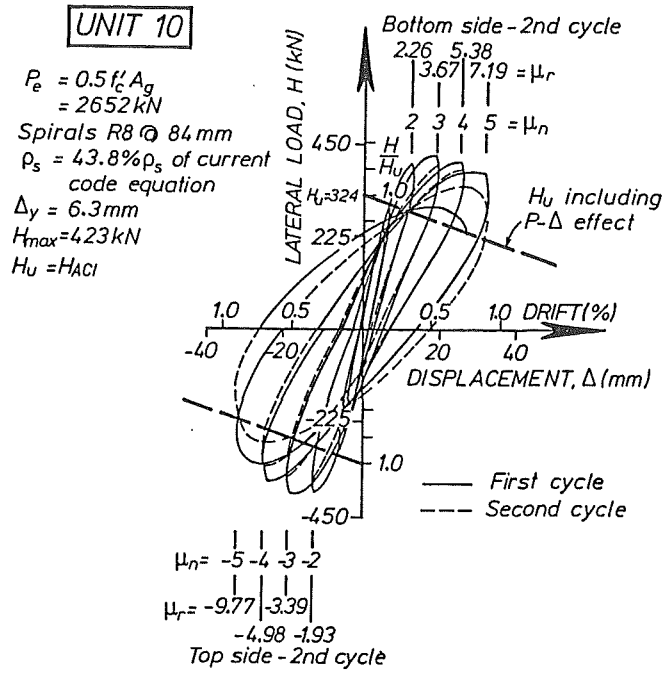

(a). Experimental Lateral Load-Displacement Hysteresis Loops for Unit 10

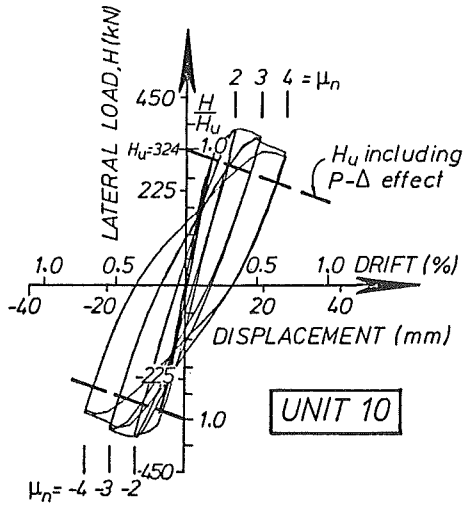

(b). Theoretical Lateral Load-Displacement Hysteresis Loops for Unit 10

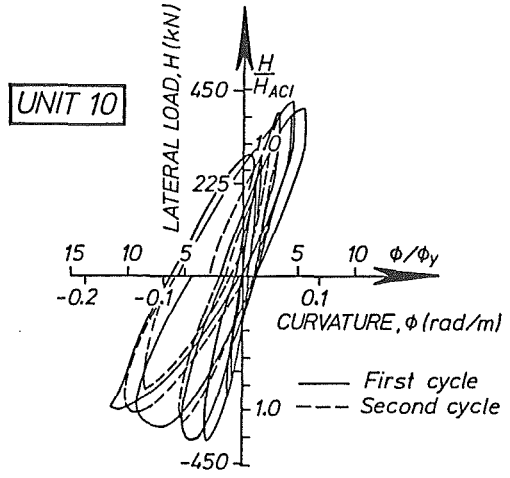

(c). Experimental Lateral Load-Top Column Curvature Hysteresis Loops for Unit 10

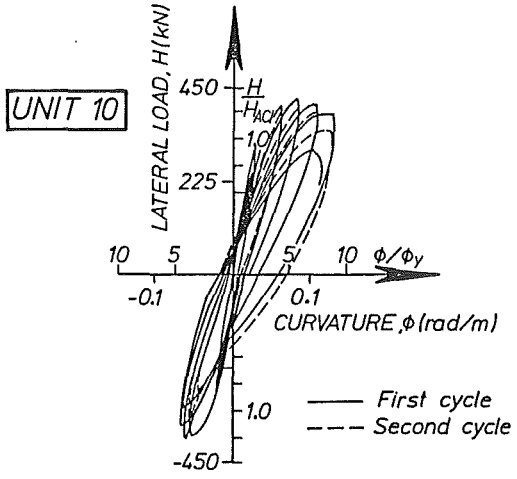

(d). Experimental Lateral Load-Bottom Column Curvature Hysteresis Loops for Unit 10

Figure 3.25: Lateral Load-Deformation Hysteresis Loops for Unit 10

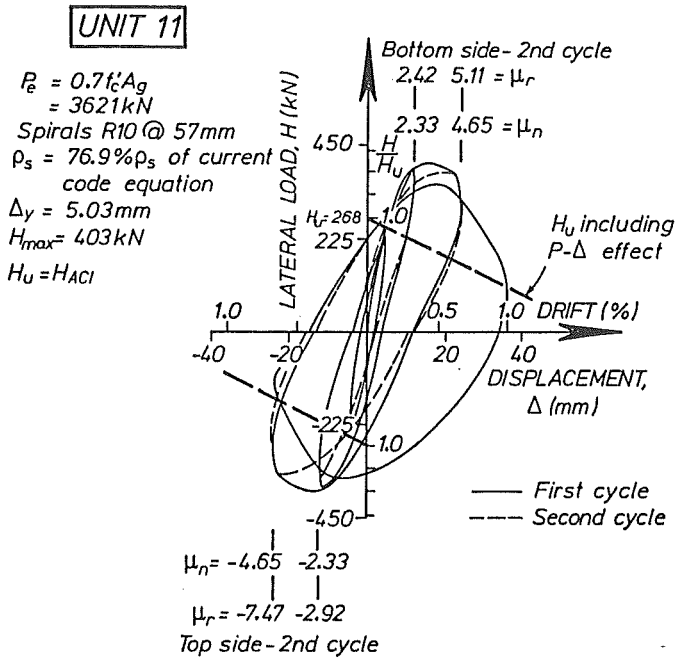

(a). Experimental Lateral Load-Displacement Hysteresis Loops for Unit 11

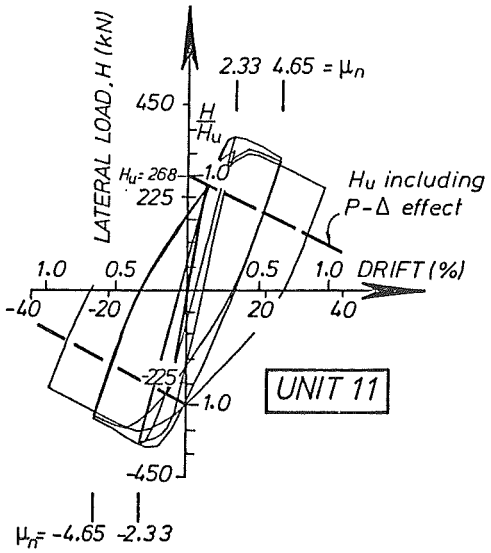

(b). Theoretical Lateral Load-Displacement Hysteresis Loops for Unit 11

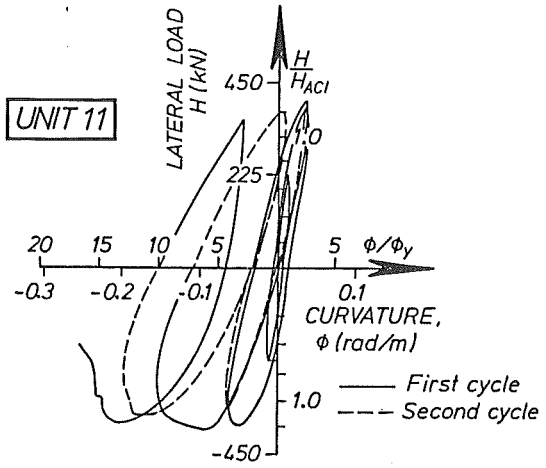

(c). Experimental Lateral Load-Top Column Curvature Hysteresis Loops for Unit 11

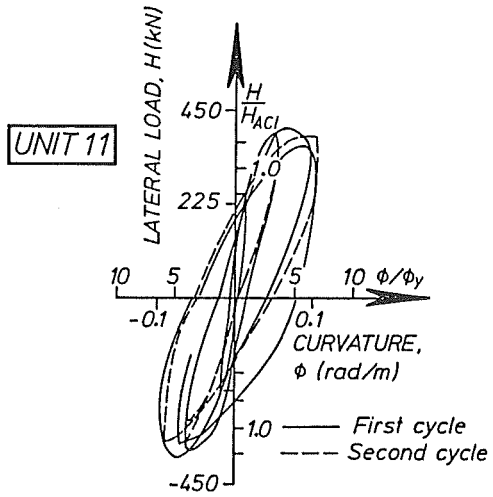

(d). Experimental Lateral Load-Bottom Column Curvature Hysteresis Loops for Unit 11

Figure 3.26: Lateral Load-Deformation Hysteresis Loops for Unit 11

The dashed lines plotted in Figs. 3.20a to 3.26a show the theoretical ideal lateral load capacity H_{ACI}, and include the $P - \Delta$ effects.

It is obvious, that the definitions of the experimental yield displacement Δ_y as described in Sec. 3.7, and its corresponding yield curvature φ_y are arbitrary. It is reasonable therefore to also measure the available displacements and curvatures in terms of drifts and curvature ductility factors. The flexural overstrength can also be clearly seen, by expressing the lateral load H as a fraction of the theoretical ultimate load H_{ACI}.

The real displacement ductility factor μ_r included the effect of the rotation of the central stub, which was due to the plastic hinge rotation concentrating mainly either above or below the stub. To find the *true* horizontal displacement of each half length of column, a horizontal displacement Δ of the centre stub, where θ is the measured rotation of the stub and l is the distance from the face of the stub to the pin at the end of the column (see Fig. 3.27). The real displacement ductility factor was then calculated from $\mu_r = (\Delta + \theta l)/\Delta_y$.

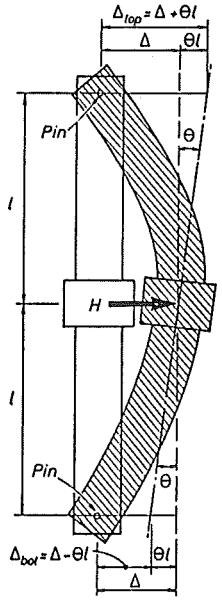

Figure 3.27: Effect of Unsymmetrical Plastic Hinge Rotations on Column Displacements

It should be noted that the ideal flexural strength of Unit 11 used during the test was calculated using the stress-strain models for concrete and steel proposed by Mander *et al.* [3], at an extreme fibre concrete compressive strain of $\epsilon_c = 0.003$, rather than the code [2] approach. The experimental values for Δ_y and φ_y were therefore recalculated using the code flexural strength, and the measured quantities were adjusted to the modified values.

Table 3.6 lists the available nominal and real displacement ductility factors, μ_n and μ_r for the column units. It is evident that the μ_r values achieved by the column units were greater than the μ_n values. Although the μ_n values imposed on all units, except for Unit 9, was less than 6, the μ_r values of Units 5, 7, 10 and 11 is greater than 6, indicating that these units have more than limited ductility.

Table 3.6: Available Displacement Ductility Factors in Column Units

Unit	$\mu_n(1)$	$\mu_r(2)$
5	5	6.7
6	4	5.4
7	3	6.3
8	3	4.0
9	> 10	> 23.3
10	5	9.8
11	4.65	7.5

Notes:

1. $\mu_n = \Delta/\Delta_y$, where Δ=lateral displacement of the central stub when the lateral load had reduced to not less than 80% of the theoretical ultimate load H_i, and Δ_y=yield displacement.
2. $\mu_r = (\Delta + \theta l)/\Delta_y$, where θ=rotation of the central stub, and l=distance from the centre of the stub to the pin.

As can be seen from Fig. 3.20a, very good performance was obtained from Unit 5 up to the final imposed displacement ductility factor of about 6. Although there was some strength degradation, the lateral load capacity was still higher than the theoretical capacity based on the code [2] approach at the end of the test.

The hysteresis loops for Unit 6 shown in Fig. 3.21a indicated that only limited ductility was available in this unit. The amount of transverse confining reinforcement in this unit was only 19% of the code [2] requirements.

Figs. 3.22a and 3.23a compare the hysteresis loops for Units 7 and 8. Although the amount of confinement provided in Unit 8 was only 72% of that provided in Unit 7, Unit 8 achieved the same nominal displacement ductility factor of μ_n=3 as Unit 7. Moreover, Unit 8 was able to complete at least one cycle of $\mu_n = 4$, while Unit 7 failed to reach that μ_n value. From this result, it is evident that the smaller diameter hoops with smaller spacings provided in Unit 8 were more efficient in preventing premature buckling of the longitudinal bars than the large diameter hoops with large spacings provided in Unit 7. However, a smaller real displacement ductility factor was reached by Unit 8 than by Unit 7.

The hysteresis loops for Unit 9 shown in Fig. 3.24a demonstrated very ductile performance of this unit. The test results gave an indication that the transverse reinforcement provided satisfactory confinement for the concrete, was capable of preventing buckling of the compressed longitudinal bars and provided sufficient shear resistance. No significant strength degradation was detected. It is worth noting that the amount of confinement provided in Unit 9 was 70% of that required by the design charts to obtain an available curvature ductility factor of 20, and was 93% of that required by the code [2] for ductile detailing.

On the other hand, Unit 11, which was designed according to the code quantity of transverse reinforcement [2] was only capable of limited ductility, as can be seen from the hysteresis loops in Fig. 3.26a. This indicated that the code equations need to be re-evaluated, if the current code requirement for adequate ductility is to be satisfied.

From the hysteresis loops for Units 10 and 11, illustrated in Figs. 3.25a and 3.26a, it can be seen that the flexural strengths of the octagonal columns were less than those of the square columns, although they had the same 400 mm lateral dimension, the same longitudinal bars, and similar concrete compressive strengths. In the octagonal column, the longitudinal bars and the concrete are concentrated closer to the plastic centroid, which results in a smaller lever arm and thus less flexural strength.

It was observed from the results of all column units, that the flexural strength enhancement factor $\phi_o = M_{max}/M_{ACI}$ increased with the axial load level. For the columns with an axial load level of $0.5f'_cA_g$, the value found for ϕ_o was about 1.5, and for the columns with an axial load level of $0.7f'_cA_g$, higher value of ϕ_o was found. Unit 9, which was well confined, reached the largest value of ϕ_o of 2.01.

The New Zealand draft loading code [39] gives a drift limitation at the end of the inelastic range of 1.7% for structures in the most severe seismic zone. This limitation is to control secondary moment $P-\Delta$ effect. Beyond this value, overall instability of frames may occur. It can be seen that Units 5,9,10 and 11 exceeded this code value. Units 6 and 7 almost reached the code value, and Unit 8 did not reach the code value. Unit 9 however, achieved the largest drift of 5.22%.

The measured maximum lateral load H_{max}, the flexural strength enhancement factor ϕ_o, the maximum displacement Δ_{max} and the measured drift are listed in Table 3.7.

3.8.3 Measured Curvature Distribution, Available Curvature Ductility Factor, Equivalent Plastic Hinge Length and Plastic Rotation

The measured curvature profiles of each column unit at the displacement ductility factor peaks are shown in Figs. 3.28 to 3.34. The values were obtained from the measurements at the potentiometer levels, and are plotted at the mid–points of the successive gauge lengths and joined by straight lines.

As expected, the measured curvatures increase as the displacement ductility factor increases. However, some irregularities do exist due to unsymmetrical plastic hinge rotations above and below the central stub, and random formation of flexural cracks. Similar curvature distributions at both plastic hinges was observed up to a displacement ductility factor of $\mu_n = 2$.

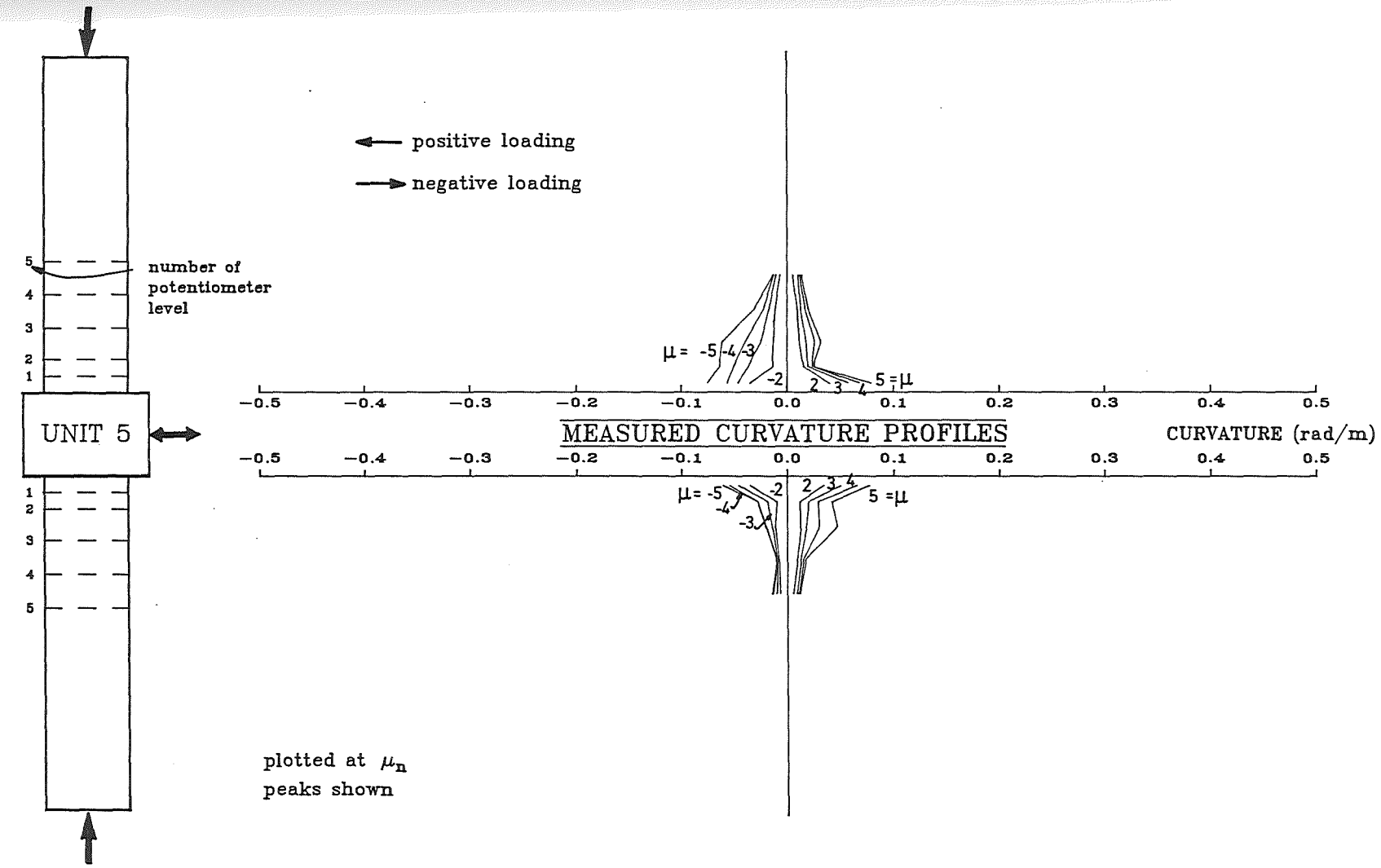

Figure 3.28: Measured Curvature Profiles for Unit 5

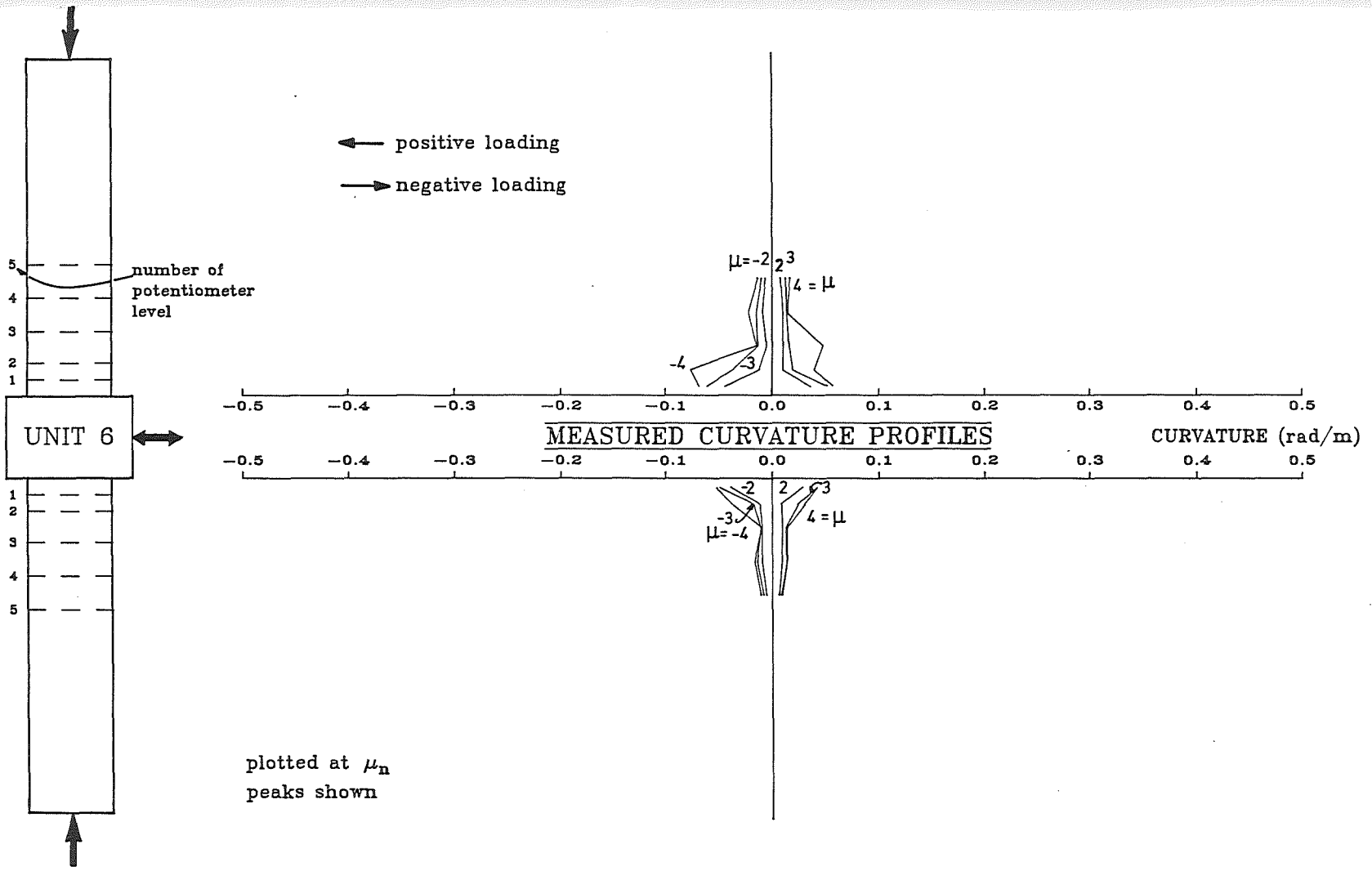

Figure 3.29: Measured Curvature Profiles for Unit 6

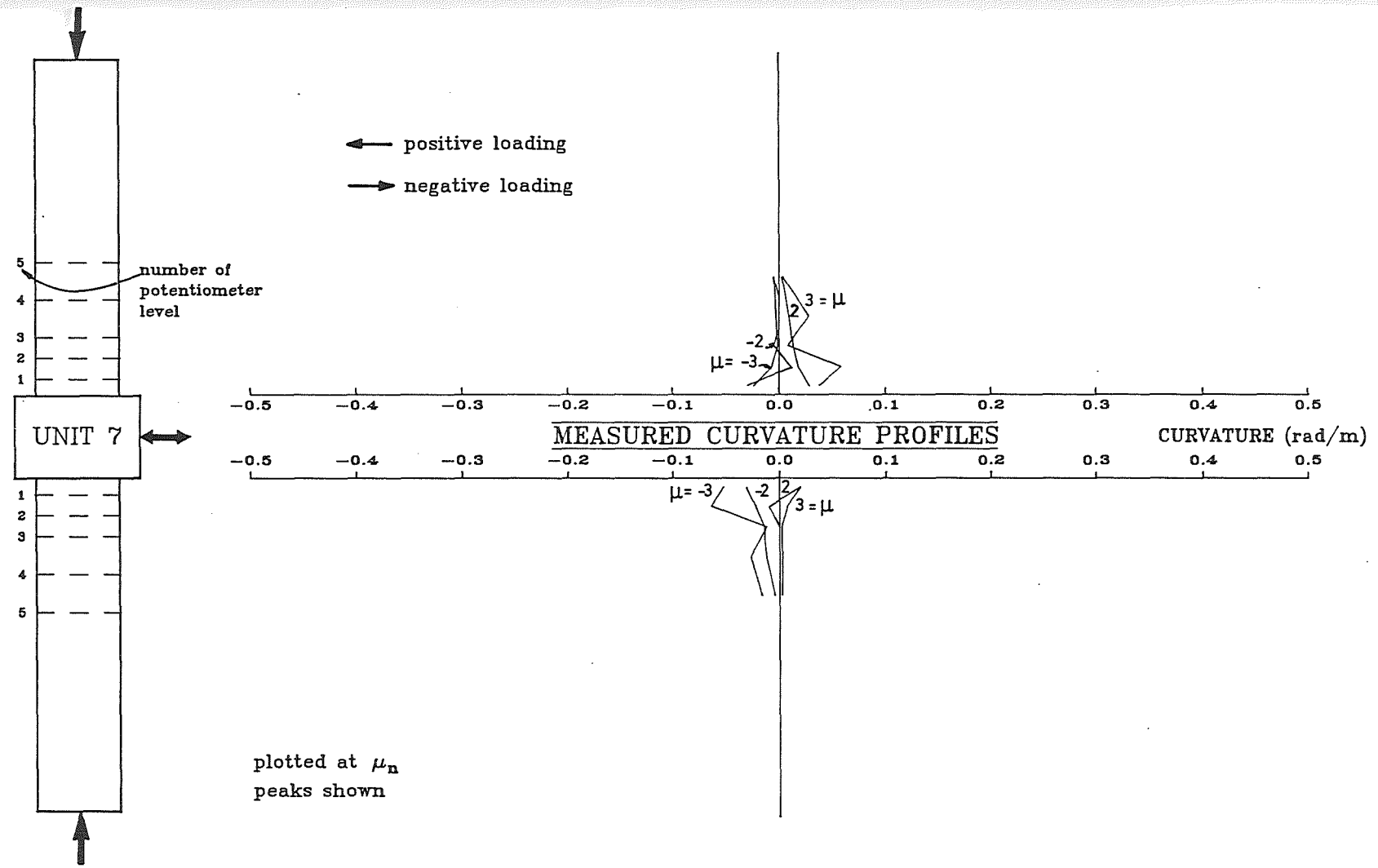

Figure 3.30: Measured Curvature Profiles for Unit 7

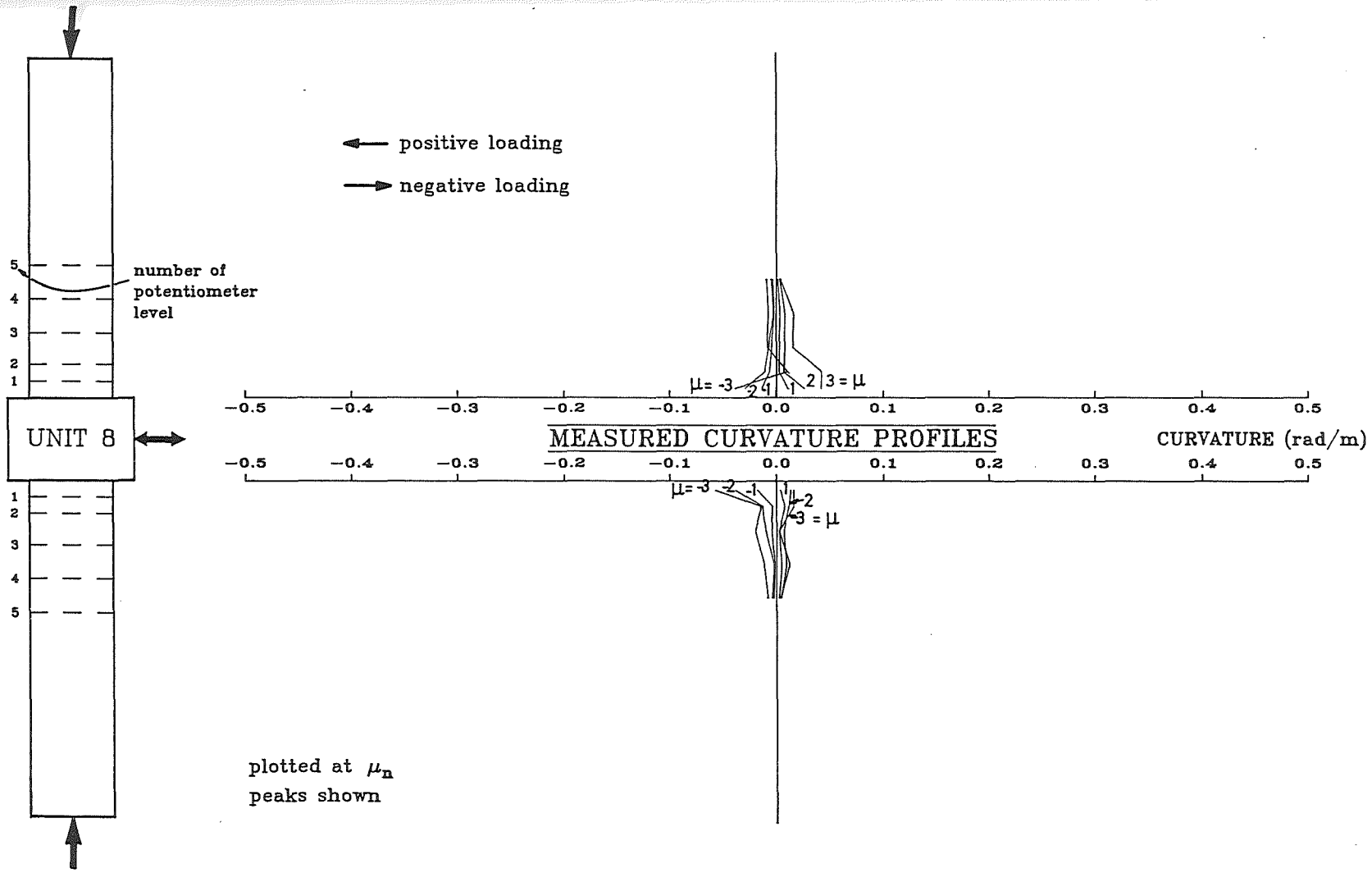

Figure 3.31: Measured Curvature Profiles for Unit 8

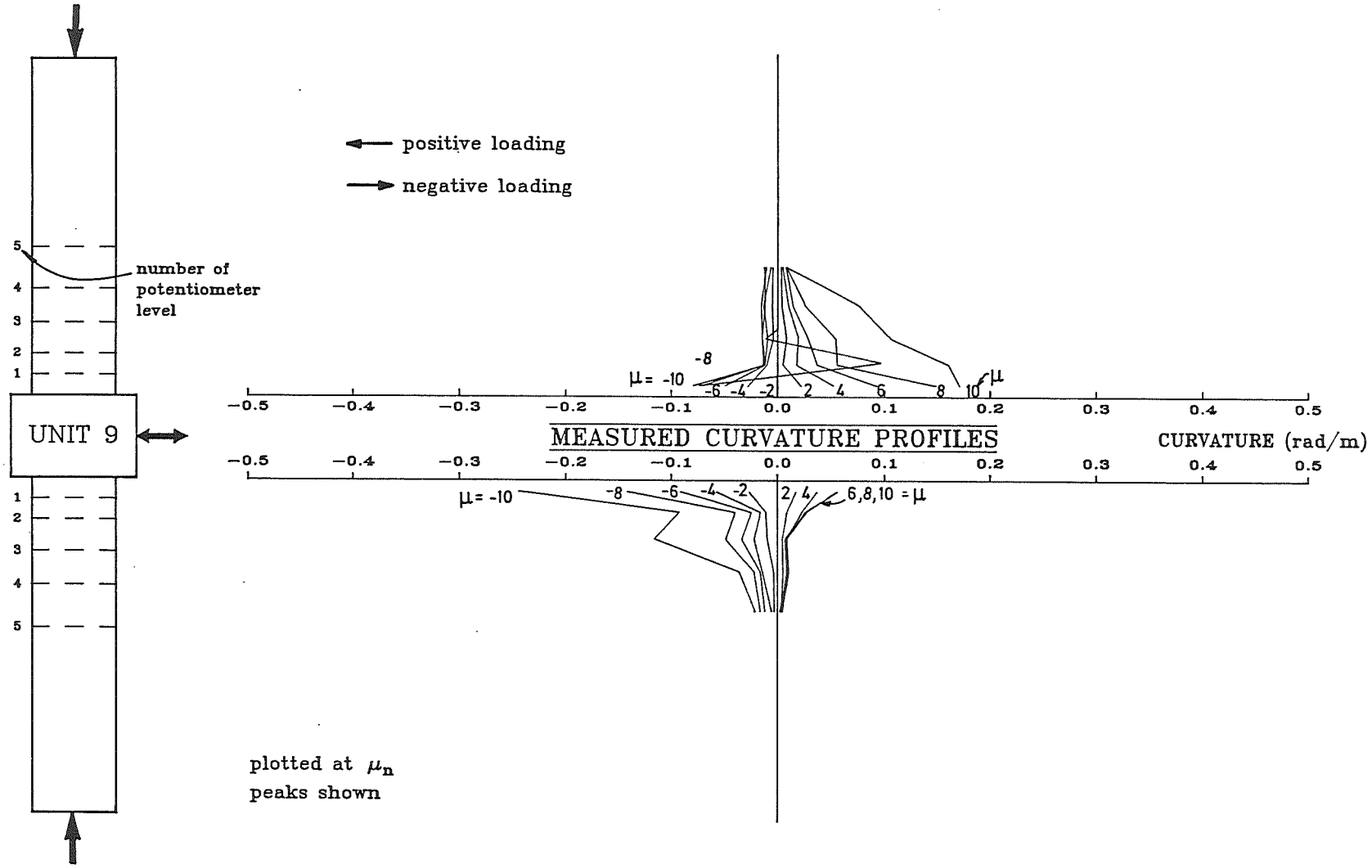

Figure 3.32: Measured Curvature Profiles for Unit 9

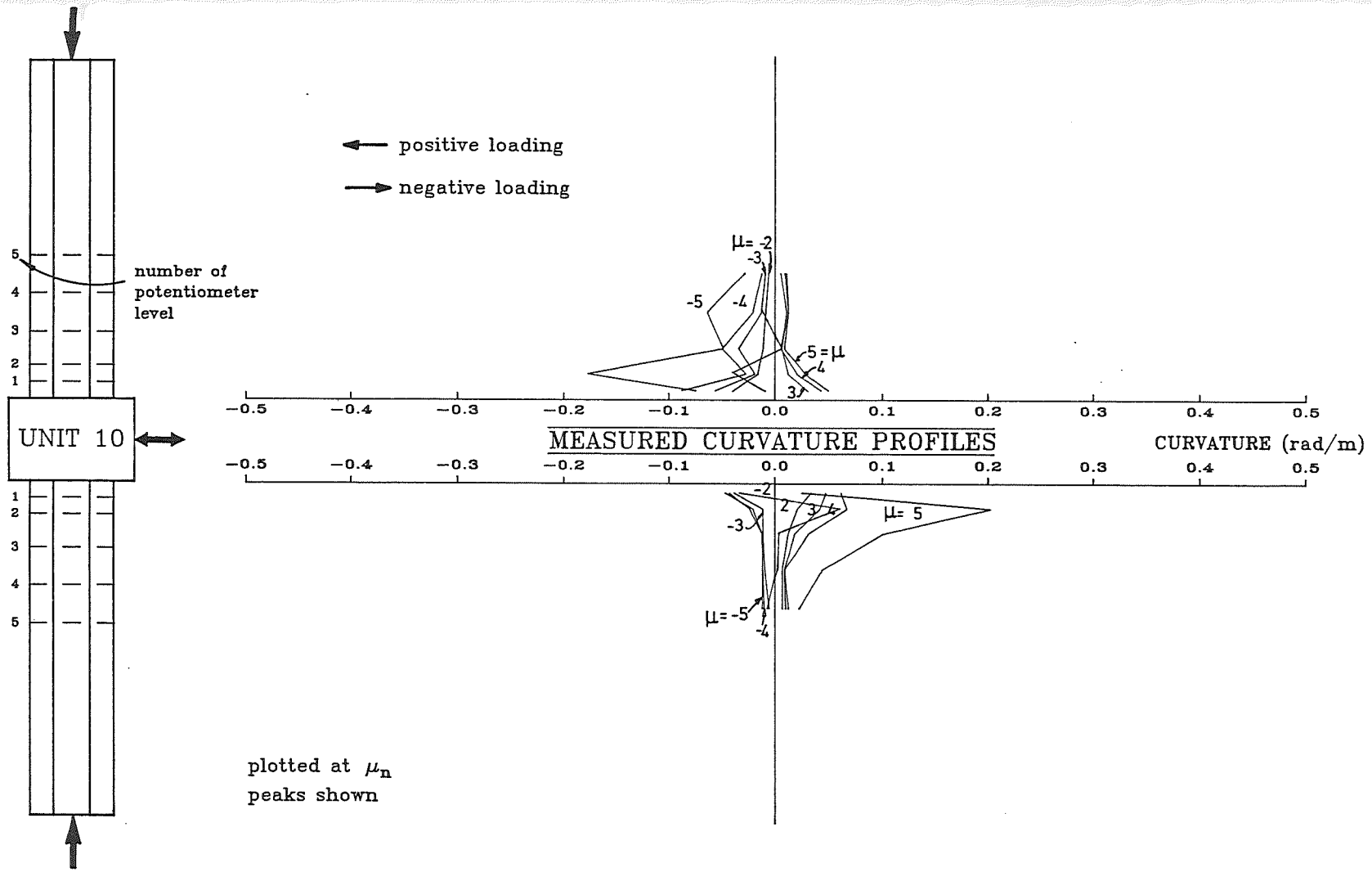

Figure 3.33: Measured Curvature Profiles for Unit 10

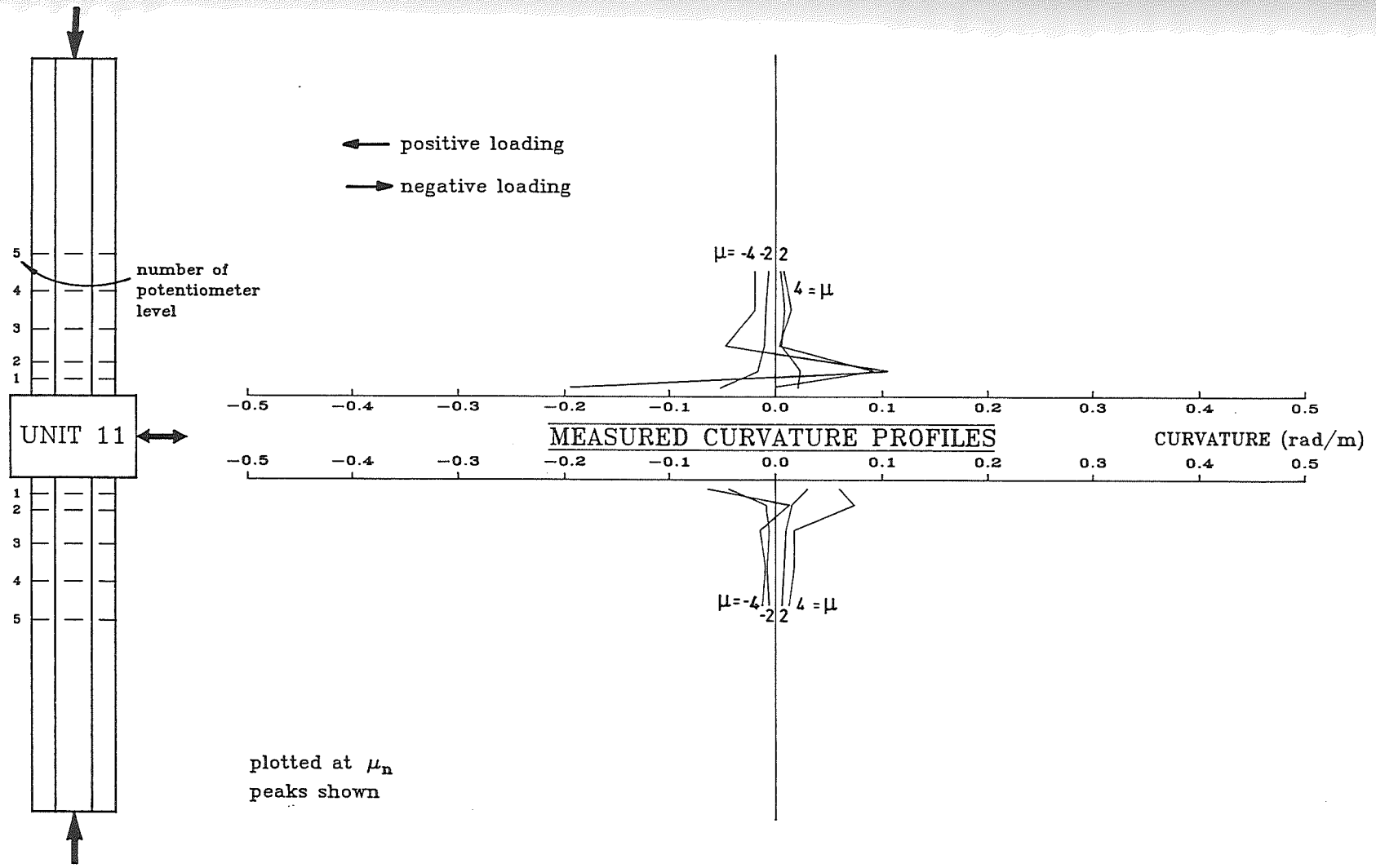

Figure 3.34: Measured Curvature Profiles for Unit 11

The curvature distribution profiles for Units 5, 6 and 8 shown by Figs. 3.28, 3.29 and 3.31, were reasonably symmetrical above and below the central stub. Unsymmetric plastic rotation of the top and bottom plastic hinges was noticeable from the curvature profiles of Units 7, 9, 10 and 11 as shown in Figs. 3.30 and 3.32 to 3.34. Again, Unit 9 exhibited the largest inelastic curvatures and very ductile behaviour.

It was observed that the curvatures measured at the first potentiometer levels were unproportionally larger than those measured at the other levels owing to the inclusion of the effects of the yield penetration of the longitudinal bars into the stub, in the measurement of the curvatures at the first level. To compensate for this effect, Zahn *et al.* [4] suggested to use the average yield curvature obtained by extrapolating the curvatures measured at the second to the fifth potentiometer levels in both direction, when calculating the experimental yield curvature φ_y (see Fig. 3.35). After testing, the φ_y could also be refined to take into account the enhancement in flexural strength. This procedure by Zahn *et al.* was dependent on contributions made by column sections along the potentiometer levels, when the yield curvature was measured. Although in some tests, this suggested measurement gave reasonably good agreement with the theoretical predictions (for example see [4,28]), it was not supported convincingly by theory, and thus the coincidence might not happen in other tests.

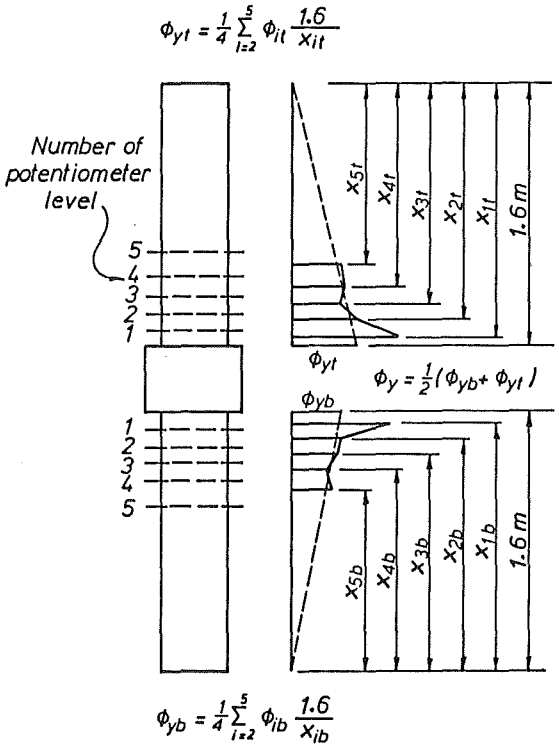

Figure 3.35: Determination of Experimental Yield Curvature According to Zahn *et al.*

It is also worth noting that in the first loading cycle, very few or even no flexural cracks were detected, since the cracking moments were equal to or larger than 75% M_{ACI}. Moreover, the central stub which was heavily reinforced, did provide additional confinement to the region surrounding the stub. Therefore, the effect of yield penetration was not very significant at the early stage of testing.

In view of these considerations, it was considered to be more reasonable to use the average curvature measured at the first potentiometer levels at both plastic hinges when determining the experimental yield curvature φ_y. To obtain φ_y, the curvature measured at the positive and negative peaks of the first cycle was extrapolated linearly, in the same manner as to determine the yield displacement Δ_y (see Fig. 3.12). By examining the lateral load-curvature hysteresis loops, it is obvious that the initial stiffness was linear, therefore such a linear extrapolation can be justified.

As a comparison, the curvature obtained by averaging the curvatures measured at the second potentiometer levels was also calculated. The regions, where the first and second potentiometers were positioned, were the regions with the greatest plastic deformations, thus the most severe damage regions.

The experimental yield curvature measured at the first and second potentiometer levels φ_{y1} and φ_{y2} ranged from 0.0096 to 0.0164, and from 0.00343 to 0.0076, respectively.

The curvature ductility factors $\varphi_{max1}/\varphi_{y1}$ and $\varphi_{max2}/\varphi_{y2}$ were calculated using φ_{max1} and φ_{max2}, that is the maximum curvatures observed at the first and second potentiometer levels at the displacement ductility peak when the strength had reduced to not less than 80% of the theoretical ultimate strength.

The larger values of yield curvatures measured at the first potentiometer levels, resulted in smaller curvature ductility factors obtained, compared to those measured at the second potentiometer levels.

Column sections with adequate ductility and limited ductility could be defined as sections with available curvature ductility factors φ_u/φ_y of approximately 20 and 10, respectively. Based on this definition, only Unit 9 has adequate ductility. Units 5 to 8, and Unit 10 have less than limited ductility, and Unit 11 has limited ductility, if the curvature ductility factors are based on the measurement at the first potentiometer level. If the measurement at the second potentiometer level is used, Unit 10 could be considered to have adequate ductility, while the other units have limited ductility.

Fig. 3.36 shows the simplified curvature distribution for the columns normally used for displacement calculations [6].

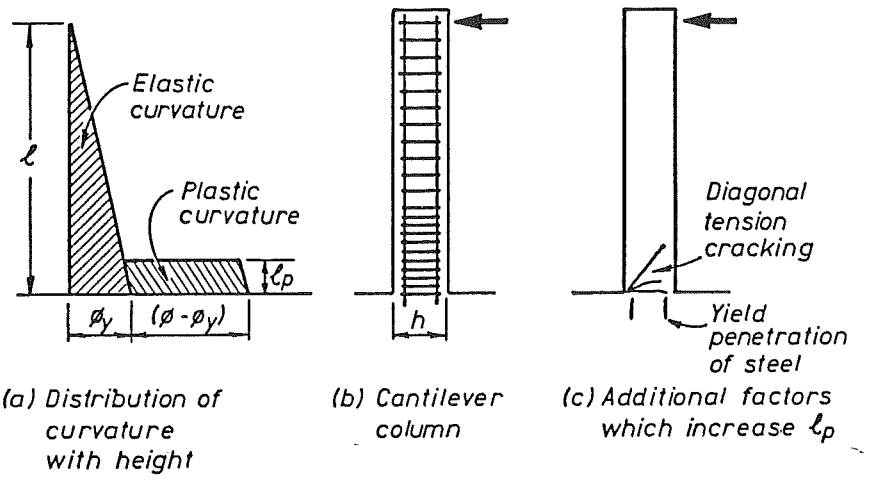

Figure 3.36: Assumed Curvature Distribution for Column Unit

The equivalent plastic hinge length ℓ_p, can be obtained from measured plastic displacement Δ_p. Now,

$$\Delta_p = (\mu_r - 1)\Delta_y \tag{3.9}$$

and also, from Fig. 3.36, Δ_p can be found by taking the first moment of area of the plastic curvature distribution about the point of contraflexure of the column as follows:

$$\Delta_p = (\varphi - \varphi_y)\ell_p(\ell - 0.5\ell_p) \tag{3.10}$$

By equating Eqs. 3.9 and 3.10, the dimensionless equivalent plastic hinge length ℓ_p/h or ℓ_p/D can be expressed as:

$$\frac{\ell_p}{h} = \frac{\ell}{h}\left(1 - \sqrt{1 - \frac{2(\mu_r - 1)\Delta_y}{\ell^2(\varphi - \varphi_y)}}\right) \tag{3.11}$$

where h (or D) is the overall depth of the column, which was 400 mm for the column units.

Since ℓ_p depends on μ_r and φ, it is more appropriate to calculate ℓ_p at successive displacement ductility factor peaks. The values of φ measured at the first and second potentiometer levels were used. According to the draft loading code [39] a ductile structure requires a displacement ductility factor of 6, and a limited ductile structure requires a displacement ductility factor of 3. The equivalent plastic hinge lengths ℓ_p were then calculated as the average values of ℓ_p at displacement ductility factors between 2 and 4 for all units, except for Unit 9, where ℓ_p was taken as the average value at displacement ductility factors of 2, 4, 6, 8 and 10.

The equivalent plastic hinge lengths calculated from Eq. 3.11 at the second cycles of real displacement ductility peaks are shown in Figs. 3.37 to 3.43. The calculated values for ℓ_p show a great deal of scatter. However, the trend is for ℓ_p to increase with increase in ductility. Note that the plastic hinge rotation θ_p is calculated from $(\varphi_u - \varphi_y)\ell_p$.

Priestley *et al.* [14] when assessing the experimental results of previous column tests at the University of Canterbury, obtained the following empirical equation for the equivalent plastic hinge length:

$$\ell_p = 0.08\ell + 6d_b \tag{3.12}$$

where ℓ is as defined in Fig. 3.36 and d_b is the diameter of the longitudinal reinforcing steel. This expression includes the spread of yielding due to yield penetration of steel into the column base (taken into account by the $6d_b$ term) and due to inclined diagonal tension cracking (see Fig. 3.36c), since those factors were included in the measurements. The fact that ℓ_p is not simply representation of the distribution of curvatures due to flexure, but also includes the effect of bond slip and shear, makes the theoretical determination of ℓ_p difficult.

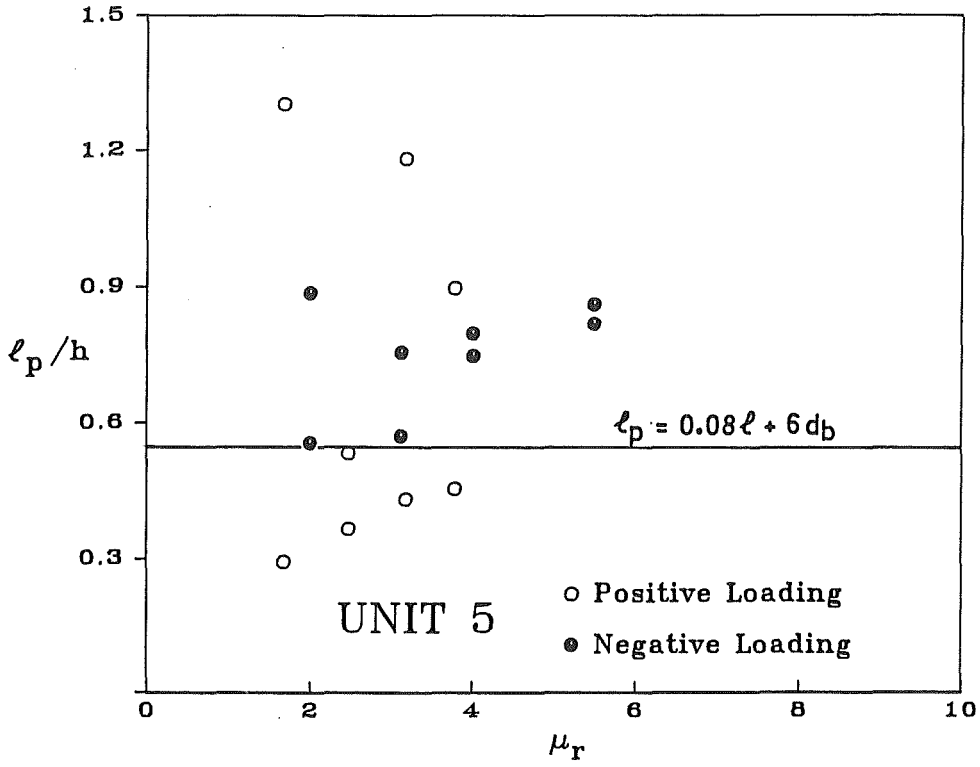

Figure 3.37: Equivalent Plastic Hinge Length-Real Displacement Ductility Factor for Unit 5

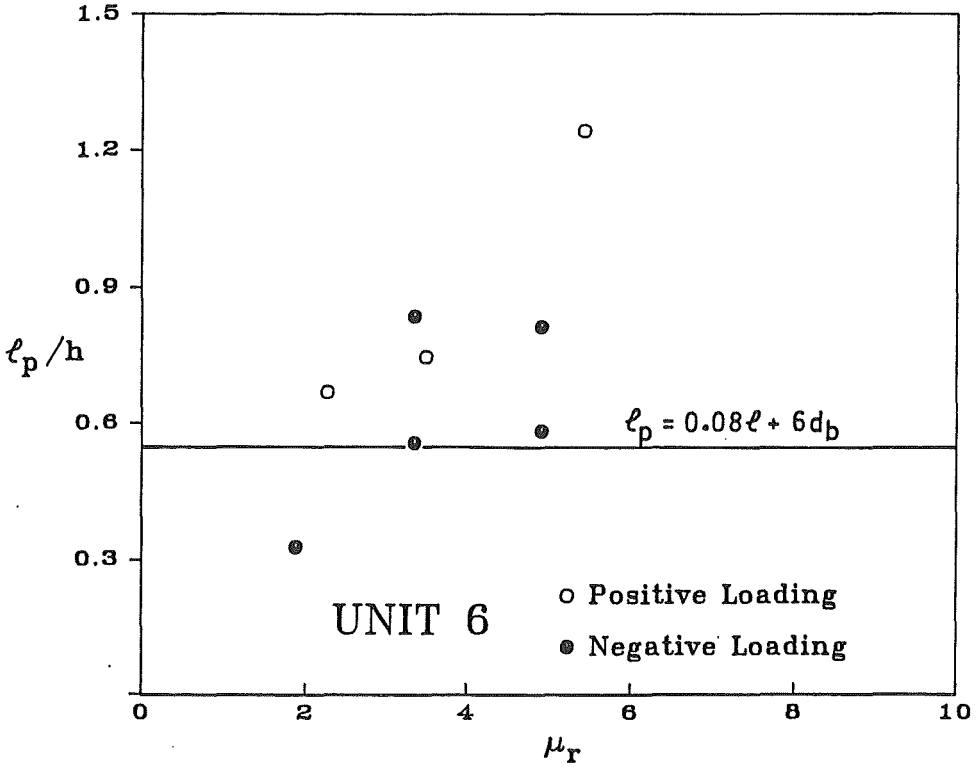

Figure 3.38: Equivalent Plastic Hinge Length-Real Displacement Ductility Factor for Unit 6

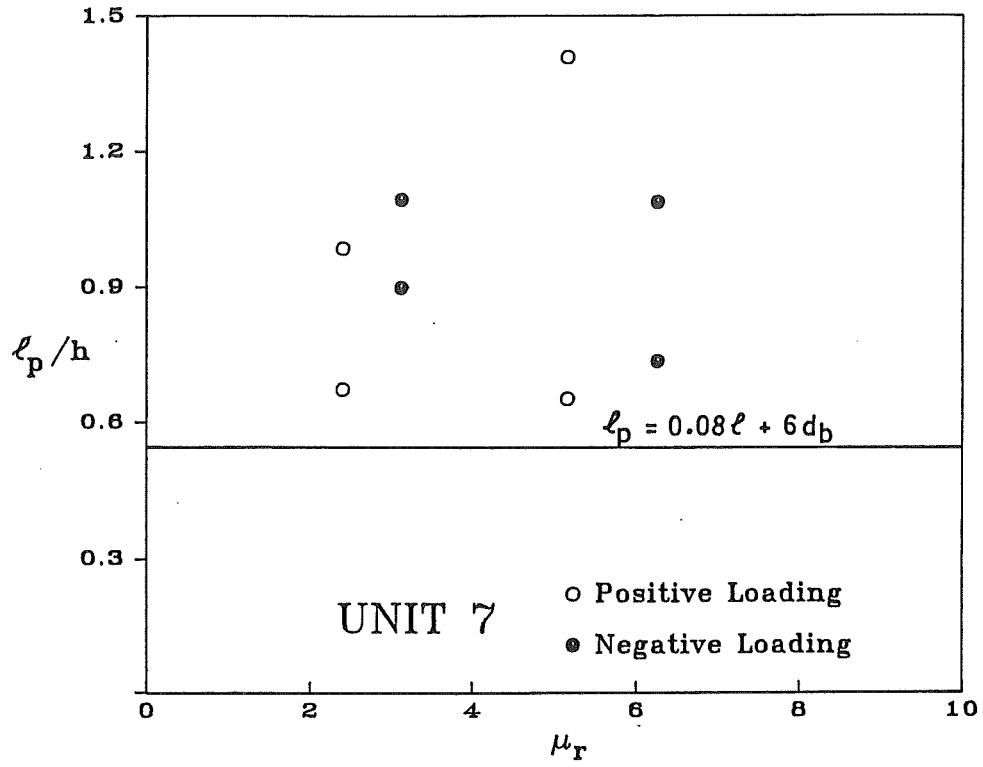

Figure 3.39: Equivalent Plastic Hinge Length-Real Displacement Ductility Factor for Unit 7

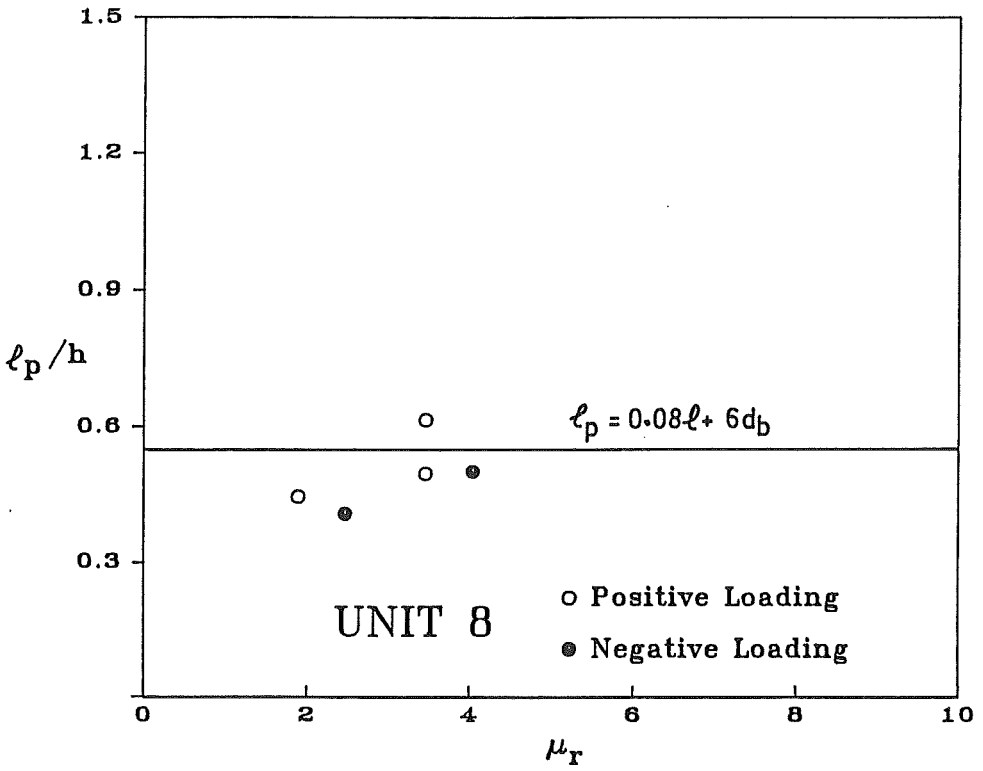

Figure 3.40: Equivalent Plastic Hinge Length-Real Displacement Ductility Factor for Unit 8

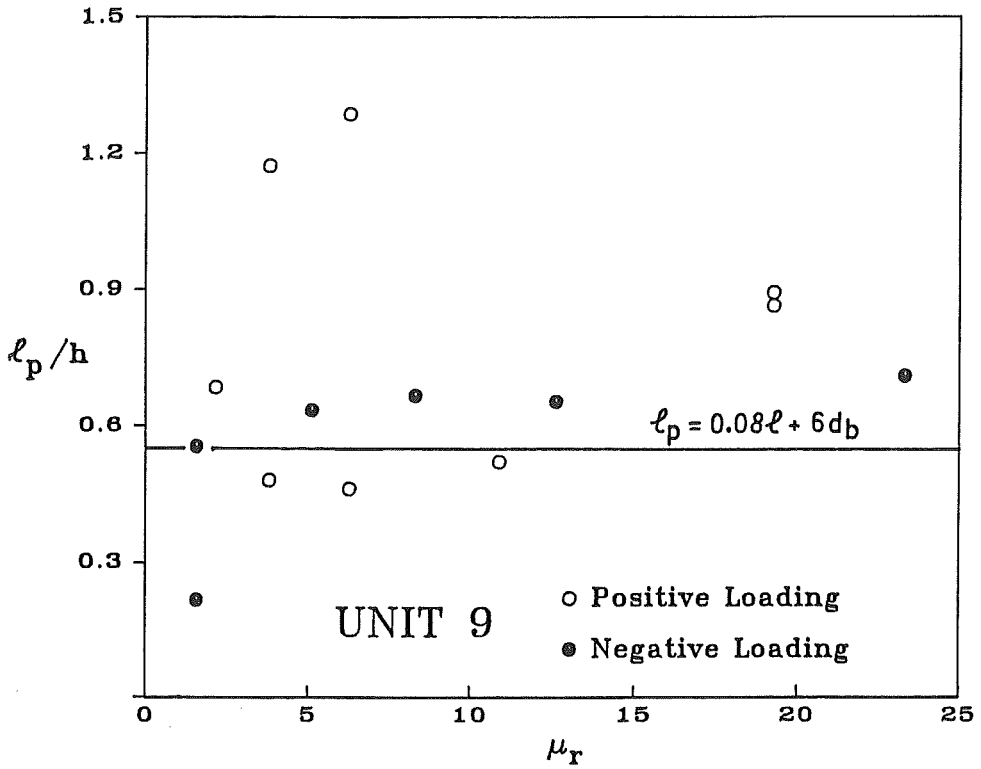

Figure 3.41: Equivalent Plastic Hinge Length-Real Displacement Ductility Factor for Unit 9

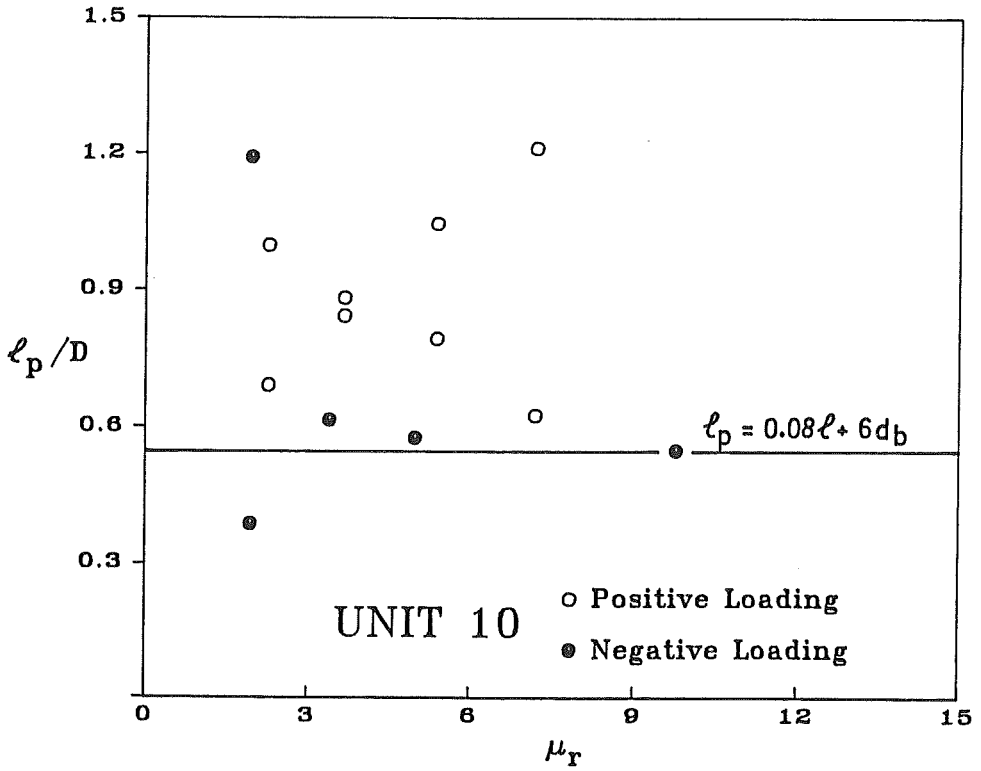

Figure 3.42: Equivalent Plastic Hinge Length-Real Displacement Ductility Factor for Unit 10

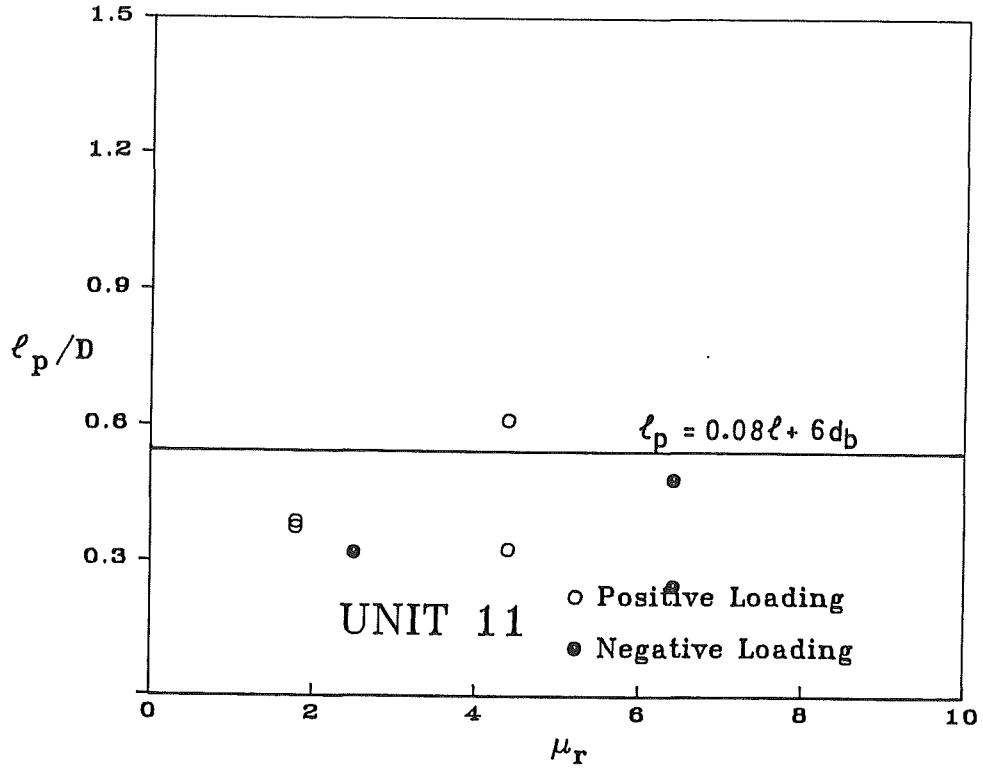

Figure 3.43: Equivalent Plastic Hinge Length-Real Displacement Ductility Factor for Unit 11

For this reason, the theoretical values of ℓ_p did not give a good agreement to the measured values. For Units 8 and 11 however, Eq. 3.12 gives a reasonably safe estimation of ℓ_p. The values of ℓ_p given by Eq. 3.12 are shown on Figs. 3.37 to 3.43.

The experimental yield displacement and curvature, Δ_y and φ_y, the measured maximum curvature φ_{max}, the curvature ductility factor φ_{max}/φ_y, the dimensionless equivalent plastic hinge length ℓ_p/h or ℓ_p/D, and the plastic rotation θ_p are given in Table 3.7.

3.8.4 Measured Strain Profiles

Graphs of strain profiles, showing the measured compressive strains on the surface of the core concrete, and the measured tensile strains on the hoops as a result of concrete confinement, at the succesive positive and negative loading peaks are illustrated in Figs. 3.44 to 3.50.

The concrete strains calculated from the potentiometer readings are plotted in the same way as for the observed curvatures. The measured strains from the strain gauge readings on the hoops are plotted at the strain gauged hoop positions and joined by straight lines.

It has been commented previously [3,4,5], that it is more appropriate to define the area of core concrete as the area of concrete within the centre-lines of the hoops, rather than within the outside of the hoops as recommended by the New Zealand code [2]. However, for design purpose, the code statement is more convenient to apply. For this reason, the concrete strains were calculated for the surface at the outside of the hoops.

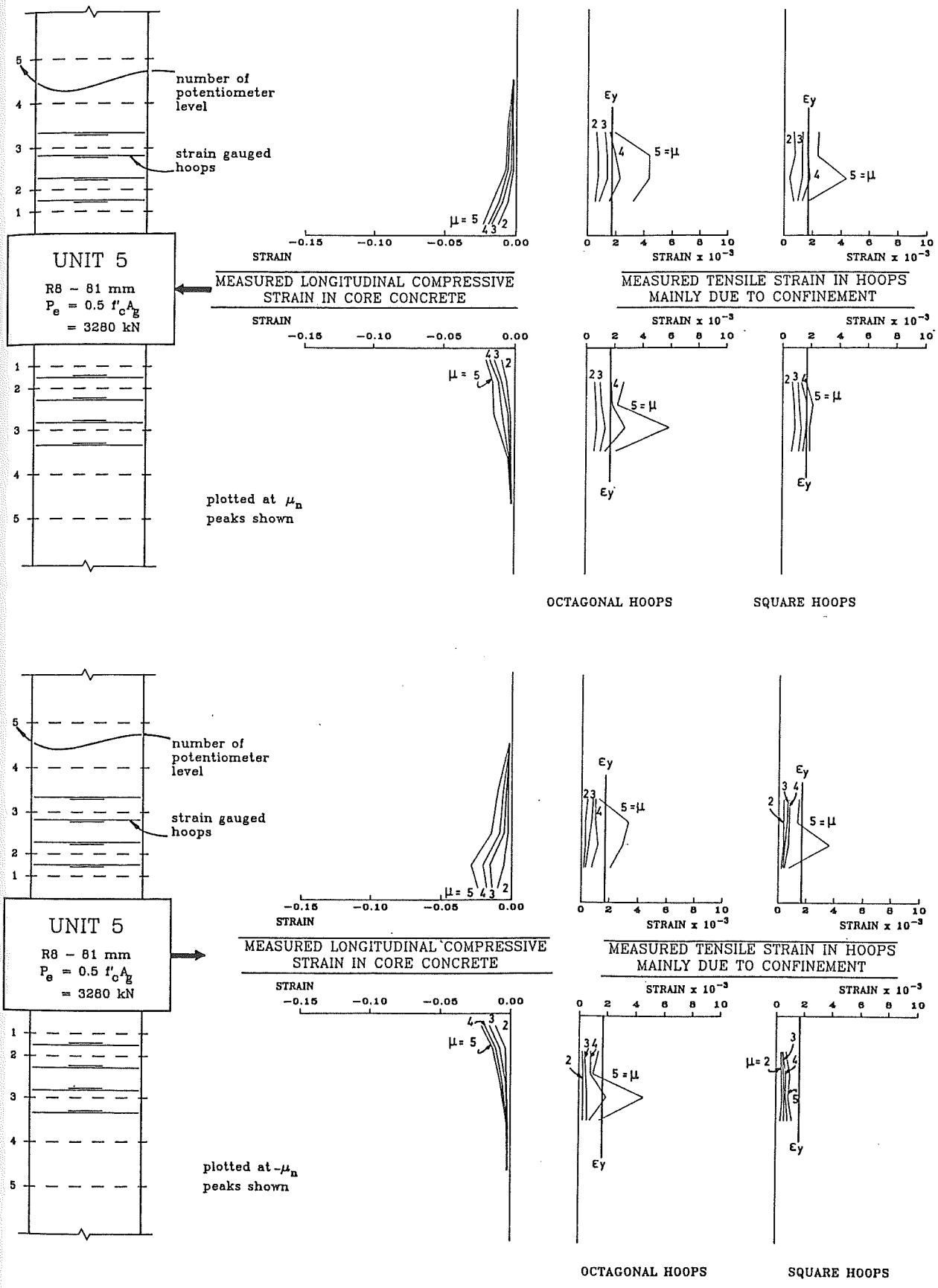

Figure 3.44: Measured Longitudinal Compressive Strains in Core Concrete and Measured Tensile Strains in Hoops Mainly Due to Confinement for Unit 5

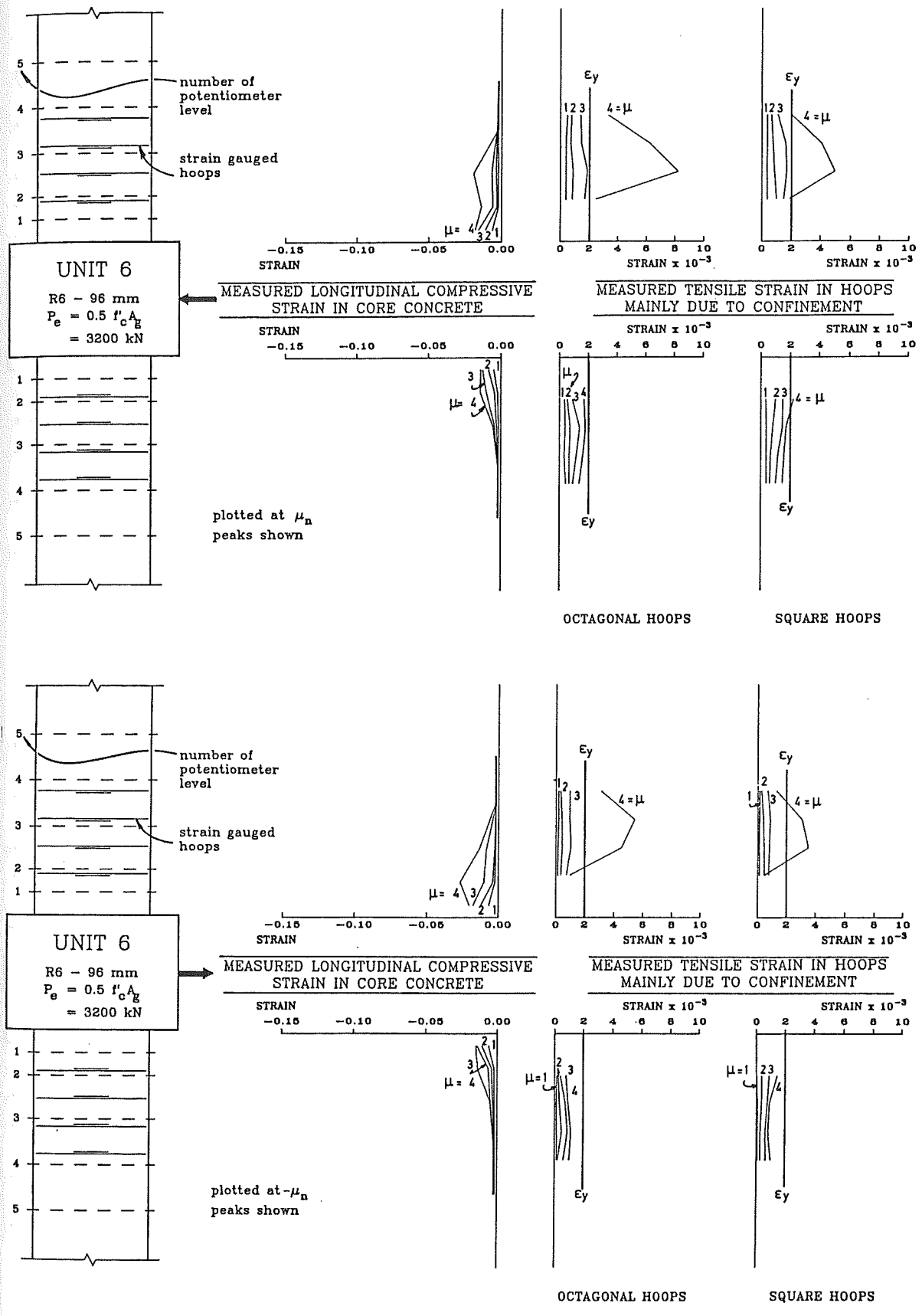

Figure 3.45: Measured Longitudinal Compressive Strains in Core Concrete and Measured Tensile Strains in Hoops Mainly Due to Confinement for Unit 6

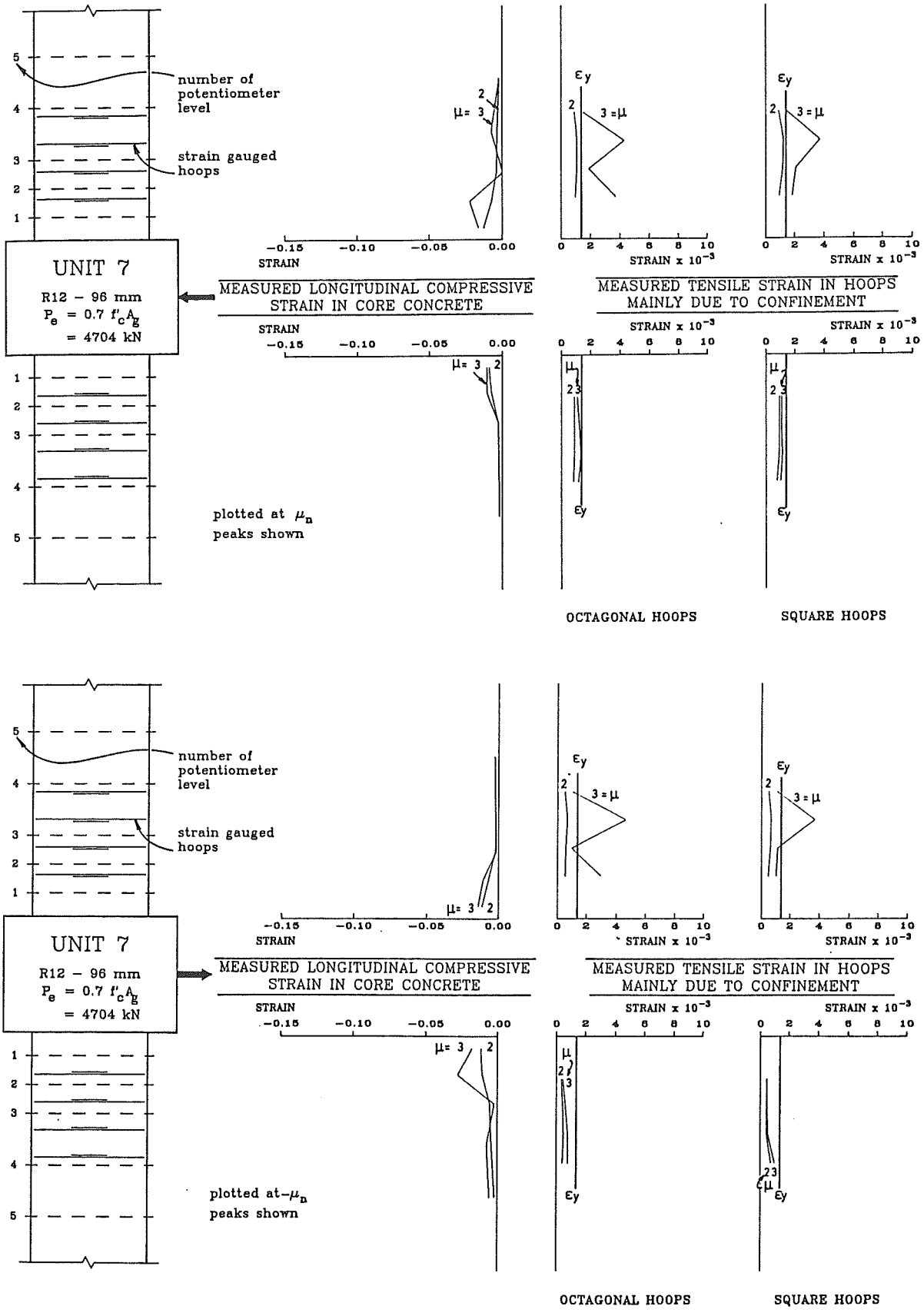

Figure 3.46: Measured Longitudinal Compressive Strains in Core Concrete and Measured Tensile Strains in Hoops Mainly Due to Confinement for Unit 7

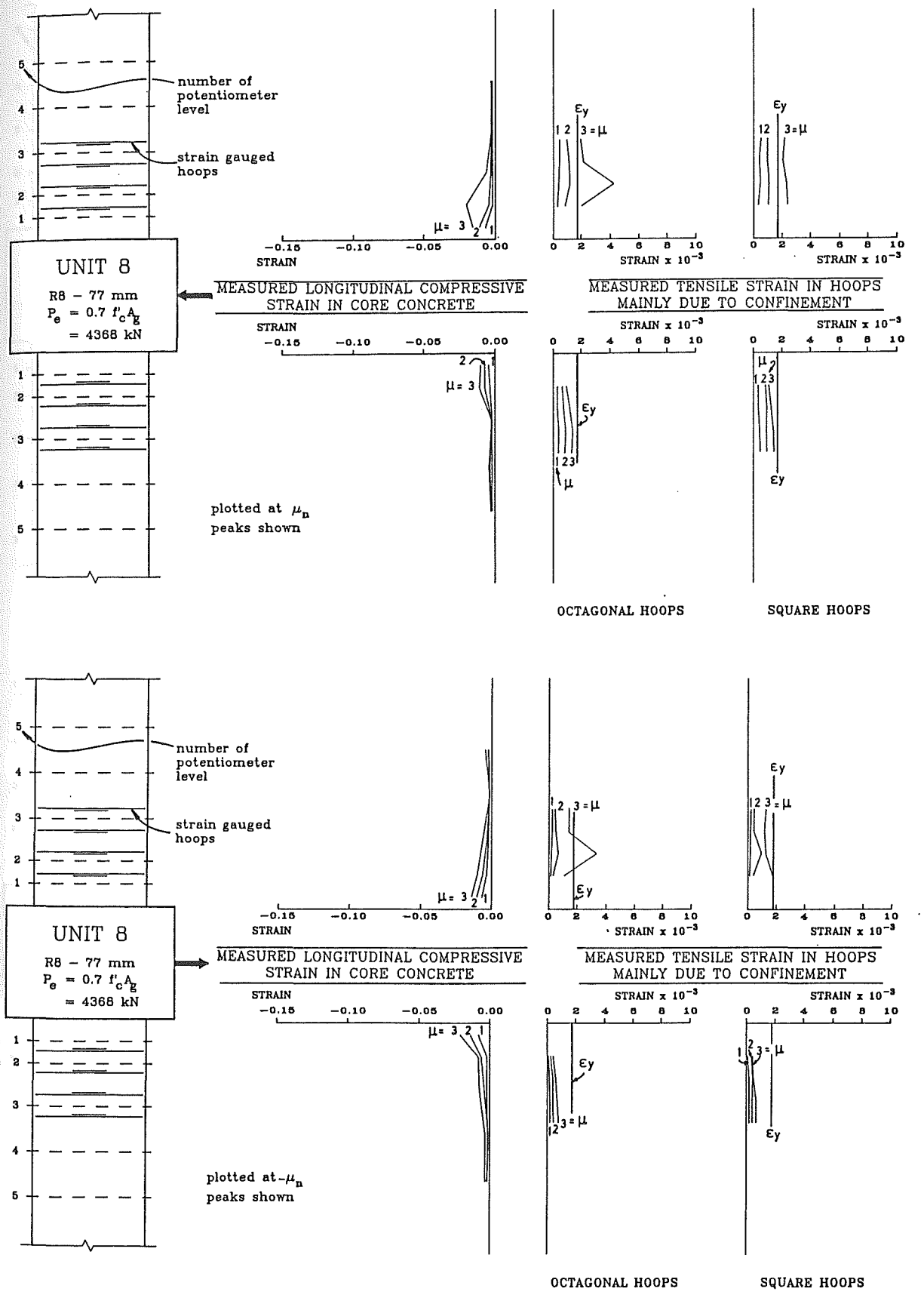

Figure 3.47: Measured Longitudinal Compressive Strains in Core Concrete and Measured Tensile Strains in Hoops Mainly Due to Confinement for Unit 8

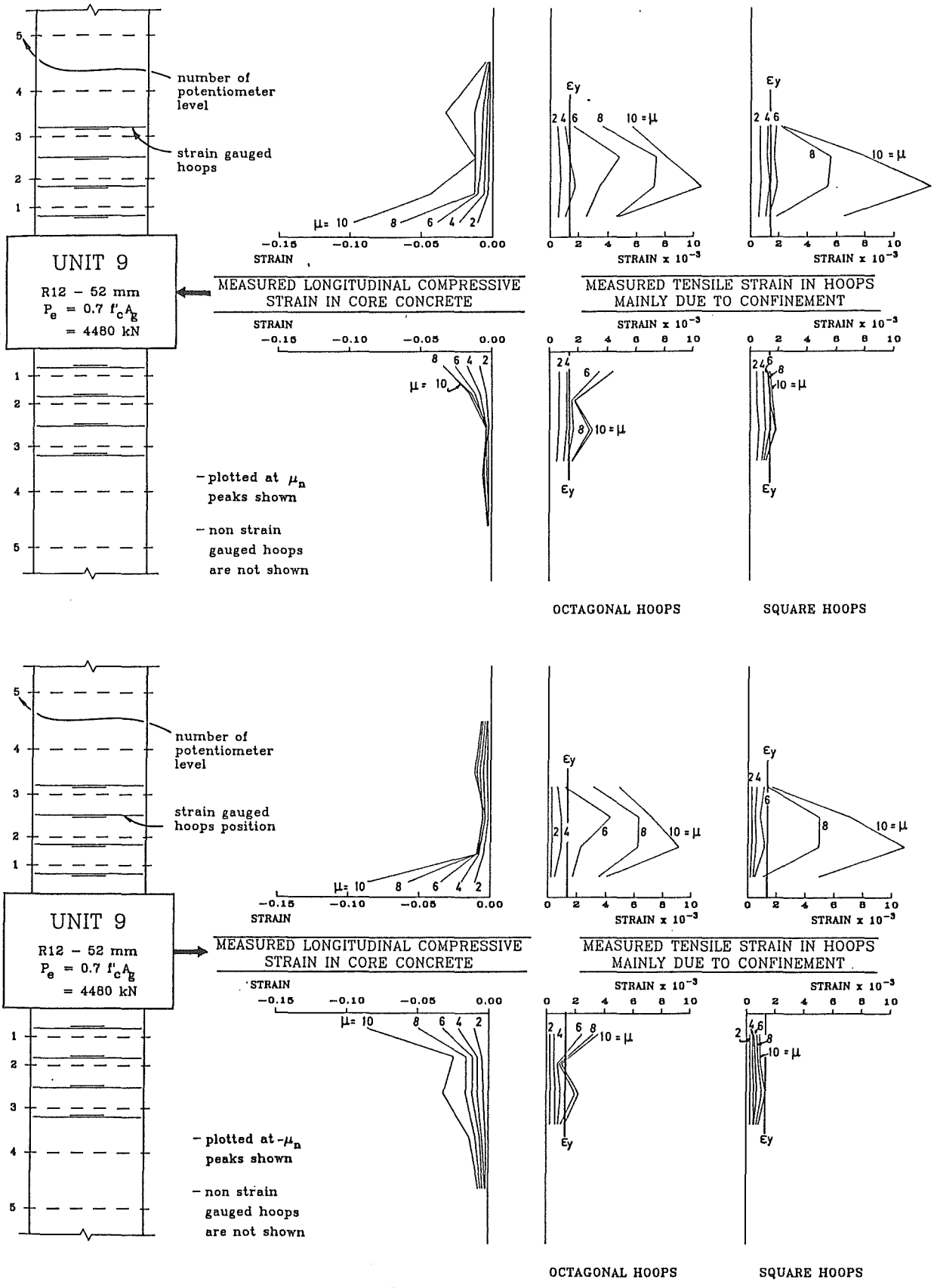

Figure 3.48: Measured Longitudinal Compressive Strains in Core Concrete and Measured Tensile Strains in Hoops Mainly Due to Confinement for Unit 9

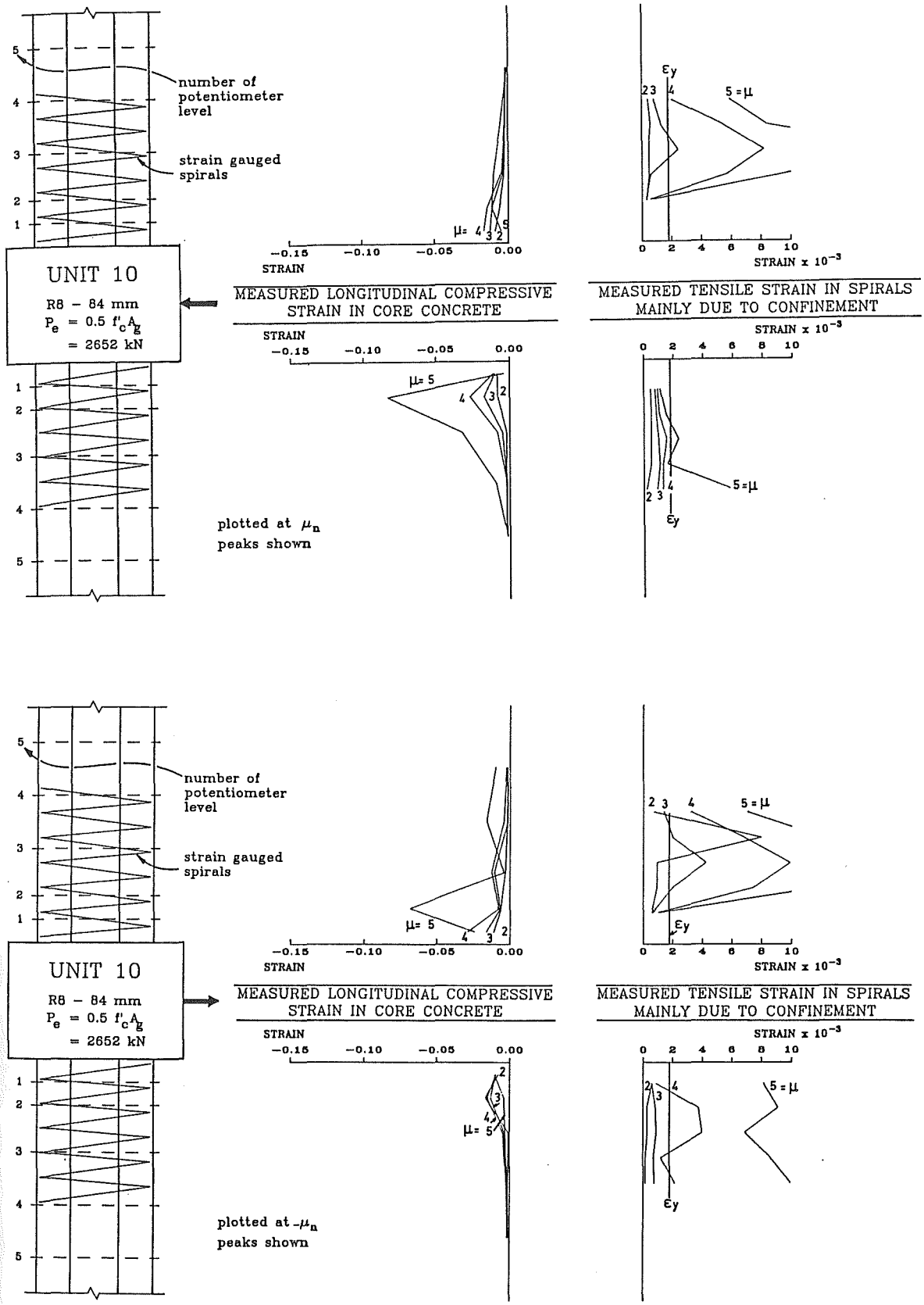

Figure 3.49: Measured Longitudinal Compressive Strains in Core Concrete and Measured Tensile Strains in Hoops Mainly Due to Confinement for Unit 10

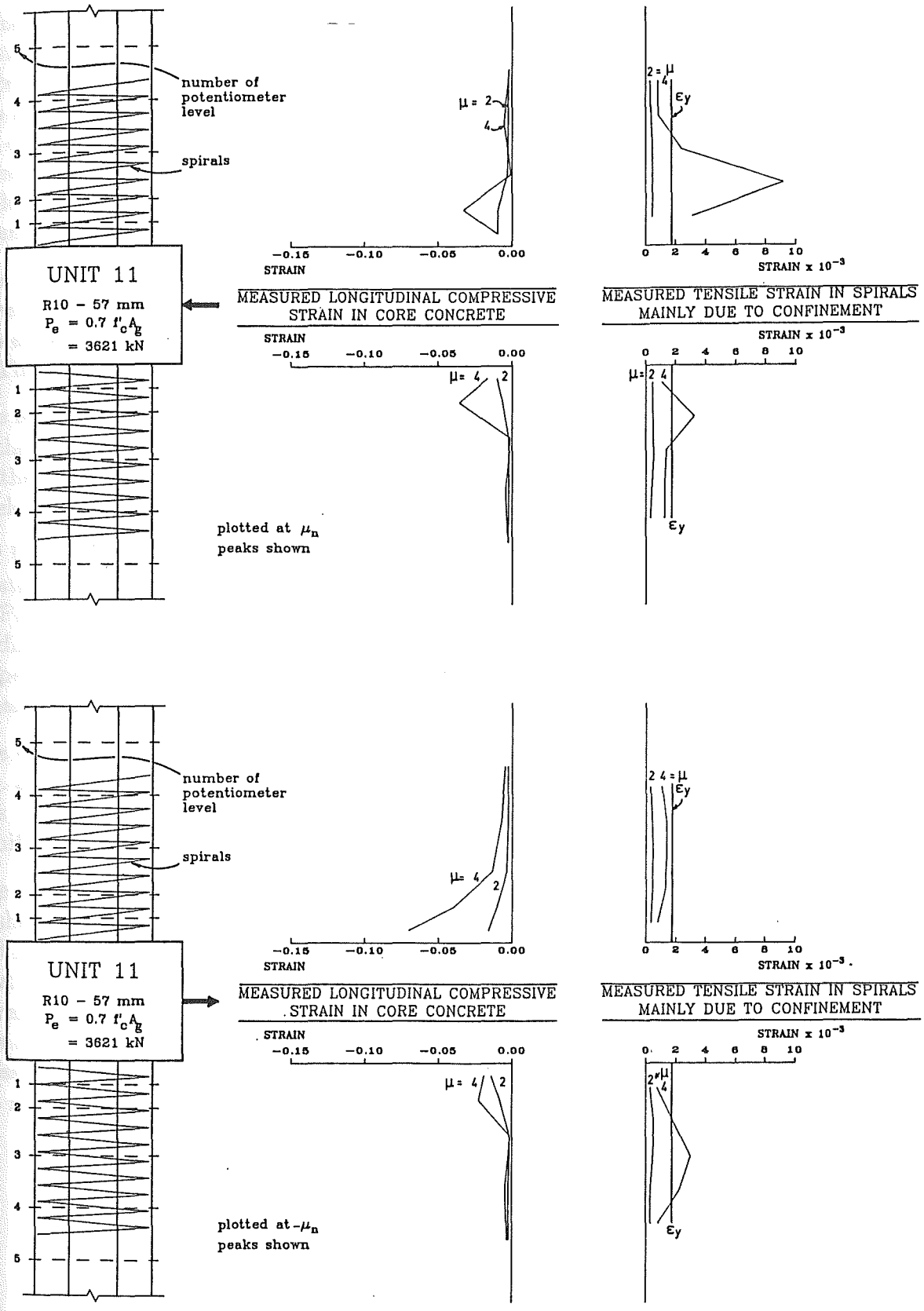

Figure 3.50: Measured Longitudinal Compressive Strains in Core Concrete and Measured Tensile Strains in Hoops Mainly Due to Confinement for Unit 11

As can be seen from Fig. 3.6, the electrical resistance strain gauges marked A in the square sections, which were placed for measuring strains mainly due to confinement of the concrete, were only attached to the hoops on one side of the column. When positive loading was applied, they gave measurements of the strains due to confinement since they were in the compression zone. However, when negative loading was applied, the strains due to confinement were smaller than those observed in the previous loading direction, since the hoops could now be in the tension zone. In fact, due to the high level of axial load, most of the column section was in compression during both loading directions.

Figs. 3.44 to 3.50 indicate that the maximum longitudinal concrete compressive strain ϵ_{cmax} when the column flexural strength was not less than 80% of the theoretical ideal strength, was approximately 0.02 to 0.03 for Units 5 to 8, 0.07 for Units 10 and 11, and 0.09 for Unit 9. The measured ϵ_{cmax} for all column units are listed in Table 3.7.

The tensile strains on the hoops indicated that the largest strain measured was at the second or the third strain gauge levels, confirming that there was additional confinement provided by the central stub, which resulted in the smaller strain recorded at the first strain gauge levels.

For Unit 11, comparing the confining strains in Fig. 3.50 with the lateral load-top column plastic hinge curvature hysteresis loops shown in Fig. 3.26c, there is an obvious discrepancy. In Fig. 3.26c, the top plastic hinge did not undergo a large rotation during the positive loading. Consequently, smaller strains should be obtained. This discrepancy was due to a lapped splice which existed in the spirals at the bottom plastic hinge which restrained the expansion of the spirals.

The electrical resistance strain gauges marked C in the square and octagonal sections (see Fig. 3.6) were attached to measure strains mainly due to shear. However, since the neutral axis depth changed significantly with the loads, the strains recorded there could also be significantly affected by flexure.

The measured tensile strains in the transverse reinforcement occuring mainly as a result of shear, are shown in Figs. 3.51 to 3.57. Most of the strains are still in the elastic range and indicate that shear was not significant in these columns which had moderate to large axial compression load levels. However, examination of Figs. 3.56 and 3.57, shows that the spirals did reach the yield range in Units 10 and 11. The octagonal columns exhibited larger strains in the transverse reinforcement than the square columns. The more uniform confining pressure in octagonal columns means that the effect of confinement was still pronounced in the region where the strain gauges measuring mainly shear were attached.

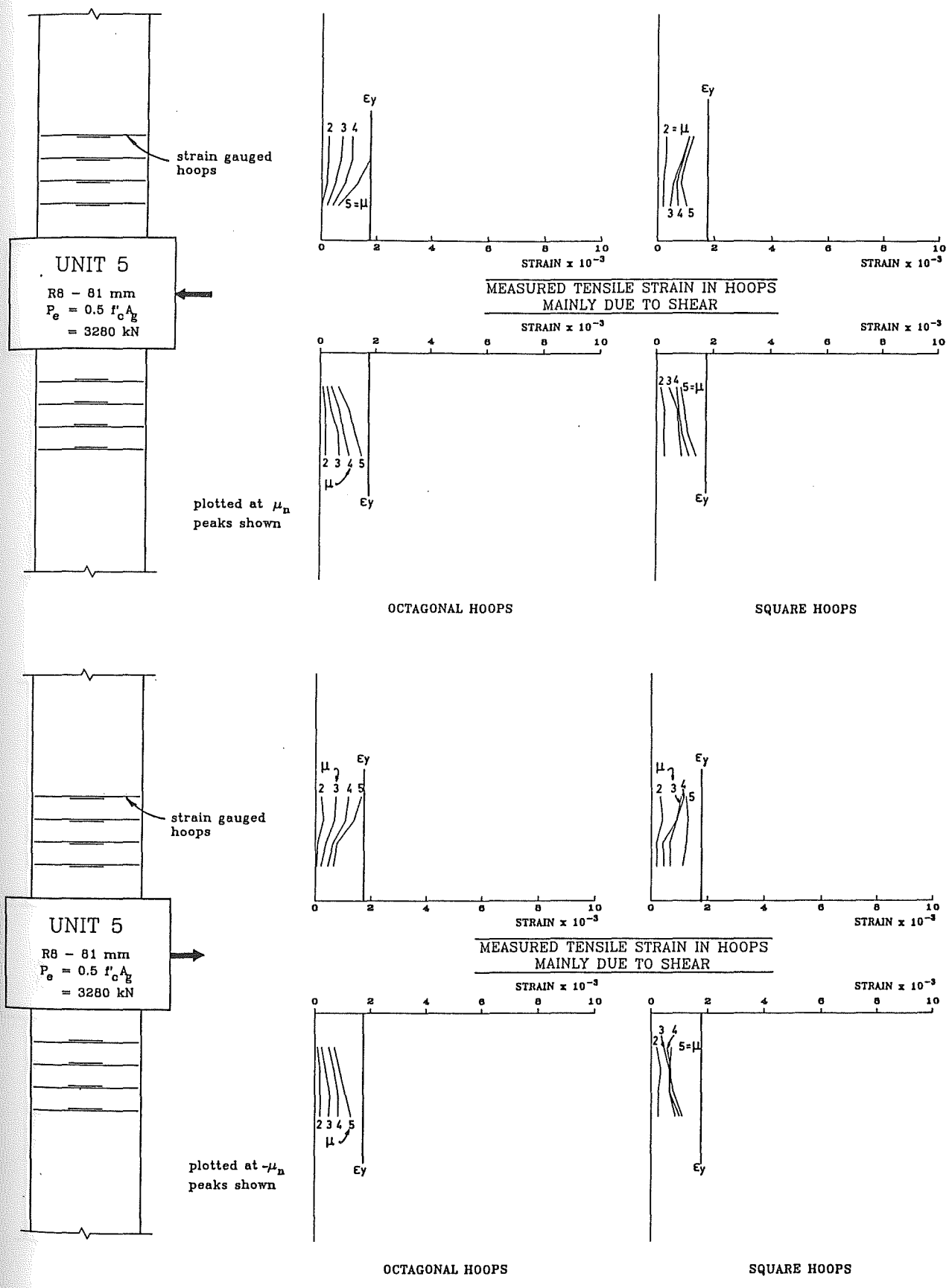

Figure 3.51: Measured Tensile Strains in Hoops Mainly Due to Shear for Unit 5

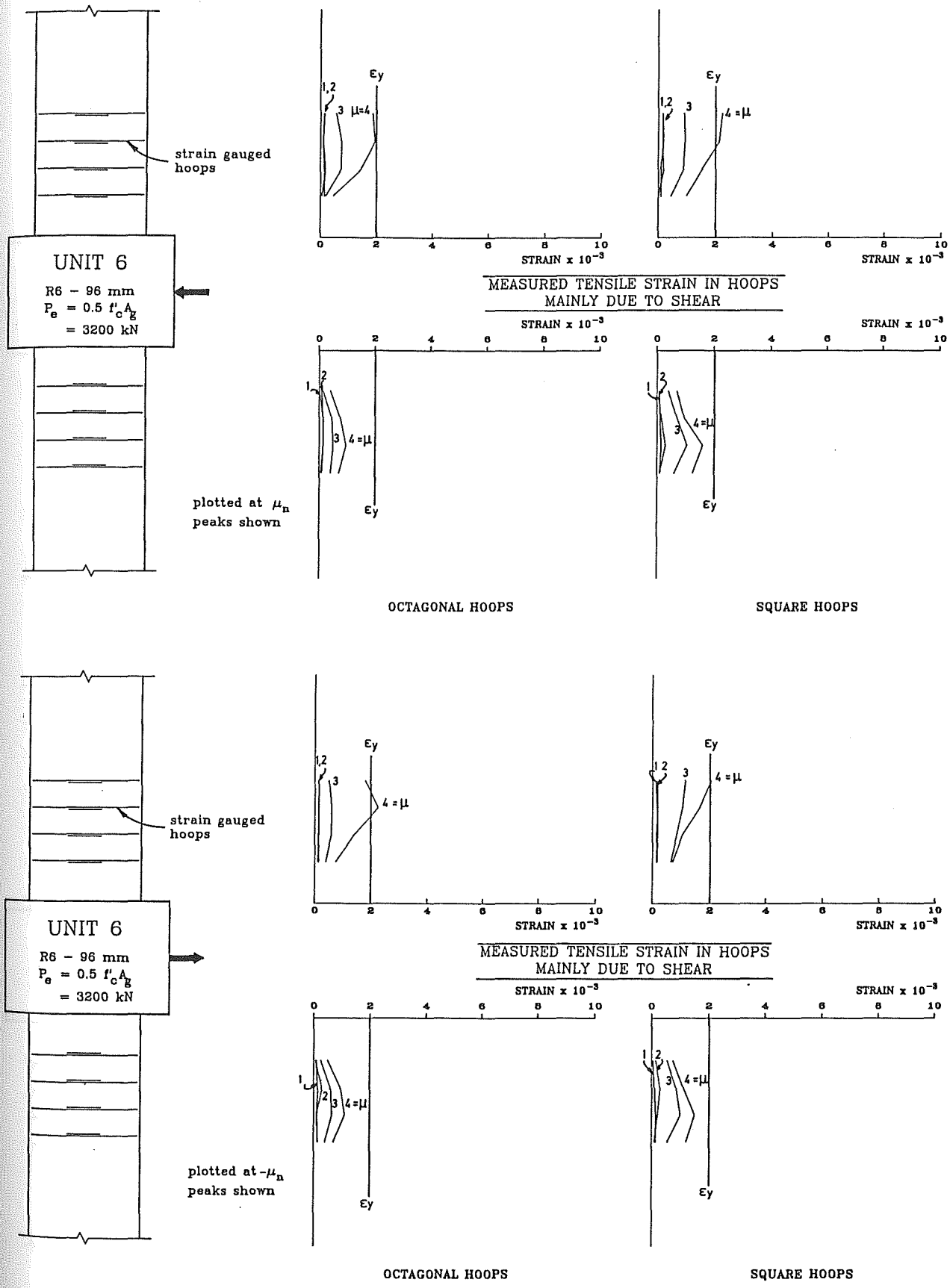

Figure 3.52: Measured Tensile Strains in Hoops Mainly Due to Shear for Unit 6

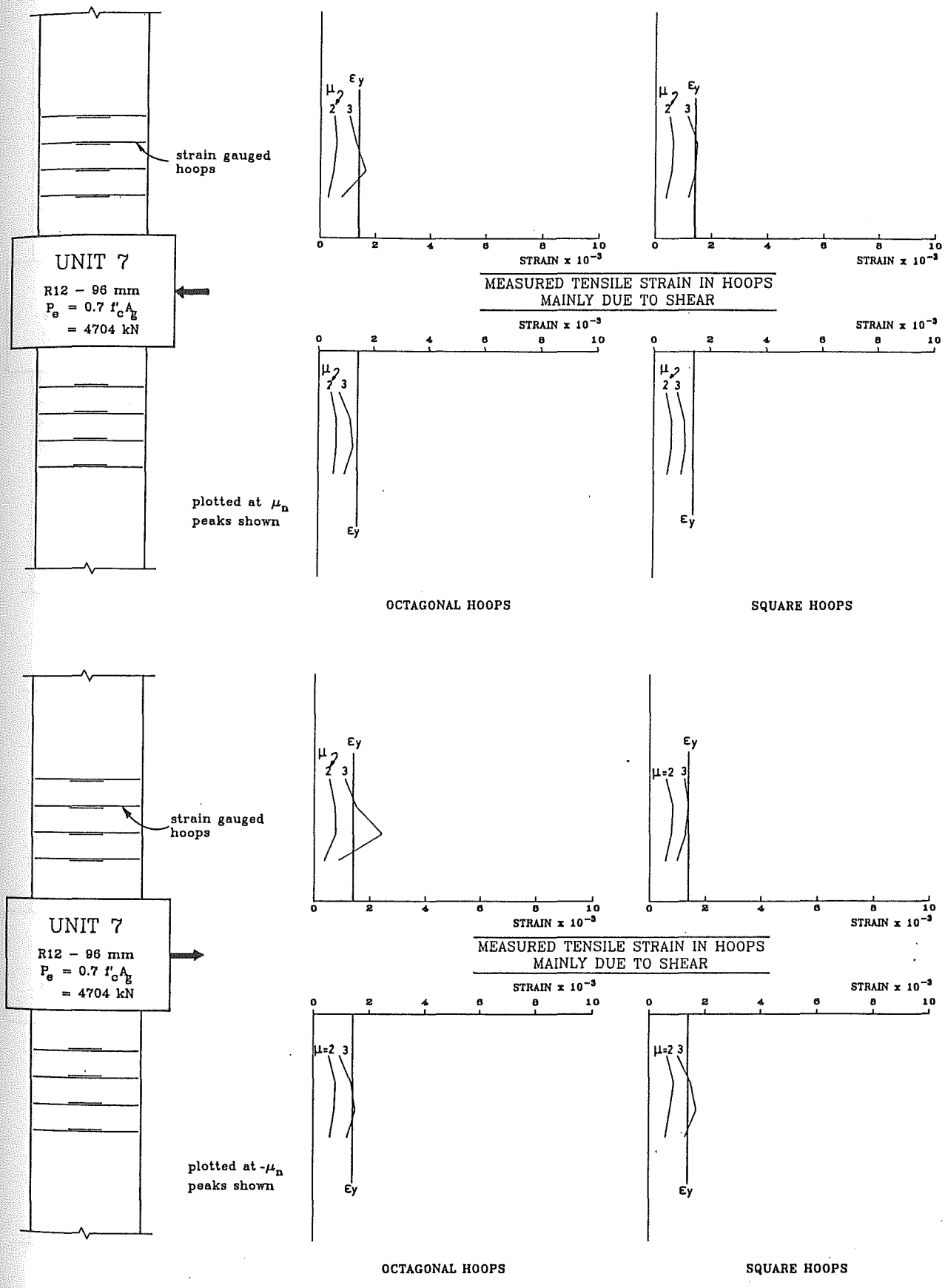

Figure 3.53: Measured Tensile Strains in Hoops Mainly Due to Shear for Unit 7

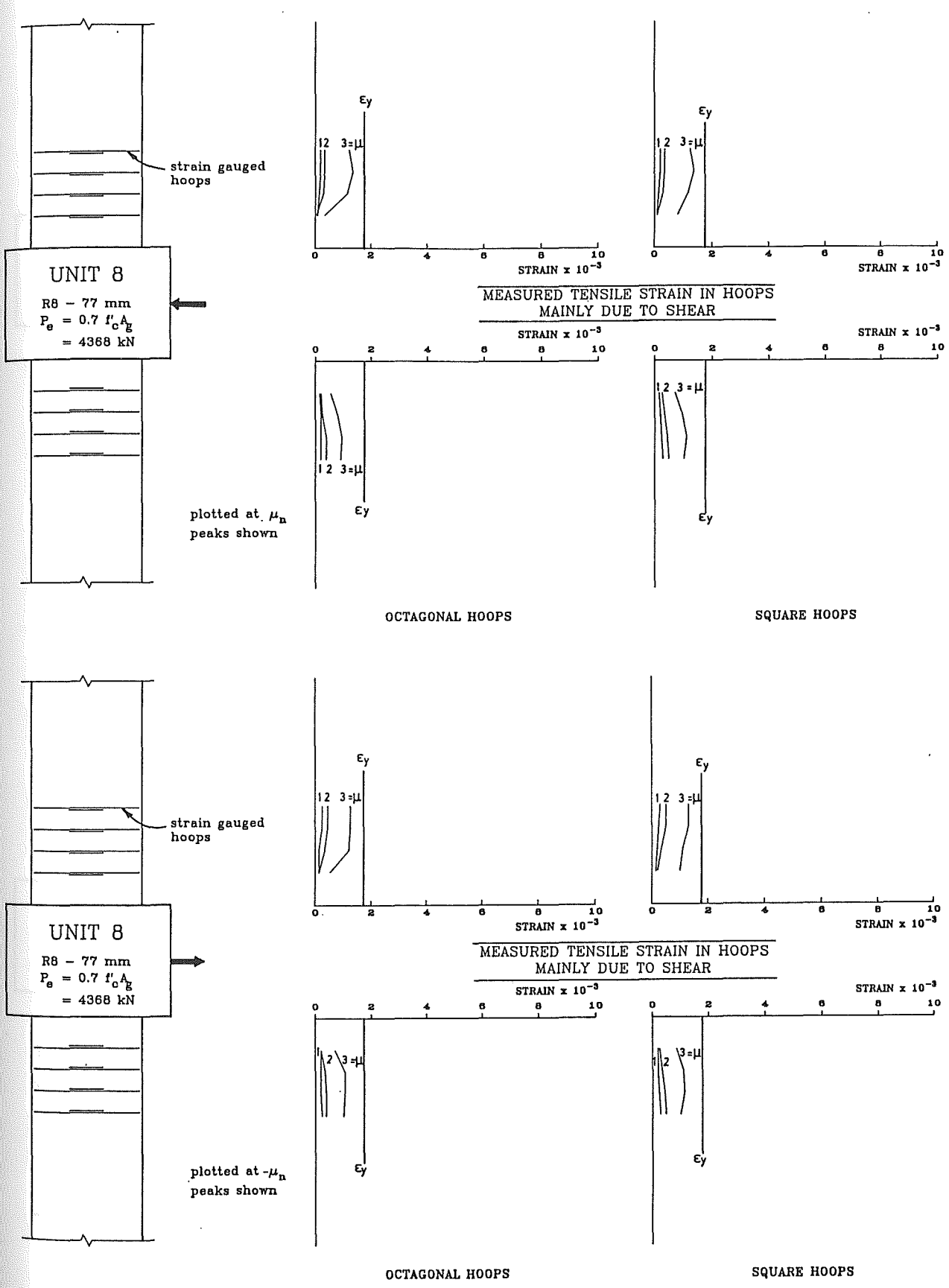

Figure 3.54: Measured Tensile Strains in Hoops Mainly Due to Shear for Unit 8

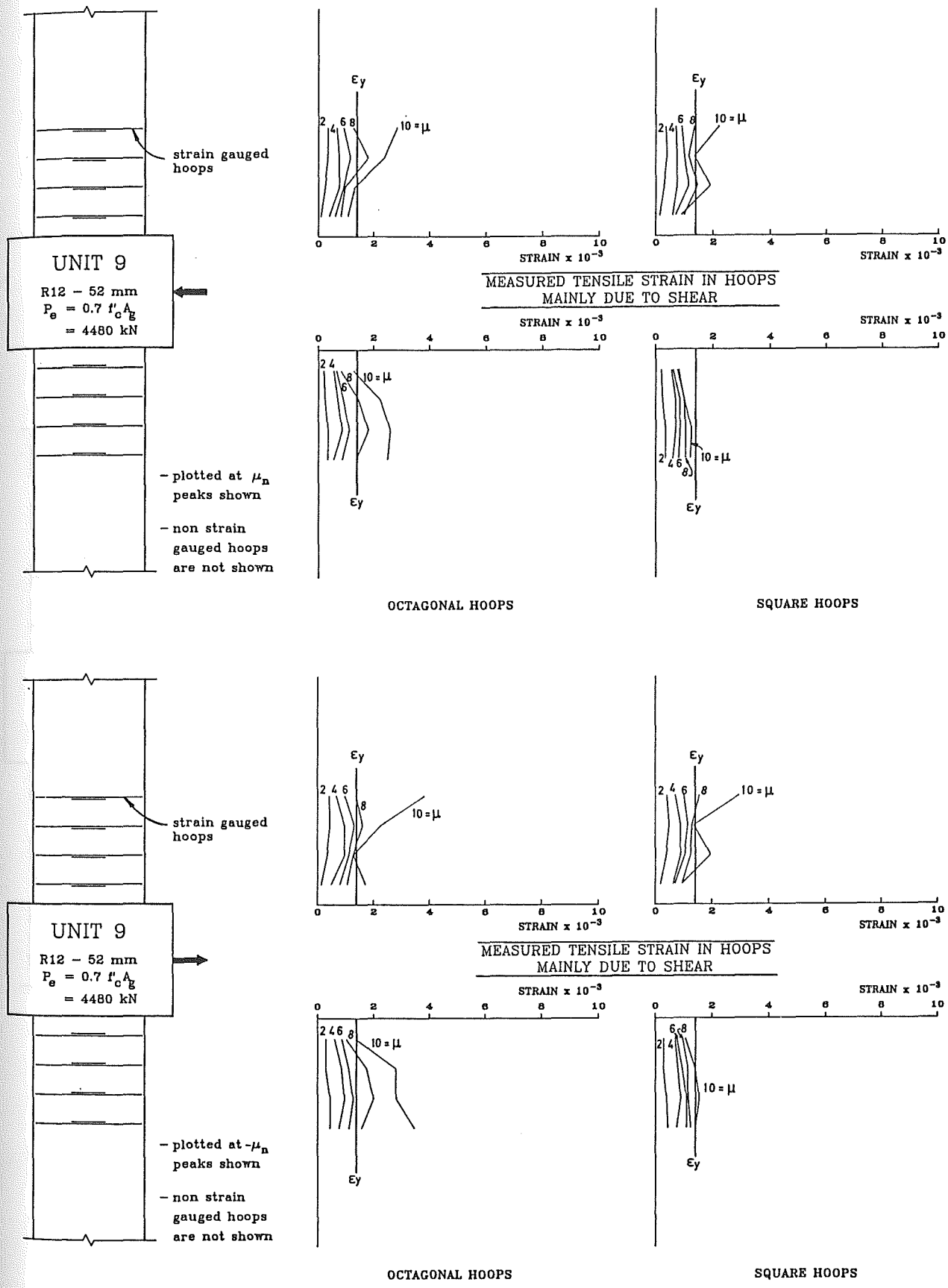

Figure 3.55: Measured Tensile Strains in Hoops Mainly Due to Shear for Unit 9

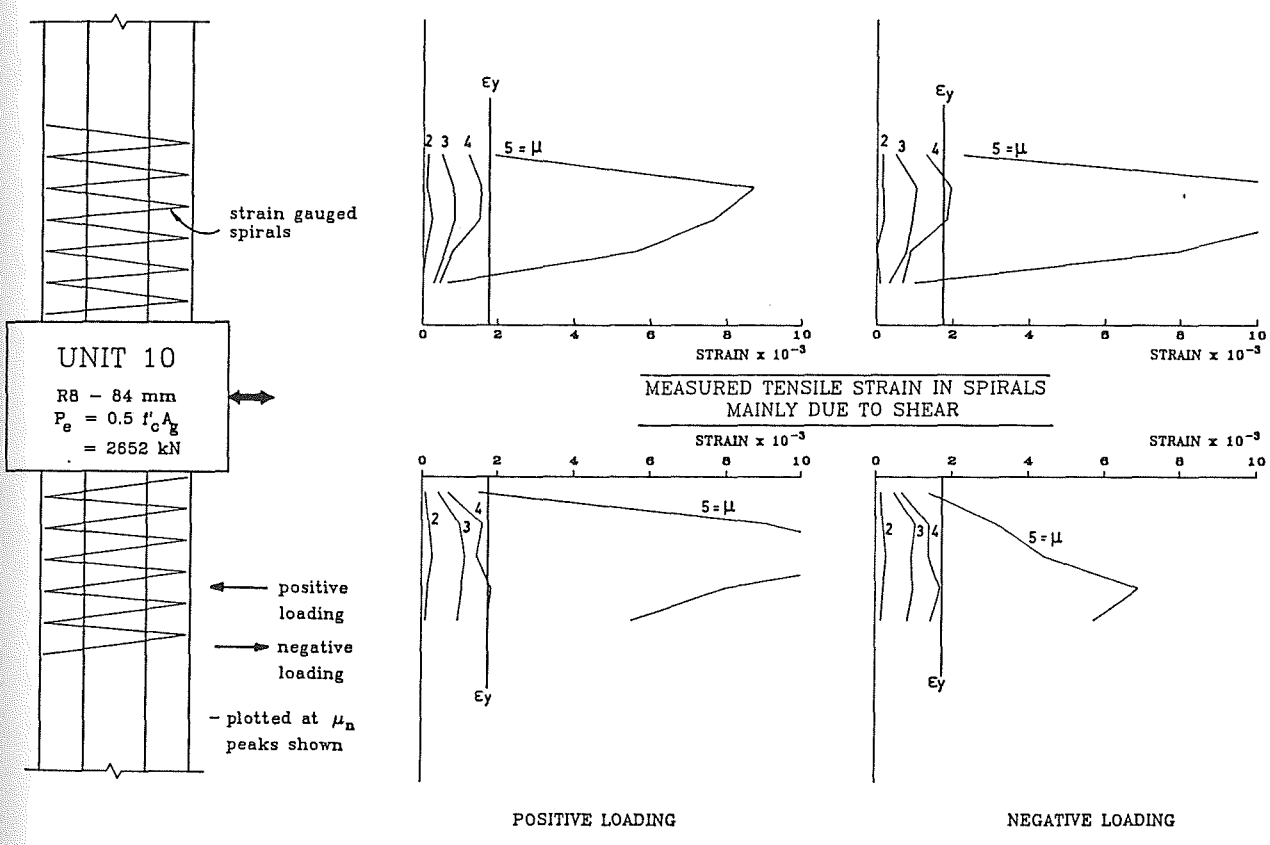

Figure 3.56: Measured Tensile Strains in Hoops Mainly Due to Shear for Unit 10

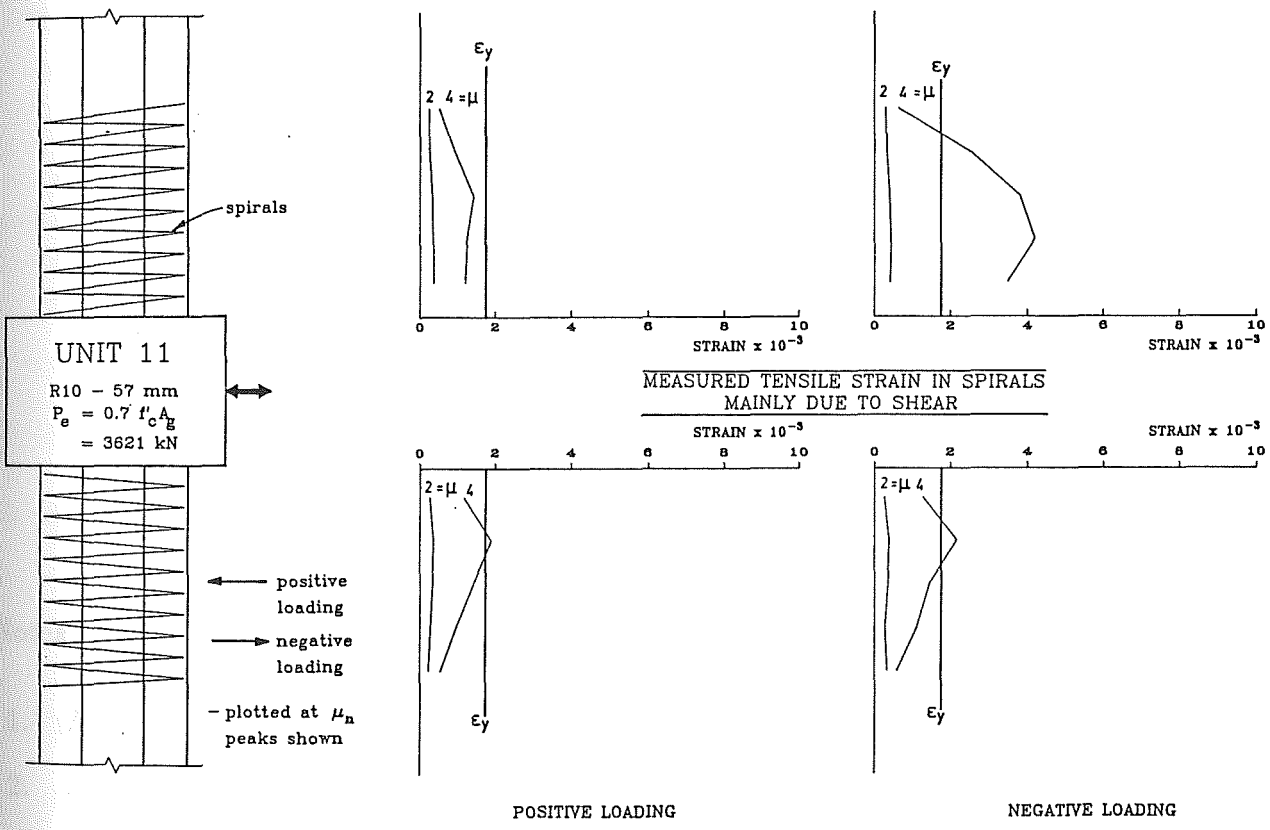

Figure 3.57: Measured Tensile Strains in Hoops Mainly Due to Shear for Unit 11

Table 3.7: Measured Quantities Obtained From the Tests of Column Units

Unit	5	6	7	8	9	10	11
Δ_y (mm)	6.15	6.25	4.75	4.50	4.35	6.30	5.03
H_{max} (kN)	580	584	589	580	608	423	403
M_{max}/M_{ACI} (1) or ϕ_o	1.38	1.40	1.70	1.79	2.01	1.50	1.70
ϵ_{spall} (10^{-3})	12.0	6.6	10.1	11.1	7.4	10.7	9.8
ϵ_{cmax} (10^{-3})	20.8	26.4	27.9	20.8	85.6	68.2	69.9
Δ_{max} (mm) (2)	43.7	29.6	29.3	17.3	94.0	70.6	36.3
Drift (%)	2.42	1.64	1.62	0.96	5.22	3.92	2.02
ℓ_p/h or ℓ_p/D	0.71	0.72	0.94	0.81	0.80	0.91	0.66
Measured at First Potentiometer Levels							
φ_y (10^{-3}rad/m)	16.4	15.9	11.2	11.1	9.6	14.6	13.1
φ_{max} (10^{-3}rad/m)	79.2	68.2	52.7	56.7	244.4	74.7	194.4
φ_{max}/φ_y	4.83	4.29	4.71	5.11	25.46	5.12	14.87
θ_p (10^{-3}rad)	17.0	13.8	10.5	13.6	54.0	18.8	35.9
Measured at Second Potentiometer Levels							
φ_y (10^{-3}rad/m)	7.6	5.2	5.6	4.9	3.4	7.0	6.3
φ_{max} (10^{-3}rad/m)	64.2	76.1	64.3	42.3	92.6	176.7	100.8
φ_{max}/φ_y	8.45	14.63	11.48	8.63	27.24	25.24	16.06
θ_p (10^{-3}rad)	15.3	18.7	14.8	11.1	20.5	53.2	18.7

Notes:

1. M_{ACI} is calculated using the code approach with measured values of f'_c and f_y
2. Rotation of the central stub was taken into account
3. The values of ℓ_p/h or ℓ_p/D shown were the average values calculated at displacement ductility peaks, using the values of φ measured at the first and second potentiometer levels
4. ℓ_p/h for Units 5 to 9, ℓ_p/D for Units 10 and 11. It is worth noting that Eq. 3.12 gives ℓ_p/h or ℓ_p/D=0.56

3.9 Comparison of the Experimental Results with Theoretical Predictions

3.9.1 General

In the following sections, a comparison of the experimental results for the column units and theoretical predictions is made. This includes the yield curvature and yield displacement, the lateral load-displacement hysteresis loops, the flexural enhancement factor, the maximum plastic rotation and curvature, and the available curvature ductility factor. The cyclic moment-curvature theory [3], and the design charts for flexural strength and ductility [4] were used to make the comparisons. The flexural strength enhancement factor is compared with an empirical prediction [13]. The predicted theoretical monotonic moment-curvature relations for all units are also compared with the experimental points.

In the cyclic moment-curvature theory, cyclic stress-strain relations for the concrete and longitudinal steel, which take into account the enhancement of strength and ductility due to confinement, and the effect of strain hardening and the Bauschinger effect, were adopted [3]. The energy balance approach was used to predict the ultimate longitudinal compressive strain of confined concrete, defined as the strain when the transverse reinforcement first fractures. This was found by equating the strain energy capacity of the transverse hoops to the work done on the concrete, and the longitudinal steel as a result of confinement.

The computer program based on the theory [3], analyzes the load-deformation behaviour of arbitrarily shaped reinforced concrete sections subjected to imposed deformations. A parabolic variation of curvature along the yielded length of the member is assumed. The effect of yield penetration and deformations due to shear are also considered. Fig. 3.58 shows these assumptions.

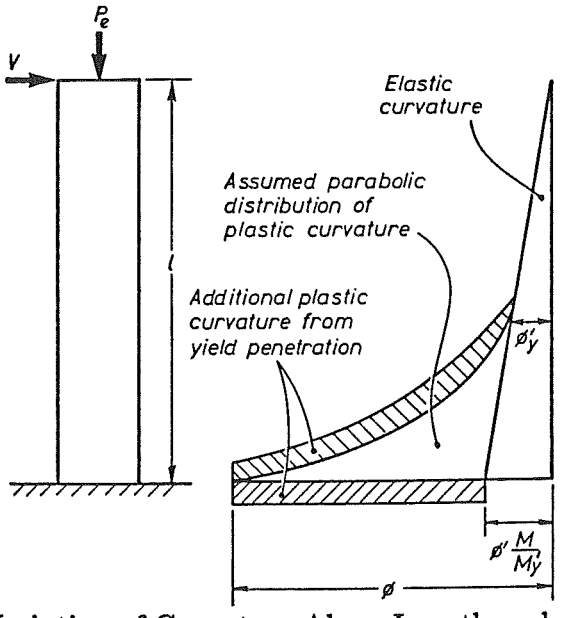

Figure 3.58: Assumed Variation of Curvature Along Length and Assumed Yield Penetration and Deformations Due to Shear in Theoretical Approach [3]

It should be noted that the cyclic moment-curvature theory by Mander *et al.* [3] was based on the concrete stress-strain relations obtained from confined reinforced concrete columns subjected to concentric axial compression. Therefore, the effect of strain gradient on the effectiveness of confinement of concrete k_e was not taken into account. It was found by Zahn *et al.* [4] that strain gradient did influence the effectiveness of confinement and a new formula for k_e was established. Instead of using the area of effectively confined concrete, the first moment of area of effectively confined concrete was used in calculating k_e. This effectiveness of confinement was denoted as k_e^*. The cyclic moment-curvature theory by Mander *et al.* [3] was modified by Zahn *et al.* [4] in that manner in order to derive the design charts for flexural strength and ductility.

3.9.2 Yield Curvature and Yield Displacement

The theoretical yield curvature φ_y was calculated by extrapolating a straight line from the origin ($M = 0, \varphi = 0$) through the first yield curvature φ'_y , to the moment at the ideal strength M_i [3,4].

On this basis:

$$\varphi_y = \frac{M_i}{M'_y}\varphi'_y \tag{3.13}$$

where φ_y and M'_y are the curvature and moment calculated at the stage when the tension steel at the extreme tension fibre yields or when the strain of concrete at the extreme compression fibre reaches 0.002, whichever occurs first.

The ideal strength M_i was originally defined as the strength of column calculated using the code [2] approach with the measured material strengths, denoted as M_{ACI} [3]. The definition however, has been modified recently [4] to the maximum moment reached before the curvature exceeds five times φ_y, taking into account the effects of enhancement of concrete compressive strength due to confinement and strain hardening of longitudinal steel. This later definition of M_i is denoted as M'_i. The yield curvature using M'_i then becomes

$$\varphi_y = \frac{M'_i}{M'_y}\varphi'_y \tag{3.14}$$

Table 3.8 compares the experimental yield curvatures with the theoretical yield curvatures, calculated from Eqs. 3.13 and 3.14, respectively, and the yield displacements for all column units. It can be seen that the measured yield curvatures at the first potentiometer levels are larger than the predicted values, evidently due to the inclusion of steel slip within the central stub in the measurement. As mentioned previously however, the measured yield curvatures at the second potentiometer levels gave reasonably good agreement. Due to the larger ideal strength M_i defined by Zahn *et al.* [4], the yield curvatures predicted by Zahn *et al.* were larger than those predicted by Mander *et al.*.

Table 3.8: Experimental and Theoretical Yield Curvatures and Yield Displacements for All Column Units

Unit	φ_y (10^{-3}rad/m)				Δ_y (mm)		
	Experimental		Theoretical		Experimental	Theoretical	
	1	2	3	4		3	4
5	16.4	7.6	7.1	8.1	6.15	5.66	6.88
6	15.9	5.2	7.1	8.4	6.25	6.27	7.36
7	11.2	5.6	5.0	6.1	4.75	4.14	6.08
8	11.1	4.9	5.0	6.3	4.50	4.17	6.23
9	9.6	3.4	5.0	7.6	4.35	4.16	6.31
10	14.6	7.0	7.7	9.5	6.30	6.34	7.85
11	13.1	6.3	5.8	8.0	5.03	4.85	6.63

Notes:

1. Measured at the first level of potentiometers (see Fig. 3.5)
2. Measured at the second level of potentiometers (see Fig. 3.5)
3. Calculated by the cyclic moment-curvature theory [3], in which the ideal flexural strength was calculated using the code [2] approach
4. Similar to 3, except the ideal flexural strength was defined as maximum moment reached before $\varphi = 5\varphi_y$ taking into account the actual material behaviour

3.9.3 Lateral Load-Displacement Hysteresis Loops

The experimental lateral load-displacement hysteresis loops for the column units are shown compared with the loops obtained from the cyclic moment-curvature theory [3] in Figs. 3.20b to 3.26b.

In order to compensate approximately for the effect of additional confinement provided by the central stub in the regions of the column adjacent to the stub, which was not considered in the theory, the compressive strength of confined concrete was increased by 15% in the analyses. This enhancement resulted in better agreement with the experimental results.

For Units 5 and 6, the shape of the experimental hysteresis loops were predicted reasonably well by the theory. The predicted compresive stress in the longitudinal reinforcement was not very significant at the end of the analysis, indicating that buckling of the longitudinal bars did not occur. On the other hand, the strain energy capacity of the hoops was violated, thus some of the hoops fractured. The tests however, exhibited buckling of longitudinal bars at the end of testing.

The theoretical hysteresis loops for Units 7 and 8 over-estimated the available ductility in the columns observed in the tests. The analysis predicted that the strength and ductility of the columns would still be maintained after completing $\mu_n = 3$. The column units however, failed at this stage of testing.

Very good agreement between the experiment and theory was shown by the hysteresis loops for Unit 9. The excellent performance exhibited by Unit 9 after completing two cycles at a nominal displacement ductility factor of 10, was very well predicted by the theory.

Fracture of some spirals in Unit 10, which was observed during the excursion to the first cycle of $\mu_n = 6$, was also shown in the analysis. However, the fracture was predicted at an earlier stage during the excursion to the first cycle of $\mu_n = 4$.

The hysteresis loops for Unit 11 given by the cyclic moment-curvature theory agreed reasonably well with the loops measured during the test. However, the theory predicted spiral fracture, whereas the buckling of longitudinal bars was observed at the end of the test.

3.9.4 Flexural Strength Enhancement Factor

Table 3.9 compares the flexural strength enhancement factors M_{max}/M_{ACI} for all column units, where M_{max} is the maximum moment obtained experimentally, or theoretically using the cyclic moment-curvature theory [3], and M_{ACI} is the ideal flexural strength of column calculated using the code [2] approach with the measured material strengths.

It was found that except for Unit 9, the strength enhancement factors given by the cyclic moment-curvature theory were generally less than those observed during the tests, indicating that the enhancement of concrete strength due to confinement was higher than predicted. If the effect of strain gradient was taken into account [4], less effectiveness of confinement would be obtained, which would result in even smaller strength enhancement.

Table 3.9: Flexural Strength Enhancement Factors for Column Units

Unit	M_{ACI}	M_{max}/M_{ACI} or ϕ_o		
	(kNm)	From Experiment	From Theory	From Empirical Eq. 3.15
5	381	1.38	1.26	1.51
6	376	1.40	1.23	1.51
7	304	1.70	1.62	1.98
8	293	1.79	1.56	1.98
9	298	2.01	2.05	1.98
10	259	1.50	1.26	1.51
11	214	1.70	1.62	1.98

In Table 3.9, the M_{max}/M_{ACI} ratios given by the empirical formula for flexural strength enhancement proposed by Ang *et al* [13] are also listed. The formula was derived from the test results of the reinforced concrete columns at the University of Canterbury in recent

years. The flexural strength enhancement of the columns plotted by Ang *et al.* to derive the equation is shown in Fig. 3.59. It is evident that the strength enhancement increases with the axial compression. The solid line indicates the average enhancement as expressed by Eq. 3.15. It was found that most results lie within the shaded area, which represents a variation of ± 15% from the average enhancement. The enhancement factors for Units 5 to 11 shown in Fig. 3.59 also lie within the shaded area, indicating that the formula gives a reasonable estimation of the flexural strength enhancement. The formula proposed by Ang *et al.* [14] is:

$$
\begin{aligned}
For P_e/(\phi f'_c A_g) < 0.1 : \frac{M_{max}}{M_{ACI}} &= 1.13 \\
For P_e/(\phi f'_c A_g) \geq 0.1 : \frac{M_{max}}{M_{ACI}} &= 1.13 + 2.35(\frac{P_e}{\phi f'_c A_g} - 0.1)^2
\end{aligned}
\tag{3.15}
$$

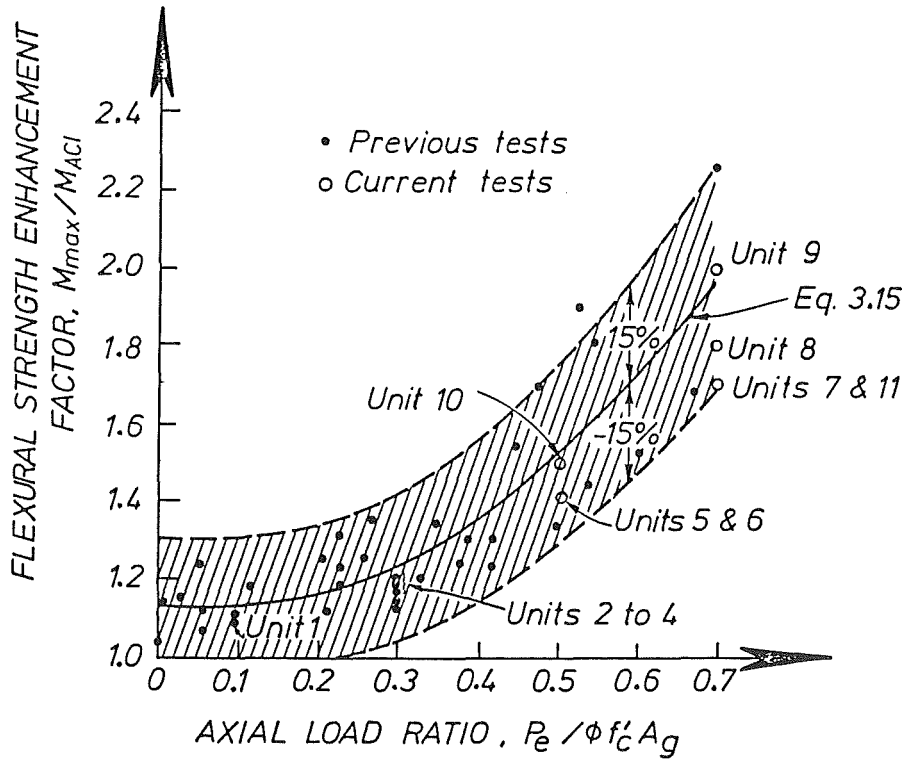

Figure 3.59: Flexural Strength Enhancement Factors of Column Units

3.9.5 Maximum Plastic Rotation and Curvature, and Available Curvature Ductility Factor

The experimentally measured maximum plastic rotations θ_p, maximum curvatures φ_{max}, and curvature ductility factors φ_{max}/φ_y for the column units are compared with the ultimate theoretical values obtained from the cyclic moment-curvature theory [3] in Table 3.10.

Table 3.10: Comparison of Experimental and Theoretical Maximum Plastic Rotations θ_p, Maximum Curvatures φ_{max}, and Curvature Ductility Factors φ_{max}/φ_y of Column Units

Unit	θ_p (10^{-3}rad)			φ_{max} (10^{-3}rad/m)			φ_{max}/φ_y		
	Experiment		Theory	Experiment		Theory	Experiment		Theory
	1	2	3	1	2	3	1	2	3
5	17.0	15.3	14.6	79.2	64.2	72.0	4.83	8.45	10.14
6	13.8	18.7	11.2	68.2	76.1	57.1	4.29	14.63	8.04
7	10.5	14.8	9.3	52.7	64.3	46.9	4.71	11.48	9.38
8	13.6	11.1	7.3	56.7	42.3	37.5	5.11	8.63	7.65
9	54.0	20.5	16.4	244.4	92.6	78.2	25.46	27.24	15.64
10	18.8	53.2	10.0	74.7	176.7	52.2	5.12	25.24	6.78
11	35.9	18.7	7.6	194.4	100.8	39.9	14.87	16.06	6.88

Notes:

1. Measured at the first level of potentiometers (see Fig. 3.5)
2. Measured at the second level of potentiometers (see Fig. 3.5)
3. Calculated by the cyclic moment-curvature theory [3]. It is worth noting that for Unit 9, the theoretical values were the maximum values when the analysis was terminated, the ultimate values would have been higher

The theoretical ultimate curvature was defined as the smallest of the following:

- When the moment reduced to 80% of the ideal flexural strength, or
- When the transverse reinforcement first fractured, or
- When the longitudinal reinforcement first fractured.

Except for Unit 9, the governing limitation for the ultimate curvature was fracture of transverse reinforcement.

Since the experimental test of Unit 9 was terminated when a nominal displacement ductility factor of 10 was obtained, the analysis was also terminated at the same stage, although no degradation in strength was detected. Thus, the maximum plastic rotations and curvatures obtained from the theoretical and the experimental results were not the ultimate values for Unit 9.

The theory predicted the maximum curvatures for Units 5 to 8 reasonably well. The predicted maximum curvatures for the other units were less than the experimentally measured values, indicating that the column units exhibited better performance than expected.

For most of the units, the theoretical curvature ductility factors lie between the experimental values measured at the first and second levels of potentiometers, except for Units 9 and 11, where the theoretical values were smaller than the experimental values.

The theoretical plastic rotations available in the column units, calculated from $(\varphi_u - \varphi_y)\ell_p$ were less than the measured values. This is due to the smaller ultimate curvatures predicted by the theory. Also, the theoretical ℓ_p of $0.56h$, calculated from Eq. 3.12 as recommended by Priestley *et al.* [14], was smaller than the experimental ℓ_p.

Probably, the most important comparisons in Table 3.10 are of the experimental and theoretical available plastic rotations, θ_p. It is to be noted that the ductility of a structure is dependent on the available plastic hinge rotation. The emphasis on curvatures has been because designers prefer to consider the behaviour of sections of members. It is of interest to note that the theoretical θ_p in Table 3.10 is always on the safe side.

3.9.6 Theoretical Monotonic Moment-Curvature Relations

The theoretical monotonic moment-curvature relations for all column units are compared with the experimental points in Figs. 3.60 to 3.66. The experimental points were measured at the first and second potentiometer levels at both the positive and negative directions. It is known that the monotonic moment-curvature relations of columns generally give an upper bound to the envelopes of cyclic performance.

Figs. 3.60 to 3.66 indicate that larger curvatures were achieved during monotonic loading than in the cyclic loading. This is because in cyclic moment-curvature analyses, the most common criterion governing the behaviour of the columns was the fracture of transverse reinforcement. In monotonic moment-curvature analyses however, this criterion is less likely to occur, since the transverse bars do not experience the accumulation of deformations as when subjected to cyclic loading. Nevertheless, the measured flexural strengths observed in the column units were generally larger than those predicted by the theory.

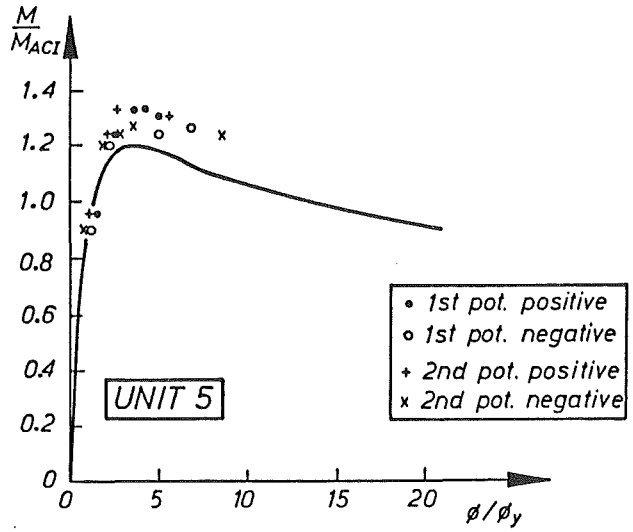

Figure 3.60: Theoretical Monotonic Moment-Curvature Relations, and Experimental Points for Unit 5

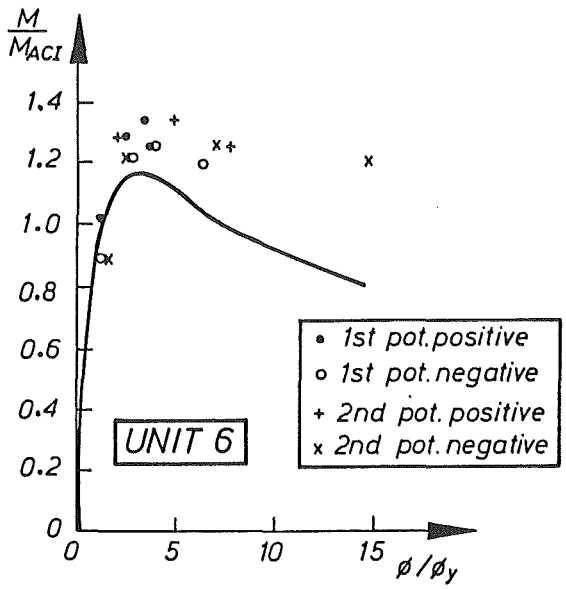

Figure 3.61: Theoretical Monotonic Moment-Curvature Relations, and Experimental Points for Unit 6

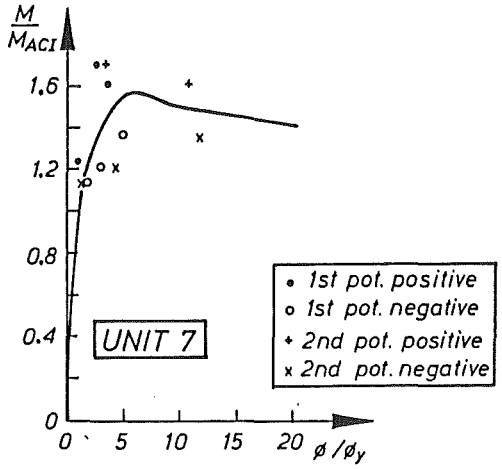

Figure 3.62: Theoretical Monotonic Moment-Curvature Relations, and Experimental Points for Unit 7

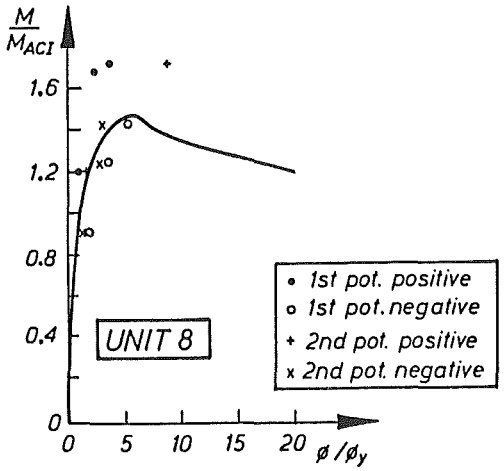

Figure 3.63: Theoretical Monotonic Moment-Curvature Relations, and Experimental Points for Unit 8

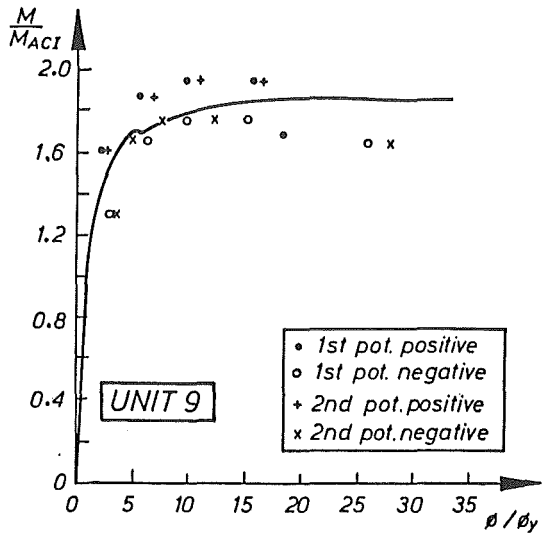

Figure 3.64: Theoretical Monotonic Moment-Curvature Relations, and Experimental Points for Unit 9

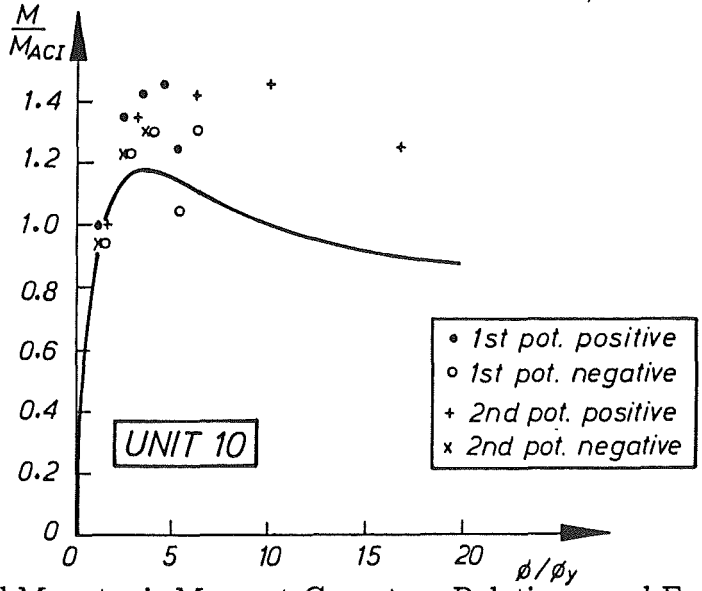

Figure 3.65: Theoretical Monotonic Moment-Curvature Relations, and Experimental Points for Unit 10

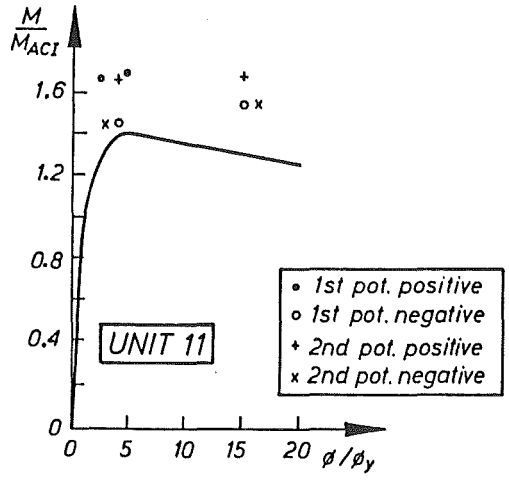

Figure 3.66: Theoretical Monotonic Moment-Curvature Relations, and Experimental Points for Unit 11

From the comparisons shown above, it is evident that although in some cases the theory under-estimated the experimental results, in general the theory is conservative.

3.10 Discussions of the Length of Confined Region of Column

3.10.1 New Zealand Code Recommended Length of Confined Regions of Columns

It is known that a sufficient length of column in plastic hinge regions needs to be adequately confined to ensure that the change of column flexural strength from the fully to nominal confined regions does not lead to failure of the column outside the confined region [7,8,14].

The current New Zealand concrete design code [2] specifies the length of confined regions of a column as follows:

- When $P_e/(\phi f'_c A_g) \leq 0.3$, not less than the larger of the longer cross section dimension in the case of a rectangular section, or the diameter in the case of a circular section, or where the moment exceeds 0.8 of the maximum moment at the critical section
- When $P_e/(\phi f'_c A_g) > 0.3$, not less than the larger of 1.5 times the longer cross section dimension in the case of a rectangular section, or 1.5 times the diameter in the case of a circular section, or where the moment exceeds 0.7 of the maximum moment at the critical section

The above requirements were determined from the assessment of test results [7,8]. The code indicates that the length increases with the axial load levels, due to the greater increase in flexural strength of the confined region which could lead to failure in the less confined adjacent region in columns with large axial compression. The bending moment used to determine the required length of confinement can be based on the assumption of a linear diagram with maximum moment at one end of the column and zero moment at the other end of the column in a storey. This conservative moment diagram was to take into account the effect of higher modes of vibration in a tall frame, which results in difficulty in predicting the bending moment diagram accurately.

3.10.2 Estimation of the Length of Confined Region Based on the Experimental Results

A great number of columns and piles have been tested at the University of Canterbury with the confined length as recommended by the code [2]. They consists of both solid [7,8,41,42,43,9,4,44,5], and hollow sections [3,4,45].

As mentioned previously however, the test of Unit 7 with axial compression of $P_e = 0.7f'_cA_g$, exhibited a region of damage up to 3 times column lateral dimension h, which is larger than the code [2] recommended region of $1.5h$. This indicated that the length of confined regions specified by the current code needs to be re-evaluated.

The required length of the confined regions can be examined using an approach, which considers the ratio of the enhancement of column flexural strength, due to concrete confinement and strain hardening of longitudinal reinforcement, to the code ideal flexural strength. Fig. 3.67 shows the assumed bending moment diagram of a column due to imposed lateral loads on the structure, and the flexural strengths of the confined and nominally confined regions of the column. To compensate for the effects of the spread of yielding due to possible diagonal tension cracking, the moment diagram is spread by $h/2$ (or $D/2$) along the member, where h=column depth (D=column diameter). The length of the region, which needs to be confined, can be estimated as follows. At the base, the column reaches its flexural strength with confinement. Outside the confined region, the code [2] calculated flexural strength is applicable. The portion of the column that needs to be confined can then be calculated from Eq. 3.16:

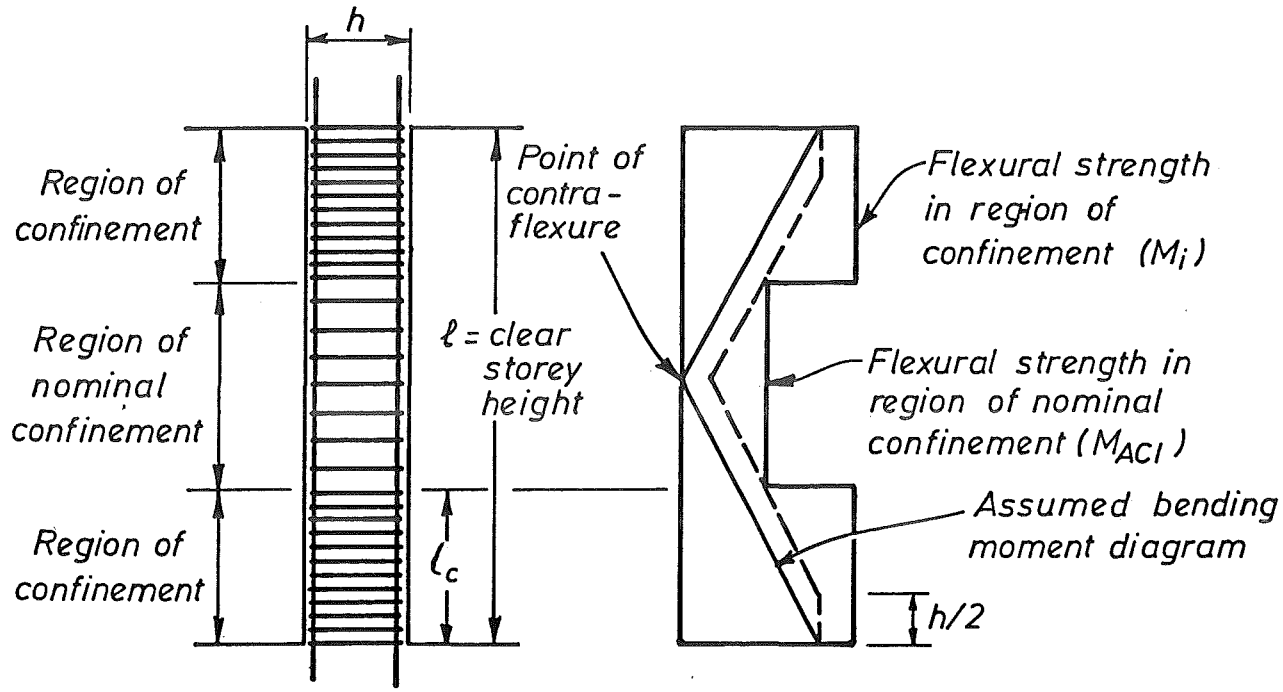

Figure 3.67: Typical Bending Moment and Flexural Strength of Column

$$l_c = \frac{l}{2}(1 - \frac{M_{ACI}}{M_i}) + \frac{1}{2}h \qquad (3.16)$$

Fig. 3.68 shows the relation of the level of column axial compression to the length of confined region l_c calculated using Eq. 3.16 for all the columns tests conducted at the University of Canterbury [7,8,41,42,43,9,4,44,5,3,4,45]. The code [2] recommendation is plotted as well. It is also obvious that the length l_c should increase with the axial load level. The other

parameters, such as the aspect ratio and the section type of the columns were found not to have a significant effect. The code recommended length was found to be insufficient for many columns, particularly for columns with large axial compression.

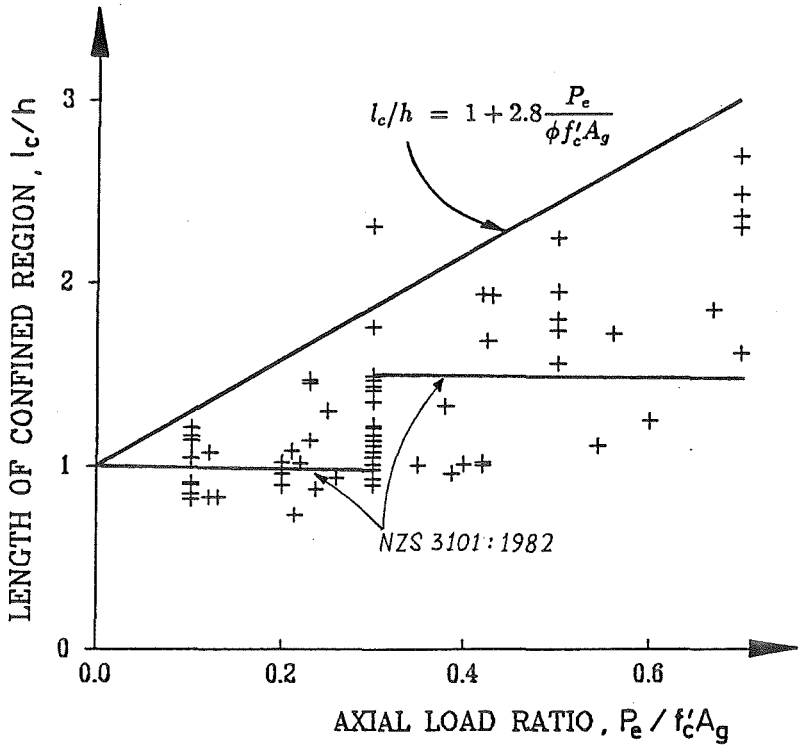

Figure 3.68: The Predicted Length of Confined Region of Columns Tested

A value for l_c which gives a safe length for most columns is:

$$\frac{l_c}{h} = 1 + 2.8\frac{P_e}{\phi f'_c A_g} \tag{3.17}$$

This gives values of $l_c = h$, and $3h$ for $P_e/(\phi f'_c A_g) = 0$ and 0.7, respectively. It is recommended that Eq. 3.17 be used in design.

3.11 Concluding Remarks

From the performance of the seven column units tested under combined cyclic flexure and constant axial load, the following conclusions can be drawn:

1. Column Units 5 and 6 with 400 mm square cross section, and column Unit 10 with 400 mm octagonal cross section, were subjected to axial compression of $P_e = 0.5 f'_c A_g$. The units which contained 38%, 19% and 44% of the confining reinforcement recommended by NZS 3101 [2] for ductile detailing, achieved real displacement ductility factors of μ_r=6.7, 5.4 and 9.8, respectively. Buckling of longitudinal bars occurred at the end of testing Units 5 and 6, and fracture of some spirals has terminated the test of Unit 10.

2. Column Units 7, 8, 9 with 400 mm square cross section, and column Unit 11 with 400 mm octagonal cross section, were subjected to an axial load level of $P_e = 0.7 f'_c A_g$. Units 7 and 8, which contained 48% and 34% of the code [2] recommended quantity of confining reinforcement for ductile detailing, achieved μ_r=6.3 and 4.0, respectively. Due to the large spacing of transverse reinforcement outside the plastic hinge regions, the hoops of Unit 7 were not capable of maintaining the strength of the column in this region. A damaged region of up to 1200 mm from the central stub was observed at the end of testing. Buckling of longitudinal bars in the plastic hinge region resulted in the termination of the test of Unit 8. Unit 9 which was designed to achieve ductile behaviour in accordance with design charts [4] and contained 93% of the code [2] recommended quantity of confining reinforcement for ductile detailing, demonstrated excellent performance. No significant degradation of strength was detected when the test was ended after completing cycles up to a nominal displacement ductility factor of 10. On the other hand, Unit 11, which contained 77% of the code quantity of confining reinforcement for ductile detailing, did not perform in a ductile manner. Buckling of longitudinal bars terminated the test of Unit 11.

3. Column Units 10 and 11 with octagonal cross sections, achieved lower stiffness and flexural strength than column Units 5 to 9 which had square cross sections, although they contained the same areas of longitudinal reinforcement. This was to be expected due to the shape of the concrete cross sections of the columns.

4. Comparisons of the experimental results and the theoretical predictions indicated that the refined cyclic moment-curvature theory and the design charts for ductility give sufficiently accurate and yet conservative predictions. This was more confirmed by the test results of Units 9 and 11. As mentioned in (2) above, Unit 9 with square cross section, and 93% of the code [2] recommended quantity of transverse confining reinforcement for ductile detailing, demonstrated ductile behaviour. Unit 11 with octagonal cross section, and 77% of the code recommended quantity of transverse reinforcement for ductile detailing, demonstrated limited ductile behaviour. These quantities were 70% and 44% of the quantities needed to achieve a curvature ductility factor of 20 according to the design charts for ductility [4]. It is evident that the design charts for ductility gives a more satisfactory prediction of the behaviour of columns, and therefore can be used to derive a refined design equation for the quantities of confining reinforcement in the potential plastic hinge region of a column.

5. The region of damage observed in Unit 7 indicated that the length of potential plastic hinge region to be confined for a column with very high axial compression, specified by the current code [2] as $1.5h$, is unconservative. For this type of column, the confined region needs to be extended to prevent failure of the column in the nominally confined region outside the code specified plastic hinge region. Based on the data obtained from the experiments, a recommendation for the length of the confined region is proposed as follows:

$$\frac{l_c}{h} = 1 + 2.8 \frac{P_e}{\phi f'_c A_g}$$

which gives values of $l_c = h$, and $3h$ for $P_e/(\phi f'_c A_g) = 0$ and 0.7, respectively.

Chapter 4

ANALYTICAL INVESTIGATION OF THE FLEXURAL DUCTILITY OF REINFORED CONCRETE COLUMNS LEADING TO A DESIGN EQUATION FOR THE QUANTITIES OF CONFINING REINFORCEMENT

4.1 Introduction

Zahn *et al.* [4] have conducted an analytical investigation of the quantities of confining reinforcement currently recommended by the New Zealand concrete design code NZS 3101:1982 [2] and found that the equations are unnecessarily conservative for columns with low to moderate axial compression.

Tests on columns conducted by Soesianawati *et al.* [5] have also shown that to achieve ductile behaviour when the axial load level is moderately small, the quantities of confining reinforcement specified by the code [2] can be substantially reduced. In those tests, two columns with square cross sections, with axial load levels of $0.1f'_cA_g$ and $0.3f'_cA_g$, containing about one-half of the code recommended quantities, were found to perform in a ductile manner.

The analytical investigation by Zahn *et al.* [4] also indicated that the code equations may be unconservative when the axial load level is high. Due to a larger neutral axis depth, the internal forces providing the moment of resistance depend more strongly on the contribution of concrete which must be more effectively confined.

It is evident, that the NZS 3101 [2] equations for the quantities of confining reinforcement need to be related more strongly to the level of axial compression loads.

Based on the design charts for ductility by Zahn *et al.* [4], an analytical investigation was carried out to derive a refined design equation for the quantities of confining reinforcement required in the potential plastic hinge regions of columns.

4.2 Parameters Investigated

It is widely known that the quantity of confining reinforcement provided in the potential plastic hinge regions of columns has a significant effect on the available curvature ductility factors of columns.

The concrete design code NZS 3101:1982 [2] specifies quantities of confining reinforcement in potential plastic hinge regions which are intended to ensure that columns have *adequate ductility*. A commonly quoted criterion for *adequate ductility* of columns is the ability to sustain a curvature ductility factor φ_u/φ_y of approximately 20. This order of curvature ductility should enable the plastic hinges at the bases of columns of multistorey moment-resisting ductile frames to develop beam sidesway mechanisms, and in the columns of one and two storey moment-resisting ductile frames developing column sidesway mechanisms, to undergo sufficient plastic rotation for frames to reach a displacement ductility factor of 4 to 6, as is implied by the level of seismic design loading for ductile structures specified by NZS 4203:1984 [30].

In this study, at the potential plastic hinge regions, a curvature ductility factor of φ_u/φ_y=20 is considered to be necessary for columns of ductile frames, and φ_u/φ_y=10 is considered for columns of frames where limited ductility, as defined by NZS 4203 would be sufficient.

A full range of parameters which has a significant influence on the available curvature ductility factors of columns was examined. These included the axial load ratio $P_e/(f'_cA_g)$, the concrete compressive strength f'_c, the mechanical reinforcing ratio $\rho_t m$ and the cover ratio c/h for square and rectangular columns, or c/D for circular columns, where c=concrete cover thickness. The range of the parameters considered is shown in Table 4.1.

The range of axial load levels of columns investigated was 0.2 to $0.7f'_cA_g$. For the axial load levels less than $0.2f'_cA_g$, most of the charts indicate no apparent limit to the curvature ductility factors available in columns, since for lightly loaded columns, the role of confining reinforcement to increase the available curvature ductility of columns is insignificant. Transverse reinforcement to prevent buckling of compression steel and to provide shear resistance is a more critical consideration.

The concrete compressive strengths of 20, 30 and 40 MPa were investigated. These strengths of concrete are widely used in design.

According to the concrete design code [2], the lower and upper limits of the ratio of area of longitudinal reinforcement $\rho_t = A_{st}/A_g$ are of 0.008 and 0.06, respectively. For yield strengths of longitudinal reinforcement of f_y=275 and 380 MPa and for concrete compressive strengths of f'_c=20 and 40 MPa, the lower and upper limits of the mechanical reinforcing ratio $\rho_t m$ are 0.065 and 1.34, respectively, where $m = f_y/0.85f'_c$.

Table 4.1: Parameters Investigated in the Derivation of a Refined Design Equation for the Quantities of Confining Reinforcement Required in Columns

	Description	Range Investigated
$P_e/(f'_c A_g)$	Axial Load Ratio	0.2 to 0.7
f'_c	Concrete Compressive Strength	20 to 40 MPa
$\rho_t m$	Mechanical Reinforcing Ratio	0.1 to 0.4
c/h	Cover Ratio	0.02 to 0.08 for square and rectangular columns
or		
c/D		0.06 for circular columns

The range of $\rho_t m$ investigated was 0.1 to 0.4. In some cases, for columns with $\rho_t m$ less than 0.1, a huge amount of confining reinforcement must be provided in the potential plastic hinge regions to achieve adequate ductility, since the ductility of columns depends significantly on the concrete which has brittle characteristics unless the concrete is well confined by closely spaced transverse reinforcement. When the value of $\rho_t m$ of a column is very high, steel congestion problems may arise, and a bigger size of column is preferred to reduce the value of $\rho_t m$. Moreover, the ductility of columns with large $\rho_t m$ depends more on the longitudinal reinforcement provided and thus the role of confining reinforcement is not as critical as for columns with smaller values of $\rho_t m$. Hence, it was decided to investigate only the range of $\rho_t m$ listed in Table 4.1.

The minimum concrete cover thickness required by the code [2] for ties, stirrups and spirals in beams and columns is 40 mm when the concrete is cast against and permanently exposed to weather, or 25 mm when the concrete is not exposed to weather. Also, the most commonly used section depth (or diameter) of columns in design is between 350 and 1500 mm. Thus, the range of the lower and upper limits of the cover ratio is 0.017 to 0.11. In this investigation, cover ratio c/h of 0.02, 0.06 and 0.08 were examined for square and rectangular columns. It was shown previously [4] that for square columns with c/h of 0.1, the flexural strength reduced quite markedly when the compressive strain of concrete at the extreme fibre reached the assumed spalling strain of 0.005.

Since the design charts for circular columns were only available for a cover ratio of $c/D = 0.06$, only this cover ratio was considered for circular columns in this investigation. However, it was found that a smaller cover ratio resulted in larger available φ_u/φ_y.

The yield strength of the longitudinal reinforcement in the investigation was held constant at 275 MPa. It was shown in the previous studies [4,45] that a change in the yield strength of the longitudinal reinforcement f_y was found to have an insignificant effect on the available curvature ductility factor of columns providing that the shape of the stress-strain curves was similar. That is, providing that the longitudinal steel has the same values for the ratios of f_{su}/f_y, ϵ_{sh}/ϵ_y and the same value for ϵ_{su} (see Fig. 4.1). The currently used New Zealand

Grade 380 steel has quite a different shape of stress-strain curve from that of Grade 275 steel (see Fig. 4.2). However, as illustrated in Fig. 4.3, the new micro-alloy Grade 380 steel manufactured in New Zealand does have a similar shape of stress-strain curve, and approximately the same ratios for f_{su}/f_y, ϵ_{sh}/ϵ_y as Grade 275 steel [46].

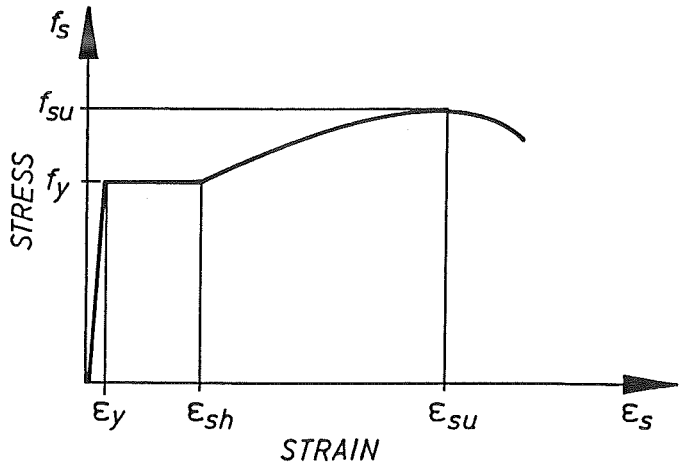

Figure 4.1: Typical Stress-Strain Curve for Reinforcing Steel

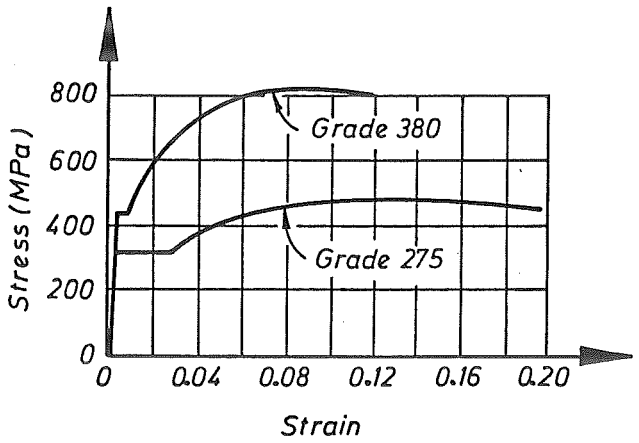

Figure 4.2: Typical Stress-Strain Curves for Grades 275 and 380 Reinforcing Steel

It was also shown [4] that the stress-strain curves for concrete confined by Grades 380 and 275 spirals are almost identical providing that the ratio of confining stress to concrete strength f_r/f_{co} and the spiral pitch s_h are similar. The earlier strain hardening of Grade 380 steel was found to have no significant effects on the stress-strain curves of confined concrete. That is, the yield force of the confining reinforcement is the most important parameter, and variation in the yield strength but with constant yield force will not change the effectiveness of confinement. Hence, the greater the yield strength, the smaller the quantity of confining reinforcement required. However, because a smaller volume of Grade 380 confining reinforcement can be used to provide the required confining stress, Grade 380 hoops or spirals are likely to fracture earlier than when using a larger volume of Grade 275 reinforcement. In this study, the yield strength of the confining reinforcement was held constant at 275 MPa.

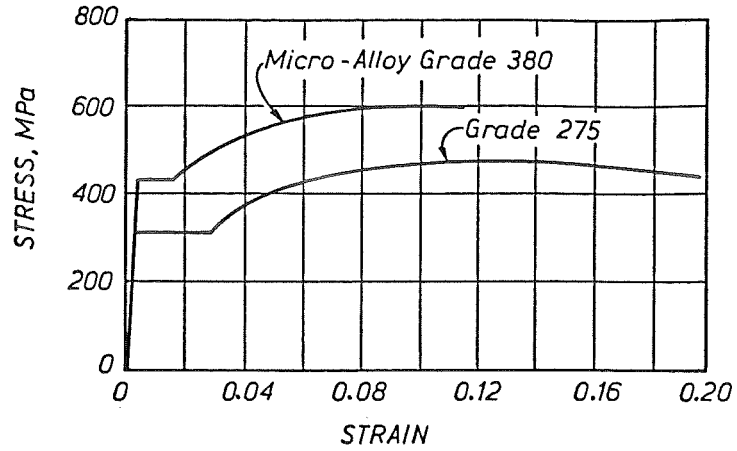

Figure 4.3: Typical Stress-Strain Curves for Grades 275 and Micro-Alloy 380 Reinforcing Steel

Fig. 4.4 shows the types of section investigated. These are circular, square, and rectangular sections with an aspect ratio of 1.5 and bending about both axes. Sets of overlapping hoops as shown in Fig. 4.4 were used as confining reinforcement for the square and rectangular sections. It has been demonstrated [14] that these hoop arrangements are more efficient than sets of overlapping rectangular hoops.

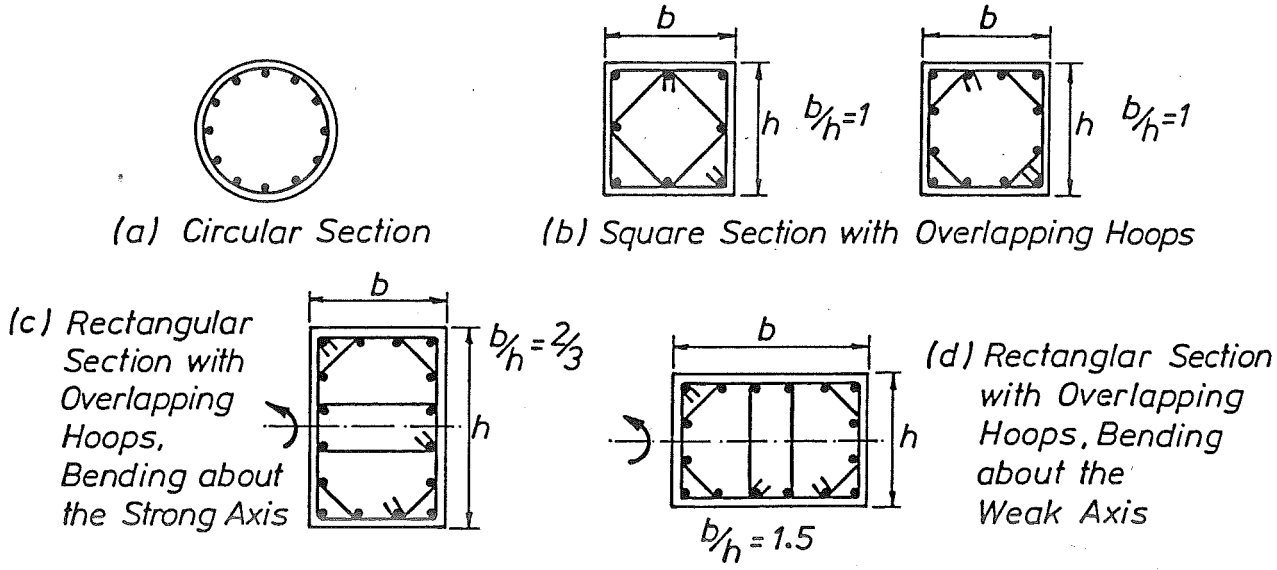

Figure 4.4: Types of Section Investigated

4.3 Design Charts for Ductility

4.3.1 Background

The New Zealand concrete design code NZS 3101:1982 [2] specifies that the volumetric ratio of confining reinforcement required in the potential plastic hinge regions of columns in seismic design should be not less than

$$\rho_s = q(\frac{f'_c}{f_{yh}})(0.5 + 1.25\frac{P_e}{\phi f'_c A_g}) \tag{4.1}$$

where $q = 0.12$ or $0.3k(A_g/A_c - 1)$, whichever is greater.

For rectangular hoop reinforcement with or without supplementary cross ties, $\rho_s = A_{sh}/(s_h h")$ and $k = 1.0$. For spiral or circular hoop reinforcement, $\rho_s = 4A_b/(s_h d_g)$ and $k = 1.5$. The notation in Eq. 4.1 is defined as follows: A_{sh} is total effective area of hoop bars in the direction under consideration, A_b is area of spiral or circular hoop, s_h is centre-to-centre spacing of hoop sets, $h"$ or d is dimension or diameter of core concrete measured to the outside of perimeter hoops or spirals, A_g is gross area of column cross section, A_c is area of concrete core of section measured perpendicular to the direction under consideration, and to the outside of peripheral hoop, f'_c is concrete compressive strength, f_{yh} is yield strength of hoops or spirals, P_e is axial compressive load due to design gravity and seismic loading and ϕ is strength reduction factor.

As mentioned previously, the code [2] equations for confining reinforcement, which were derived from theoretical monotonic moment-curvature analyses for a range of column cross sections with different axial load compression, is aimed at ensuring an available curvature ductility factor of at least 20 [14]. However, laboratory tests and recent theoretical studies conducted at the University of Canterbury (see for example Refs. [14,3,4]), have shown that columns subjected to high axial compression loads and cyclic flexure may undergo a deterioration of flexural strength. The theoretical work has greatly improved the understanding of the interaction between the confining reinforcement and the confined core concrete. In particular, the refined cyclic stress-strain models developed by Mander *et al.* [3], for steel and confined concrete, have provided an accurate basis to model analytically the behaviour of columns during cyclic flexure.

In addition, Mander *et al.* [3] have proposed an *energy balance* approach to predict the stage of hoop or spiral bar fracture. The approach reflects the principle that the lateral expansion of core concrete at large compression strains is passively resisted by confining reinforcement, which has to follow that expansion, thus absorbing strain energy. The increase in the strain energy capacity of compressed concrete due to confinement is equivalent to the strain energy stored by the confining reinforcement as it yields in tension. Hoop or spiral fracture occurs when the strain energy stored in the compressed concrete, plus the additional strain energy required to yield the longitudinal reinforcement in compression, is equal to the strain energy capacity of the confining reinforcement.

The strain energy of concrete is equal to the difference in area between the stress-strain curves for confined and unconfined concrete up to the longitudinal strain at first hoop fracture (see

the shaded area in Fig. 4.5) multiplied by the volume of confined concrete. The strain energy of the longitudinal reinforcement is equal to the area under the compression stress-strain curve of that steel up to the longitudinal strain at first hoop fracture, multiplied by the volume of that steel. The strain energy capacity of the confining reinforcement is equal to the area under the stress-strain curve of the confining steel up to the fracture strain multiplied by the volume of that steel confining the concrete. If the strain energy accumulated in a hoop or spiral bar over a number of curvature cycles in the inelastic range has reached the strain energy absorption capacity of the transverse reinforcement, causing it to fracture, the section may be considered to be at an ultimate limit state, since the concrete is no longer effectively confined. The longitudinal strain of concrete at this stage can be considered to be the ultimate strain.

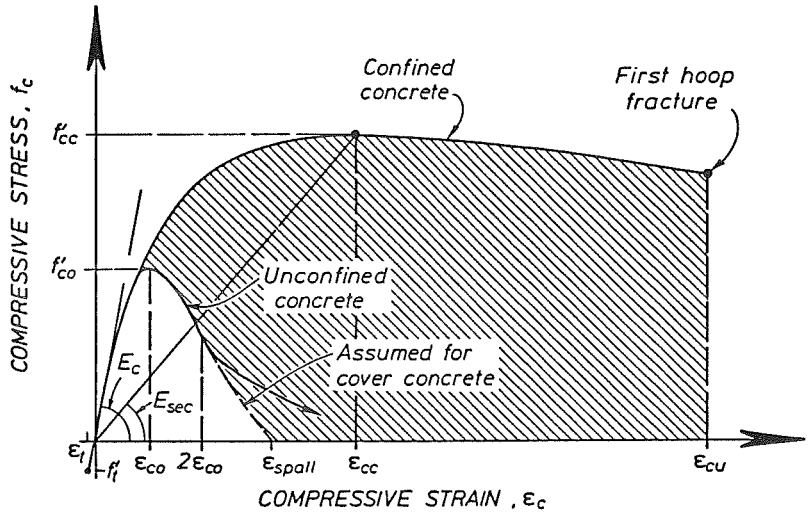

Figure 4.5: Typical Compressive Stress-Strain Curves for Confined and Unconfined Concrete

It is evident that the possible reduction in the flexural strength of columns during cyclic flexure, and the possible fracture of confining reinforcement due to an accumulation of strain energy as a result of cyclic loading, may have a major effect on the available curvature ductility of a column. Therefore, it was considered necessary to derive design charts from cyclic moment-curvature analyses rather than from monotonic moment-curvature analyses. A computer program developed by Mander *et al.* [3], which takes these effects into account was modified to include a set of criteria to determine whether the section is at an ultimate limit state.

4.3.2 Assumptions and Definitions Used in the Design Charts for Ductility

For the preparation of the design charts [4,47], some assumptions and definitions have been made. These are described in the following sections.

Curvature History and Available Ultimate Curvature

It has been observed that the available ductility of a member depends on the imposed curvature history. The ultimate curvature resulting from monotonic flexure will be greater than that resulted from cyclic flexure with full reversals. It is therefore necessary to define a suitable standard curvature history to measure the available curvature ductility of a column. Moment-curvature analysis which shows a relation between the quantity of confining reinforcement and the available curvature ductility must then follow the standard curvature history. Cyclic stress-strain models for concrete and steel must also be incorporated in the analysis.

A sequence of four identical cycles of imposed bending moment, to curvatures of equal magnitude in both positive and negative directions, was adopted [4] as a standard by which the available curvature ductility factor of a column section is measured. The section is considered to have achieved its ultimate curvature when one or more of the following ultimate limit state conditions is reached:

- The moment reached at either positive or negative curvature peak of the last cycle has reduced to 0.8 M_i, where M_i is the ideal flexural strength of the section (see Fig. 4.6)
- The strain energy accumulated in the confining reinforcement at the end of the fourth cycle is equal to its strain energy absorption capacity and it fractures (see Fig. 4.7)
- The longitudinal reinforcing steel fractures or buckles

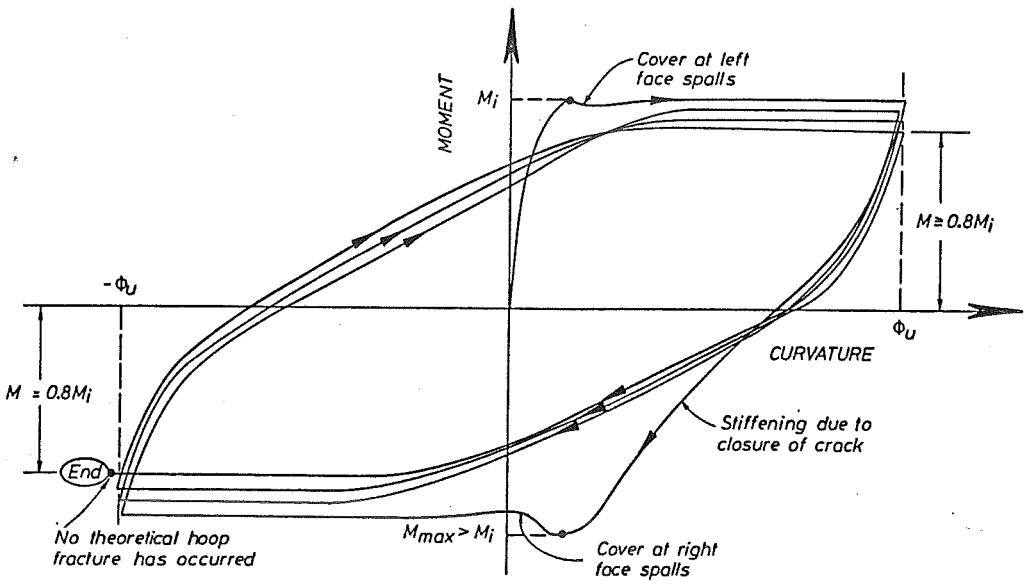

Figure 4.6: Theoretical Cyclic Moment-Curvature Relation of a Column where Moment Deterioration Governs the Available Ultimate Curvature

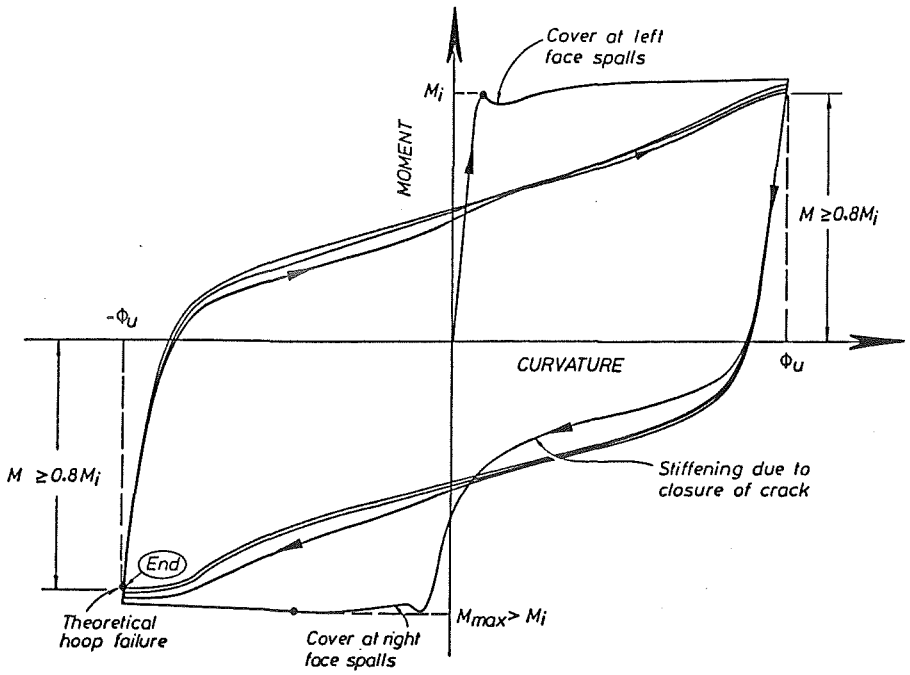

Figure 4.7: Theoretical Cyclic Moment-Curvature Relation of a Column where Hoop Fracture Governs the Available Ultimate Curvature

The peak curvature when one or both of the above conditions applies is defined as the available ultimate curvature, φ_u.

The criterion of four loading cycles to a particular ductility level without the flexural capacity reducing by more than 20% is similar to that stated in the NZS 4203:1984 [30].

Before commencing the analysis, it is not known whether four cycles to a particular curvature peak, φ_{peak}, will produce the ultimate limit state as defined above. The available ultimate curvature has to be determined by an iterative process. The section is analysed for the standard sequence of four cycles to the first estimate of φ_{peak}. If the ultimate limit conditions are not satisfied, the entire cyclic analysis is repeated with an improved estimation of φ_{peak} until one or more of the ultimate limit state conditions is reached, indicating that the final value of φ_{peak} is equal to the available ultimate curvature, φ_u.

In conducting this analysis, no explicit limitations were imposed on the longitudinal steel strains. It was found from the tests [4] that at the levels of ultimate curvature required in design, fracture of longitudinal bars in tension did not occur. Also, premature buckling of the bars in compression can be suppressed by ensuring that the transverse reinforcement provided in the potential plastic hinge regions of columns satisfies the code [2] requirements for stability of longitudinal compression bars (that is, a spacing not greater than six times longitudinal bar diameter), and for restraint of longitudinal bars (that is a tie force not less than one sixteenth of the force in the compressed longitudinal bar being tied, at 100 mm centres).

Yield Curvature, Yield Moment and Ideal Moment

As defined in Chapter 3 (refer to Section 3.9.2), the yield curvature is obtained by extrapolating a straight line joining the origin with the point (φ_y',M_y'), as shown in Fig. 4.8.

Hence

$$\varphi_y = \frac{M_i}{M'_y}\varphi'_y \tag{4.2}$$

where φ'_y and M'_y are the curvature and the corresponding moment calculated at the stage when the steel at the extreme tensile fibre of the section reaches yield or when the concrete compressive strain at the extreme fibre reaches 0.002, whichever occurs first. This definition of first yield was preferred to that when the steel first yields only. In columns with high axial compression loads, the tension steel will normally not yield until the section has lost a considerable amount of flexural stiffness. The curvature corresponding to when the concrete compressive strain at the extreme fibre reaches 0.002 in columns with high axial compression loads is equivalent to the curvature corresponding to first yield of the tension steel in columns with low axial compression loads.

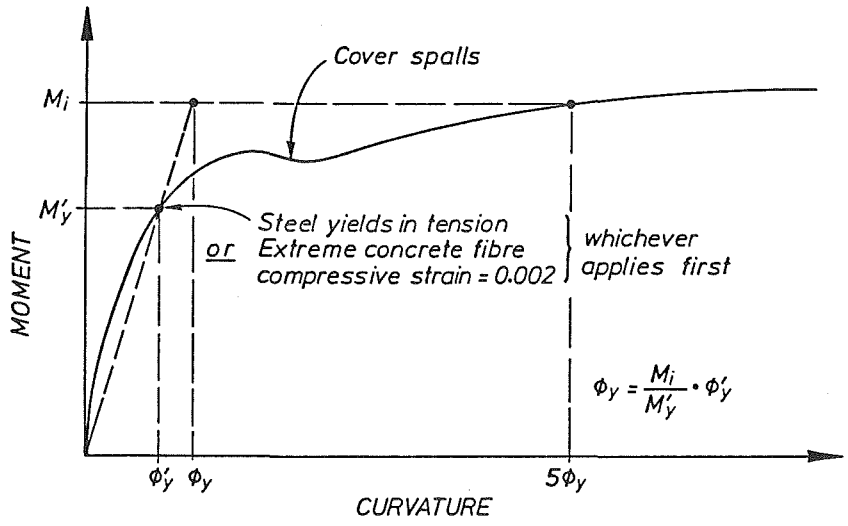

Figure 4.8: Definitions of Yield Curvature φ_y, Yield Moment M'_y, and Ideal Moment M_i

The ideal moment M_i is defined as the maximum moment reached in the initial (positive) half cycle before the section curvature exceeds five times the yield curvature. This means that any strength enhancement of concrete due to confinement is taken into account in the calculation of M_i, but strain hardening of longitudinal reinforcement has not usually commenced at that stage.

Material Properties Assumed for Concrete

For columns, the compressive strength of unconfined concrete f'_{co} loaded at a quasi-static strain rate is assumed to be equal to $0.85f'_c$ and its corresponding strain ϵ_{co} is taken as 0.002. The initial tangent modulus E_c is equal to $5000\sqrt{f'_c}$ (MPa).

The cover concrete is assumed to cease carrying load once the compressive strain has exceeded the assumed spalling strain of 0.005.

The tensile strength of concrete is neglected once the modulus of rupture of concrete of $f_t' = 0.6\sqrt{f_c'}$ (MPa) has been exceeded.

The cyclic stress-strain model proposed by Mander *et al.* [3] for confined and unconfined concrete is used (see Fig. 4.5). The monotonic stress-strain curve is given by

$$f_c = \frac{f_{cc}' x r}{r - 1 + x^r} \tag{4.3}$$

in which

$$x = \frac{\epsilon_c}{\epsilon_{cc}} \tag{4.4}$$

$$r = \frac{E_c}{E_c - E_{sec}} \tag{4.5}$$

$$E_c = 5000\sqrt{f_c'} \tag{4.6}$$

$$E_{sec} = \frac{f_{cc}'}{\epsilon_{cc}} \tag{4.7}$$

where f_{cc}' and ϵ_{cc} are the maximum strength and the corresponding strain of confined concrete, and have to be determined.

As indicated by Mander *et al.* [3], the most significant parameter affecting the shape of confined concrete stress-strain curve is the effective confining stress f_l' provided by confining reinforcement. The efficiency of the various possible arrangements of transverse reinforcement was taken into account by defining a confinement effectiveness coefficient k_e. Mander *et al.* determined the value of k_e for various section shapes with various confining steel configurations as follows:

For sections confined by circular hoops :

$$k_e = \frac{(1 - 0.5s'/d_c)^2}{1 - \rho_{cc}} \tag{4.8}$$

For sections confined by spirals :

$$k_e = \frac{1 - 0.5s'/d_c}{1 - \rho_{cc}} \tag{4.9}$$

For rectangular sections :

$$k_e = \frac{(1 - 0.5s'/b_c)(1 - 0.5s'/h_c)(1 - \sum_{i=1}^{n} \frac{w_i'^2}{6b_c h_c})}{1 - \rho_{cc}} \tag{4.10}$$

where s' is the clear spacing between hoop sets or spiral bars, w_i' is the clear spacing between longitudinal bars supported by the corner of a hoop or by a cross tie, d_c is the core diameter of a section confined by a circular hoop or spiral, b_c and h_c are the core dimensions of a rectangular section, and ρ_{cc} is the volumetric ratio of the longitudinal steel with respect to the confined core concrete. All core dimensions are measured to the centre-line of the perimeter hoop or spiral. The counter n in Eq. 4.10 is the number of arches between longitudinal bars in the plane of a rectangular section, and is equal to the number of longitudinal bars (or bundles of bars) supported by the corner of a hoop or by a cross tie. The notation is illustrated in Fig. 4.9.

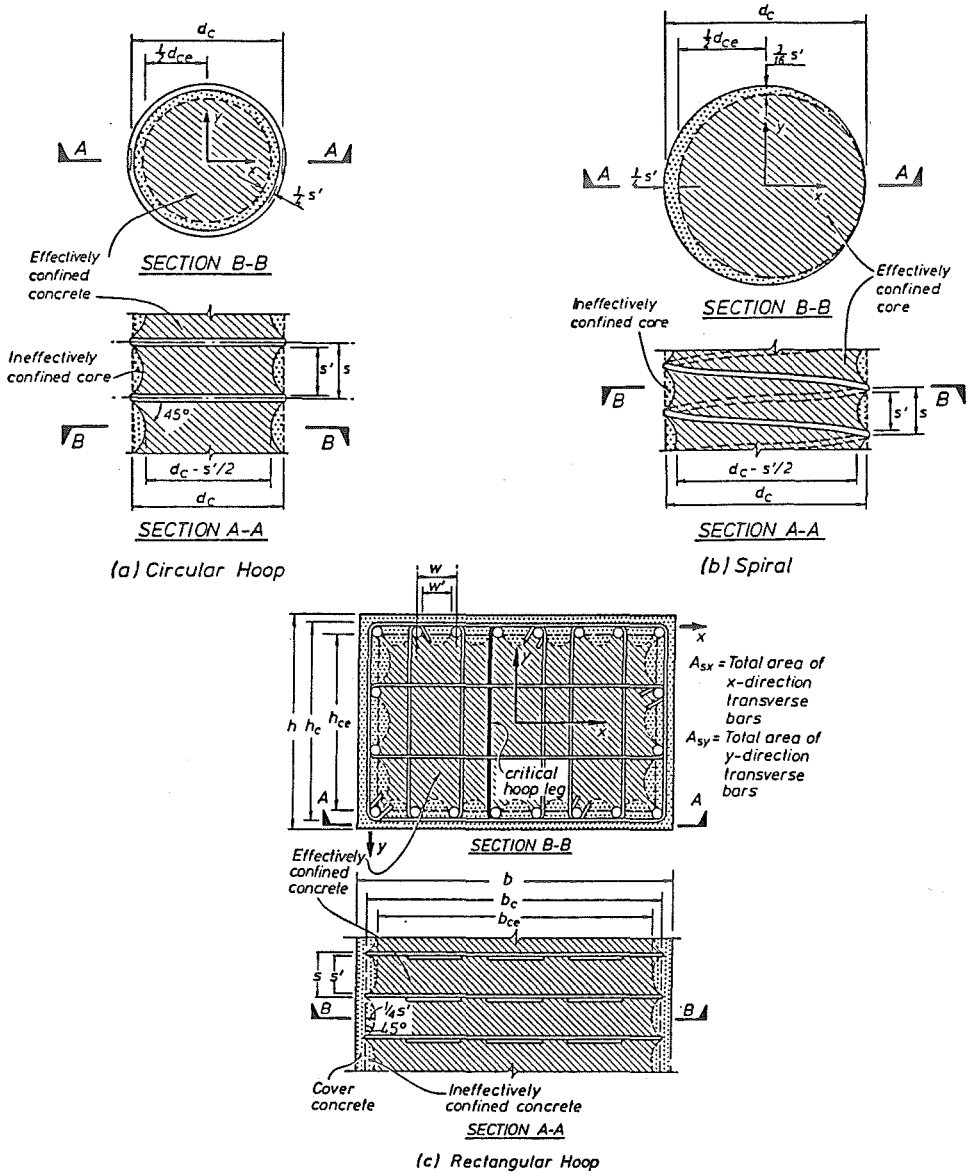

Figure 4.9: Confined Core Concrete of Column Sections

To determine the enhancement of concrete compressive strength due to the effective confining stress f_l', Mander *et al.* [3] evaluated an ultimate strength surface given by a model suggested by Willam and Warnke [48]. This model predicts the ultimate strength surface of concrete in triaxial compression with unequal lateral confining pressures. The results of the calculations are conveniently presented diagrammatically in Fig. 4.10, which can be used to read off the value of $k_{cc} = f_{cc}'/f_{co}'$ for any set of dimensionless confining stresses f_{lx}'/f_{co}' and f_{ly}'/f_{co}' in two perpendicular directions of a rectangular section. It is worth noting that in the figure, $f_{lx}' \geq f_{ly}'$.

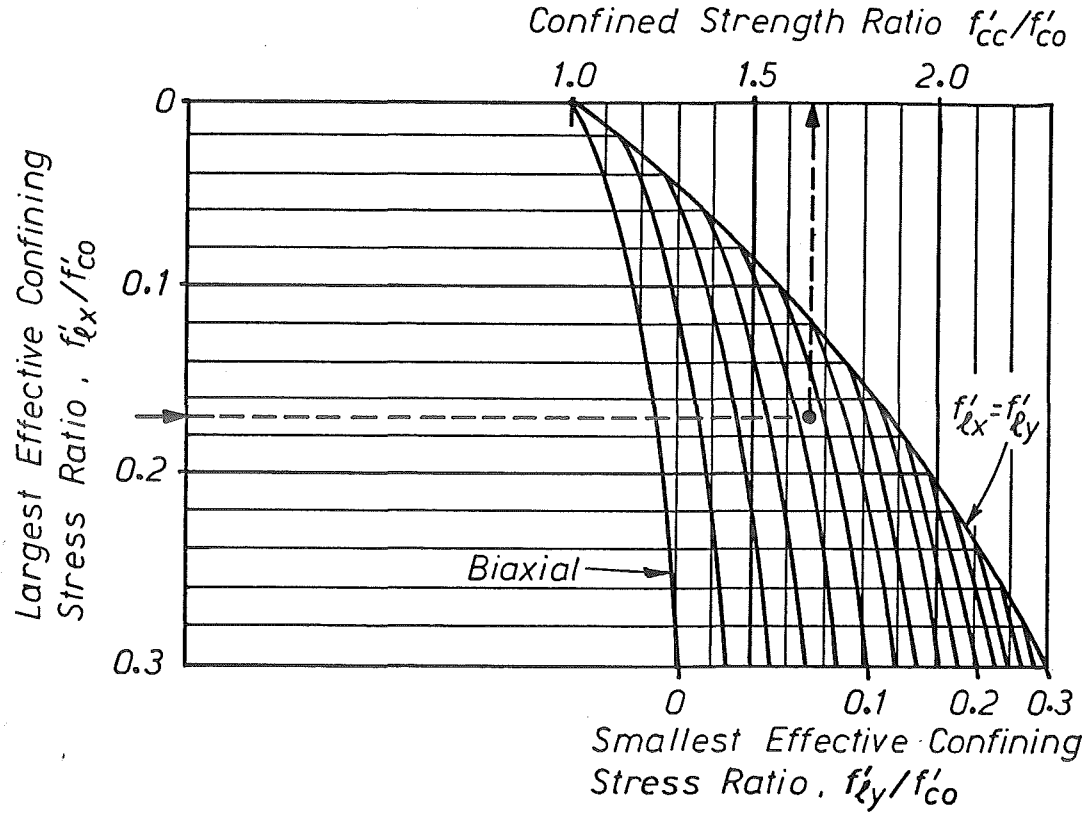

Figure 4.10: Determination of the Strength of Confined Concrete from the Effective Confining Stresses

For equal effective confining stresses in both directions, that is $f_{lx}' = f_{ly}' = f_l'$, as in the case of circular sections confined by spirals or circular hoops, or most square sections, Fig. 4.10 contains a curve which is explicitly described as follows:

$$k_{cc} = \frac{f_{cc}'}{f_{co}'} = -1.254 + 2.254\sqrt{1 + 7.94\frac{f_l'}{f_{co}'}} - 2.0\frac{f_l'}{f_{co}'} \tag{4.11}$$

It was shown [4] that Eq. 4.11 gives a good approximation for cases where $f_{lx}' \neq f_{ly}'$ by substituting $f_l' = \frac{1}{2}(f_{lx}' + f_{ly}')$, providing that the ratio of f_{lx}'/f_{ly}' is between 0.4 and 2.5.

The radial confining stress f_l and the transverse confining stresses in x and y directions, f_{lx} and f_{ly} are calculated as in Fig. 4.11. Then the effective confining stresses are given by:

For circular sections:

$$f_l' = k_e f_l = \frac{1}{2} k_e \rho_s f_{yh} \tag{4.12}$$

where ρ_s is volumetric ratio of spiral or circular hoop to confined concrete=$4A_b/(s_h d_c)$, and f_{yh} is yield strength of confining reinforcement.

For rectangular sections:

$$f_{lx}' = k_e f_{lx} = k_e \rho_{sx} f_{yh} \tag{4.13}$$

$$f_{ly}' = k_e f_{ly} = k_e \rho_{sy} f_{yh} \tag{4.14}$$

where ρ_{sx} and ρ_{sy} are the volumetric ratios of effective confining reinforcement in x and y directions, and are calculated as follows:

$$\rho_{sx} = \frac{A_{sx}}{s_h h_c} \tag{4.15}$$

$$\rho_{sy} = \frac{A_{sy}}{s_h b_c} \tag{4.16}$$

where A_{sx} and A_{sy} are the effective areas of x-direction and y-direction transverse bars, respectively (see Fig. 4.9c).

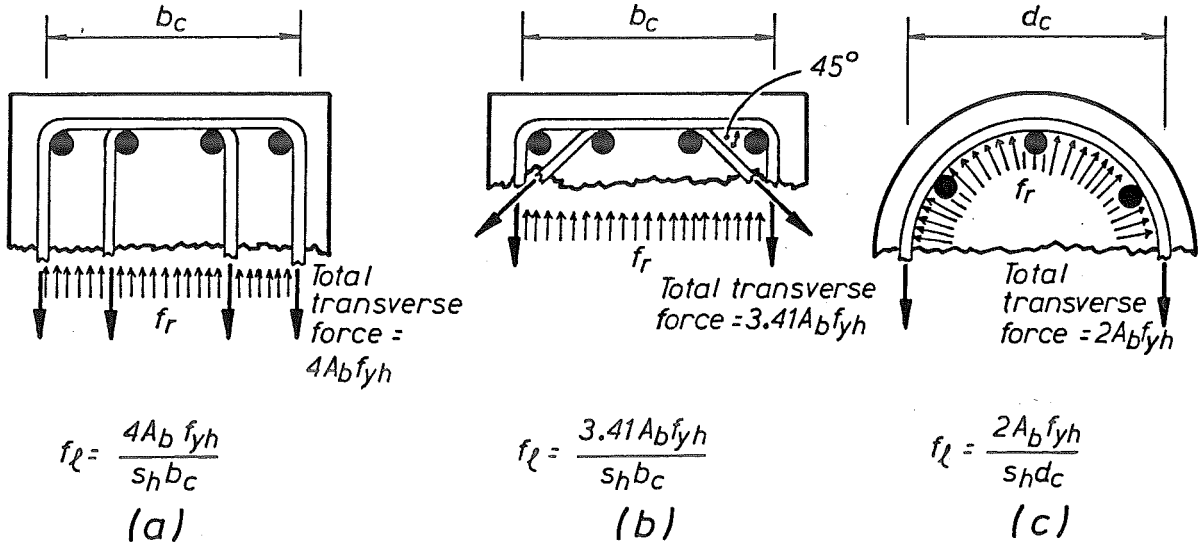

Figure 4.11: Confining Stresses Provided by Different Arrangements of Transverse Reinforcement

Once k_{cc} has been determined, the value of ϵ_{cc} can be obtained from the following expression:

$$\epsilon_{cc} = \epsilon_{co}(1 + R(k_{cc} - 1)) \tag{4.17}$$

where $R = (\epsilon_{cc} - \epsilon_{co})/(f'_{cc} - f'_{co})$ is the ratio of strain increase to stress increase at the peak strength of confined concrete, due to confinement and is assumed to be 5.

It should be noted that the value of $R = 5$ was calibrated from the experimental results of concentrically loaded specimens. When only a part of section is in compression, Zahn *et al.* [4] suggested that a smaller value of R (say $R = 3$) would be more appropriate.

Alternatively, instead of using a smaller value for the parameter R to allow for the smaller efficiency of confining reinforcement when a strain gradient exists, Zahn *et al.* [4] considered that it would be more logical to refine the definition of the efficiency factor k_e, from that defined by Mander *et al.* [3].

The parameters examined in this study, which are expected to have an influence on the efficiency of a particular arrangement of confining reinforcement, were similar to those examined previously [3], namely:

- The form of confining reinforcement, i.e. spirals, circular hoops, or sets of rectangular hoops with or without cross ties;
- The spacing of spiral or hoop bars along the column axis;
- The spacing of longitudinal bars across the section that are effectively restrained from buckling by transverse bars;
- The ratio of hoop bar spacing to longitudinal bar diameter.

In addition, the proportion of the section area in compression was taken into account by considering only the compressed part of core area when calculating the efficiency factor. The ratio of effectively confined area to overall core area hence becomes smaller. In this case, the ratio of the first moment of areas rather than the areas themselves should be used in defining the efficiency factor [4]. As an approximation, the moment could be taken about the centroidal axis of the section. The modified k_e, which is denoted as k_e^*, is calculated as:

$$k_e^* = \frac{S_{ce}}{S_{cc}} \tag{4.18}$$

where S_{ce} and S_{cc} are the first moment of effectively confined core area and total core area of concrete about the centroidal axis of the section, respectively.

For circular sections confined by circular hoops or spirals:

$$k_e^* = \frac{(1 - 0.5\alpha)^3}{1 - (\rho_{cc} + g'^2)^{1.5} + g'^3} \tag{4.19}$$

For square and rectangular sections:

$$k_e^* = \frac{(1-0.5\alpha)^2(\beta-0.5\alpha)}{\beta(1-1.6g'\rho_{cc})}\left[1-\frac{8(0.58+0.11g')}{\beta}\left(\frac{w_i'}{h_c}\right)^2+\frac{0.93}{\beta}\left(\frac{w_i'}{h_c}\right)^3\right] \quad (4.20)$$

where $\alpha = s'/d_c$ for circular sections, or s'/h_c for square and rectangular sections, $\beta = b_c/h_c$, g'=distance between the centres of longitudinal bars in the extreme faces divided by the core dimension, and the other notation is similar to that defined previously.

The term outside the rectangular brackets in Eq. 4.20 allows for the arching between hoop levels, and can be taken as unity when the centre-to-centre hoop spacing s_h is not greater than four times the diameter of longitudinal bars.

The effective radial confining stress provided by circular hoops or spirals is now given by:

$$f_r = \frac{1}{2}k_e^*\rho_s f_{yh} = 2\frac{A_b f_{yh}}{s_h d_c}k_e^* \quad (4.21)$$

and the effective confining stresses in rectangular sections in x and y directions are given by:

$$f_{rx} = k_e^*\frac{A_{sx}}{s_h h_c}f_{yh} = k_e^*\frac{X_{eff}A_b}{s_h h_c}f_{yh} \quad (4.22)$$

$$f_{ry} = k_e^*\frac{A_{sy}}{s_h b_c}f_{yh} = k_e^*\frac{Y_{eff}A_b}{s_h b_c}f_{yh} \quad (4.23)$$

where A_b is the area of transverse bar, X_{eff} and Y_{eff} are the effective number of transverse bars in the x and y directions, respectively, each with area A_b.

As with the previous examination of f_l', if the values of the effective confining stresses in each direction f_{rx} and f_{ry} are different, the average value of f_{rx} and f_{ry} may give a good estimation of the confined concrete properties, providing that the ratio of f_{rx}/f_{ry} is between 0.5 and 2.0. The average effective confining stress is then

$$f_r = \frac{1}{2}(f_{rx}+f_{ry}) = \frac{1}{2}\frac{A_b f_{yh}}{s_h}k_e^*\left(\frac{X_{eff}}{h_c}+\frac{Y_{eff}}{b_c}\right) \quad (4.24)$$

The ratio of f_r/f_{co} is the main parameter in the moment-curvature analyses conducted to develop the design charts for ductility.

The effective confining stresses given by Eqs. 4.21 to 4.24 were used in this study.

Material Properties Assumed for Steel

A cyclic stress-strain model for steel proposed by Mander *et al.* [3] was used in the moment-curvature analysis. A complete description of the model can be found in Chapter 2 of Ref. [3].

A standard skeleton curve for Grades 275 and 380 deformed steel bars had to be established, and the following parameters are needed for both monotonic tension and compression:

- yield strength, f_y
- Young's modulus, E_s
- strain hardening strain, ϵ_{sh}
- tangent modulus when the strain hardening commences, E_{sh}
- ultimate stress, f_{su} and
- ultimate strain ϵ_{su}.

The specified values of yield strengths of 275 MPa and 380 MPa were used, although these are somewhat conservative. For the other parameters in tension, the average values obtained from a number of specimens tested at the University of Canterbury in recent years were used. The values used to define the skeleton stress-strain curve for steel in tension are summarized in Table 4.2.

Table 4.2: Parameters for the Skeleton Stress-Strain Curve for Steel in Tension

	Grade 275	Grade 380
f_y (MPa)	275	380
E_s (MPa)	204000	204000
ϵ_{sh}	0.022	0.010
E_{sh} (MPa)	4900	8800
f_{su} (MPa)	420	615
ϵ_{su}	0.20	0.15

As investigated by Mander *et al.* [3], the parameters obtained from tensile testing do not precisely describe the skeleton curve in compression, due to the reduced ultimate strain and stress of steel in compression, resulting from inelastic buckling. However, an approach was suggested to calculate the parameters necessary to describe the compression skeleton curve. Table 4.3 summarizes the values adopted to define the skeleton stress-strain curve, for steel in compression assuming that the longitudinal bars are effectively braced by spiral bars, rectangular hoops, or cross ties at $4d_b$ centres, where d_b is the diameter of longitudinal bars. It should be noted that s/d_b=4 is the lower bound of range of spiral or hoop spacings used in design.

Table 4.3: Parameters for the Skeleton Stress-Strain Curve for Steel in Compression

	Grade 275	Grade 380
f_{yc} (MPa)	275	380
E_{sc} (MPa)	204000	204000
ϵ_{shc}	0.012	0.006
E_{shc} (MPa)	6860	12320
f_{suc} (MPa)	400	590
ϵ_{suc}	0.070	0.060

Zahn *et al.* [4] established the relationships of the longitudinal compression steel strain ϵ_{suc}, and the ratios of buckling stress to yield stress f_{suc}/f_y, to the hoop spacing ratio s_h/d_b necessary to control buckling, for Grades 275 and 380. The results are shown in Figs. 4.12 and 4.13.

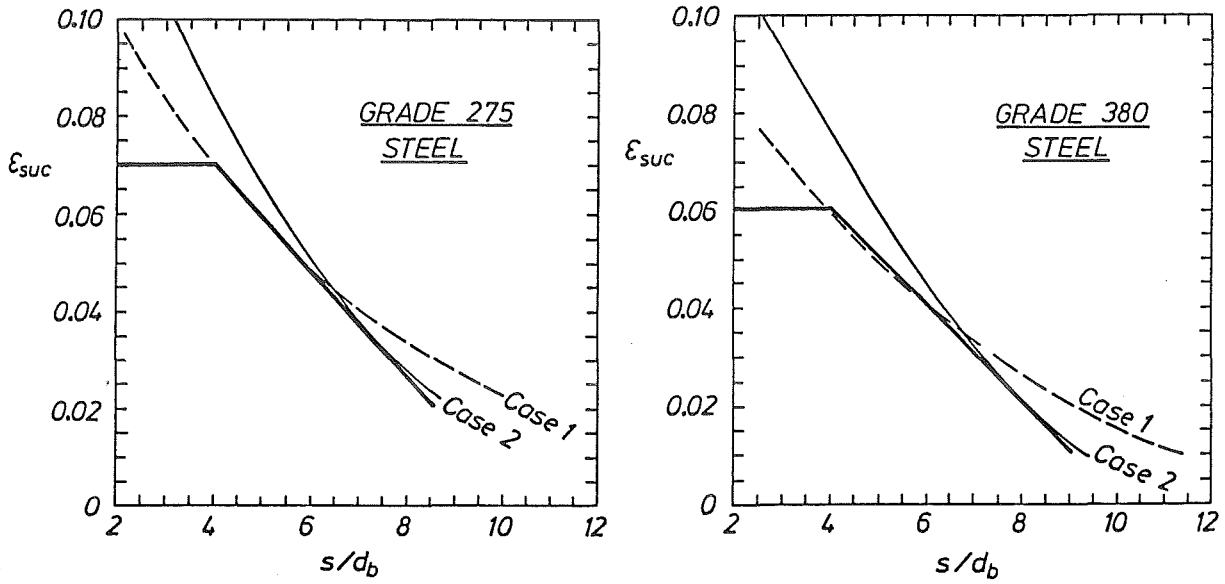

Figure 4.12: Theoretical Longitudinal Buckling Strains for Grade 275 and 380 Steel

Two cases were considered for each steel grade, as shown in Figs. 4.12 and 4.13. For case 1, the specified yield strength f_y, and the average values of ultimate tensile stress f_{su}, and strain hardening modulus E_{sh}, obtained from the tests, were used. For case 2, the average values of f_y and f_{su}, and the lowest value of E_{sh}, obtained from the the tests were used. A linear expression, which is shown by heavy lines, was chosen to represent a lower bound of the strains and stresses calculated for the two cases. It is worth noting that the increase in the buckling stress and strain for $s_h/d_b < 4$ was neglected.

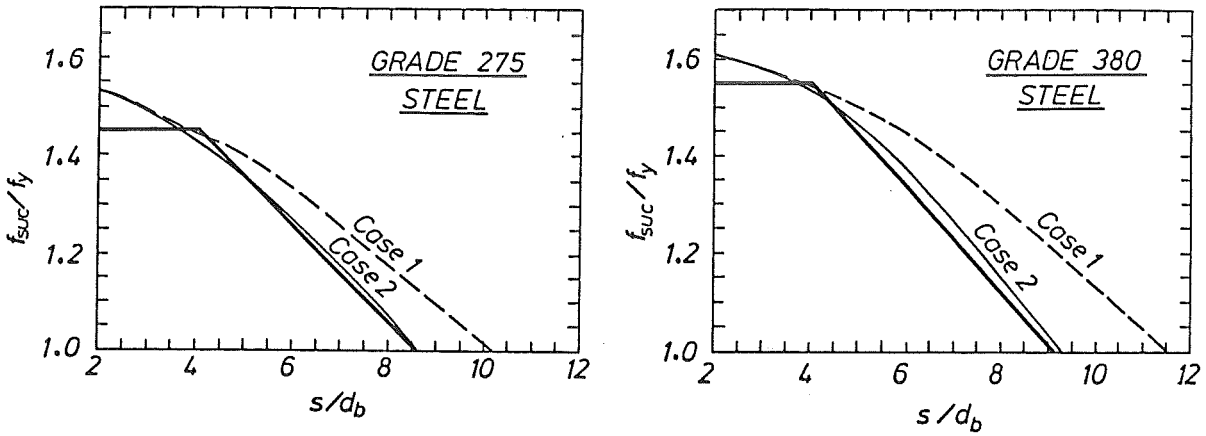

Figure 4.13: Ratio of Theoretical Buckling Stress to Yield Strength of Grades 275 and 380

The maximum steel strain reached during the initial half cycle was used as the basic strain to determine the s_h/d_b necessary to control buckling. This cycle is identical to the monotonic moment-curvature relation. By this way, the relationships given in Figs. 4.12 and 4.13, which were derived from the monotonic stress-strain curves, were applied to the cyclic analysis.

In order to allow for a possible increase in the compressive steel strain during the following cycles to φ_u, it was assumed that the increase in the basic strain per cycle depends linearly on the axial load ratio $P_e/(f'_c A_g)$. For zero axial load, the compressive strain was assumed not to increase at all with further cycles, while a 15% increase during each cycle was assumed for an axial compressive load level of $0.7f'_c A_g$. The compressive strain increase per cycle for columns with axial load ratios between 0.0 and 0.7 was given by a linear interpolation between 0% and 15%.

Dynamic Strain Rate Effects

The strengths of both steel and concrete are enhanced when the loading takes place at a dynamic strain rate such as during earthquakes.

Scott *et al.* [49] found that an increase in the strain rate resulted in an increase in the peak stress, strain at the peak stress, and slope of the falling branch of stress-strain curve for confined concrete.

Mander *et al.* [3] found that an increase in strain rate resulted in a decrease in the strain at maximum stress of unconfined concrete, an increase in the tangent modulus, and an increase in the slope of the falling branch of both unconfined and confined concrete.

In this study however, no dynamic strain rate effects were considered, since initial analyses showed that use of the dynamic material properties results in little, if any, change in the calculated ultimate curvature ductility factor.

4.3.3 Presentation of the Design Charts for Ductility

Fig. 4.14 shows a typical example of the design charts developed for circular spirally reinforced column sections. The chart relates the available curvature ductility factor φ_u/φ_y at the critical section of potential plastic hinge region to the ratio of the magnitude of effective confining stress acting on the core concrete to unconfined concrete strength, f_r/f_{co}. As expected, the axial load ratio $P_e/(f'_cA_g)$ is the major parameter. The charts are presented in a dimensionless form to facilitate their use for different section dimensions.

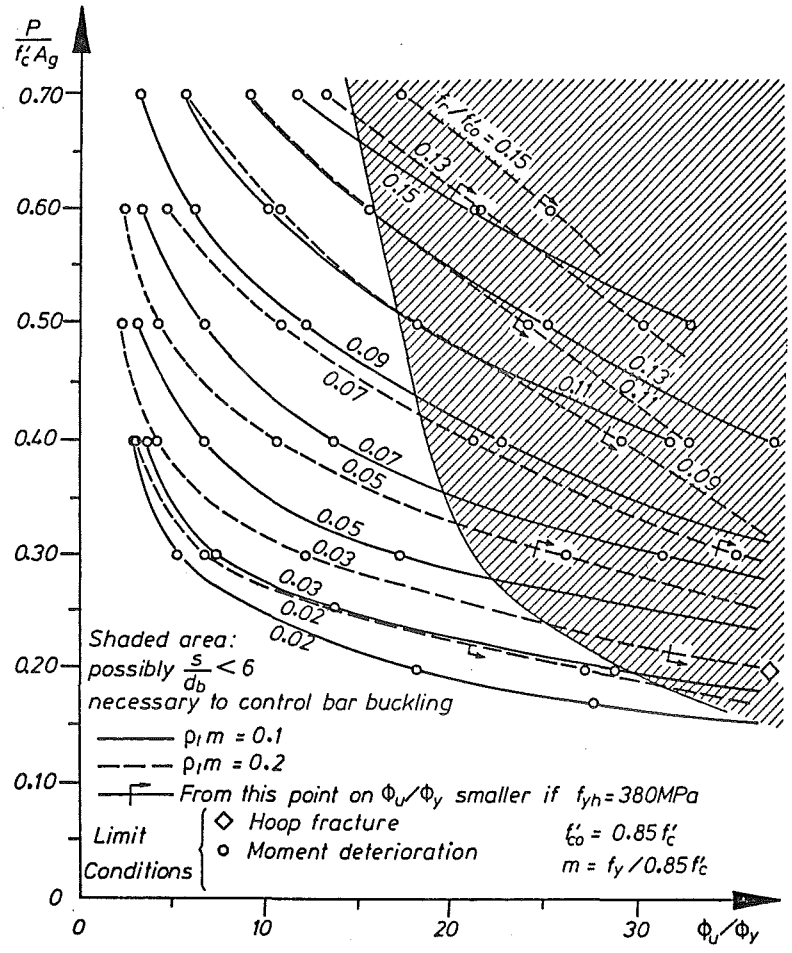

Figure 4.14: Example of Design Chart for Ductility for a Circular Section

The chart shown in Fig. 4.14 is for a circular section with f'_c=30 MPa, f_y=275 MPa, f_{yh}=275 MPa, $\rho_t m$=0.1 and 0.2, and c/D=0.06, where f'_c is concrete compressive strength, f_y and f_{yh} are the yield strengths of longitudinal and transverse reinforcement, respectively, $\rho_t m$ is mechanical reinforcing ratio=$\rho_t f_y/f'_c$, c is concrete cover thickness and D is overall diameter.

Examination of Fig. 4.14 indicates that:

- The available curvature ductility factor φ_u/φ_y rapidly decreases with increase in the axial compressive load ratio $P_e/(f'_cA_g)$.

- At very low axial load ratios, say $P_e/(f'_c A_g) < 0.15$, extremely large curvature ductility factors are theoretically available with only small quantities of confining reinforcement. It is obvious however, that there are other factors that govern the quantity of transverse reinforcement in such cases, such as the requirements for shear and prevention of buckling of the longitudinal compression bars.
- The most common factor which governs the ultimate curvature ductility of a section is the cyclic flexural strength deterioration, as indicated by the "o" symbols in Fig. 4.14.
- The available φ_u/φ_y, for a given effective confining stress ratio f_r/f_{co}, may be less when Grade 380 steel is used, as shown by the "↱" symbols in Fig. 4.14.
- The available φ_u/φ_y increases with the mechanical reinforcing ratio $\rho_t m$.
- The available φ_u/φ_y is limited by the line separating the shaded area from the unshaded area. The curvature ductilities within the shaded area can be expected only if excessive buckling of the longitudinal reinforcement does not occur. This can be achieved by providing smaller spacings of transverse reinforcement than the $6d_b$ required by the code.

Zahn *et al.* [4,47] also developed other design charts, similar to that shown in Fig. 4.14, for circular, square and rectangular column sections with different values of mechanical reinforcing ratio and cover ratio:

Circular Sections

The design charts are for sections with mechanical reinforcing ratios of $\rho_t m$=0.1,0.2,0.3 and 0.4. The charts were derived assuming a concrete compressive strength of f'_c=30 MPa, yield strengths of longitudinal and transverse reinforcement, f_y and f_{yh}, of 275 MPa, and a cover ratio of $c/D = 0.06$.

For columns with the values of $\rho_t m$ in between those investigated, linear interpolation is possible. For f'_c between 20 and 40 MPa, the φ_u/φ_y are modified by a factor of $\gamma f'_c$. Other modification factors are for the influence of other yield strengths of longitudinal and transverse reinforcement, γf_y and γf_{yh}, respectively, and the influence of other cover ratios $\gamma c/D$. Considering the large scatter found in the values of γf_y, it may be more reasonable to neglect this influence completely. Due to the limited samples examined for different cover thickness, it is possible that the influence of the c/D ratio was not comprehensively determined in the investigation. However, for columns with large diameter, where the cover ratio is only 0.02 to 0.04, the available curvature ductility factor is at least 15% greater than the values obtained from the charts. All of these modification factors are presented in a form of charts.

Square and Rectangular Sections

The design charts are for sections with $\rho_t m$ of 0.1, 0.15, 0.2, 0.3 and 0.4. As for circular sections, the charts were also derived assuming f'_c=30 MPa and f_y of 275 MPa. Yield strengths of confining reinforcement f_{yh} of 275 and 380 MPa were examined, and the c/h

ratios investigated were 0.02, 0.06 and 0.08. Linear interpolation is also possible for values of $\rho_t m$ and c/h in between those investigated.

Although values for the modification factors $\gamma f'_c$, γf_y and γf_{yh} were not investigated, it is likely that they are not significantly different from those calculated for circular sections [4].

The charts however, are also applicable for sections with the New Zealand manufactured Grade 380 longitudinal bars, providing that $\rho_t m \leq 0.3$. The influence of f'_c may be neglected providing that $25 \leq f'_c \leq 35$ MPa. Although the charts were developed for square sections, they can be applied to rectangular sections by modifying the cover ratio by a factor α, which depends on the section side ratio b/h.

4.4 Application of the Design Charts and Derivation of Refined Design Equation

4.4.1 Applications of the Design Charts for Ductility and Comparisons with the NZS 3101:1982 Equations

The work of Zahn *et al.* [4,47] was extended in this present study by using the design charts to derive a design equation for determining the quantities of confining reinforcement required in potential plastic hinge regions of columns.

The applications of the design charts for this derivation is illustrated as follows. First, the value of $\rho_t m$ is chosen for the column section type. From the corresponding design charts, the ratio of f_r/f_{co} is found for the various levels of axial compressive load on the column for values of φ_u/φ_y of 20 and 10. From the confining stress f_r, the required quantity of confining reinforcement to provide that confining stress can be calculated. The quantity of confining reinforcement is expressed by the volumetric steel percentage ρ_s. The core concrete is measured to the outside of the perimeter hoops or spirals as specified by the code [2].

For circular sections, according to the Eq. 4.21, the relation between f_r and ρ_s is expressed by:

$$f_r = \frac{1}{2} k_e^* \rho_s f_{yh} \tag{4.25}$$

Therefore

$$\rho_s \frac{f_{yh}}{f'_c} = \frac{2}{k_e^*} \frac{f_r}{f'_c} = \frac{1.7}{k_e^*} \frac{f_r}{f'_{co}} \tag{4.26}$$

where f'_{co}=compressive strength of unconfined concrete, taken as 0.85 f'_c.

Zahn *et al.* [4] suggested that a value of k_e^*=0.85 to be used for confined circular columns. Eq. 4.26 then becomes

$$\rho_s \frac{f_{yh}}{f'_c} = 2\frac{f_r}{f'_{co}} \tag{4.27}$$

Using the values of f_r/f'_{co} obtained from the corresponding design charts, the relations between $\rho_s f_{yh}/f'_c$ and the axial load ratio $P_e/(f'_c A_g)$ can be plotted for all combinations of the parameters listed in Table 4.1. Two of the graphs for circular sections are shown plotted in Figs. 4.15 and 4.16 for f'_c=30 MPa, $c/D = 0.06$ and φ_u/φ_y=20 and 10, respectively. For comparison, the code [2] recommended value of $\rho_s f_{yh}/f'_c$ as given by Eq. 4.1 is also plotted in those figures.

For the square sections shown in Fig. 4.4b, $A_{sh} = Y_{eff} A_b, h_c = b_c$, and the values of X_{eff} and Y_{eff} in Eq. 4.24 are equal to 3.41. Thus, if $\rho_s = A_{sh}/(s_h b_c)$, from Eq. 4.24

$$\rho_s = \frac{1}{k_e^*}\frac{f_r}{f_{yh}} = \frac{0.85}{k_e^*}\frac{f_r}{f'_{co}}\frac{f'_c}{f_{yh}} \tag{4.28}$$

For $k_e^* = 0.7$ as assumed by Zahn *et al.* [4], Eq. 4.28 can be rewritten as:

$$\rho_s \frac{f_{yh}}{f'_c} = 1.214\frac{f_r}{f'_{co}} \tag{4.29}$$

As for circular sections, the relation between $\rho_s f_{yh}/f'_c$ and $P_e/(f'_c A_g)$, for φ_u/φ_y values of 20 and 10, can be plotted. The graphs for f'_c=30 MPa and $c/h = 0.06$ are shown and compared with the code [2] equation Eq. 4.1 in Figs. 4.17 and 4.18.

For the rectangular section shown in Fig. 4.4c, $A_{sh} = Y_{eff} A_b, X_{eff} = 5.41, Y_{eff} = 3.41$, and $h_c = 1.5 b_c$. If $\rho_s = A_{sh}/(s_h b_c)$, Eq. 4.24 then becomes:

$$\rho_s = 1.18\frac{f_r}{f'_{co}}\frac{f'_c}{f_{yh}} \tag{4.30}$$

For the rectangular section shown in Fig. 4.4d, $A_{sh} = Y_{eff} A_b, X_{eff} = 3.41, Y_{eff} = 5.41$, and $h_c = \frac{2}{3} b_c$. Thus, if $\rho_s = A_{sh}/(s_h b_c)$, Eq. 4.24 becomes:

$$\rho_s \frac{f_{yh}}{f'_c} = 1.25\frac{f_r}{f'_{co}} \tag{4.31}$$

The relations between $\rho_s f_{yh}/f'_c$ and $P_e/(f'_c A_g)$ for rectangular sections with bending about the strong axis or the weak axis, and $f'_c = 30MPa$, $c/h = 0.06$, and $\varphi_u/\varphi_y = 20$ or 10, are illustrated and compared with the code [2] equation Eq. 4.1 in Figs. 4.19 to 4.22.

From this investigation, it was observed that the current code equations are unnecessarily conservative for columns with low to moderate axial compression. The code equations result in an available curvature ductility factor of greater than 20 in such cases. However, for

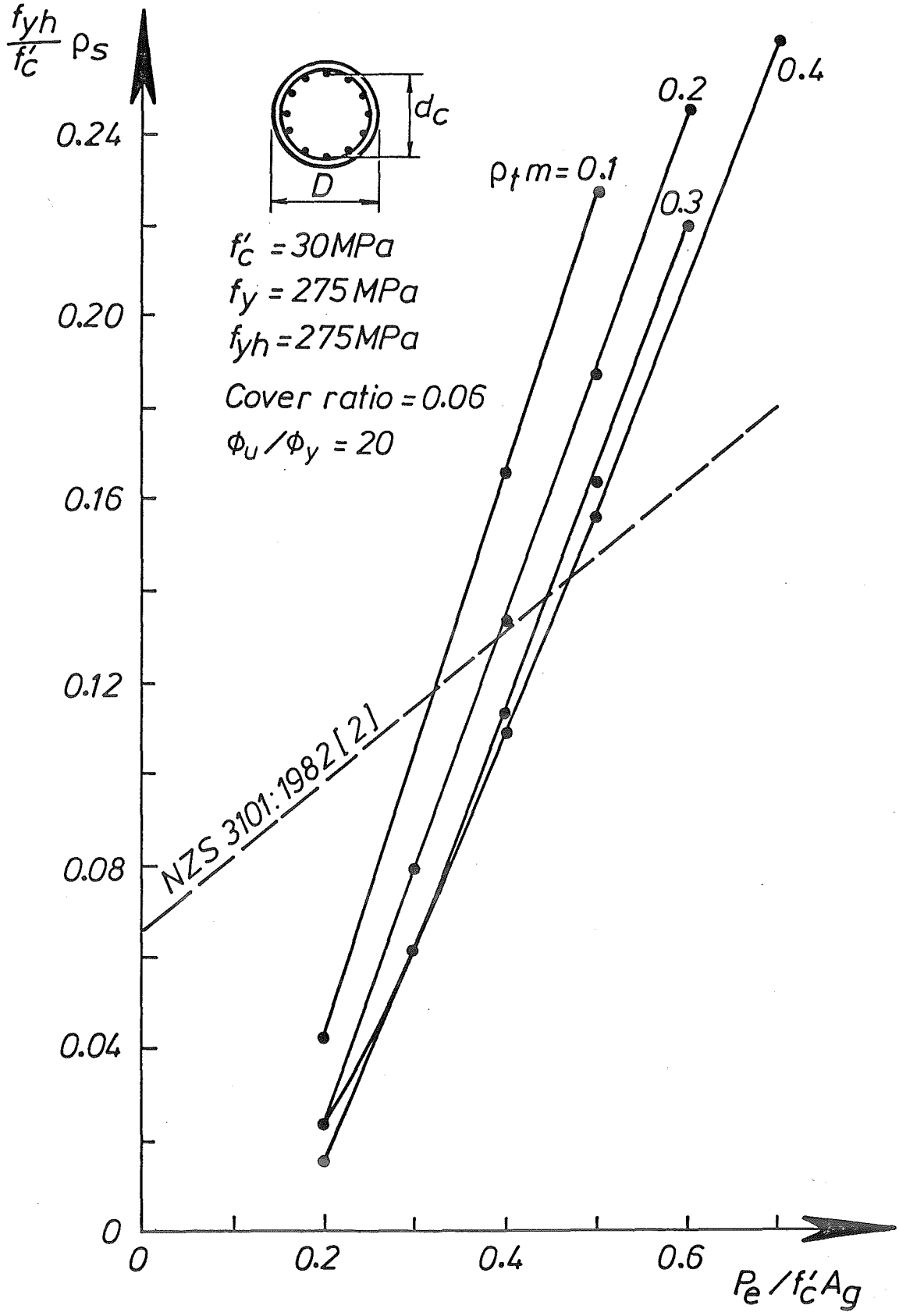

Figure 4.15: Required Quantities of Confining Reinforcement in the Potential Plastic Hinge Regions of Circular Columns to Achieve $\varphi_u/\varphi_y = 20$, and Comparison with the Code Requirement [2]

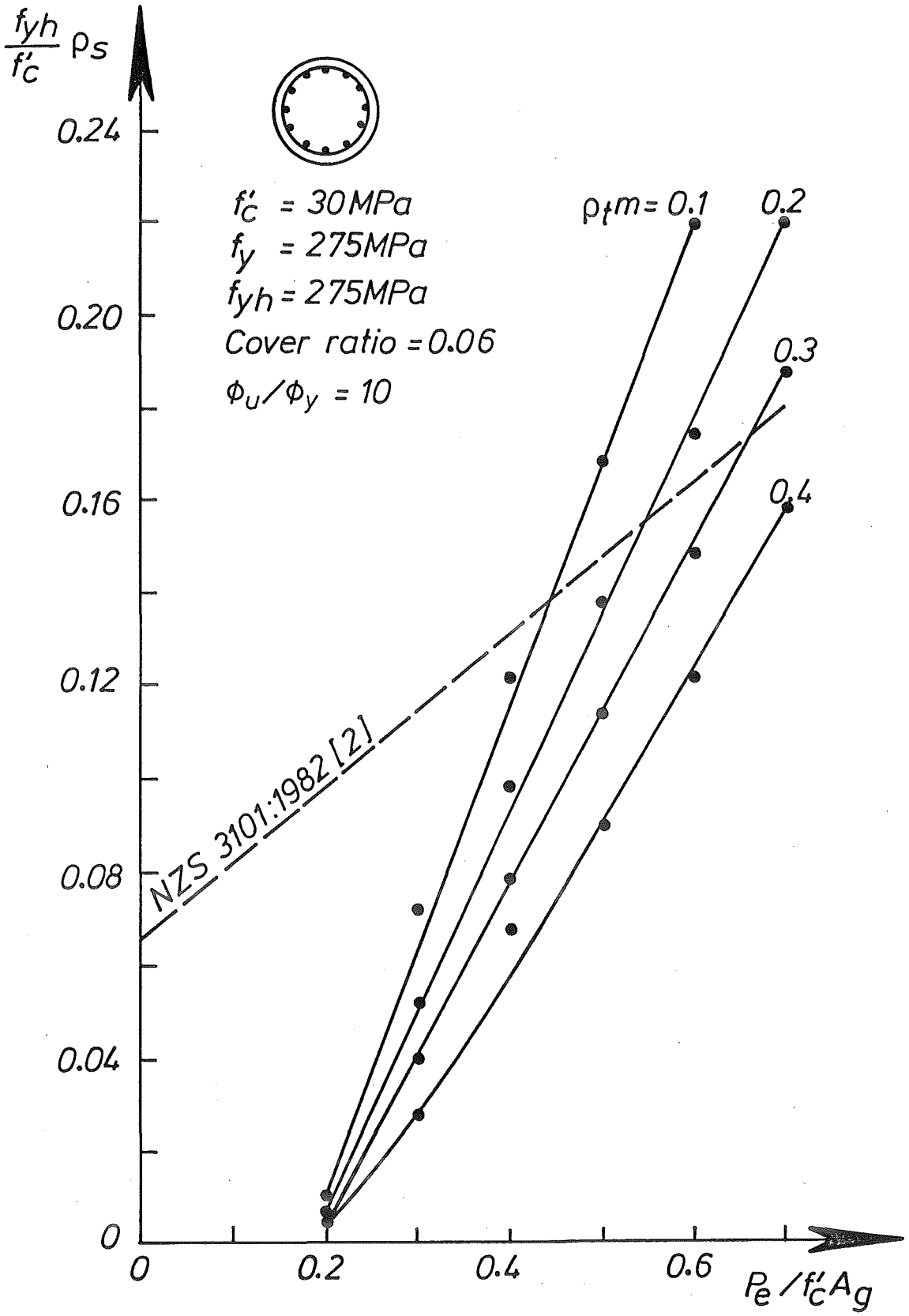

Figure 4.16: Required Quantities of Confining Reinforcement in the Potential Plastic Hinge Regions of Circular Columns to Achieve $\varphi_u/\varphi_y = 10$, and Comparison with the Code Requirement [2]

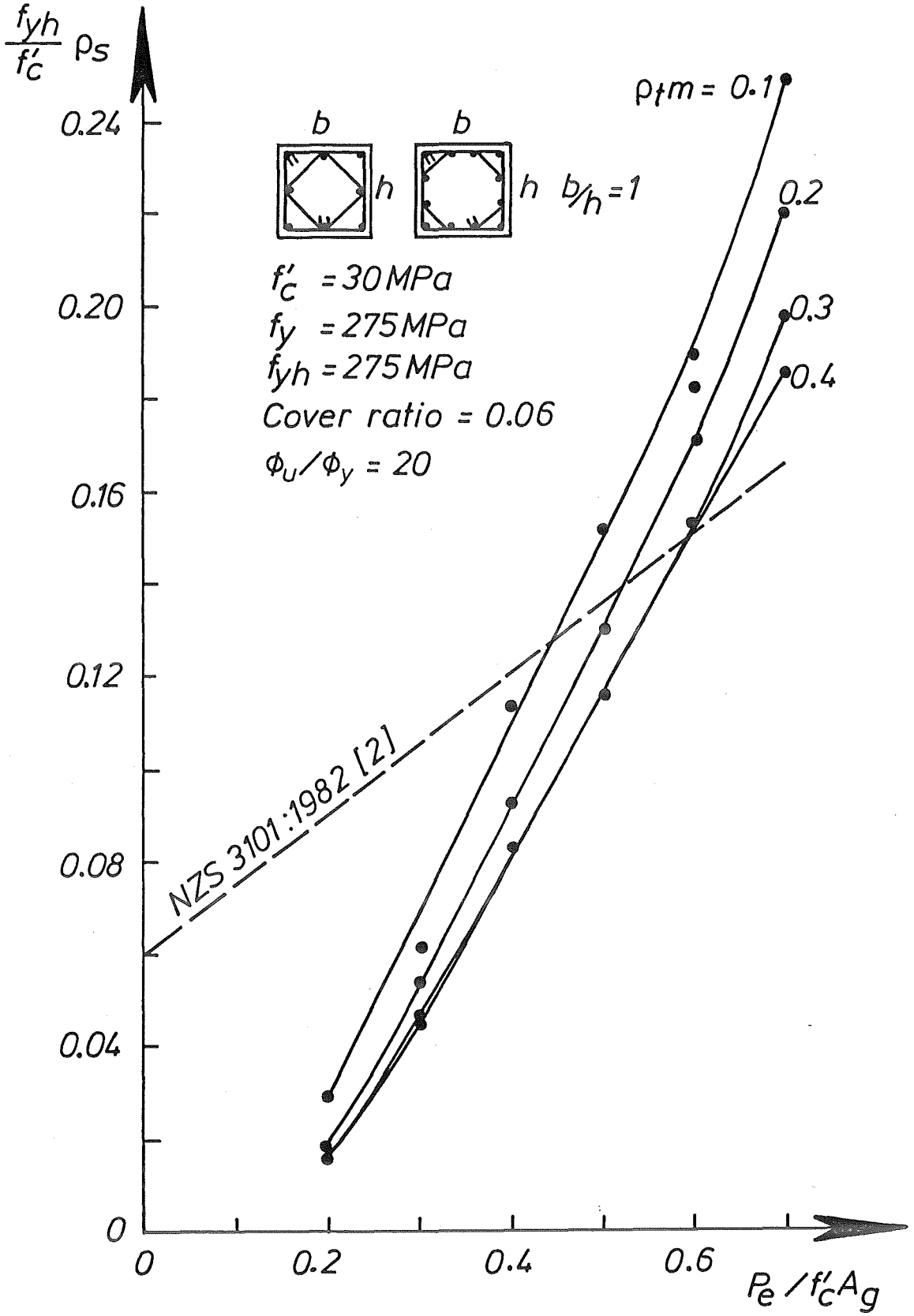

Figure 4.17: Required Quantities of Confining Reinforcement in the Potential Plastic Hinge Regions of Square Columns to Achieve $\varphi_u/\varphi_y = 20$, and Comparison with the Code Requirement [2]

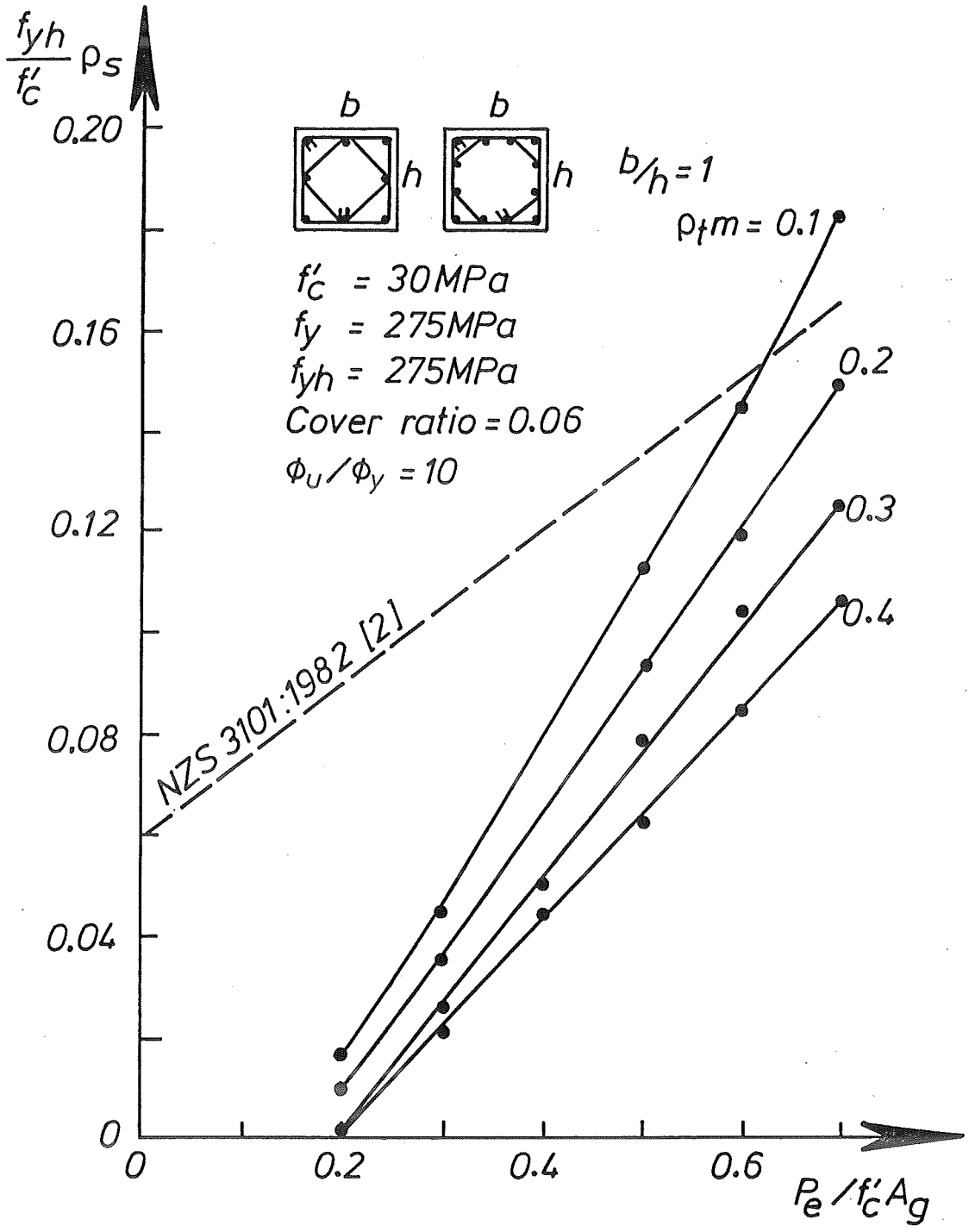

Figure 4.18: Required Quantities of Confining Reinforcement in the Potential Plastic Hinge Regions of Square Columns to Achieve $\varphi_u/\varphi_y = 10$, and Comparison with the Code Requirement [2]

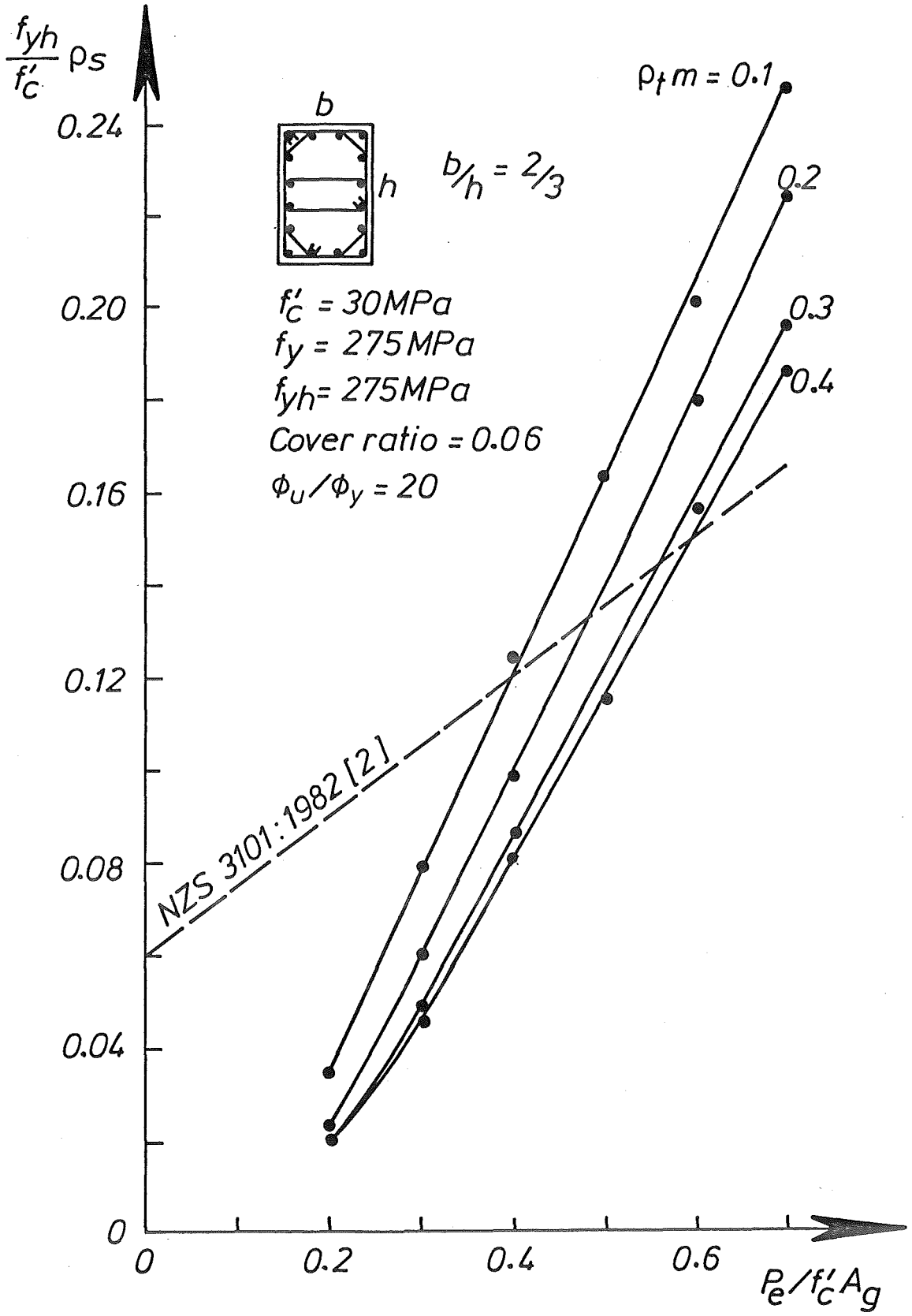

Figure 4.19: Required Quantities of Confining Reinforcement in the Potential Plastic Hinge Regions of Rectangular Columns with Bending about Strong Axis, to Achieve $\varphi_u/\varphi_y = 20$, and Comparison with the Code Requirement [2]

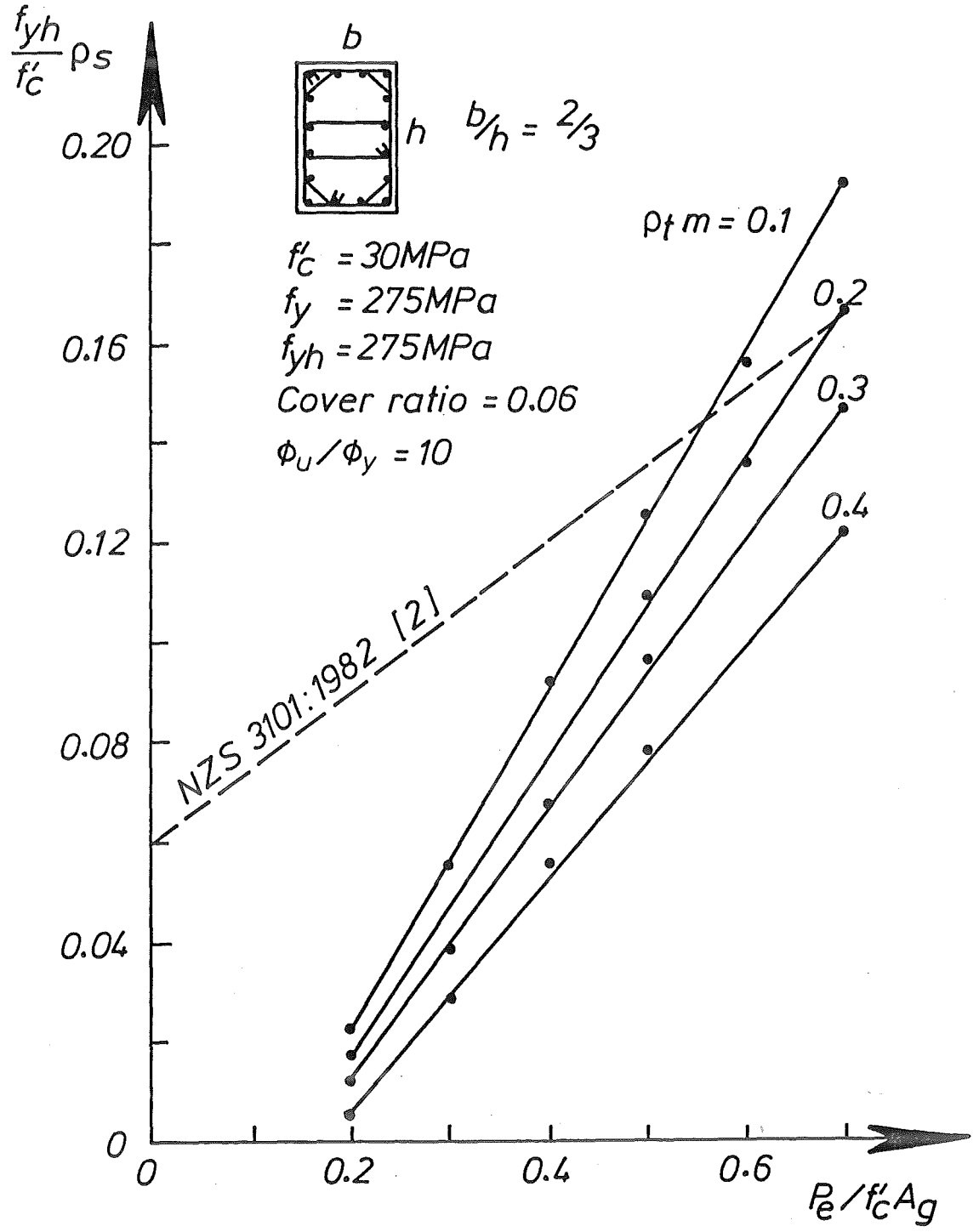

Figure 4.20: Required Quantities of Confining Reinforcement in the Potential Plastic Hinge Regions of Rectangular Columns with Bending about Strong Axis, to Achieve $\varphi_u/\varphi_y = 10$, and Comparison with the Code Requirement [2]

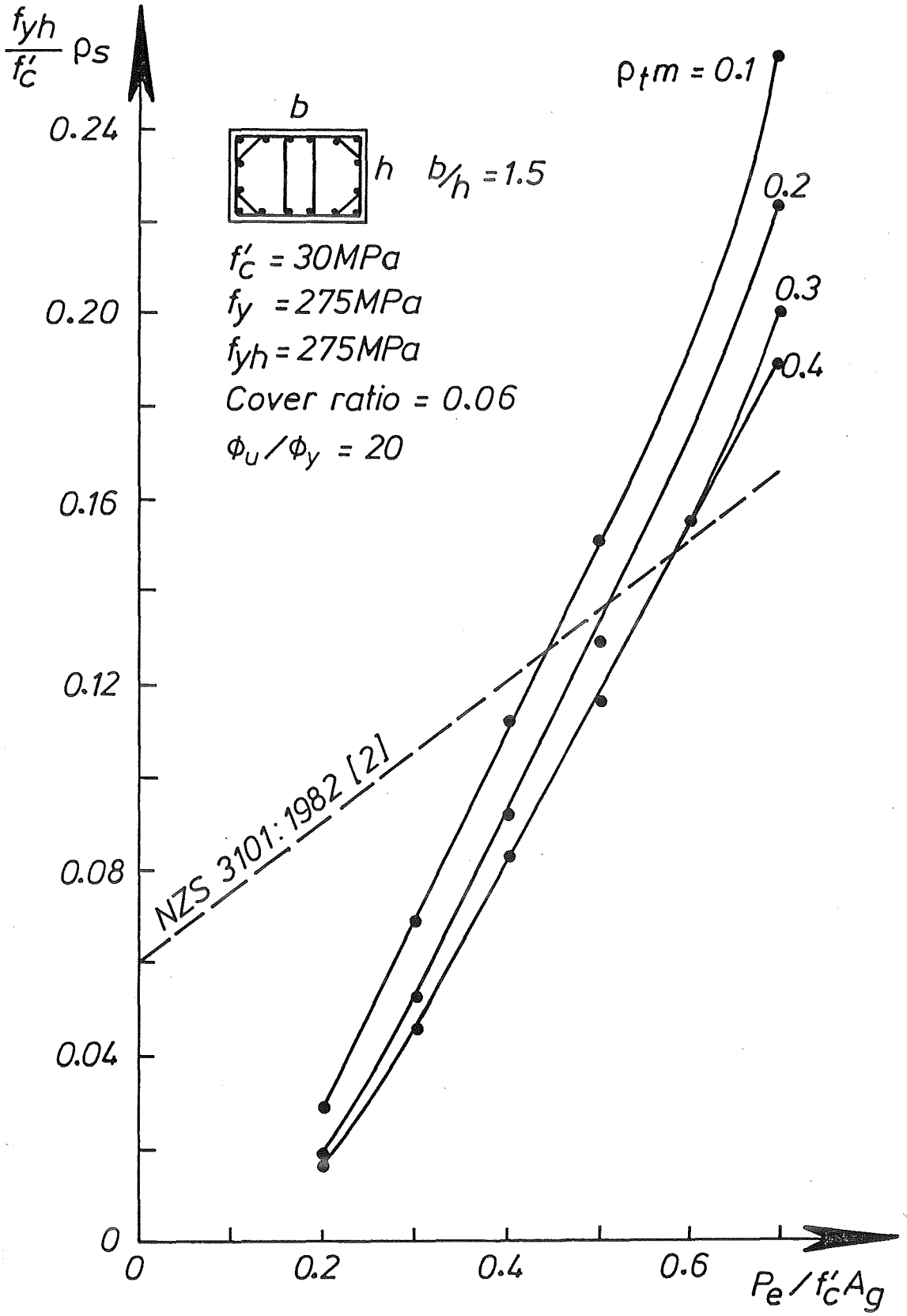

Figure 4.21: Required Quantities of Confining Reinforcement in the Potential Plastic Hinge Regions of Rectangular Columns with Bending about Weak Axis, to Achieve $\varphi_u/\varphi_y = 20$, and Comparison with the Code Requirement [2]

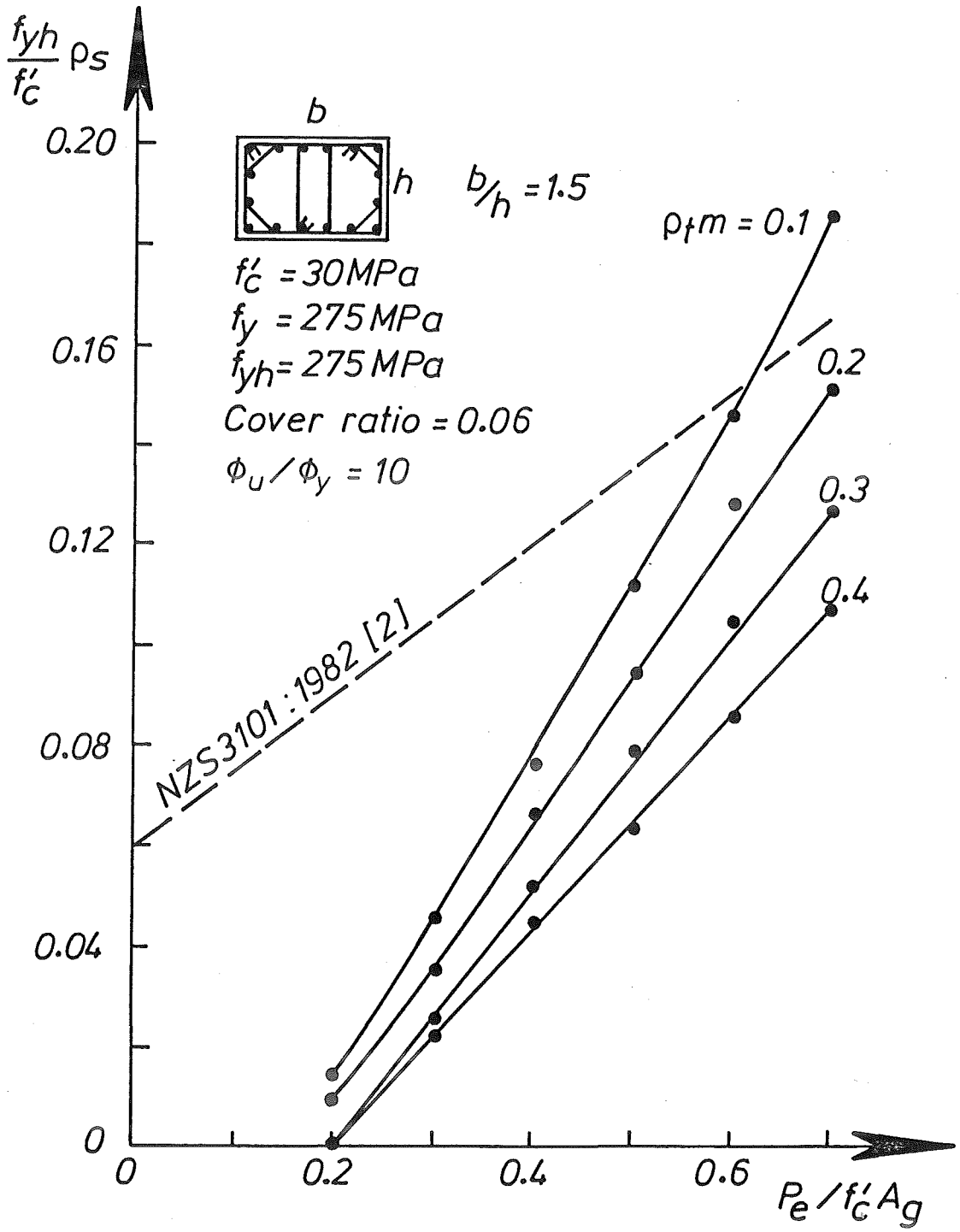

Figure 4.22: Required Quantities of Confining Reinforcement in the Potential Plastic Hinge Regions of Rectangular Columns with Bending about Weak Axis, to Achieve $\varphi_u/\varphi_y = 10$, and Comparison with the Code Requirement [2]

columns with high axial compression, large cover thickness, and small flexural steel content, the code equations can be unconservative. In such cases, the code equations can result in an available curvature ductility factor of less than 10. If the existing code requirement of an available curvature ductility factor of 20 for ductile column sections is to be maintained, the quantity of confining reinforcement recommended by the code can be reduced for low axial compression loads, but needs to be increased for high axial compression loads in some cases.

4.4.2 Derivation of Refined Design Equation for the Quantities of Confining Reinforcement Required in Columns for Adequate Ductility

Examination of the relations between the required confining reinforcement and the axial compression load ratio for columns for a particular curvature ductility factor, such as shown in Figs. 4.15 to 4.22, leads to the following conclusions concerning the influence of the parameters listed in Table 4.1.

Axial Compression Load Ratio $P_e/(f'_c A_g)$

It was observed that the required transverse reinforcement for concrete confinement for a particular curvature ductility factor increases significantly as the axial load ratio increases. When the axial load is high, the flexural strength of columns is more dependent on the concrete compressive stress distribution. As a result, more transverse reinforcement is required to provide adequate confinement. Also, the cyclic curvature history used in the analysis (i.e. four identical, symmetrical cycles to the ultimate curvature) leads to greater strength deterioration of the concrete than in the case of monotonic loading.

Mechanical Reinforcing Ratio $\rho_t m$

The required confining reinforcement increases when the flexural steel content ρ_t decreases. This is because of the smaller contribution due to strain hardening of longitudinal bars to the flexural strength, and a greater proportional contribution of the concrete compressive stress distribution to the flexural strength. To compensate for this effect, a larger quantity of transverse reinforcement is needed to confine concrete when $\rho_t m$ is small.

Section Type Factor f

It was observed that the type of section has a significant effect on the required quantity of confining reinforcement. As expected, to achieve the same curvature ductility factor, the ρ_s required for circular section is markedly different from the ρ_s required for square and rectangular sections. The values of ρ_s for square and rectangular sections are not significantly different. This indicates therefore, that the square and rectangular sections used in this investigation may represent a wide range of rectangular sections used in design.

Cover Ratio c/D or c/h and Concrete Compressive Compressive Strength f'_c

Although figures illustrating the relation between $\rho_s f_{yh}/f'_c$ and $P_e/(f'_c A_g)$ for $f'_c \neq 30MPa$ and c/D or $c/h \neq 0.06$ are not presented here, it was found that these parameters also have considerable effects on the quantity of confining reinforcemet.

A small cover thickness means a larger area of concrete core, resulting in more ductile behaviour of the concrete and hence less confining reinforcement is required.

Concrete with a high compressive strength is more brittle, and hence the quantity of transverse steel required for confinement is larger.

Based on the above considerations, it was decided that a refined design equation for the quantities of confining reinforcement in columns needs to be related to the required curvature ductility factor φ_u/φ_y, and it would have to include all the parameters examined above, that is $P_e/(f'_c A_g)$, $\rho_t m$, f, c/D or c/h, f'_c and f_{yh}. For convenience, the influence of the relative cover thickness c/D or c/h is expressed by the ratio of A_g/A_c, where A_g is gross area of section and A_c is area of concrete core.

Figs. 4.23 to 4.30 illustrate all values of $\rho_s f_{yh}/f'_c$ obtained from the design charts for the range of parameters listed in Table 4.1, to achieve curvature ductility factors of 20 and 10.

It can be seen that the values of $\rho_s f_{yh}/f'_c$ for circular sections (indicated by "o" symbols) are larger than those for square and rectangular sections (indicated by "•" symbols) for the same values of $\rho_t m$, $P_e/(f'_c A_g)$ and c/D or c/h. It was decided therefore, to evaluate only the values of $\rho_s f_{yh}/f'_c$ for square and rectangular sections, and a section type factor f could then be applied to obtain the value of that index for circular sections. Large scatter is also indicated by the results plotted in those figures. However, a suitable linear design equation could be fitted using the procedure described below.

The 95% upper tail values and the mean values of $\rho_s f_{yh}/f'_c$ are also plotted in Figs. 4.23 to 4.30. To obtain the most desirable design equation, more interpolation points are needed. Therefore, the 95% upper tail values of $\rho_s f_{yh}/f'_c$ for φ_u/φ_y of 15 were also calculated.

For those 95% upper tail values, the best fit linear equation of $\rho_s f_{yh}/f'_c$ as a function of $P_e/(f'_c A_g)$, for each $\rho_t m$ and φ_u/φ_y was then determined by the *Least Square* method. The equations obtained are given in Table 4.4.

The coefficients of $P_e/(f'_c A_g)$ listed in Table 4.4, were next plotted as a function of $\rho_t m$ for each φ_u/φ_y, as shown in Fig. 4.31.

The best-fit linear equations are shown in Fig. 4.31 as Eqs. A. Clearly, the slopes are not significantly different and a value of -0.41 fits all equations reasonably well. Equations for A could then be written as follows:

$$\begin{aligned} For\ \varphi_u/\varphi_y = 10,\ A &= -0.41\rho_t m + 0.419 \\ For\ \varphi_u/\varphi_y = 15,\ A &= -0.41\rho_t m + 0.469 \\ For\ \varphi_u/\varphi_y = 20,\ A &= -0.41\rho_t m + 0.543 \end{aligned} \tag{4.32}$$

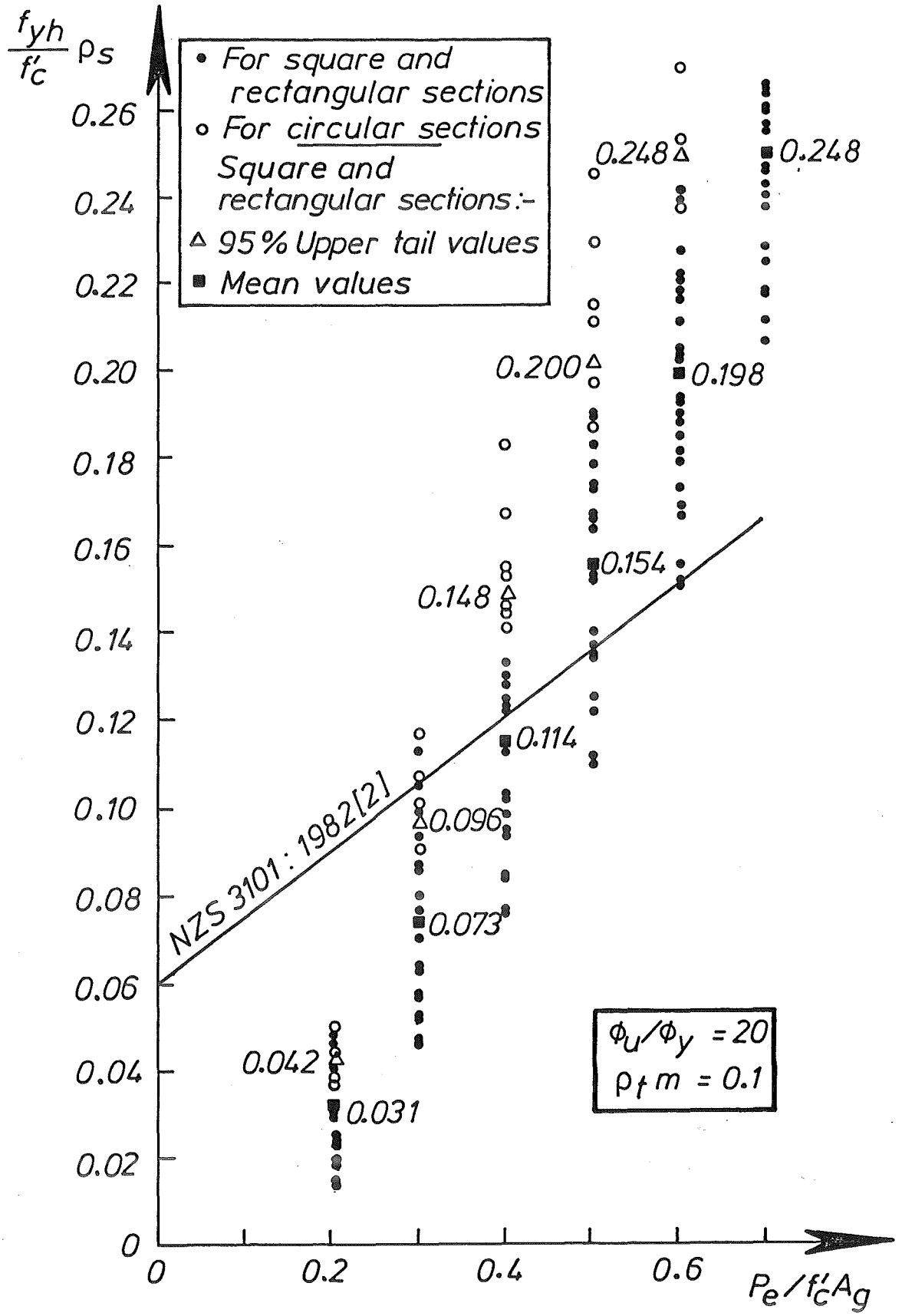

Figure 4.23: Required Quantities of Confining Reinforcement in the Potential Plastic Hinge Regions of Columns with $\rho_t m$=0.1 Obtained from Design Charts to Achieve φ_u/φ_y=20, and Comparison with the Code Requirement [2]

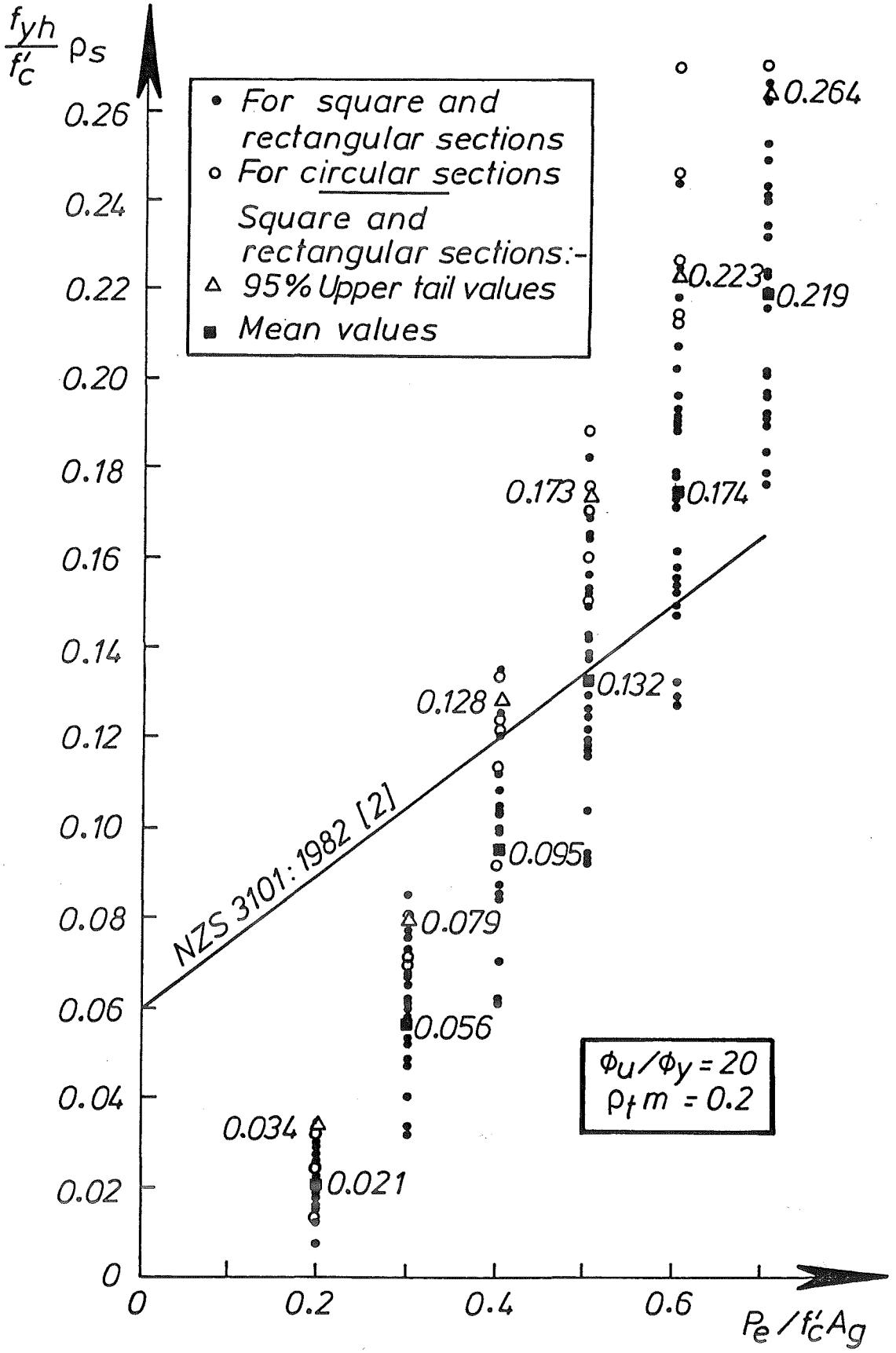

Figure 4.24: Required Quantities of Confining Reinforcement in the Potential Plastic Hinge Regions of Columns with $\rho_t m$=0.2 Obtained from Design Charts to Achieve φ_u/φ_y=20, and Comparison with the Code Requirement [2]

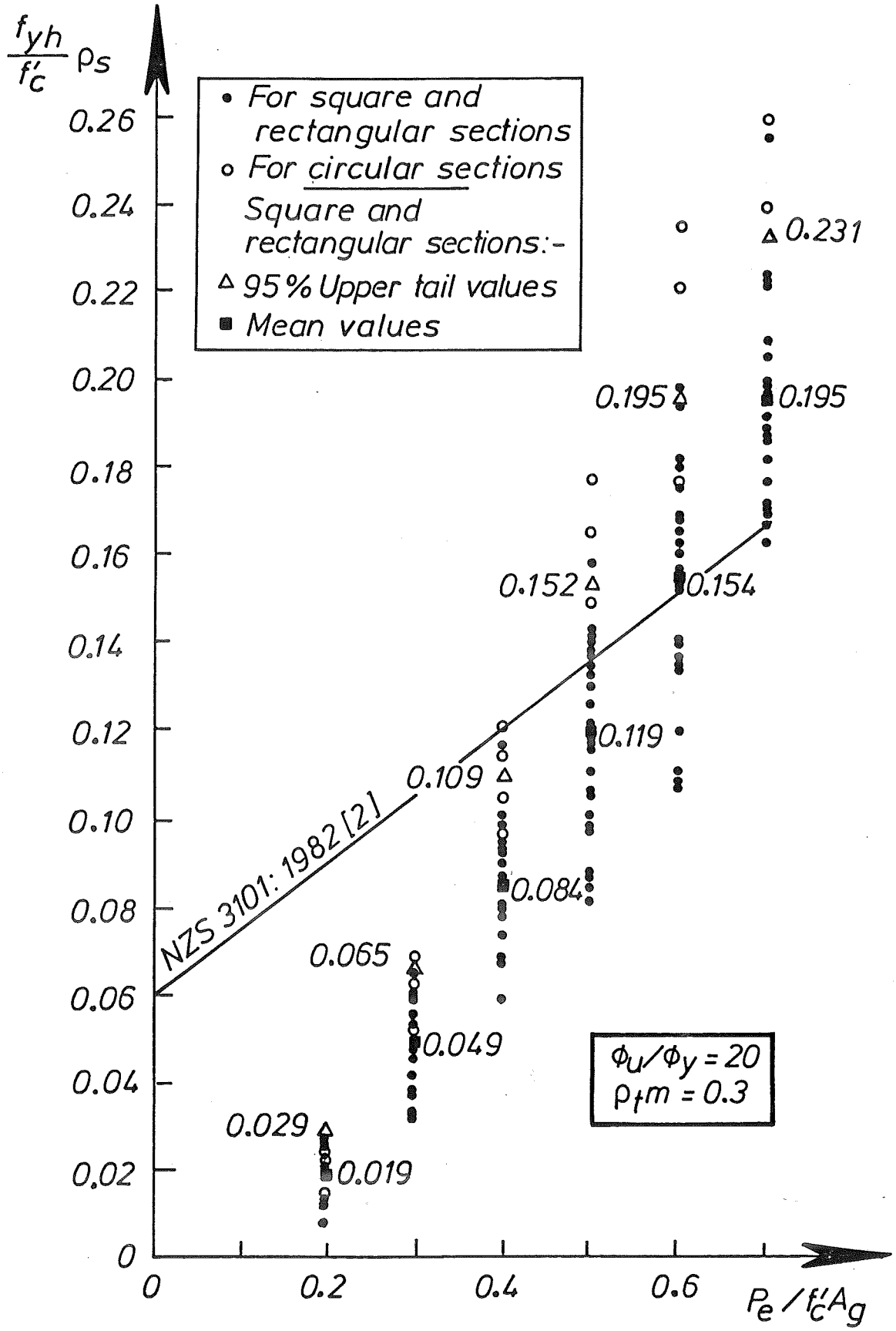

Figure 4.25: Required Quantities of Confining Reinforcement in the Potential Plastic Hinge Regions of Columns with $\rho_t m$=0.3 Obtained from Design Charts to Achieve φ_u/φ_y=20, and Comparison with the Code Requirement [2]

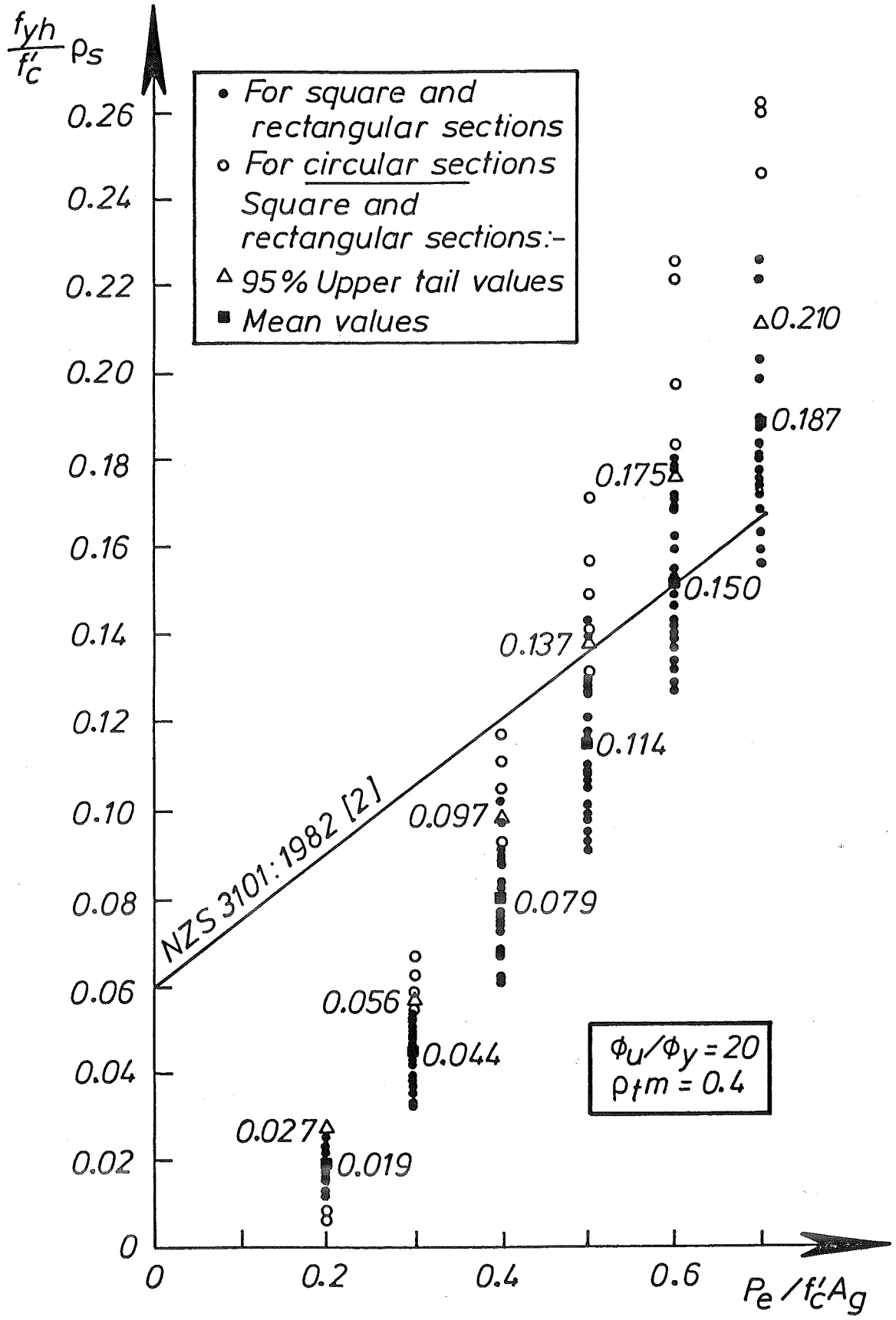

Figure 4.26: Required Quantities of Confining Reinforcement in the Potential Plastic Hinge Regions of Columns with $\rho_t m$=0.4 Obtained from Design Charts to Achieve φ_u/φ_y=20, and Comparison with the Code Requirement [2]

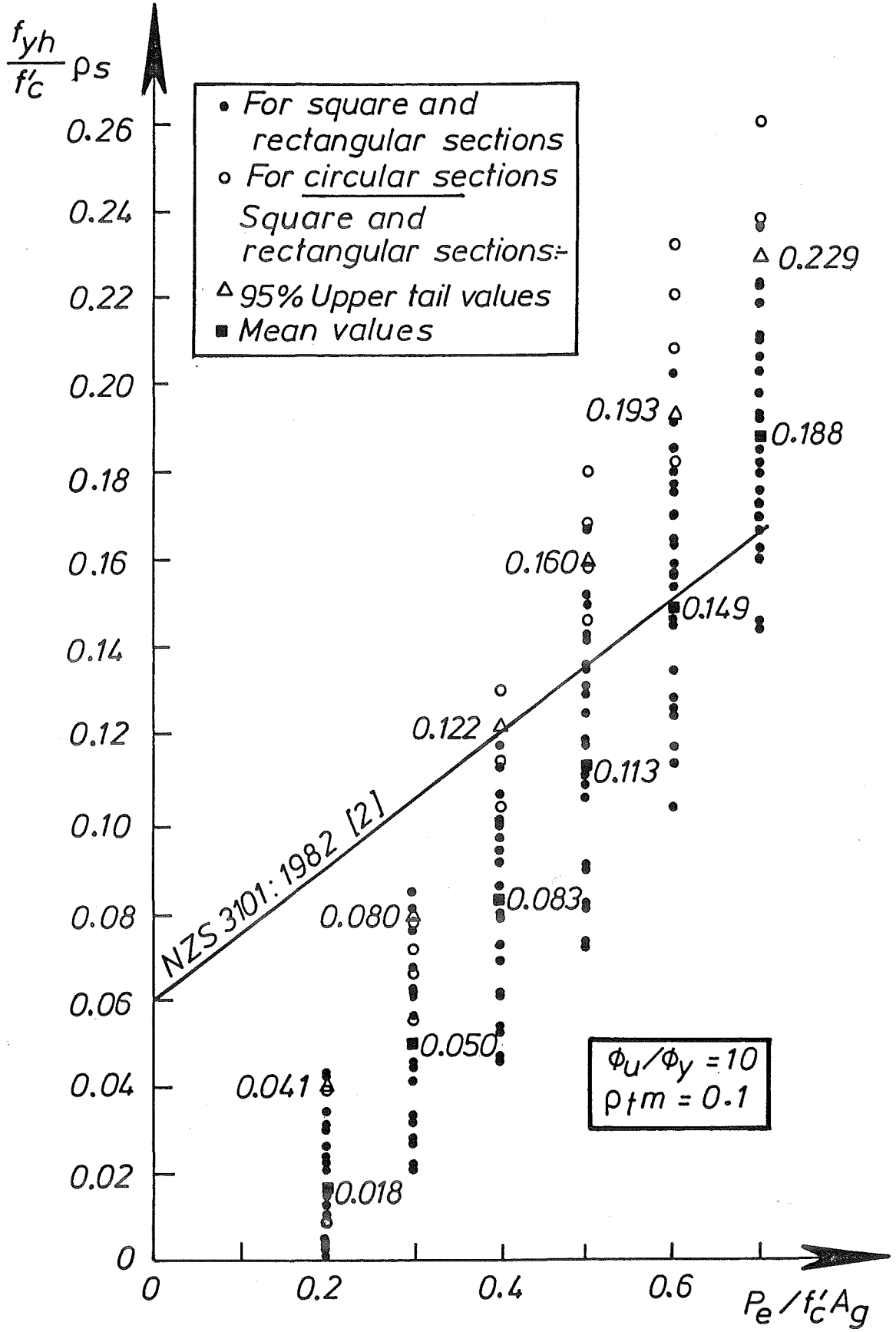

Figure 4.27: Required Quantities of Confining Reinforcement in the Potential Plastic Hinge Regions of Columns with $\rho_t m$=0.1 Obtained from Design Charts to Achieve φ_u/φ_y=10, and Comparison with the Code Requirement [2]

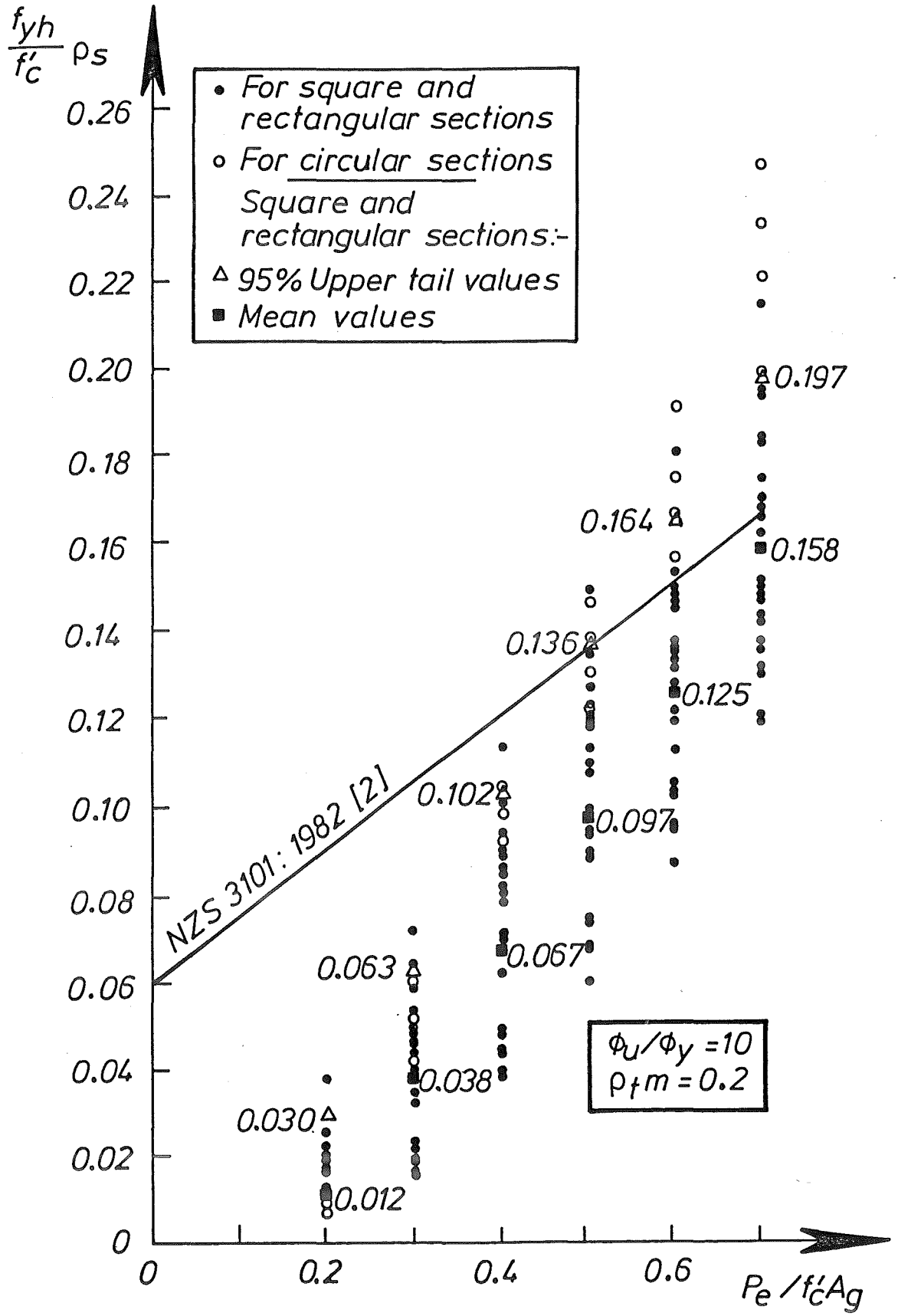

Figure 4.28: Required Quantities of Confining Reinforcement in the Potential Plastic Hinge Regions of Columns with $\rho_t m$=0.2 Obtained from Design Charts to Achieve φ_u/φ_y=10, and Comparison with the Code Requirement [2]

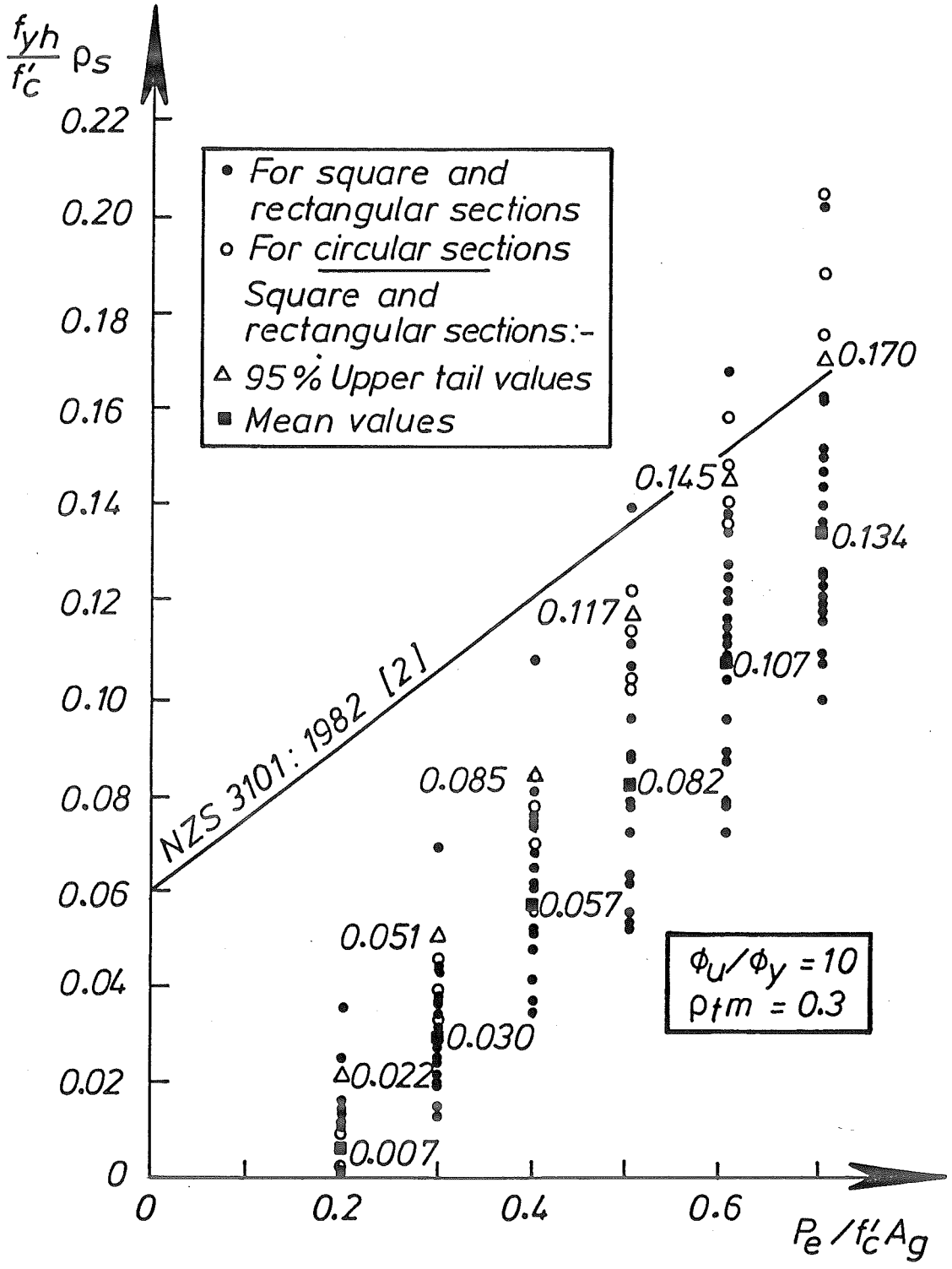

Figure 4.29: Required Quantities of Confining Reinforcement in the Potential Plastic Hinge Regions of Columns with $\rho_t m$=0.3 Obtained from Design Charts to Achieve φ_u/φ_y=10, and Comparison with the Code Requirement [2]

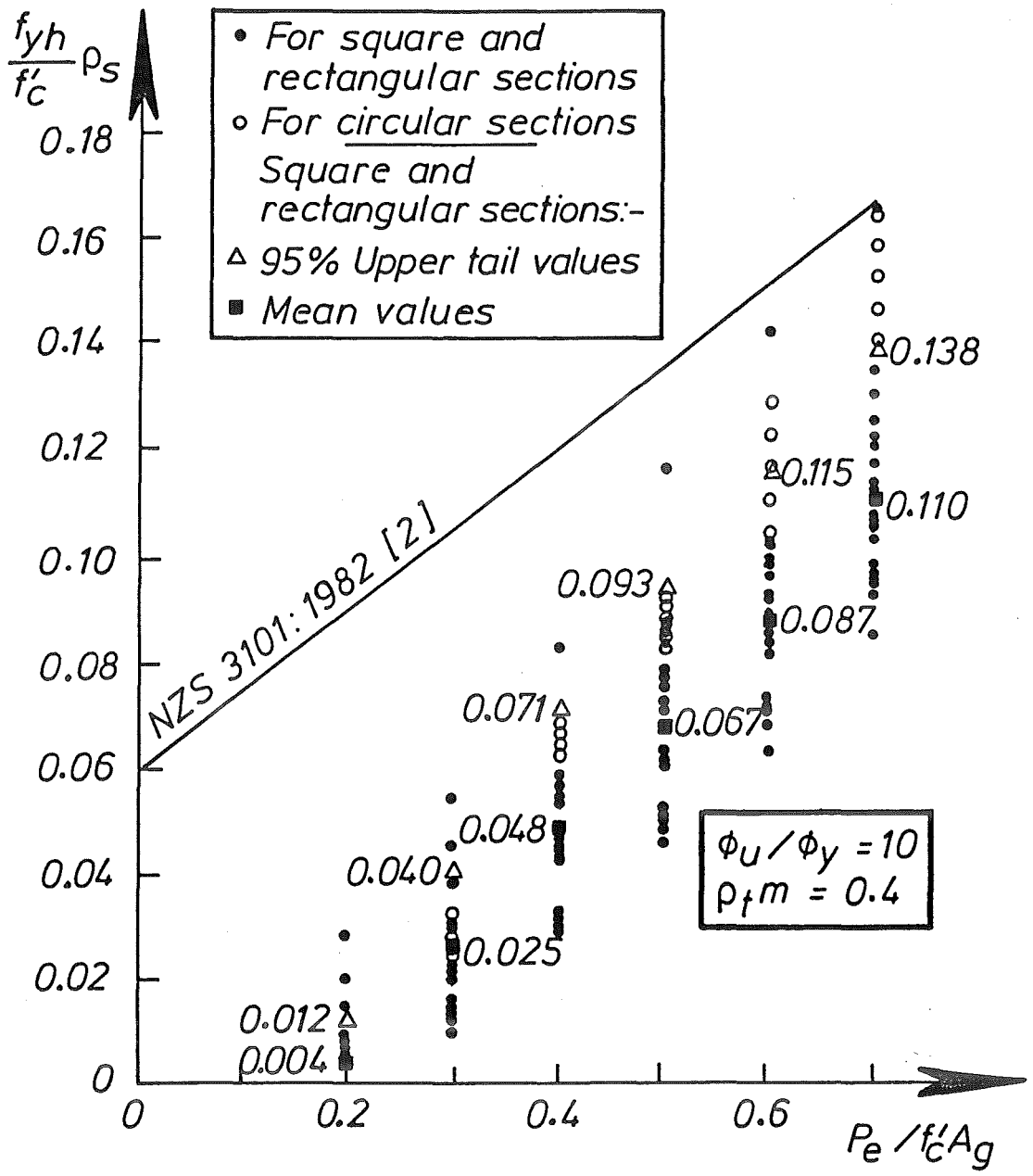

Figure 4.30: Required Quantities of Confining Reinforcement in the Potential Plastic Hinge Regions of Columns with $\rho_t m$=0.4 Obtained from Design Charts to Achieve φ_u/φ_y=10, and Comparison with the Code Requirement [2]

Table 4.4: The Best-Fit Equations for the 95% Upper Tail Values of $\rho_s f_{yh}/f'_c$ for Square and Rectangular Columns

	The Best-Fit Equations		
$\rho_t m$	φ_u/φ_y=10	φ_u/φ_y=15	φ_u/φ_y=20
0.1	$y = 0.377x - 0.032$	$y = 0.426x - 0.039$	$y = 0.497x - 0.053$
0.2	$y = 0.336x - 0.036$	$y = 0.387x - 0.048$	$y = 0.465x - 0.059$
0.3	$y = 0.302x - 0.038$	$y = 0.333x - 0.046$	$y = 0.413x - 0.056$
0.4	$y = 0.252x - 0.035$	$y = 0.303x - 0.042$	$y = 0.372x - 0.050$

where $y = \rho_s f_{yh}/f'_c$ and $x = P_e/(f'_c A_g)$

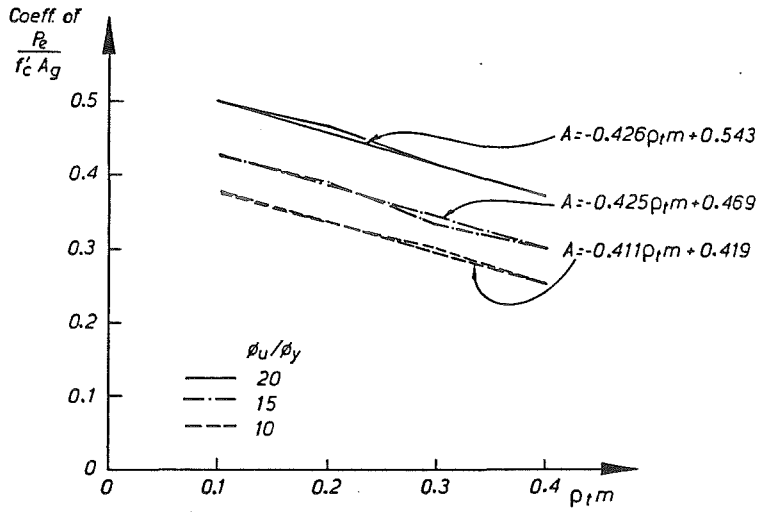

Figure 4.31: Relationships between $\rho_t m$ and Coefficients of $P_e/(f'_c A_g)$

The constants in Eq. 4.32, that is 0.419, 0.469, and 0.543, are shown in Fig. 4.32 and a linear equation $B = 0.0123\varphi_u/\varphi_y + 0.292$ can be fitted to them. Eq. 4.32 could now be brought together as:

$$A = -0.41\rho_t m + 0.0123\varphi_u/\varphi_y + 0.292 \tag{4.33}$$

The constants in the equations for y listed in Table 4.4 are shown plotted in Fig. 4.33. The linear equations for these constants for each φ_u/φ_y, denoted as Eqs. C, indicated that the slopes (the variation with $\rho_t m$) are very small and can be neglected. Eqs. C were then rewritten as follows:

$$\begin{aligned} \varphi_u/\varphi_y = 10,\ C &= 0.033 \\ \varphi_u/\varphi_y = 15,\ C &= 0.042 \\ \varphi_u/\varphi_y = 20,\ C &= 0.058 \end{aligned} \tag{4.34}$$

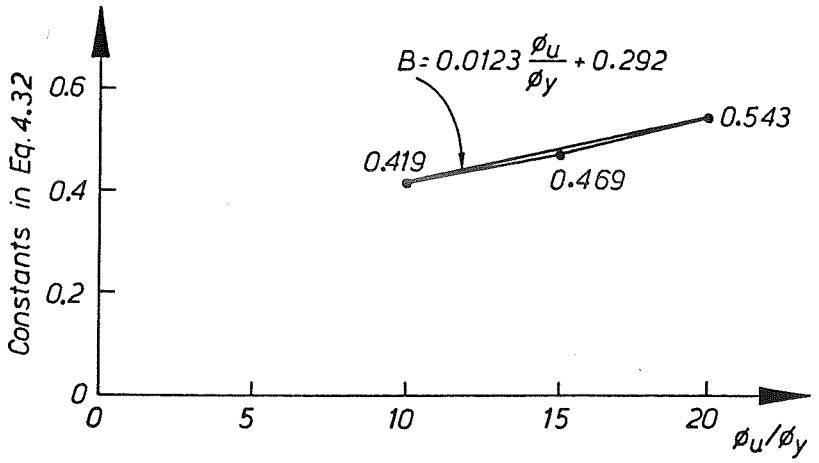

Figure 4.32: Relationships between Constants in Eq. 4.32 and φ_u/φ_y

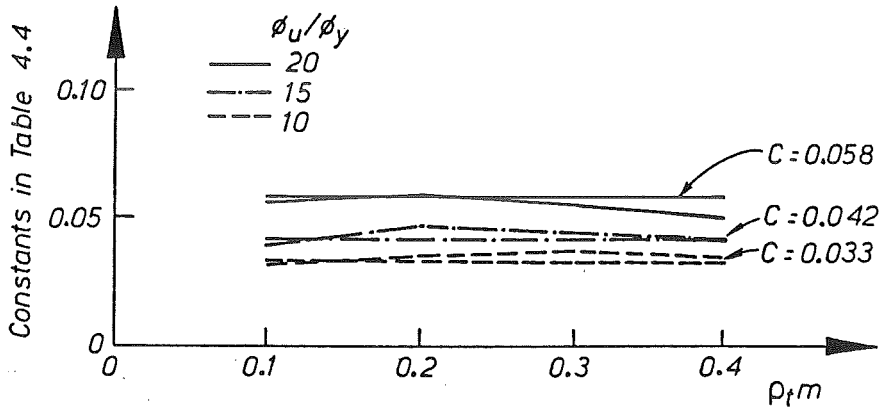

Figure 4.33: Relationships Between $\rho_t m$ and Constants in Table 4.4

These values for C of 0.033, 0.042 and 0.058 are plotted as shown in Fig. 4.34 as a function of φ_u/φ_y. A parabolic curve D was found to fit very well, where

$$D = 1.4 \times 10^{-3}(\varphi_u/\varphi_y)^2 - 1.7 \times 10^{-2}(\varphi_u/\varphi_y) + 0.036 \tag{4.35}$$

By combining Eqs. 4.33 and 4.35, the following equation can then be obtained for square and rectangular columns:

$$\rho_s \frac{f_{yh}}{f'_c} = (-0.41\rho_t m + 0.0123\varphi_u/\varphi_y + 0.292)\frac{P_e}{f'_c A_g} - 1.4 \times 10^{-3}(\varphi_u/\varphi_y)^2 - 1.7 \times 10^{-2}(\varphi_u/\varphi_y) + 0.036 \tag{4.36}$$

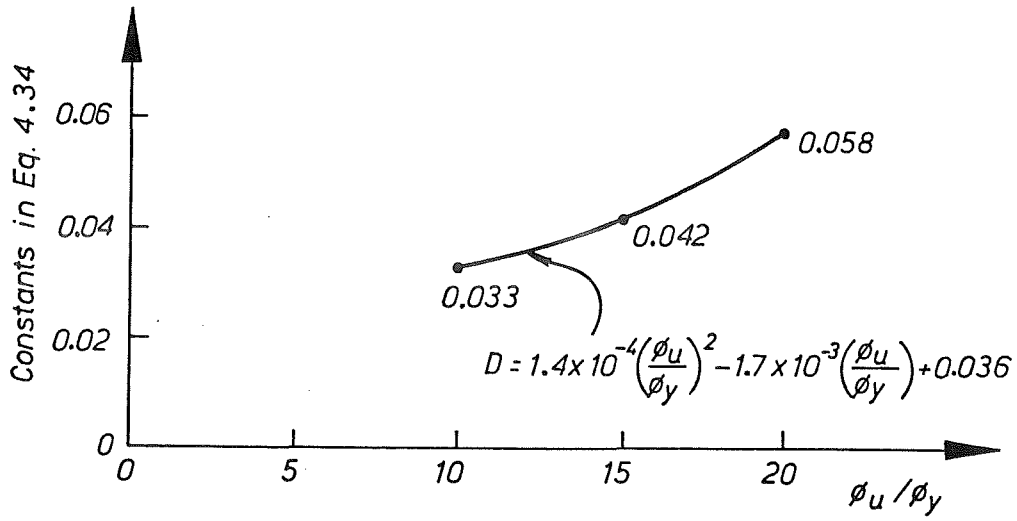

Figure 4.34: Relationships between Constants in Eq. 4.34 with φ_u/φ_y

Note that Eq. 4.36 was derived from the 95% upper tail values of $\rho_s f_{yh}/f'_c$ appropriate for $c/h = 0.08$. To obtain a refined design equation which is applicable to the range of cover ratios commonly used in design, Eq. 4.36 can be written as follows for square or rectangular columns.

$$\rho_s \frac{f_{yh}}{f'_c} = \frac{A_g}{A_c}(-0.3\rho_t m + 0.009\varphi_u/\varphi_y + 0.208)\frac{P_e}{f'_c A_g} - 1.4 \times 10^{-3}(\varphi_u/\varphi_y)^2 - 1.7 \times 10^{-2}(\varphi_u/\varphi_y) + 0.036 \quad (4.37)$$

It is worth noting that in determining Eq. 4.37, it was found that the influence of the cover ratio in the second term is small, and it was therefore decided to ignore it.

The section type factor f, which relates the values of ρ_s for circular sections to that for square or rectangular sections for the same values of $P_e/(\phi f'_c A_g)$, f'_c, $\rho_t m$ and cover thickness, was found to be approximately 1.4.

Thus, for circular columns, Eq. 4.37 becomes:

$$\rho_s \frac{f_{yh}}{f'_c} = 1.4\left\{\frac{A_g}{A_c}(-0.3\rho_t m + 0.009\varphi_u/\varphi_y + 0.208)\frac{P_e}{f'_c A_g} - 1.4 \times 10^{-3}(\varphi_u/\varphi_y)^2 - 1.7 \times 10^{-2}(\varphi_u/\varphi_y) + 0.036\right\} \quad (4.38)$$

Inspection of Eqs. 4.37 and 4.40 shows that the second term is insignificant compared to the first term. Moreover, if it is multiplied by the ratio of f'_c/f_{yh}, the second term becomes even less significant. Therefore, a constant number can be adopted for approximation. The refined design equations for both section types can be written in the following forms with a strength reduction factor ϕ included in the axial load ratio.

For square or rectangular sections:

$$\rho_s = \frac{A_g}{A_c}\frac{(\varphi_u/\varphi_y - 33\rho_t m + 22)}{111}\frac{f'_c}{f_{yh}}\frac{P_e}{\phi f'_c A_g} - 0.006 \tag{4.39}$$

where $\rho_s = A_{sh}/(s_h h_c) \geq 0$.

For circular sections:

$$\rho_s = 1.4\frac{A_g}{A_c}\frac{(\varphi_u/\varphi_y - 33\rho_t m + 22)}{111}\frac{f'_c}{f_{yh}}\frac{P_e}{\phi f'_c A_g} - 0.008 \tag{4.40}$$

where $\rho_s = 4A_b/(s_h d_c) \geq 0$.

4.4.3 Alternative Derivation of Refined Design Equation Using Optimization Methods

General

In this section, an alternative procedure to derive a refined equation using optimization theory is described. The derived equation is then compared to that given in Eq. 4.39, and the preferred design equation is suggested.

Multi-Variable Optimization and Its Application

The basic mathematical optimization problem is to minimize a scalar function E (known as an objective function), which is the value of a function of a set of dependent parameters, $x_1, x_2, ...x_n$.

In this derivation, the dependent parameters consist of:

A_g/A_c	denoted as x_1
φ_u/φ_y	denoted as x_2
$\rho_t m$	denoted as x_3
f'_c/f_{yh}	denoted as x_4
$P_e/(\phi f'_c A_g)$	denoted as x_5

In a multi-variable optimization, the quantity to be minimized is not only a function of controlled parameters but also of independent variables. If $A_1, A_2, ...A_m$ denote the values of the independent variables at the m available sample points, the form of the objective function can then be written as:

$$E = f[g(\mathbf{x}, A_1)g(\mathbf{x}, A_2), ...g(\mathbf{x}, A_m)] \tag{4.41}$$

where $\mathbf{x}$ is a column vector of x.

The values of the independent variables may be incorporated into the function $g(\mathbf{x})$ to yield the following equation:

$$E = f[G_1(\mathbf{x})G_2(\mathbf{x}), ...G_m(\mathbf{x})] \tag{4.42}$$

In this study, the values of the independent variables are the values of $\rho_s f'_c/f_{yh}$ obtained from the design charts.

The choice of the objective function is an important issue in optimization problems as it greatly influences the optimum point and the ease by which it is found.

The form of the function f is termed the error criterion. The most widely used error criterion is the *Least Squares* values with the following general form:

$$Minimize\ E = \sum_{i=1}^{m}[w_i G_i(\mathbf{x})]^2 \tag{4.43}$$

where $w_1, w_2, ...w_m$ are termed weights or penalties, and have the effect of emphasizing errors of importance in the formulation of the problems.

A predicted equation was chosen to take the form as the right hand side of the refined equation shown in Eq. 4.39 as follows:

$$F = x_1(Ax_2 + Bx_3 + C)x_4x_5 + D \tag{4.44}$$

The figures in Eq. 4.39 were used as the first estimated values of A, B, C and D in the process of optimization. The objective function E can then be written as:

$$E = \sum_{i=1}^{m}(\rho_{si}\frac{f'_c}{f_{yh}} - x_{1i}(Ax_{2i} + Bx_{3i} + C)x_{4i}x_{5i} + D)^2 \tag{4.45}$$

The E value obtained from Eq. 4.45 is the sum of the errors at the data points. Using optimization methods, the minimized E can be found.

Since the $\rho_s f'_c/f_{yh}$ obtained from the design charts are well spread, it was decided to take the weighting value w_i in Eq. 4.43 as unity.

The following step is now to decide the method of performing the optimization. For multi-variable optimization, the methods fall naturally into two classes, although they are not completely separate, namely *Search methods* which use objective function evaluation only, and *Gradient methods* which in addition require gradient information [51].

In general, Gradient methods are superior to Search methods if the functions involved have continuous derivatives which can be evaluated analytically. For functions for which the derivative information is not readily available, the application of Search methods is normally required. However, a Gradient method that only requires objective function evaluations has been recently formulated in a form of subroutine library **VF04AD** [50]. In this routine, derivative information is not necessarily supplied, as an estimation of the gradient was found numerically from either the Finite or Central Difference formula. The basic method and its derivation may be found in Refs. [52,53].

Using the gradient optimization [50], the following optimum equations were found:

For $\varphi_u/\varphi_y = 10$ for square or rectangular columns:

$$\rho_s = \frac{A_g}{A_c}\frac{(2\varphi_u/\varphi_y - 0.1\rho_t m + 1)}{100}\frac{f'_c}{f_{yh}}\frac{P_e}{\phi f'_c A_g} - 0.004 \tag{4.46}$$

For $\varphi_u/\varphi_y = 20$ for square or rectangular columns:

$$\rho_s = \frac{A_g}{A_c}\frac{(2\varphi_u/\varphi_y - 0.2\rho_t m - 8.2)}{100}\frac{f'_c}{f_{yh}}\frac{P_e}{\phi f'_c A_g} - 0.006 \tag{4.47}$$

It is obvious that in Eqs. 4.46 and 4.47 that the parameter $\rho_t m$ has little significance. In the previous analysis however, it was shown that this parameter did influence the quantities of confining reinforcement significantly.

Fig. 4.35 compares the quantities of confining reinforcement required in a square or rectangular column section, as suggested by Eqs. 4.39, 4.46 and 4.47, and by the code [2].

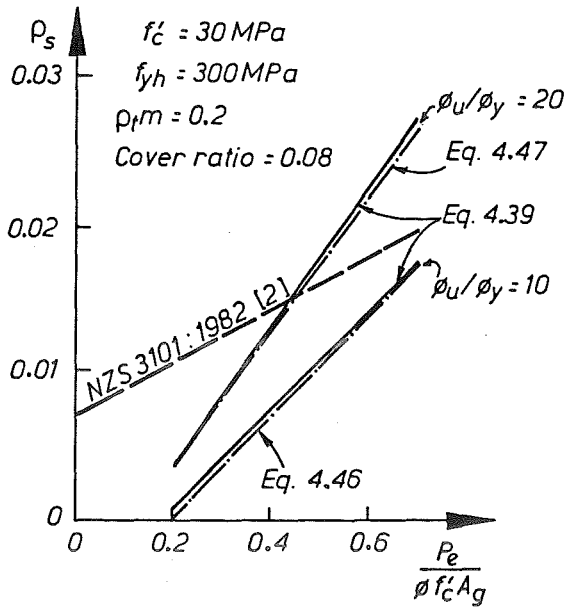

Figure 4.35: Comparison of Quantities of Confining Reinforcement in a Square or Rectangular Column Section, as Suggested by Eqs. 4.39, 4.46 and 4.47, and by the Code [2]

It can be seen from Fig. 4.35 that the required quantities of confining reinforcement ρ_s predicted by the equation obtained from the 95% upper tail values, agreed very well with those obtained from the optimization theory. In general however, Eq. 4.39 gives greater quantities of confining reinforcement than those equations derived from the Optimization method. To obtain the optimum fitted-curve, which means to search for the minimum errors at the data points, the values of ρ_s obtained from the chart should be evenly distributed above and below the optimum curve. On the other hand, Eq. 4.39 was derived from the 95% upper tail design chart values of ρ_s, which means that the values of ρ_s obtained from the chart are generally below the the values of ρ_s given by Eq. 4.39. This difference is reflected in Fig. 4.35 in which although the two approaches gave similar results, Eq. 4.39 indicates more conservatism. It is also clearly seen from Fig. 4.35 that the current code [2] equation of confining reinforcement is more than sufficient to provide curvature ductility factor φ_u/φ_y of 20 for columns with low to medium axial compression, but it is not sufficient for columns with large axial compression. Based on the above considerations, it was decided to suggest Eq. 4.39 as a refined design equation to replace the current code [2] equations.

4.5 Verification of the Refined Design Equation

A comparison of the quantities of confining reinforcement obtained from the proposed refined design equation, with the quantities provided in the column units tested by various researchers [7,8,9,4,5] is necessary, to ensure that the proposed equation is not unduly conservative, and yet reasonably accurate.

Except for some columns tested by Potangaroa [8], the results of the columns tested previously at the University of Canterbury [7,8,9,4], which were generally designed to the New Zealand code recommended quantities of confining reinforcement, showed that the columns behaved in a ductile manner. No significant strength degradation was detected before the tests were terminated. Moreover, the load-displacement hysteresis loops were still rising, indicated that the units maintained sufficient reserve strength.

For the tests carried out as a part of the present study (see Chapter 3), it was also found that Units 1, 2 and 9 indicated ductile behaviour. It is worth noting, that Units 1 and 2 only contained about one-half of the code recommended quantities for ductile detailing. Unit 9 however, was designed to have adequate ductility as predicted by the cyclic moment-curvature theory [4] on which the design charts were based.

Figs. 4.36 compares the quantities of confining reinforcement provided in the column units mentioned above, with the quantities required by the refined design equation to achieve $\varphi_u/\varphi_y = 20$.

It is evident that the quantities provided in the columns tested were generally greater than the quantities required for adequate ductility according to the refined design equation. Although the maximum experimental values of φ_{max}/φ_y attained by some of the columns were less than 20 (see Table 2.2, Chapter 2), this was due to the termination of the tests after completing two cycles to a displacement ductility factor of 6 or 8. If the tests had been carried on to higher displacement ductility factors, $\varphi_{max}/\varphi_y = 20$ would easily have been obtained since the hysteresis loops were still showing an increase in load with displacement at the

end of testing. Therefore the prediction of the refined design equation that the quantities provided were excessive to achieve the expected level of ductility was confirmed.

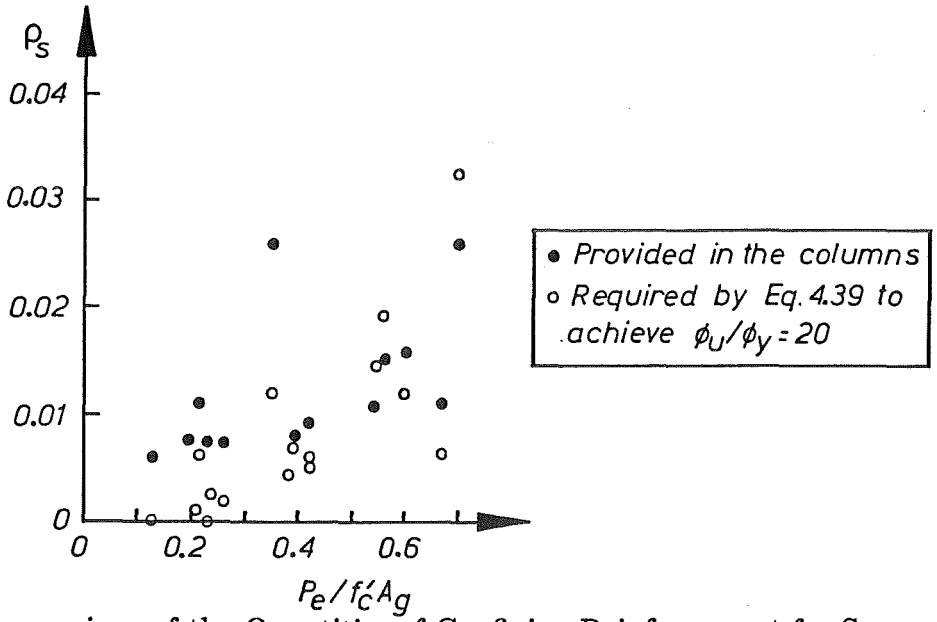

Figure 4.36: Comparison of the Quantities of Confining Reinforcement for Square and Circular Reinforced Concrete Columns

The quantities of confining reinforcement in the columns tested by Potangaroa [8] were less than those required by the refined design equation to achieve $\varphi_{max}/\varphi_y = 20$. However, it was shown that those units did not indicate ductile performance. The maximum curvature ductility factor obtained from the test was less than 10. This indicated therefore that the quantities provided in the columns should be increased as given by Eq. 4.40.

The refined design equation therefore gives a more accurate, and yet sufficiently conservative prediction, and therefore it is suitable for use in design.

4.6 Concluding Remarks

The conclusions reached from this investigation may be summarized as follows:

1. The parameters which have significant influences on the available curvature ductility factor in the potential plastic hinge regions of reinforced concrete columns during cyclic flexure were examined, namely the axial load ratio $P_e/(f'_cA_g)$, the concrete compressive strength f'_c, the mechanical reinforcing ratio $\rho_t m$, and the cover ratio c/h for square and rectangular columns, or c/D for circular columns.

2. The investigation indicated that the current code [2] equations for confining reinforcement are just sufficient to ensure an available curvature ductility factor of φ_u/φ_y=20, when the axial load ratio $P_e/(f'_cA_g)$ is approximately 0.35, and the mechanical reinforcing ratio $\rho_t m$ is greater than 0.2. For columns with large axial compression and large cover thickness, the code equations are not sufficient to provide a curvature ductility factor of 20, particularly when ρ_t is small.

3. Using the design charts for ductility [4], and considering a range of the critical parameters as mentioned in (1), two methods were used to derive a refined design equation for the quantities of confining reinforcement required in potential plastic hinge regions of square and rectangular columns.

   In the first method, the 95% upper-tail values of $\rho_s f_{yh}/f'_c$ obtained from the design charts were determined. Using a regression analysis, the best-fit equation was obtained by the Least Square method, as follows:

$$\rho_s = \frac{A_g}{A_c}\frac{(\varphi_u/\varphi_y - 33\rho_t m + 22)}{111}\frac{f'_c}{f_{yh}}\frac{P_e}{\phi f'_c A_g} - 0.006$$

   where $\rho_s = A_{sh}/(s_h h_c) \geq 0$.

   In the second method, the refined design equation was derived using the gradient optimization methods. The following equations for the quantities of confining reinforcement were found:

   For $\varphi_u/\varphi_y = 10$:

$$\rho_s = \frac{A_g}{A_c}\frac{(21 - 0.1\rho_t m)}{100}\frac{f'_c}{f_{yh}}\frac{P_e}{\phi f'_c A_g} - 0.004$$

   For $\varphi_u/\varphi_y = 20$:

$$\rho_s = \frac{A_g}{A_c}\frac{(31.8 - 0.2\rho_t m)}{100}\frac{f'_c}{f_{yh}}\frac{P_e}{\phi f'_c A_g} - 0.006$$

   where $\rho_s = A_{sh}/(s_h h_c) \geq 0$.

   Since the equation obtained from the Least Square method generally gives more conservative values of the quantities of confining reinforcement than those obtained from the Optimization method, the first equation is proposed to replace the current code [2] equations.

4. The quantities of confining reinforcement needed in the potential plastic hinge regions of circular columns are markedly different from those in columns with square and rectangular sections. with the same axial load level, mechanical reinforcing ratio and curvature ductility demand. However, the same refined design equation for confining reinforcement section type factor f to account for section shape. The f factor was found to be 1.4.

5. The proposed refined design equation ensures that the specified curvature ductility factor φ_u/φ_y in columns is available for axial compressive load levels up to $0.7f'_c A_g$.

6. The refined design equation gives only the transverse reinforcement required for concrete confinement. The transverse reinforcement provided must also be checked to ensure that the stability of longitudinal compression bars, and shear requirements are satisfied.

Chapter 5

COMPARISON OF THE INELASTIC DYNAMIC RESPONSE OF REINFORCED CONCRETE FRAMES OF LIMITED DUCTILITY AND DUCTILITY

5.1 Introduction

Section 14 of the New Zealand concrete design code NZS 3101:1982 [2] covers the design and detailing requirements for members in structures of limited ductility subjected to earthquake induced loading.

Structures of limited ductility need to be designed for higher seismic loadings than those used in the design of ductile structures. The design seismic loadings are part-way between those for ductile structures and those for elastically responding structures, and hence because the ductility requirements are not as high as for ductile structures, the application of capacity design becomes less important and is not necessary. This exemption presents a potential problem because of the difficulty of identifying possible modes of collapse. Column sidesway mechanisms can occur due to dynamic effects of higher modes of vibration which are more pronounced when the fundamental periods of vibration of structures increase. For structures of four storeys or less however, the effect of higher modes is not so prominent and therefore the ductility demand at the plastic hinges at the column ends may not be so great.

According to NZS 4203:1984 [30], frames of limited ductility have a maximum height of four storeys or 18 m, or if the roof and wall mass are less than 150 kg/m^3 of floor area a maximum height of 5 storeys or 22.5 m. Section 14 of NZS 3101 [2] states that for buildings of more than four storeys, column sidesway mechanisms may result in poor performance of buildings and a special study is needed.

The following structures are appropriate for design as structures of limited ductility:

- Low rise buildings which have a greater inherent strength than required for ductile structures, and hence low ductility demand is expected even under the strongest seismic attack
- Multi-storey buildings which have been designed for lateral wind loads greater than required by the code seismic loadings for ductile behaviour
- Less important buildings which do not warrant detailing for full ductility.

In this study, the response of typical four, six and twelve storey reinforced concrete frames under seismic attack is investigated. The frames were designed for ductility and limited ductility. Two different approaches were adopted. For ductile frames, the capacity design procedure proposed by Park and Paulay [6] was applied. For limited ductile frames, instead of using capacity design, the conventional strength design method was applied to apportion the strengths of the members, and some relaxation of detailing was considered in recognition of a smaller ductility demand. The dynamic response of the buildings was examined and compared, including the deformation response and ductility demand, column axial forces, beam and column bending moments and shear forces, and the required longitudinal and transverse reinforcement content in the beams and columns. The frames were assumed to be located in a less severe seismic zone in New Zealand, and were designed for combinations of gravity and code seismic loadings. These, as discussed above, are likely to be the types of structures most suitable for limited ductility design. However, the response of the non-capacity designed structures under the strongest seismic attack in New Zealand was also examined in the dynamic analyses, and the results from this excitation are discussed.

A proposed draft replacement for NZS 4203:1984, prepared by a committee of the Standards Association of New Zealand has been circulated for comment. The draft DZ4203 [39] proposes changes to the load factors and the seismic design loadings, as summarized in a NZNSEE study group report [1]. For the frames investigated in this study, the load factors and seismic design loadings recommended in the draft DZ4203 were adopted.

The inelastic dynamic analyses in this study were carried out using a two-dimensional non-linear dynamic computer program RUAUMOKO [55].

5.2 Structural Layout and Description of the Buildings

The buildings analysed, were designed in accordance with the requirements for limited ductility and ductility specified in the New Zealand codes. The component of horizontal earthquake loading perpendicular to the plane of the frames considered was assumed to be resisted by structural walls or some other structural systems. The effect of vertical component of earthquake loading on the response of the buildings was neglected. Torsional moments and $P-\Delta$ effects were not considered in the design. All non-capacity designed frames, and the four storey capacity designed frame were designed according to the draft New Zealand loadings code DZ 4203:1986 [39] and the New Zealand concrete design code NZS 3101:1982 [2]. The six and twelve storey capacity designed frames, designed by Tompkins *et al.* [54],

according to the requirements of DZ3101:1978 [10] and NZS4203:1976 [29], were used for comparison. The basic dimensions of the buildings are given in Tables 5.1 to 5.4, and Figs. 5.1 to 5.3.

Table 5.1: Member Dimensions for the Four Storey Frames Designed for Limited Ductility and for Ductility (All Dimensions are in mm)

Member	Floors 1 to 4
Main Beams	400 × 750
Secondary Beams	350 × 600
Columns 1 and 4	500 × 500
Columns 2 and 3	600 × 600
Slab	160

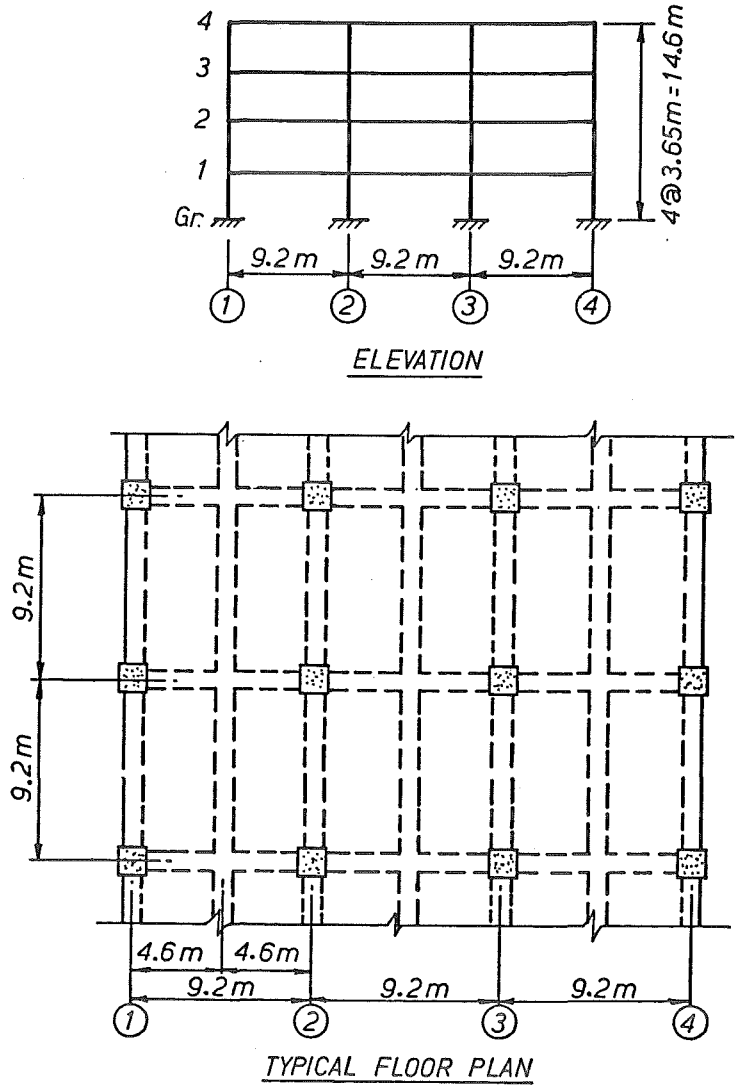

Figure 5.1: Principal Dimensions of the Four Storey Frames

Table 5.2: Member Dimensions for the Six Storey Frames Designed for Limited Ductility (All Dimensions are in mm)

Member	Floor	
	1 to 4	5 and 6
Main Beams	400 × 750	400 × 750
Secondary Beams	350 × 600	350 × 600
Columns 1 and 3	500 × 550	500 × 500
Column 2	600 × 600	550 × 550
Slab	160	160

Table 5.3: Member Dimensions for the Six Storey Frames Designed for Ductility (All Dimensions are in mm)

Member	Floor	
	1 to 4	5 and 6
Main Beams	400 × 750	400 × 750
Secondary Beams	350 × 600	350 × 600
Columns 1 and 3	500 × 575	500 × 500
Column 2	650 × 650	600 × 600
Slab	160	160

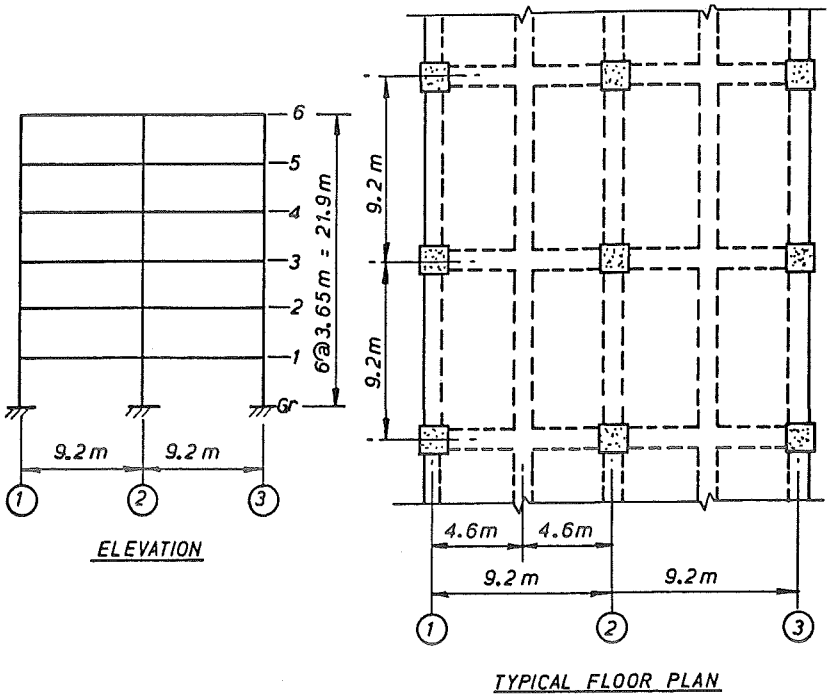

Figure 5.2: Principal Dimensions of the Six Storey Frames

Table 5.4: Member Dimensions for the Twelve Storey Frames Designed for Limited Ductility and for Ductility (All Dimensions are in mm)

Member	Floor				
	1 to 3	4 to 6	7 and 8	9 and 10	11 and 12
Main Beams	400 × 750	400 × 750	400 × 700	400 × 650	400 × 600
Secondary Beams	350 × 600	350 × 600	350 × 600	350 × 600	350 × 600
Columns 1 and 3	500 × 725	500 × 625	500 × 575	500 × 525	500 × 500
Column 2	725 × 725	675 × 675	625 × 625	575 × 575	550 × 550
Slab	160	160	160	160	160

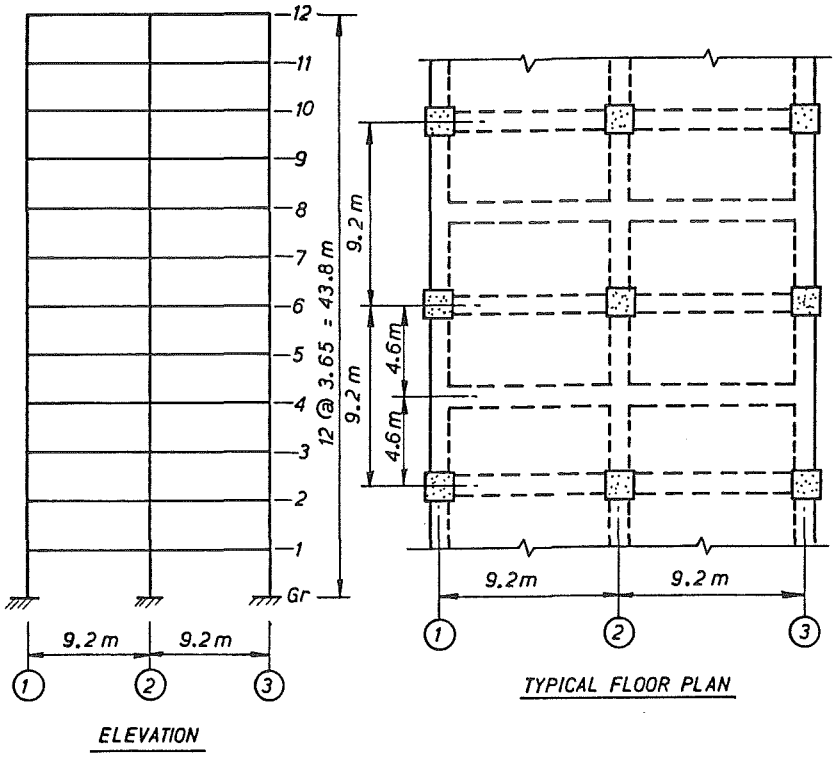

Figure 5.3: Principal Dimensions of the Twelve Storey Frames

Frames with greater number of bays than shown in Figs. 5.1 to 5.3 were also considered. It was found however, that the results of the inelastic dynamic response analyses of those frames were quite similar to the results of the frames with a lesser number of bays. It was decided therefore to report only the response of the frames shown in Figs. 5.1 to 5.3.

The load factors used, as specified in the draft New Zealand Loadings Code DZ 4203:1986 [39] were as follows:

$$\begin{aligned} U &= 1.2D + 1.6L_r \\ U &= 1.2D + 1.2L_s \pm E \\ U &= 0.9D \pm E \end{aligned} \tag{5.1}$$

where D is the dead load, L_r and L_s are the reduced live load and live load at serviceability state respectively, and E is the earthquake load.

A unit weight of 23 $\mathsf{kN/m^3}$ was assumed for concrete. A uniformly distributed dead load of 0.5 kPa and unreduced live load of 2.5 kPa (as for offices for general use [39]) were assumed. The live load at serviceability state was taken as 0.8 kPa. The reduced live load was obtained from unreduced live load multiplied by a reduction factor R_l of

$$R_l = 0.4 + 2.7/\sqrt{A} \tag{5.2}$$

where A=tributary area per floor, in square metres.

A concrete compressive strength of 30 MPa was assumed. According to a News Release of the Standards Association of New Zealand [56], Grades 275 and 380 reinforcing steel in New Zealand will be replaced by Grades 300 and 430 reinforcing steel, respectively. These new, greater characteristic yield strengths, were used for the beam and column longitudinal reinforcement, respectively.

5.3 Equivalent Lateral Static Load Analysis

According to the DZ4203:1986 [39], the total horizontal seismic shear force at the base of a regular structure, V shall be computed from

$$V = C_\mu RZW_t \tag{5.3}$$

where

- C_μ = a basic seismic coefficient read from one of the sets of normalized curve, as shown in Fig. 5.4. The set is chosen to be appropriate for normal and soft soil conditions, the degree of structure ductility μ available, and the value for the natural period of vibration of astructure

- R = a risk factor, varies between 0.4 and 1.3, which modifies the design load when either diminished failure risk is required or enhanced failure risk is acceptable.
- Z = a zone factor accounting for regional seismicity
- W_t = gravity load of structure considered to be present during the earthquake, which was calculated by adding the dead load D and one third of the unreduced live load L.

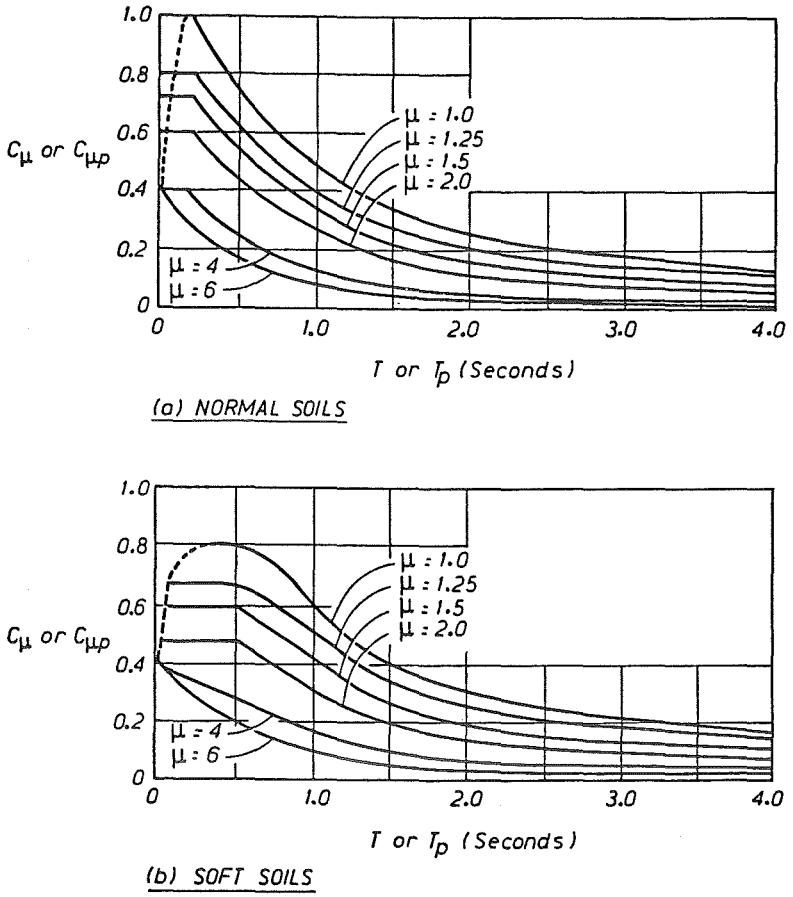

Figure 5.4: Basic Seismic Coefficients Proposed in the Draft Code DZ4203:1986 [39]

The distribution of seismic lateral load applied at level i of the structure shall be obtained from

$$F_i = (V - F_t)\frac{W_i h_i}{\sum W_i h_i} \tag{5.4}$$

where F_t=addition seismic load to be applied at the top of the structure, W_i and h_i=seismic weight and height at level i of the structure, respectively. When the natural period of the structure in the direction under consideration is less than 0.7 seconds, F_t shall be taken as zero. Otherwise,

$$F_t = 0.08V \tag{5.5}$$

and this quantity shall be added to F_i at the top of the structure.

The displacement ductility factors for ductile moment resisting reinforced concrete frames and for reinforced concrete moment resisting frames of limited ductility recommended by DZ4203 [39] are 6 and 3, respectively. This can be checked against the values calculated using the assumptions of NZS 4203:1984 [30] as follows. Based on the equal displacement concept, a relationship between the structural type factor S and the displacement ductility factor μ can be written as:

$$\mu = \frac{4}{SM} \tag{5.6}$$

where according to the NZS 4203:1984 [30] the structural material factor is taken as M=0.8 for reinforced concrete, and the structural type factor is taken as S=0.8 for ductile frames, S=1.0 to 2.0 for ductile cantilever structural walls depending on the height/horizontal length ratio, and S=2.0 for frames and cantilever structural walls of limited ductility. The code [30] recommended values for μ for the frames are then 2.5 and 6.25. In this study μ=6 and μ=3, were used for ductile and limited ductile moment resisting frames, respectively.

A risk factor of R=1.0 and a zone factor of Z=0.5 were adopted. However, when the response of the buildings under the most severe earthquake generated in New Zealand [65] was examined, Z=0.85 was used.

With member stiffnesses as shown in Table 5.5, and assuming that columns have full base fixity, an elastic analysis due to a unit base shear was carried out using a two dimensional structure computer program [57].

Table 5.5: Assumed Stiffnesses of Structural Members

Properties	Beams	Columns
Area	$0.5A_g$	$0.8A_g$
Shear Area	$0.5A_v$	$0.8A_v$
Second Moment of Area	$0.5I_g$	$0.8I_g$

Note: A_v is shear area, and A_g and I_g are area and second moment of area of the gross section, respectively.

According to DZ 4203:1986 [39], the natural period T may be computed from the Rayleigh formula:

$$T = 2\pi\sqrt{\frac{\sum W_i d_i^2}{g\sum F_i d_i}} \tag{5.7}$$

where W_i, d_i and F_i are seismic weight, displacement and lateral load of level i, respectively, and g is acceleration due to gravity.

Defining d_i' as the displacement due to a unit base shear, Eq. 5.7 can be rewritten as:

$$T = 2\pi\sqrt{\frac{\sum W_i(d_i')^2}{g\sum \frac{F_i}{V}d_i'}} \tag{5.8}$$

in which F_i/V can be found from Eq. 5.4. This means that the displacement at each level due to a unit base shear can be used in calculating T [58]. The calculated T for the buildings are given in Table 5.6 below.

Table 5.6: Natural Period of Limited Ductility and Ductile Buildings

Number of Storeys	T for *Buildings LD* (secs.)	T for *Buildings D* (secs.)
Four	0.80	0.80
Six	1.19	1.15
Twelve	2.39	2.27

Note: *LD* denotes limited ductility and *D* denotes ductility

It is worth noting that the values of T for the twelve storey limited ductility buildings are slightly different from those for ductile buildings ($\approx 5\%$), although the dimensions of the two buildings are similar. This is probably due to a small difference in the calculation of the weight of the buildings.

Assuming that the buildings were located on normal soils, the basic seismic coefficient C_μ was found from Fig. 5.4 using the appropriate design μ. The base shear V was then calculated from Eq. 5.3, and an elastic analysis was carried out to obtain the axial and shear forces, and the bending moments, in the beams and columns due to various combinations of loadings as given in Eq. 5.2.

DZ4203:1986 [39] recommends that the maximum difference between the horizontal deflections of consecutive floor levels shall not exceed $Z/50$ times the difference in elevation of those levels (i.e. drift $\leq Z/50$). The inclusion of the zone factor Z ensures that the ratio of the $P-\Delta$ moment to total moment at any level is practically independent on the geographic location of a structure. The code limitations for the drifts are 1% and 1.7% for $Z = 0.5$ and $Z = 0.85$, respectively.

5.4 Design of Prototype Frames

5.4.1 General

In the design of the prototype frames, the design procedure given by Paulay [63] was adopted.

A moment redistribution technique developed by Paulay [64] was applied to the beam moments obtained from elastic frame analysis. The aim of using moment redistribution is to utilize as much as possible of the beam moment capacity. For example, NZS 3101:1982 [2] recommends that in the potential plastic hinge region the compression reinforcement ratio should not be less than half of the tension reinforcement ratio.

Redistribution of beam moments at column centre-lines was carried out leading to reductions of up to 30% of the maximum moment as recommended by NZS 3101 [2]. Redistribution of column moments of up to 20% of their maximum original values was also made.

Once the design actions in columns were calculated, a computer package [66] was used to design the columns. The column charts given in the New Zealand Reinforced Concrete Design Handbook [67] were used as the first design estimation.

As mentioned previously, separate design procedures were adopted for designing ductile frames and frames of limited ductility.

5.4.2 Design of Ductile Frames

General

The capacity design approach proposed by Park and Paulay [6] was used to design the earthquake load dominated ductile frames. In the capacity design, the maximum probable actions that can be generated in the beams due to overstrength, need to be estimated before the design actions in the columns can be assessed. The column design actions are also assessed taking into account the possible effects of higher modes of vibration and concurrent loading effects. The procedure is intended to provide a high degree of protection against the formation of column sidesway mechanisms in any storey during very severe seismic loading [2]. That is, a strong column-weak beam concept is used. This enables the desired mechanism of inelastic deformation, namely plastic hinging in the beams is assured. Capacity design procedures are also used to provide adequate reserve shear strength in beams, columns and beam-column joints.

The flexural strength requirements for beams and columns, and the-step-by-step design procedures, are described in detail in the Commentary of the code [2]. The code also specifies the use of a strength reduction factor of $\phi = 0.9$ for the design of beam sections for flexure, and $\phi = 1.0$ for the design of column sections and all members and joints for shear, with design actions derived from the overstrengths of adjacent members in accordance with capacity design.

Design Actions

Design of Beams

The design moment envelopes for the beams, obtained from the elastic frame analysis and moment redistribution, were used to proportion the longitudinal reinforcement required in the beams. The maximum probable moment input from beam to column, which could

develop during large inelastic deformations, was determined using the beam flexural overstrength factor ϕ_o at the column centre-line at each floor and in each direction of loading. ϕ_o is the ratio of the maximum probable flexural overstrength developed by the beam to the flexural strength required by the code [2].

The design shear forces in the beams were calculated from the combinations of the static lateral forces, with the flexural overstrength being developed at the most probable location of the critical sections in the beams, and the gravity load with an appropriate load factor.

Dynamic Magnification of Column Moments

A dynamic magnification factor ω is also introduced to take into account the dynamic effects of higher modes of vibration, which result in a departure of the column moment pattern from that obtained from an elastic frame analysis for the code static load distribution [2].

Higher mode effects are more prominent in the upper storeys and when the natural period of vibration of the structures T increases. The code [2] relates ω and T as follows:

For one-way frames

$$\omega = 0.6T + 0.85 \tag{5.9}$$

but not less than 1.3 nor more than 1.8.

For two-way frames

$$\omega = 0.5T + 1.0 \tag{5.10}$$

but not less than 1.5 nor more than 1.9.

In the design examples of frames considered here, it is assumed that the lateral load in the other direction is resisted entirely by structural walls, hence the ω values for one-way frames are used. At roof and base levels, where column plastic hinging is acceptable, ω is taken as unity. At the top storey, the development of a column sidesway mechanisms is acceptable and the minimum value of ω=1.3 may be taken. At the first storey a point of contraflexure does not normally occur in a column, since the columns are stiff relative to the beams, and therefore cantilever action of the columns will dominate. This reduces the effects of higher modes and thus ω=1.3 can be taken in the first storey.

Column Design Axial Forces

Based on the assumption that with an increasing number of storeys the proportion of the beam plastic hinges at which the flexural overstrength may simultaneously occur is reduced, an axial force reduction factor R_v is introduced [2]. Thus, the earthquake induced axial force in a column should not be less than

$$P_{eq} = R_v \sum V_{oe} \tag{5.11}$$

where $\sum V_{oe}$ is the sum of the earthquake induced beam shear forces at all floors above the level considered, developed at all sides of the column, taking into account the beam overstrengths and the appropriate sense of the forces. The R_v factor varies between 0.54 to 0.97, depending on the number of floors above that level and ω.

Column Design Moments

The code [2] specifies that in each principle direction, column design moment to be used together with the appropriate axial load for the determination of the ideal strength of the column, should not be less than

$$M_{col} = \phi_o M_{code} - 0.3 h_b V_{col} \tag{5.12}$$

or when the total design axial load on the column does not exceed $0.1 f'_c A_g$, and hence column yielding is more acceptable, the design column moment can be reduced and taken as follows:

$$M_{col,red} = R_m(\phi_o M_{code} - 0.3 h_b V_{col}) \tag{5.13}$$

where M_{code} is column bending moment derived from the code specified seismic loading, V_{col} is column design shear force and h_b is the beam depth.

The R_m factor varies between 1.0 and 0.3 depending on ω and the axial load level.

Column Design Shear Forces

The design shear force in a column of one-way frames can be computed from the following expressions [2]:

At upper storey columns

$$V_{col} = 1.3 \phi_o V_{code} \tag{5.14}$$

At first storey columns, in addition to satisfying the requirement above (Eq. 5.14), the shear force given by Eq. 5.15 should also be considered:

$$V_{col} = \frac{M_{o,col} + 1.3 \phi_o M_{code,top}}{l_n + 0.5 h_b} \tag{5.15}$$

where $M_{o,col}$ is the flexural overstrength capacity of the base section, and $M_{code,top}$ is the value of M_{code} for the first storey columns at first floor level.

For two-way frames, the 1.3 in Eq. 5.14 becomes 1.6, and 1.3 in Eq. 5.15 becomes 1.5. Again, in the design examples of frames examined here, it is considered that due to the presence of structural walls in the other direction the frames can be treated as one-way frames.

Gravity Load Dominated Frames

In low rise frames, particularly those with long span beams, and commonly in the upper storeys of multi-storey frames, often the gravity load rather than seismic load requirements will govern the design strengths of beams. This results in flexural strengths of the beams which may be greater than those required by the code for seismic loading. The indiscriminate application of the capacity design philosophy as described above, to such a structure would therefore lead to unnecessary conservatism, particularly in the design of columns.

To overcome this problem, the formation of plastic hinges in some columns is permitted. However, two design criteria should be satisfied:

- No column sidesway mechanisms (soft storeys) should be able to form. This can be achieved by assuring the outer columns remain in the elastic range, and that plastic hinges can only form in the inner columns.
- Reduction of the ductility demand in the frame, since the formation of plastic hinges in columns is undesirable. This can be achieved by increasing the lateral load resistance of the frame, which means increasing the strengths of the members. As a result, the inelastic response of the frame to the design earthquake decreases, and thus reduces the ductility demand. Hence, instead of using the capacity design approach, a non-capacity design approach for frames with less ductility demand could be applied.

5.4.3 Design of Frames of Limited Ductility

General

As mentioned previously, the frames of limited ductility studied here were designed using the conventional strength design method rather than the capacity design procedure.

Design Actions

The design actions in the beams and columns due to various combination of loadings were obtained directly from two-dimensional elastic theory structural analysis, and the members were designed according to the most critical combination of loadings.

A similar amount of redistribution of beam and column moments was also applied to the non-capacity designed frames of limited ductility as was used for the capacity designed ductile frames.

The design shear forces of beams are calculated assuming that the flexural overstrengths developed at both ends of the beams simultaneously (see Fig. 5.5a), and the design shear forces of columns are calculated assuming that moments at both ends of the columns reached the code strengths M_{ACI} simultaneously (see Fig. 5.5b).

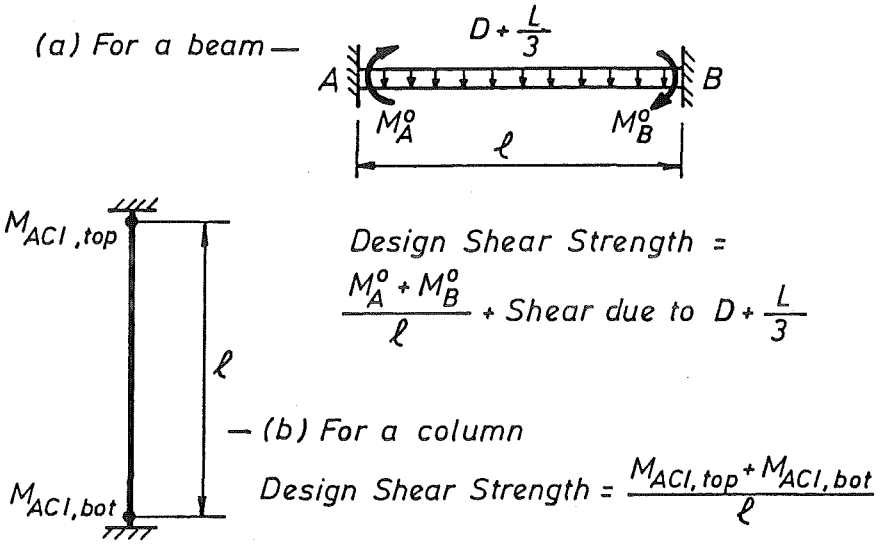

Figure 5.5: Assumption for Determining Design Shear Forces

Design Strengths

The beams and columns were designed such that the dependable strengths in the members, that is ϕ times the ideal strengths, had to be at least equal to the design actions, where ϕ=strength reduction factor:

ϕ	=	0.9	for flexure
ϕ	=	0.9	for flexure and axial load
ϕ	=	0.85	for shear

It is worth noting that according to the code [2], a strength reduction factor of ϕ=0.7 for flexure and axial load shall be used for columns not detailed for ductility, that is if the columns are not sufficiently confined for an available curvature ductility factor of φ_u/φ_y=20. However, since in these frames, confinement for φ_u/φ_y=10 is provided, and other brittle types of failure are prevented, ϕ=0.9 was used in the design of these columns.

5.5 Investigation of Dynamic Behaviour of Frames of Limited Ductility

5.5.1 General

Since the capacity design procedure is not applied in the design of frames of limited ductility, yielding is likely to develop in columns, and brittle failure due to inadequate flexural ductility or shear resistance may occur. Therefore, to fully investigate the behaviour of this type of frame, the worst condition for the possibility of the formation of the plastic hinges in the columns, and the occurence of shear failure, need to be examined. Two sets of dynamic analyses were then conducted.

5.5.2 Dynamic Analysis to Examine the Flexural Behaviour of Columns

In this case, the beam flexural overstrengths of $M = \phi_o M_i$ were used, where ϕ_o is the beam flexural overstrength factor, taken as 1.25, and M_i is the ideal flexural strength $\approx A_{st} f_y jd$, where A_{st}=area of tension steel, f_y=yield strength of longitudinal steel, jd=lever arm between the centroid of tension steel and the centre of concrete compressive block. For columns, the flexural strengths of $M = \phi M_{ACI}$ were used, where ϕ is strength reduction factor, taken as 0.9 and M_{ACI} is ideal flexural strength, calculated using the code [2] approach. These flexural strengths, with the greatest beam strengths and the smallest column strengths, will result in the greatest column plastic hinge rotations and the most likely situation for the formation of a column sidesway mechanism.

5.5.3 Dynamic Analysis to Examine the Shear Behaviour of Columns

As for the examination of the flexural behaviour, the beam flexural overstrengths of $M = \phi_o M_i$ were used. For columns however, the *real* flexural strengths of $M = \phi M_{real}$ were used, where M_{real} is real flexural strength, taking into account enhancement in concrete strength due to confinement, and increase in steel stress due to strain hardening. In this calculation, P_e was used, and the strength was taken as the maximum moment reached before the curvature exceeds five times the yield curvature φ_y. These flexural strengths, with the greatest beam strengths and the greatest column strengths, will result in the greatest shear forces.

5.6 Computer Modelling and Selected Ground Acceleration Record

5.6.1 Computer Program

The two-dimensional inelastic time-history analysis program RUAUMOKO [55] was used to investigate the response of the designed structures under simulated seismic attack.

In this program, a step-by-step numerical integration process is used to solve the equations of motion governing the response of a structure to a given input base excitation. The time step, Δt used for the numerical integration process is an important parameter. In RUAUMOKO, the numerical integration is based on the Newmark $\beta = \frac{1}{4}$ scheme [59]. Instability in analysis may arise if Δt is not sufficiently small due to response phase shift, implicit equivalent damping of the integration technique, and amplitude modification. Two main factors which influence the value of Δt are the economic feasibility and the need to ensure stability. Generally, a time step must be sufficiently smaller than the lowest period of vibration. For a framed structure, a time step of 1/100 sec. is normally sufficient.

The program also requires the specification of stiffness properties (axial and shear areas, moment of inertia, Young's and shear moduli) which are considered constant throughout

the time history analysis. Below flexural yield conditions, no adjustment is made to member stiffnesses which might represent the effects of cracking, previous inelastic deformations, and changing axial load in columns.

Structural components are modelled by a one dimensional prismatic member element with a spring hinge at each end. The nonlinear ends of the elastic member model incorporate rigid end blocks which locate, through a modification to the transformation matrix, the potential yielding section away from the intersection of the member centre lines.

The mass of a prototype frame can be modelled as either equivalent lumped masses at the nodes or as consistent distributed mass in the structural members [62].

The secondary moment $P - \Delta$ is also included in the program. At each time step, the member properties are redefined in terms of the updated joint coordinates.

Four viscous damping models are available, namely Rayleigh [60] damping models using either initial or tangent stiffness, and two other models with linear and trilinear variation of damping with initial elastic natural frequencies. The Rayleigh damping model based on initial stiffness is usually preferred to that based on the tangent stiffness. The stiffness degradation of a structure after yielding means that damping based on the tangent stiffness decreases during the excursions which is not consistent with the intuitive idea that damping should increase with the onset of plasticity. However, it has been shown, that the Rayleigh damping model based on the tangent stiffness might lead to realistic results [61].

The velocity-dependent viscous damping force matrix $[C]$ is computed from

$$[C] = a_1[M] + a_2[K] \tag{5.16}$$

where $[M]$ is system generalized mass matrix, and for Rayleigh damping model based on initial stiffness, $[K]$ is initial stiffness matrix. The coefficients a_1 and a_2 are calculated from

$$a_1 = \frac{2\omega_1\omega_2(\omega_1\lambda_2 - \omega_2\lambda_1)}{\omega_1^2 - \omega_2^2} \tag{5.17}$$

$$a_2 = \frac{2(\omega_1\lambda_1 - \omega_2\lambda_2)}{\omega_1^2 - \omega_2^2} \tag{5.18}$$

where ω_1 and ω_2 are any two circular frequencies, and λ_1 and λ_2 are the respective fractions of critical damping applicable to the vibration modes with the frequencies mentioned. Other modes are constrained to have amounts of viscous damping such that:

$$\lambda_n = \frac{1}{2}(\frac{a_1}{\omega_n} + a_2\omega_n) \tag{5.19}$$

5.6.2 Input for Dynamic Analysis

The computer program RUAUMOKO [55] requires the following information as input data:

- Nodal geometry. The geometrical position of nodes must be provided to define the structure. Some information regarding possible nodal fixity or inter-nodal coupling is also given
- Member positions. All members making up the structure are specified by reference to the nodes which bound the members
- Stiffness properties. For each member, values of cross-sectional area, shear area and second moment of area are required. The member stiffness used in the design, which is simply assumed to be a fraction of the stiffness based on the gross section is shown in Table 5.6. Young's and shear moduli were taken as 25 and 11 GPa, respectively
- Length of Rigid End Blocks. The lengths of rigid end blocks for beams and columns were taken as one-half of the column and beam depths, respectively
- Strength properties. The strengths of the columns were given in the form of the simplified moment-axial load interaction diagram shown in Fig. 5.6.

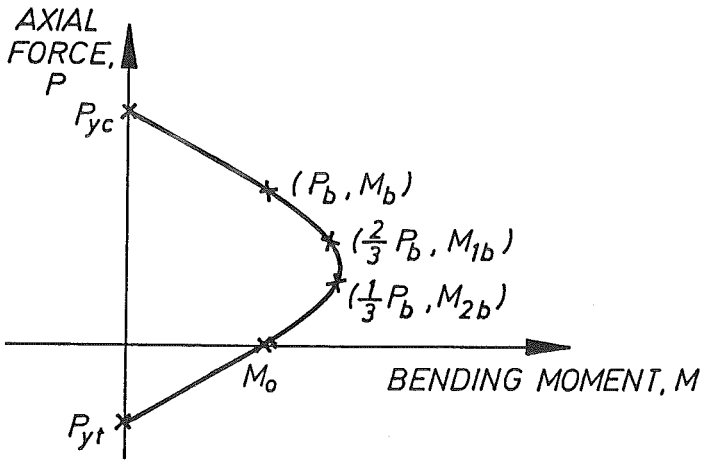

Figure 5.6: Axial Force Moment Yield Interaction Surface

The values of the flexural strengths of beams and columns supplied for non-capacity designed and capacity designed frames were given as follows:

For non-capacity designed frames of limited ductility

The strengths of beams and columns were calculated as mentioned in Section 5.5. To obtain the moment-axial load interaction diagram for the columns, the concrete compressive strength f'_c was used for the flexural investigation, and the confined strength of concrete f'_{cc} was used for the shear investigation.

For capacity designed ductile frames

The beam flexural overstrengths of $M = \phi_o M_i$, and the column flexural strengths of $M = \phi M_{ACI}$ were used, with ϕ is strength reduction factor = 1.0.

It is worth noting, that for beams and columns in frames of limited ductility, and for beams in ductile frames, where flexural yielding is expected, the strengths were multiplied by 0.95, to allow for a moment overshoot before the flexural yielding was

detected during the tracking of the moment-curvature hysteresis loops. This over-estimation of moment results from the assumption of linear behaviour for the duration of each constant length time step.

The bilinear moment-curvature hysteretic model, illustrated in Fig. 5.7, with a factor controlling post yield stiffness of $r = 0.02$, was used for the beams and columns.

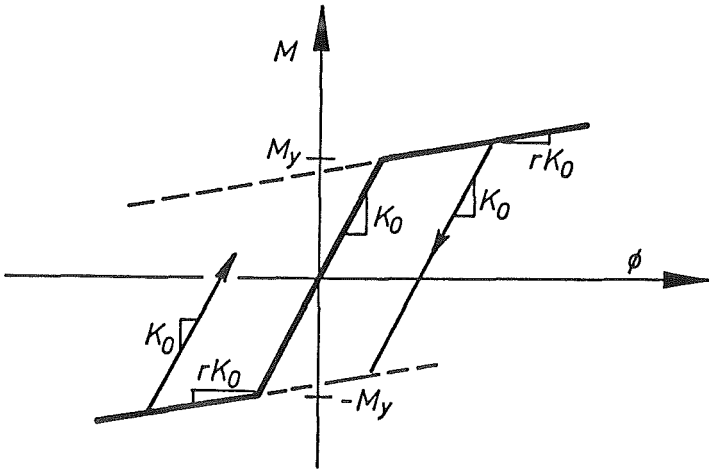

Figure 5.7: Bi-linear Moment-Curvature Hysteresis Model Used in Dynamic Analysis

- Nodal masses. Lumped nodal masses and inertia are required for the horizontal, vertical and rotational degrees of freedom to calculate the inertia forces and moments. The nodal masses were assessed using a tributary area approach, and the nodal weights were calculated as the sum of the external vertical loads and the internal beam shears. Rotational inertias were approximated as the off diagonal term of the consistent mass matrix [62] of a straight beam segment with uniformly distributed mass and was taken as $\sum(ml/420) \times 4l^2$, where m=the mass per unit length, based on the gravity load of $D + L_r/3$, and l=the length of each member connected to the node.

- Miscellaneous data. Some additional information such as the time step Δt used in the numerical solution of the equations of motion, and the fraction of critical damping are needed. A value of Δt=0.01 sec., and Rayleigh damping based on the initial stiffness with 5% of critical damping to the first and fifth modes of vibration were used in the analysis. This value of damping is commonly accepted as reasonable for reinforced concrete structures.

5.6.3 Sources of Inaccuracy in Time History Analysis

Due to the unsophisticated nature of modelling and selection of input data, some inaccuracies may occur in a time history analysis as listed below:

Modelling

- The assumed deformation patterns, which are based on finite element models may not fit some types of member well.

- The basic stiffness of members is generally held constant throughout the analysis, regardless of the influence of varying axial load.
- The viscous damping models used may not accurately reflect the true nature of the phenomenon.
- The behaviour of a structure obviously depends on the effects of torsion on members and on three dimensional effects. However, the modelling does not include these effects.
- The influences of non-structural elements and site conditions are not taken into account.

Input Data

- The assumed stiffness of the structural elements may not accurately reflect the effect of cracking and degradation of material properties of the elements. This affects the frequency characteristics of a structure, which may result in different deformation responses.
- The actual strengths of the members may not be accurately estimated, which will influence the onset of yielding and thus the overall response of the structure.
- The assumptions of full base fixity and floor slab rigidity may not be precise.
- The use of historical earthquake records, which were strongly affected by local conditions, may not accurately reflect typical ground motions.

5.6.4 Selected Ground Acceleration Records

General

Due to the large computing time required to produce a time history response of a non-linear two-dimensional frame, it was decided to use only four ground motion records, namely the El Centro May 1940 North- South component, Parkfield No. 2 June 1966 North 65°-East component, Pacoima Dam February 1971 South 14°-West component and an artificial generated NZS4203A earthquake records. For the first three records, the buildings were subjected to the first fourteen seconds of strong motion only. However, since the artificial earthquake has a long duration of strong motion, the first twenty second motion were applied to the buildings. The reasons for the selection of these particular earthquake records are given below.

El Centro May 1940 N-S Component Record

The 1940 Imperial Valley, California earthquake had a magnitude of 6.4 on the Richter scale. The El Centro accelerograph, 9 km from the epicentre, was the first accelerograph recorded in the immediate region of a moderately strong seismic event. Until the Parkfield

earthquake in 1966, the El Centro peak ground acceleration of $0.34g$ was the largest ground motion ever recorded. For those reasons, the El Centro ground motion has been used as the basis for the design response spectra in many countries including New Zealand [29,30,39]. It was therefore considered necessary to study the response of the structures under this ground motion.

Parkfield June 1966 No. 2 N65°E Component Record

The 1966 Parkfield earthquake had a magnitude of only at 5.6 on the Richter scale. However, propagation of rupture towards the No. 2 station resulted in a considerable concentration of energy in the motion in the direction of this station. The maximum ground acceleration recorded at the Parkfield No. 2 accelerograph, which was located at 32 km from the epicentre, was $0.48g$. Since this record ranks as the second strongest ground motion record after the Pacoima Dam, it was considered reasonable for use in this study.

Pacoima Dam February 1971 S15°W Component Record

Although the 1971 San Fernando earthquake had a magnitude of only 6.4 on the Richter scale, the Pacoima Dam ground motion which was recorded at 9 km from the epicentre is the strongest ever measured and had a maximum ground acceleration of $1.15g$. The Pacoima Dam accelerogram has exceptionally long duration pulses which results in very large ground velocity increments and thus imposes large displacement excursions on a structure. This ground motion was selected in this study since it represents the upper bound to a possible seismic event, in the context of the New Zealand seismicity.

Artificial Generated NZS4203A Earthquake Record

An artificial earthquake record was generated using SIMQKE [65] to match the design acceleration response spectra proposed in the draft DZ4203:1986 [39] for the most severe seismic zone in New Zealand. This record can then be considered as a typical earthquake in New Zealand, and therefore it is of interest to study the response of the buildings under this earthquake record. With a zone factor of $Z = 0.85$, the behaviour of the non-capacity designed buildings under this record was examined, although the buildings were designed for $Z = 0.5$.

5.7 Inelastic Dynamic Response of Non-Capacity Designed Frames of Limited Ductility and Comparison with the Inelastic Dynamic Response of Capacity Designed Ductile Frames

5.7.1 Inelastic Dynamic Response of Non-Capacity Designed Frames of Limited Ductility

The Response Analyses

The response of the four, six and twelve storey frames designed for limited ductility, under the above earthquake records was analysed. The envelopes of the extreme structural deformations and member actions are presented as follows:

- inter-storey drifts;
- column axial forces;
- beam and column bending moments, shear forces, plastic rotations and curvature ductility demands;
- the development of plastic hinge formation during the excitations.

For comparisons of shear forces, the results obtained from the second set of dynamic analysis were used. For the other comparisons, the results of the first set of dynamic analysis were used.

It should be noted that some of the observed values are not drawn on the graphs due to their similarity with the values obtained from the other earthquake records. An outline of the information presented in subsequent figures is given below.

Interstorey Drifts and Displacements

The inter-storey drift envelopes and the maximum horizontal displacement response at the top storeys, observed during the excitations are presented. The maximum interstorey drifts permitted by the draft code DZ4203:1986 [39] of $Z/50$ (Z=zone factor) are shown. For $Z = 0.5$ and $Z = 0.85$, the code limitations for the drifts are 1.0% and 1.7%, respectively.

Maximum and Minimum Column Axial Forces

The maximum and minimum axial force envelopes in columns obtained from the dynamic analyses are presented, and are compared with the design axial forces calculated from elastic frame analysis. The maximum design axial load P_{des} was found from the combination of $1.2D + 1.2L_s + E$ or $1.2D + 1.6L_r$, and the minimum design axial load was found from the combination of $0.9D - E$.

Maximum Beam and Column Bending Moment Envelopes

The dependable flexural strengths of the beams after moment redistribution, calculated as $0.9M_i \approx 0.9A_{st}f_yjd$, and the flexural overstrengths of beams of $1.25M_i$, are compared with the maximum moment envelopes which occurred during the excitations. In frames of limited ductility, higher beam flexural strengths are available, which means that the extent of plastic hinge rotations of the beams are not as severe as that in ductile frames. From the response of the frames, it was shown that the percentage of moment redistributed as mentioned earlier was not excessive.

The dependable flexural strength of the columns ϕM_{ACI} was calculated using the code [2] approach. In the calculation of the real flexural strength of columns M_{real}, which take into account the contribution of the enhancement of the concrete compressive strength due to confinement and the strain hardening of longitudinal steel, the stress- strain curves for confined concrete and steel due to Mander *et al.* [3] were adopted. Since the columns are expected to have limited ductility, the amount of confining reinforcement provided was found from the refined design equation derived in Chapter 4 to achieve a curvature ductility factor of φ_{max}/φ_y=10. Using the axial loads obtained from the dynamic analyses, the real flexural strength M_{real} can be found. Both the ϕM_{ACI} and M_{real} are compared with the maximum observed moment envelopes.

The bending moment envelopes presented, are the maximum values, which occurred at either end of the beams, and at the top or bottom ends of the columns.

Maximum Beam and Column Shear Envelopes

The design shear forces of beams, obtained from the assumption as shown in Fig. 5.5a, are compared with the shear forces observed during the dynamic analyses.

The design shear forces of columns calculated assuming that moments at both ends of the columns reached the code flexural strengths M_{ACI} simultaneously (see Fig. 5.5b), are compared with the observed shear forces. The shear forces calculated assuming that the real flexural strengths M_{real} reached at both ends of the columns are also plotted. This will give an understanding of whether the design shear force based on the M_{ACI} is adequate or a higher design shear force based on the M_{real} has to be used.

Maximum Beam and Column Curvature Ductility and Plastic Rotation

The curvature ductility demands in beams and columns observed during the seismic excitations φ_{max}/φ_y are derived. For beams, the values were calculated from the computer program [55]. For columns, the program calculates the yield moment and curvature based on the axial load at the balance point. The real yield moment and curvature however, should be based on the real axial load occurred during the excitations. In this study, these values were obtained from a monotonic moment-curvature analysis.

The maximum plastic rotations, may be written as:

$$\theta_p = (\varphi_{max} - \varphi_y)\ell_p = (\frac{\varphi_{max}}{\varphi_y} - 1)\varphi_y\ell_p \tag{5.20}$$

In this calculation, ℓ_p is the equivalent plastic hinge length, and may be taken as one-half of the beam and column section depths [14].

More ductile behaviour (that is greater available φ_u/φ_y) can usually be expected in beams than in columns, which means that larger plastic rotations can be sustained in the beams. However, in a limited ductility frame, greater flexural strengths are available, and therefore the plastic rotation demand in the beams is not so large. Hence the required level of ductility can generally be achieved easily. For columns however, more stringent requirements are needed to provide adequate ductility. For this reason, the plastic rotation demand in columns is usually of greatest interest.

In a column section of limited ductility, φ_{max}/φ_y=10 has been considered to be sufficient for the ductility demand (refer to Chapter 4). Eq. 5.20 then indicates that the column plastic hinge rotation obtained during dynamic analysis should not exceed

$$\theta_p = 9\varphi_y\frac{h}{2} \tag{5.21}$$

From the first principles, $\varphi_y(h/2)$ can be considered to be reached when the concrete compressive strain ϵ_c at the extreme compressive fibre is approximately 0.002. A plastic rotation of θ_p=0.018 rad. can be considered as a reasonable maximum available value in a column section of limited ductility. It was observed during the analyses that only a few columns underwent significant plastic rotations. It was decided therefore to compare the maximum plastic rotations in those columns with the value of 0.018 radians.

To provide more information however, the observed plastic rotation envelopes in the beams are also derived and plotted.

Development of Plastic Hinges

The main objective in this study was to investigate whether column sidesway mechanisms occurred or not during the excitations, if the columns are not protected against hinging using the capacity design approach. And if such mechanisms do occur, what is the largest curvature ductility demand in the columns.

From the dynamic analyses, the graphs illustrating the sequence of the formation of the plastic hinges in the structural members at each time step can be obtained. However, the graphs only show the instants when major changes in the formation of the plastic hinges occurred.

Since the program calculates the yield moment and curvature based on the axial load at the balance point P_b, and not the real axial load observed during the excitation, the plastic hinge rotations in the columns plotted in the graphs could be unrealistic.

Results for the Four Storey Building

The results obtained from the dynamic analyses in terms of the interstorey drift index, axial force, bending moment, shear force, curvature ductility factor and plastic hinge formation during the seismic excitations for the four storey frame are shown in Figs. 5.8 to 5.15.

The horizontal displacements at the top storey obtained from the dynamic analyses indicated that the maximum displacements were 0.39%, 0.69%, 0.82%, and 0.42% of the total height of the building during the response to the El Centro, Parkfield, Pacoima Dam and Artificial generated New Zealand earthquakes, respectively.

Fig. 5.8 shows the inter-storey drift envelopes during the excitations. Clearly, the maximum drift recorded during the El Centro and Parkfield excitations of 0.44% and 0.75% were less than the code limitation of 1.0%. However, during the Pacoima Dam excitation the maximum inter-storey drift imposed was 1.2%, which was larger than the code limitation [39]. The drift observed during the Artificial earthquake of 0.5% was less than the drift index specified by the code for the highest seismic zone of 1.7%.

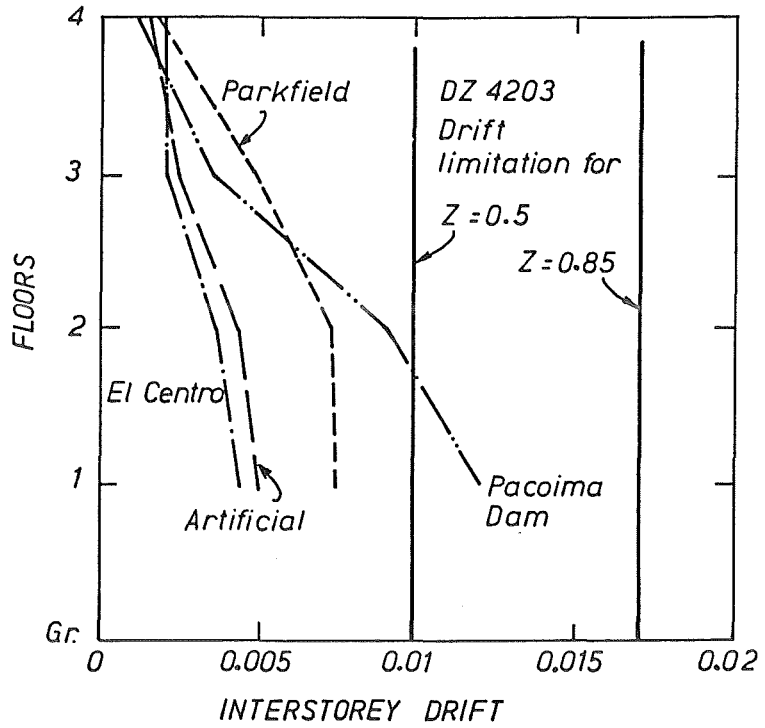

Figure 5.8: Maximum Inter-Storey Drift Envelopes for Non-Capacity Designed Four Storey Frame of Limited Ductility

The observed axial loads in the columns were generally within the maximum and minimum design envelopes (see Figs. 5.9a,b and Figs. 5.10a,b). For the exterior columns, the observed values of the maximum axial forces were very similar to the design forces. The observed minimum axial forces however, were slightly less than the design forces. This indicates that the induced axial tension forces due to earthquakes were larger than those assumed in the design. However, since the observed minimum axial forces were still in compression, uplift of the substructure due to the earthquake induced tension axial forces did not occur.

For the interior columns, the observed axial forces were quite similar during all seismic excitations, since the axial forces induced by an earthquake were insignificant in the interior columns, and therefore the observed axial forces were mainly due to a gravity load of $D + L_r/3$, which is assumed to be the most likely gravity load that occurs during an earthquake. The maximum design values were larger than the maximum observed values, because the

design values were governed by $1.2D + 1.6L_r$, which are much larger than those due to $D + L\ /3 + E$ adopted in the dynamic analyses. It is worth noting that E is reasonably small for the interior columns. On the other hand, the minimum observed values were greater than the design values, since the minimum design axial forces were governed by $0.9D$-E, while the observed forces were determined by $D + L\ /3 - E$.

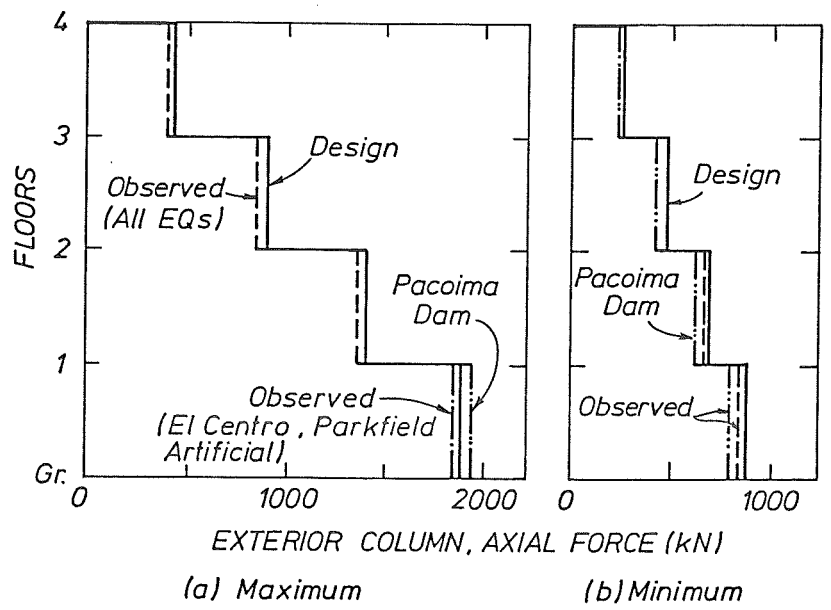

Figure 5.9: Maximum and Minimum Axial Force Envelopes for Exterior Columns in Non-Capacity Designed Four Storey Frame of Limited Ductility

The envelopes for the maximum bending moments in the beams, shown in Fig. 5.11a, indicate that the overstrength moments were reached by the observed values. However, at the first floor, the observed moments were larger than the overstrength moments. This was possible due to the bi-linear hysteresis rule used in the analyses, which had a post-yield strength r of 0.02. At the other floors, the observed values were only slightly greater than the design values. At the top floor, the observed values were almost similar to the overstrength values. Compared with those resulted from the other excitations, the moments reached during the Pacima Dam record were the largest. For comparison, the design bending moments of $0.9M_i$ were also plotted (Fig. 5.11a). Obviously, the design moments were less than those observed during the seismic excitations.

For the exterior columns, the envelopes for the observed maximum bending moments exceeded the code design flexural strengths in the columns. The real flexural strengths based on the confined concrete, were reached by most of the columns, as illustrated in Fig. 5.11b, except for the column at the second floor, where only the observed bending moment during the Pacoima Dam earthquake was greater than the design moment.

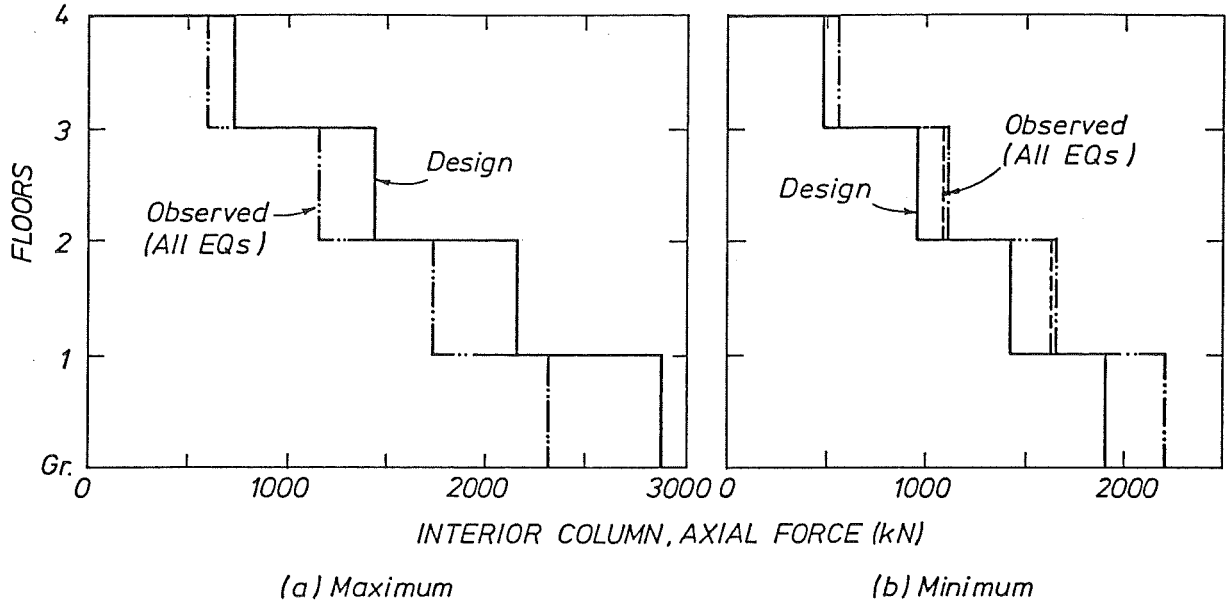

Figure 5.10: Maximum and Minimum Axial Force Envelopes for Interior Columns in Non-Capacity Designed Four Storey Frame of Limited Ductility

Fig. 5.11c shows that the design bending moments were attained by most of the interior columns, except for the column at the second level. At the first level, the observed bending moments during the Pacoima Dam was greater than the design moment. However, the real flexural strengths of the columns were not reached.

Fig. 5.12 illustrates the design and the observed shear forces for the beams, exterior and interior columns. As indicated in Fig. 5.12a, the design shear forces of the beams assuming that the overstrength moments developed at both ends of the beams, were reasonably close to the observed forces. The observed shear forces during the El Centro and Parkfield excitations were quite similar.

It is obvious from Figs. 5.12b and c, that the design shear forces based on the assumption that M_{ACI} developed at the both ends of the columns were sufficient. The shear forces calculated assuming that the both ends of the columns reached their real flexural strength were much larger than the observed shear forces. The shear forces observed during the Pacoima Dam and the Artificial New Zealand earthquakes were generally greater than those observed during the Parkfield and the El Centro excitations.

Fig. 5.13a indicates that the required ductility demand decreases at the higher floors. A maximum φ_{max}/φ_y in the beams at the first floor of 5.9 was observed during the Pacoima Dam excitation.

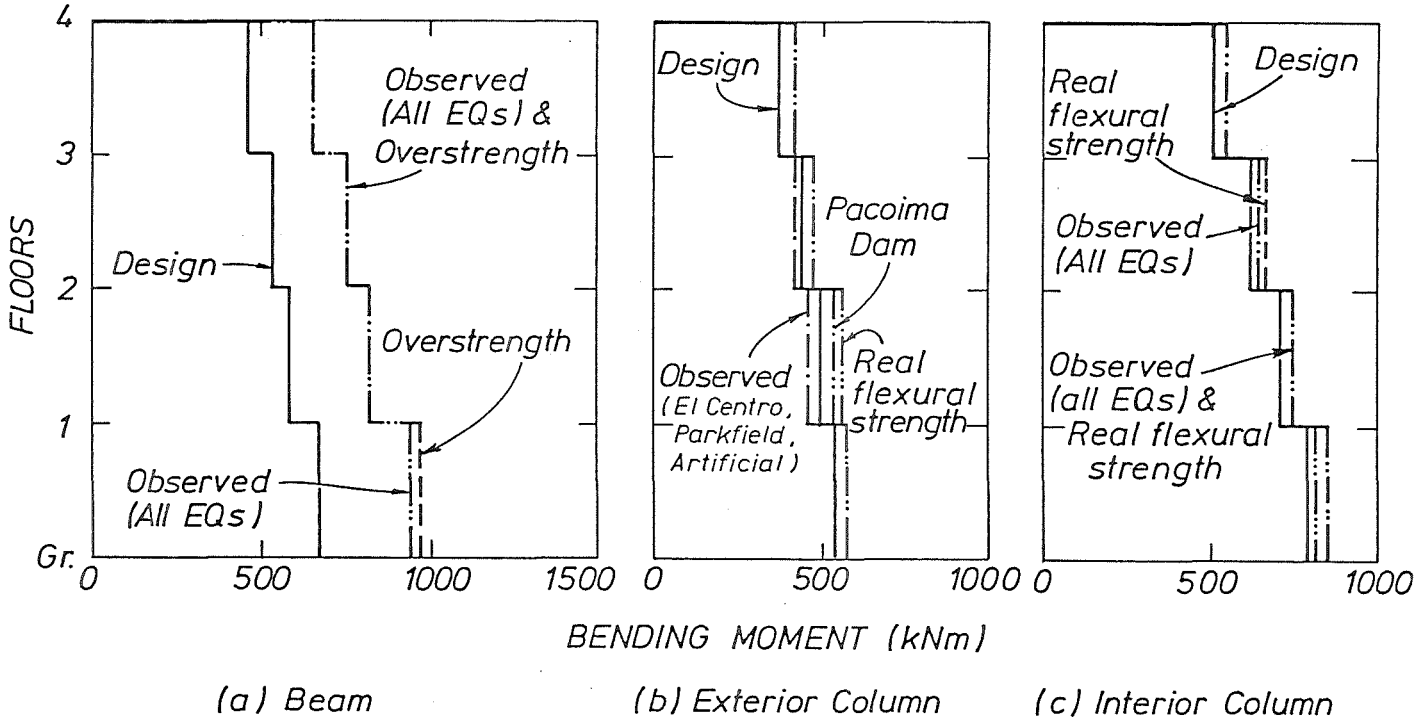

Figure 5.11: Maximum Bending Moment Envelopes for Beams and Columns in Non-Capacity Designed Four Storey Frame of Limited Ductility

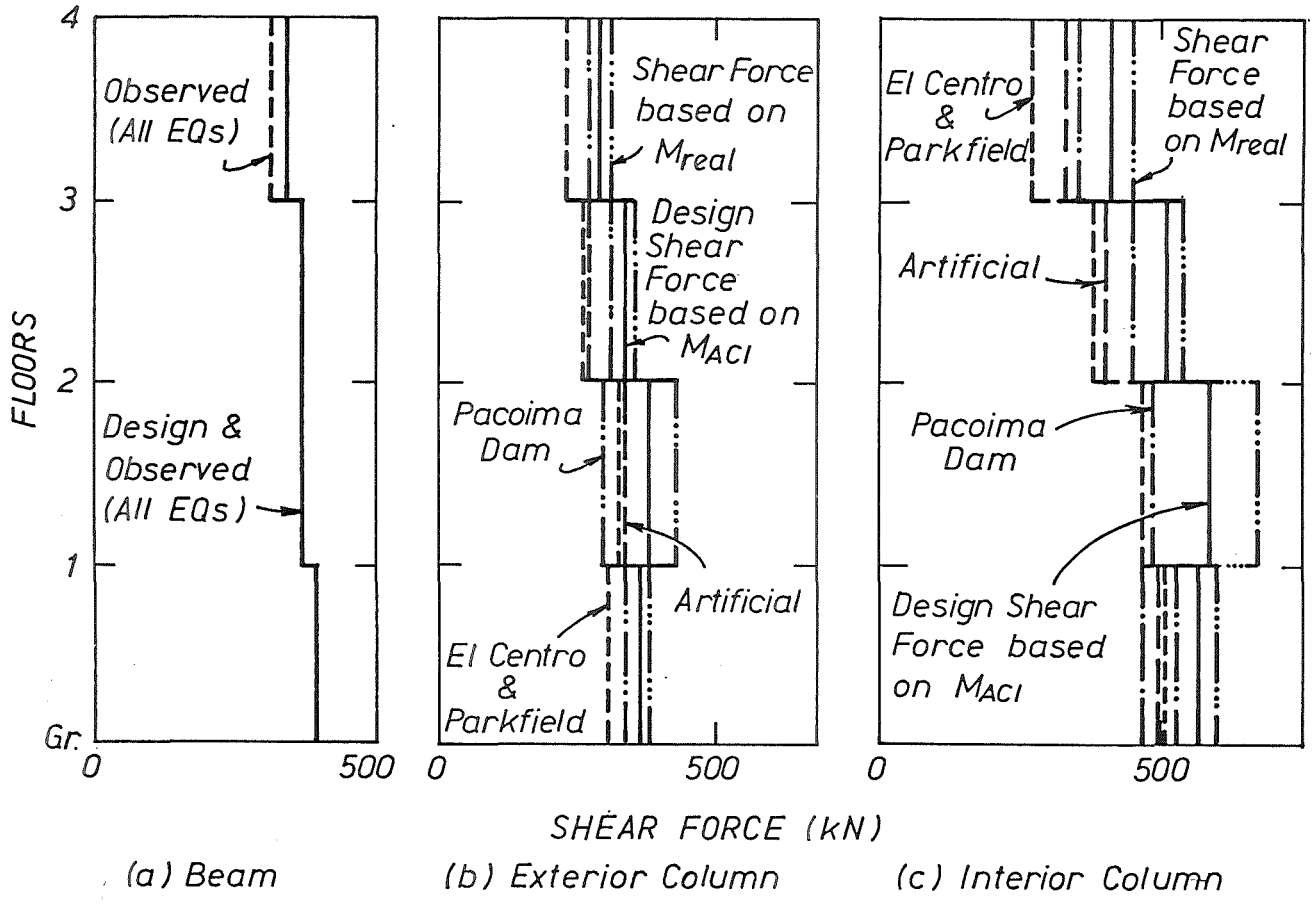

Figure 5.12: Maximum Shear Force Envelopes for Beams and Columns in Non-Capacity Designed Four Storey Frame of Limited Ductility

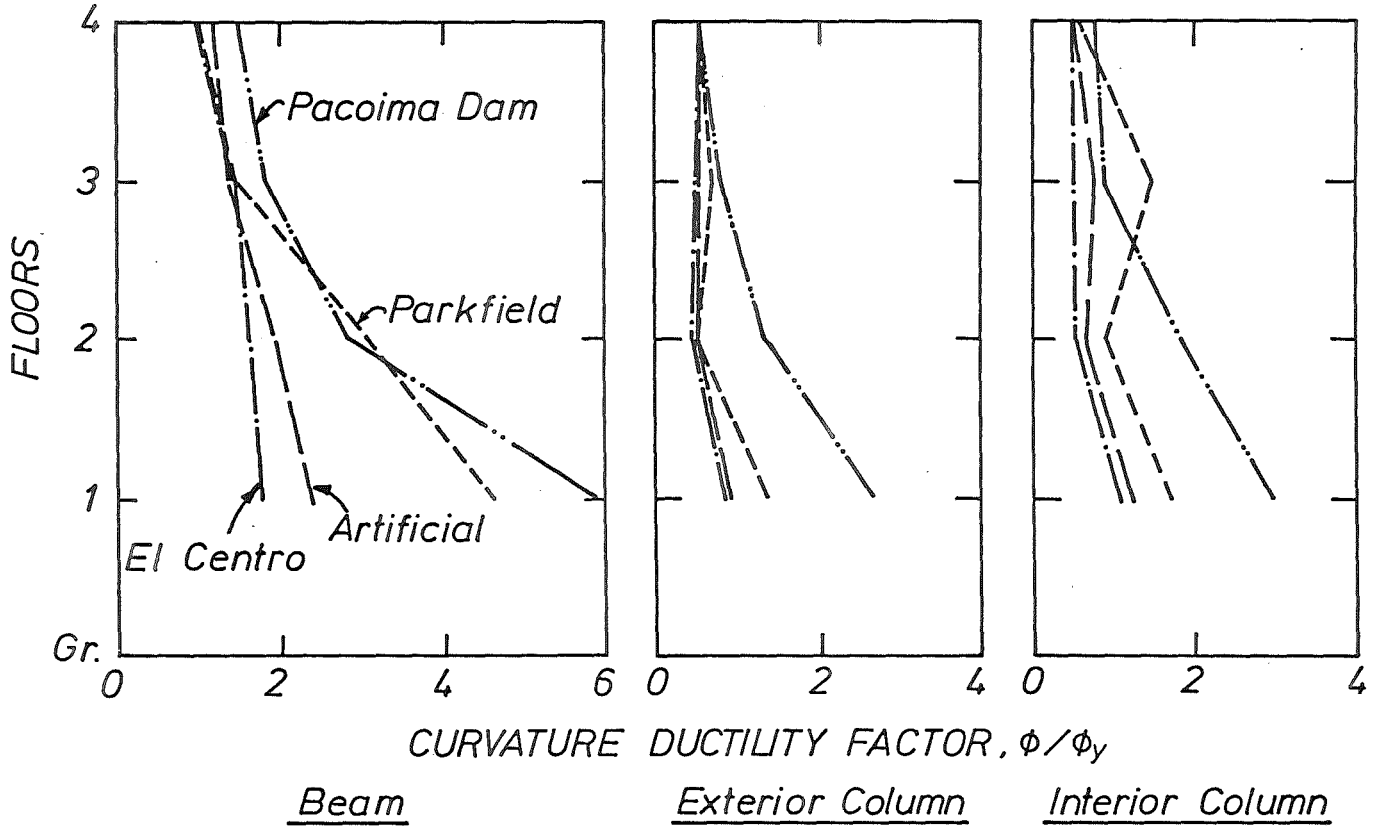

Figure 5.13: Maximum Curvature Ductility Envelopes for Beams and Columns in Non-Capacity Designed Four Storey Frame of Limited Ductility

From the observed curvature ductility factors φ_{max}/φ_y in the columns shown in Figs. 5.13b and c, it was found that the largest φ_{max}/φ_y demand was 2.7 and 3.0 for the exterior and interior columns, respectively, which occurred at the base, and were recorded during the Pacoima Dam excitation. During the El Centro and the Artificial New Zealand earthquakes, the exterior columns remained in the elastic range. Moreover, under these excitations, the largest curvature ductility demand required by the interior columns at the first level, where yielding mostly occurred, was only about 1.2.

Due to very small plastic rotations that occurred, only the plastic rotations in the beams are plotted (see Fig. 5.14). It can be seen that the maximum observed plastic rotation was only 0.0022 rads., and recorded during the Pacoima Dam excitation.

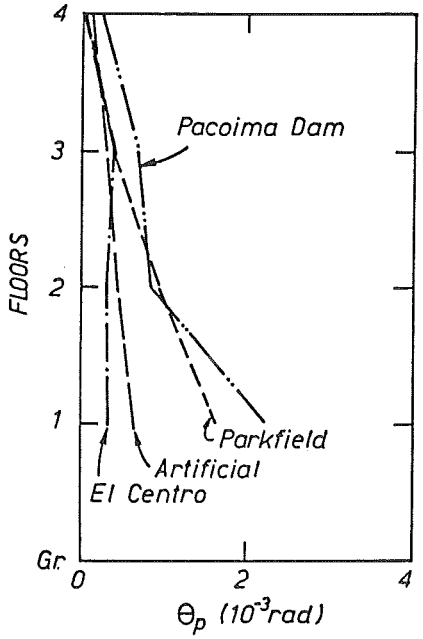

Figure 5.14: Maximum Plastic Rotation Envelopes for Beams in Non-Capacity Designed Four Storey Frame of Limited Ductility

As mentioned previously, a plastic rotation of up to 0.018 rad. is generally available in a column section of limited ductility. From the calculated plastic rotations in the columns as given in Table 5.7, it can be seen that the maximum observed plastic hinge rotations in the exterior and interior columns were only 0.0036 and 0.0042 rads., and occurred at the base of the columns during the Pacoima Dam excitations.

Table 5.7: Maximum Plastic Rotations Occuring in Columns in the Non-Capacity Designed Four Storey Frame of Limited Ductility (in rad.)

	Exterior Column	Interior Column
El Centro	-	-
Parkfield	0.0008 (ground)	0.0014 (ground)
Pacoima Dam	0.0036 (ground)	0.0042 (ground)
NZ Artificial	-	-

The response of the building during the Pacoima Dam excitation was the most severe. For this reason, only the formation of plastic hinges during the Pacoima Dam excitation is shown (see Fig. 5.15). It can be seen that the maximum number of the plastic hinges formed in the columns was 6, The plastic hinges developed at both ends of the lower interior columns, and at the bottom end of the exterior columns at the ground floor during the interval of 2.96 to 2.98 secs., 3.34 to 3.56 secs, and 4.10 to 4.15 secs. However, soft storey mechanisms did not occur throughout this excitation, which has been considered as the strongest credible seismic event.

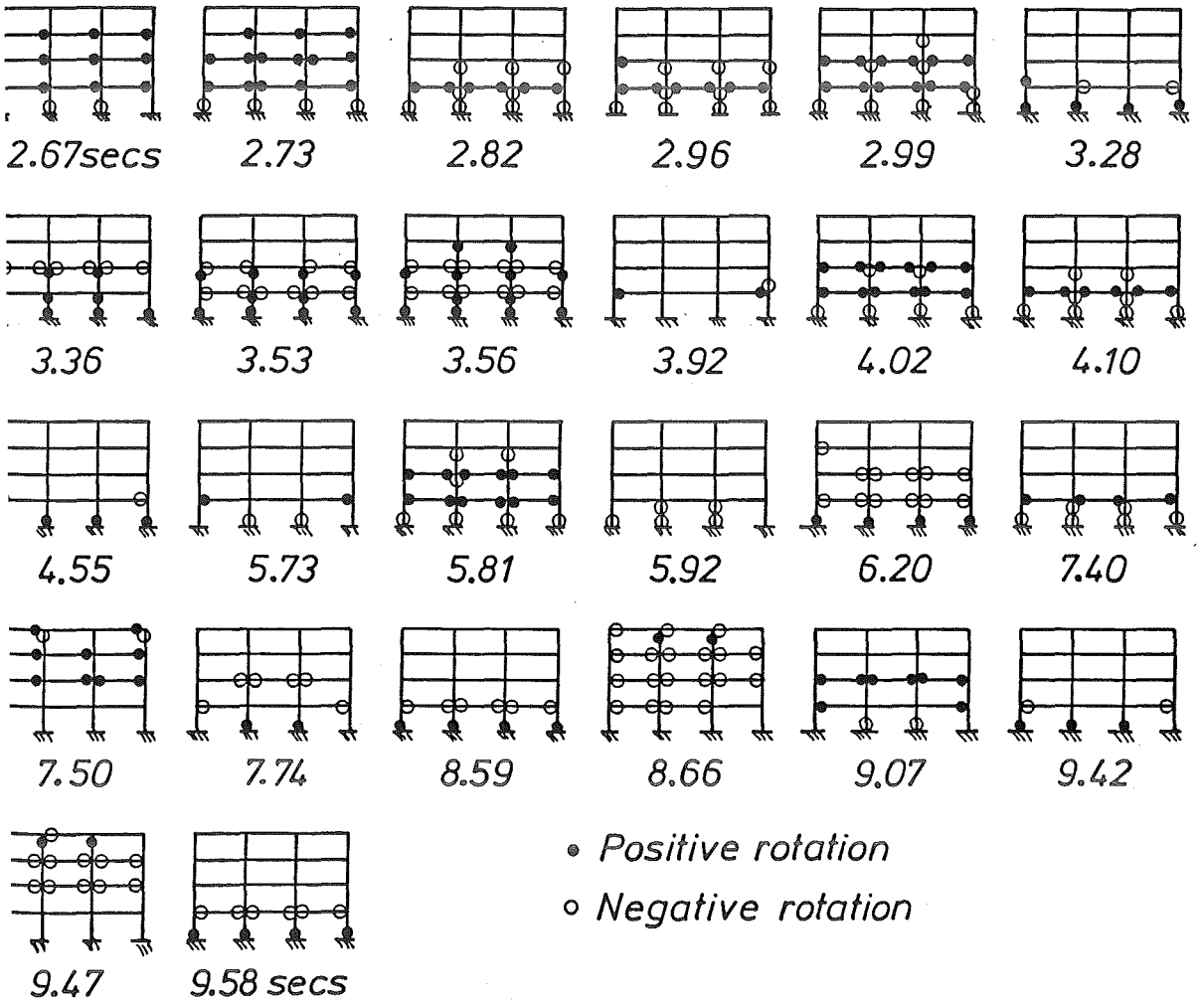

Figure 5.15: The Sequence of the Development of Plastic Hinge Formation in Non-Capacity Designed Four Storey Frame of Limited Ductility During the Pacoima Dam Excitation (Seconds After Start of Earthquake)

Results for the Six Storey Building

The observed maximum displacements at the top storey during the El Centro, Parkfield, Pacoima Dam and Artificial generated New Zealand earthquakes were 0.35%, 0.52%, 0.85% and 0.74% of the total height of the building. It is shown in Fig. 5.16 that the maximum drifts occurred at the first floor, and were 0.44%, 0.94%, 1.74% and 1.0% during the above excitations. Except for that observed during the Pacoima excitation, the drift limitations specified by the code [39] of 1.0% for the buildings located at the region with Z=0.5, and of 1.7% for the buildings located at the region with Z=0.85, were not exceeded.

The maximum and minimum axial force envelopes for the exterior and interior columns observed during the excitations were reasonably close to the maximum and minimum design axial forces (see Figs. 5.17a,b and Figs. 5.18a,b). Similar comments to the results for the four storey frame are applied. The maximum design values exceeded the observed values, and the minimum design values were less than the observed values in the case of the interior columns, but slightly greater than the observed values in the case of the interior columns. It should be noted that due to the configuration of the building, the axial forces induced by earthquakes are practivally zero for the interior columns.

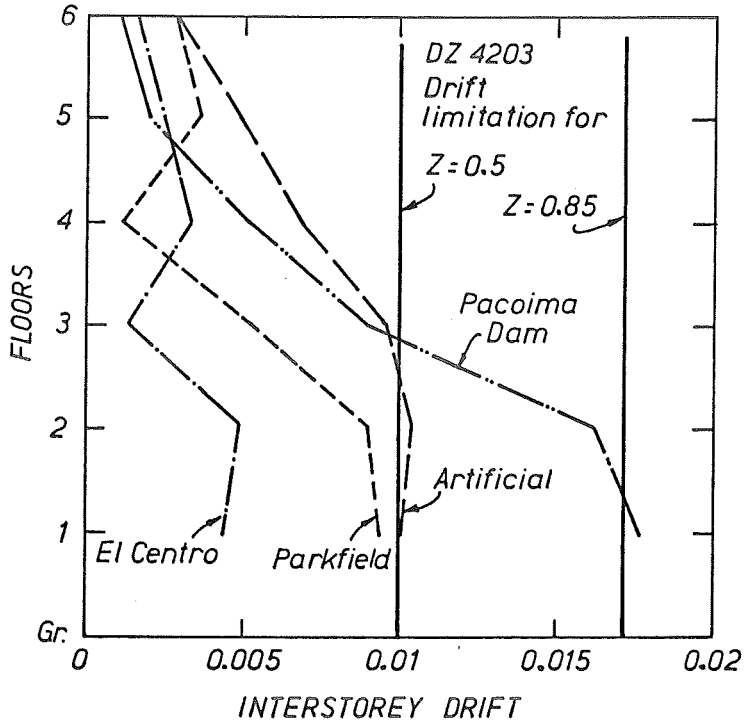

Figure 5.16: Maximum Inter-Storey Drift Envelopes for Non-Capacity Designed Six Storey Frame of Limited Ductility

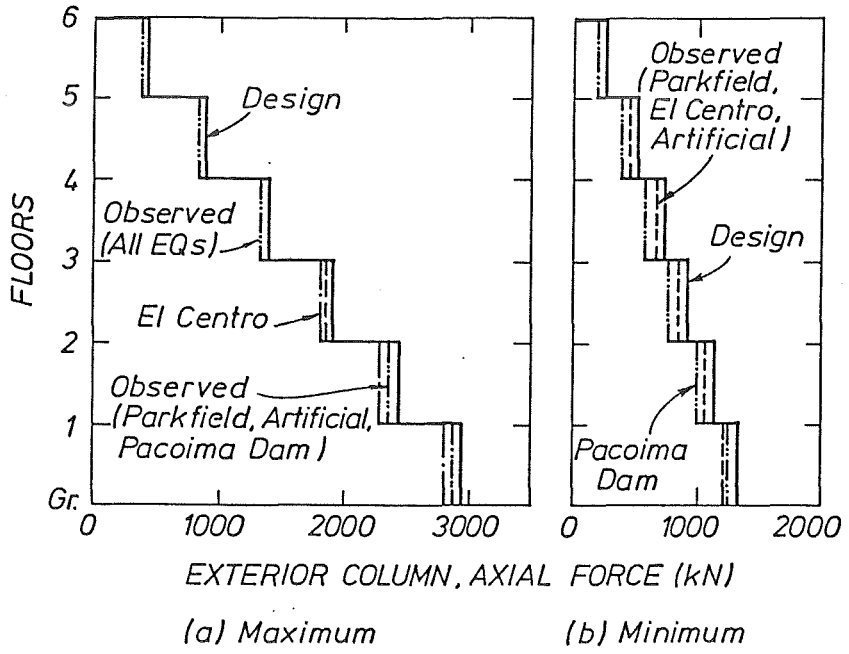

Figure 5.17: Maximum and Minimum Axial Force Envelopes for Exterior Columns in Non-Capacity Designed Six Storey Frame of Limited Ductility

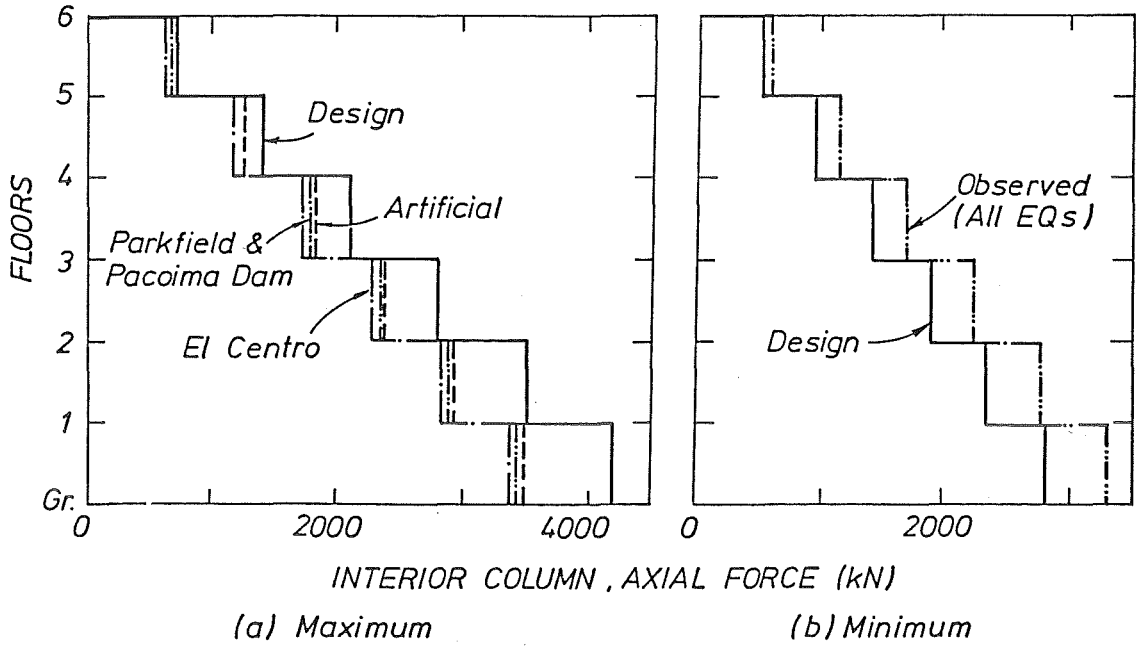

Figure 5.18: Maximum and Minimum Axial Force Envelopes for Interior Columns in Non-Capacity Designed Six Storey Frame of Limited Ductility

Fig. 5.19a compares the observed maximum bending moment envelopes in the beams with the overstrength moments of the beams used in the dynamic analyses. The overstrength moments of the beams at the low storeys were smaller than the observed values. At the top floor however, only the observed moment under the Pacoima Dam excitation reached the overstrength moment.

As shown in Figs. 5.19b and c, the code design moments of $0.9M_{ACI}$ for the columns at all levels, were generally exceeded during most of the excitations. During the El Centro excitation however, the design moments were not even reached, at the middle levels of the structure. The real flexural strengths of the columns, which were based on the confined strength of concrete to achieve a curvature ductility factor of φ_{max}/φ_y=10, were equal or greater than the observed moments. As expected, the Pacoima Dam earthquake gave the largest response, followed by the Artificially generated New Zealand, Parkfield and El Centro earthquakes.

The design shear forces in the beams calculated from the assumption shown in Fig. 5.5a, were found to be sufficient (see Fig. 5.20a). The maximum shear forces observed under the earthquake records used in this study were quite similar to each other.

As illustrated in Figs. 5.20b and c, the design shear forces in the columns, based on the assumption that the code flexural strengths developed at both ends of the columns, were adequate under all seismic excitations. At the second to forth levels, the design shear forces were very conservative. Obviously, the design shear forces calculated from the real flexural strengths developed at the columns would be unnecessarily conservative.

Fig. 5.21a, which shows the curvature ductility factor envelopes for the beams indicates that a curvature ductility factor of approximately 9.0 was required in the beams during the Pacoima Dam excitation. The largest curvature was recorded at the first floor and curvatures became less at the higher floors.

As shown in Figs. 5.21b and c, maximum curvature ductility factors of φ_{max}/φ_y=3.2 and 3.4 were observed at the base of the exterior and interior columns during the Pacoima Dam excitation. The graphs indicate that the plastic hinge rotation was greatest at the ground and roof levels. The response of the building under the El Centro excitation was very good, the required curvature ductility was insignificant.

The maximum plastic rotation envelopes for the beams plotted in Fig. 5.22 also show that only small plastic rotations required in the beams. As listed in Table 5.8, the largest plastic rotation of 0.0044 rad. was recorded at the base of the interior columns during the Pacoima Dam excitation.

The graphs showing the sequence of the formation of plastic hinges during the Pacoima Dam excitation pointed out that the plastic hinges formed in both the beams and columns. The maximum number of the plastic hinges developed was 18 and 12 plastic hinges formed in the beams and columns at 3.50 secs. (see Fig. 5.23).

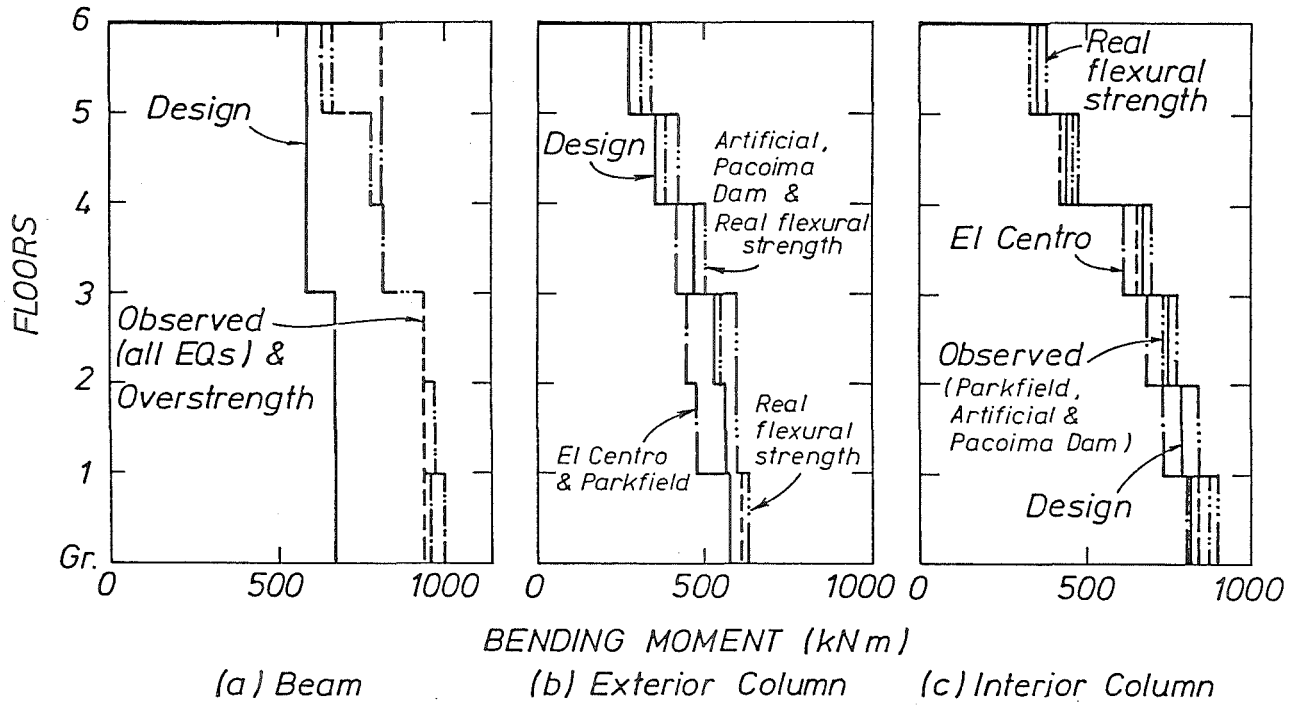

Figure 5.19: Maximum Bending Moment Envelopes for Beams and Columns in Non-Capacity Designed Six Storey Frame of Limited Ductility

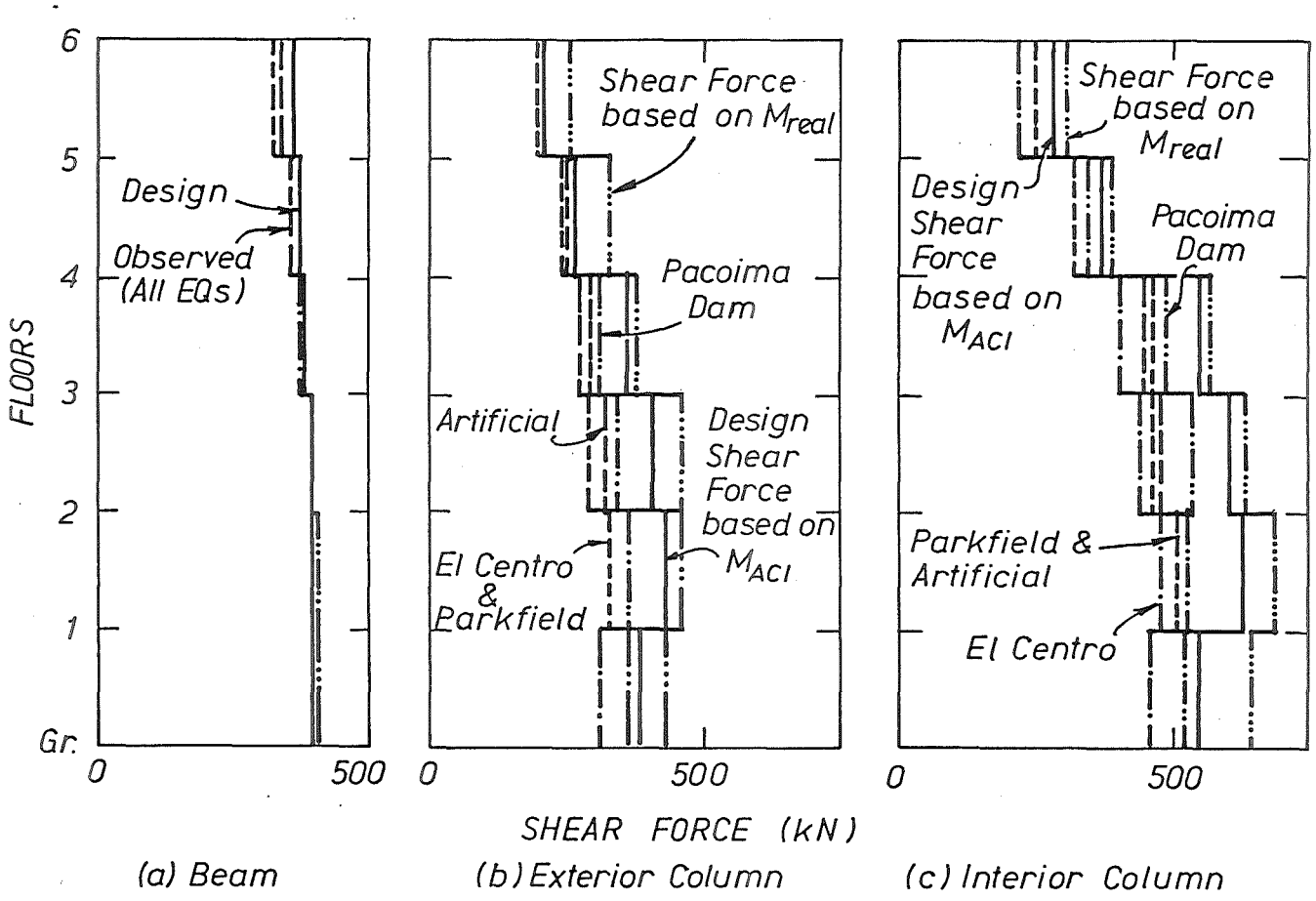

Figure 5.20: Maximum Shear Force Envelopes for Beams and Columns in Non-Capacity Designed Six Storey Frame of Limited Ductility

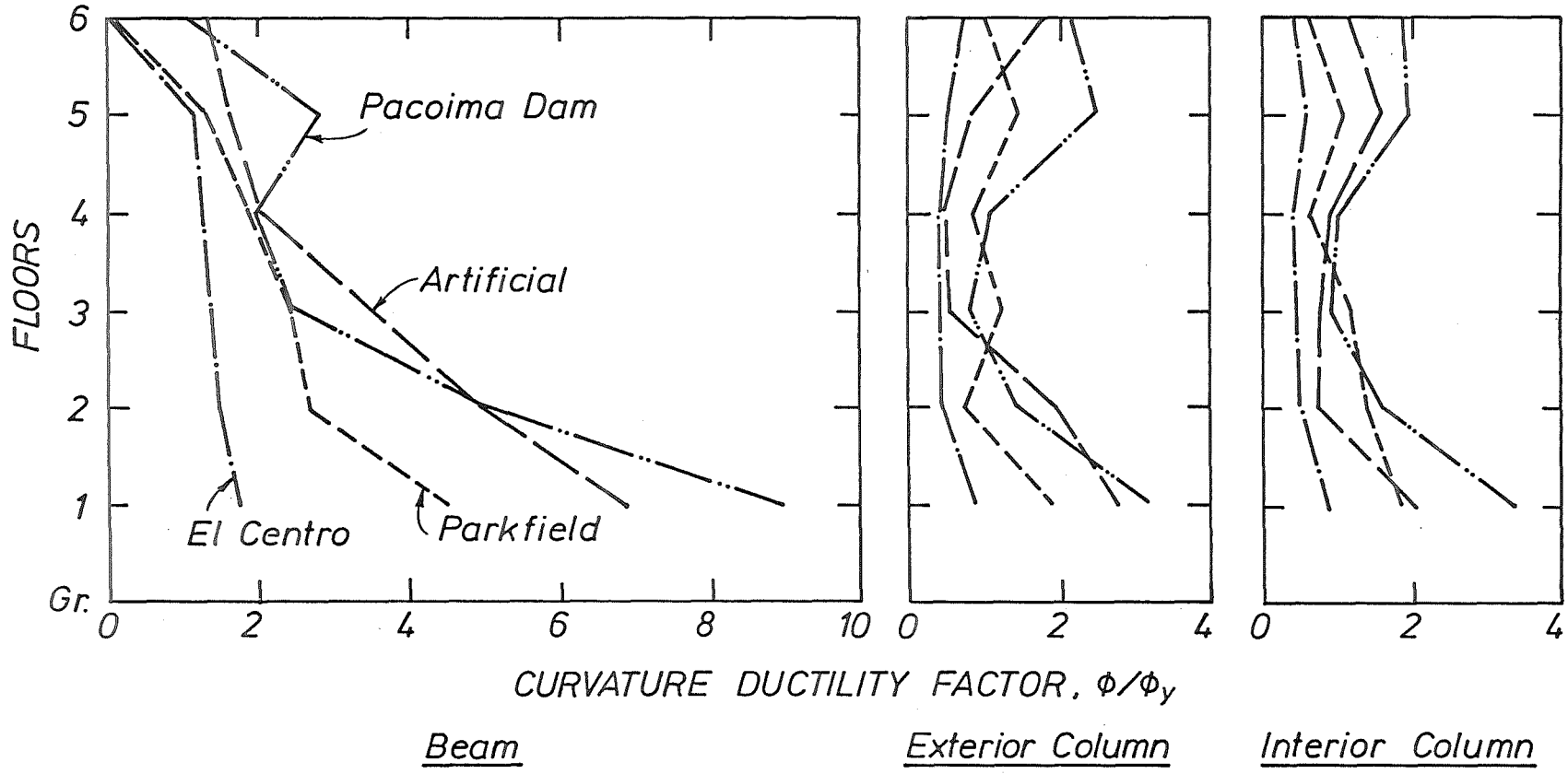

Figure 5.21: Maximum Curvature Ductility Envelopes for Beams and Columns in Non-Capacity Designed Six Storey Frame of Limited Ductility

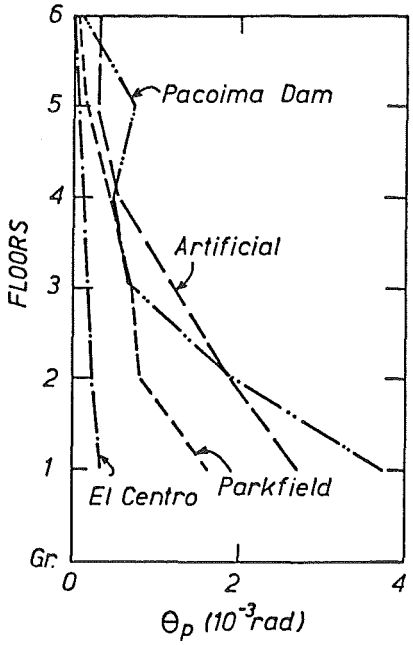

Figure 5.22: Maximum Plastic Rotation Envelopes for Beams in Non-Capacity Designed Six Storey Frame of Limited Ductility

Table 5.8: Maximum Plastic Rotations Occuring in Columns in the Non-Capacity Designed Six Storey Frame of Limited Ductility (in rad.)

	Exterior Column	Interior Column
El Centro	-	-
Parkfield	0.0021 (ground)	0.0016 (ground)
Pacoima Dam	0.0038 (ground)	0.0044 (ground)
NZ Artificial	0.0030 (ground)	0.0019 (ground)

Less column hinges formed during the El Centro and Parkfield records. Although the artificial earthquake used in this study is for the most severe seismic zone, the plastic hinges formed during this excitation were less than those recorded during the Pacoima Dam with a lower seismic zone factor.

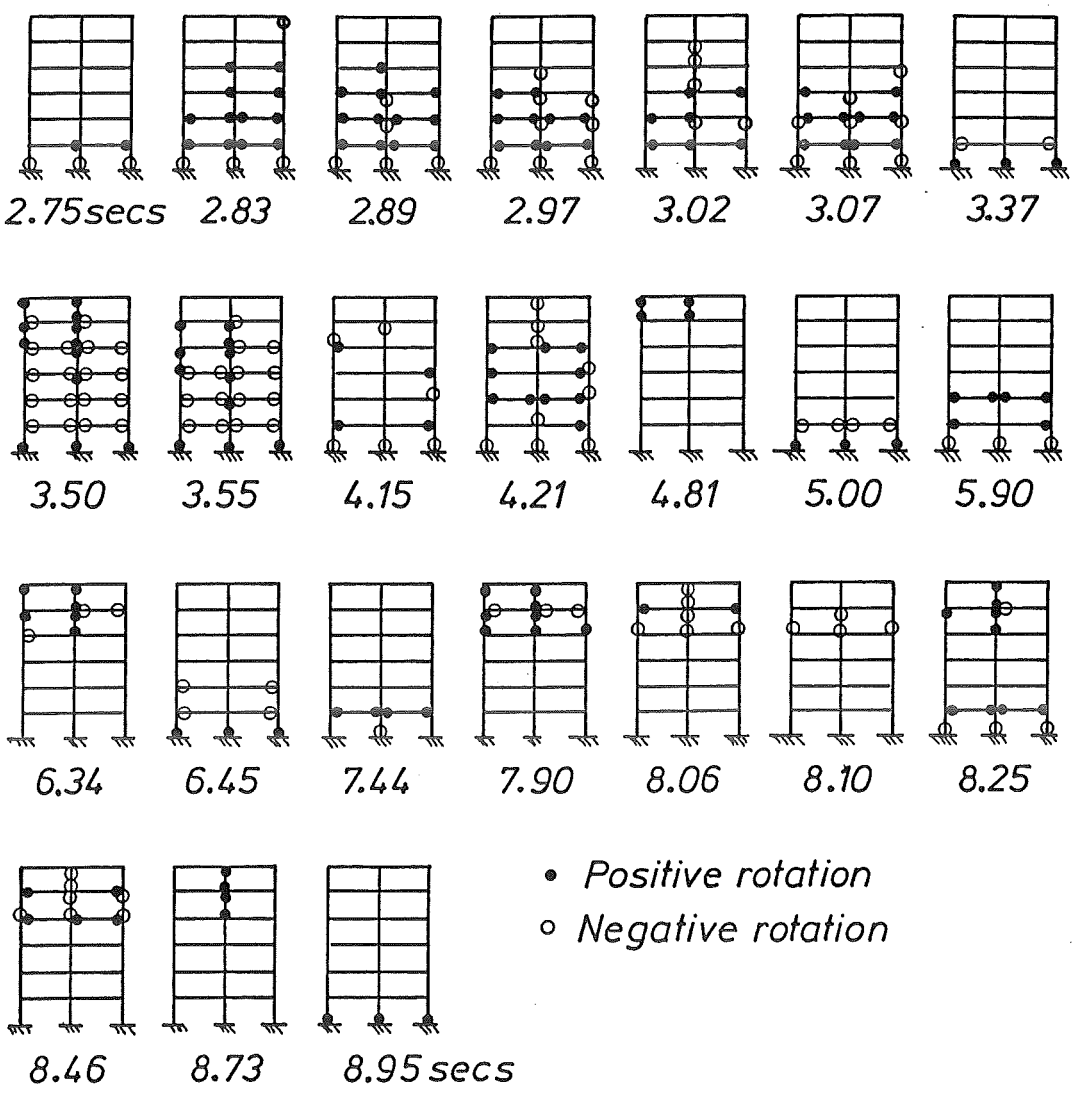

Figure 5.23: The Sequence of the Development of Plastic Hinge Formation in Non-Capacity Designed Six Storey Frame of Limited Ductility During the Pacoima Dam Excitation (Seconds After Start of Earthquake)

Results for the Twelve Storey Building

The inter-storey drift envelopes shown in Fig. 5.24 indicate that during the Parkfield and Pacoima Dam excitations the drift limitation specified by the code was exceeded. Maximum drifts recorded were 0.61%, 1.13%, 1.66%, and 1.08%, during the El Centro, Parkfield, Pacoima Dam and Artificial earthquake excitations, respectively.

The maximum displacements at the top storey observed under the El Centro, Parkfield, Pacoima Dam and Artificial earthquake records, were 0.38%, 0.71%, 0.86%, and 0.49% of the total height of the building.

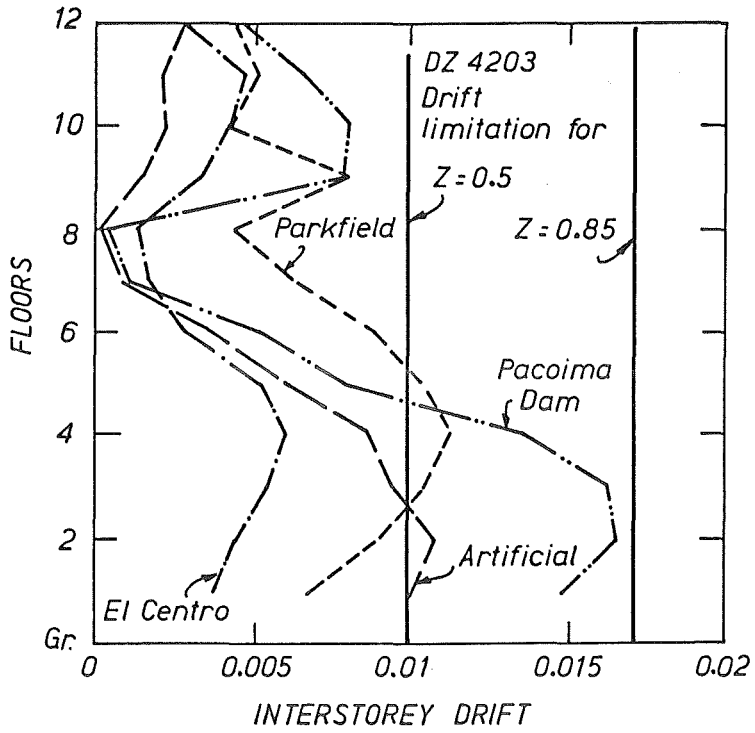

Figure 5.24: Maximum Inter-Storey Drift Envelopes for Non-Capacity Designed Twelve Storey Frame of Limited Ductility

The maximum observed axial force envelopes for the exterior and interior columns during the excitations were well within the maximum design axial forces. As for the previous buildings, the minimum observed axial forces were less than the design values (see Figs. 5.25a,b and Figs. 5.26a,b). The response of the building due to the El Centro earthquake was the most satisfactory, and the response due to the Pacoima Dam earthquake was the most severe.

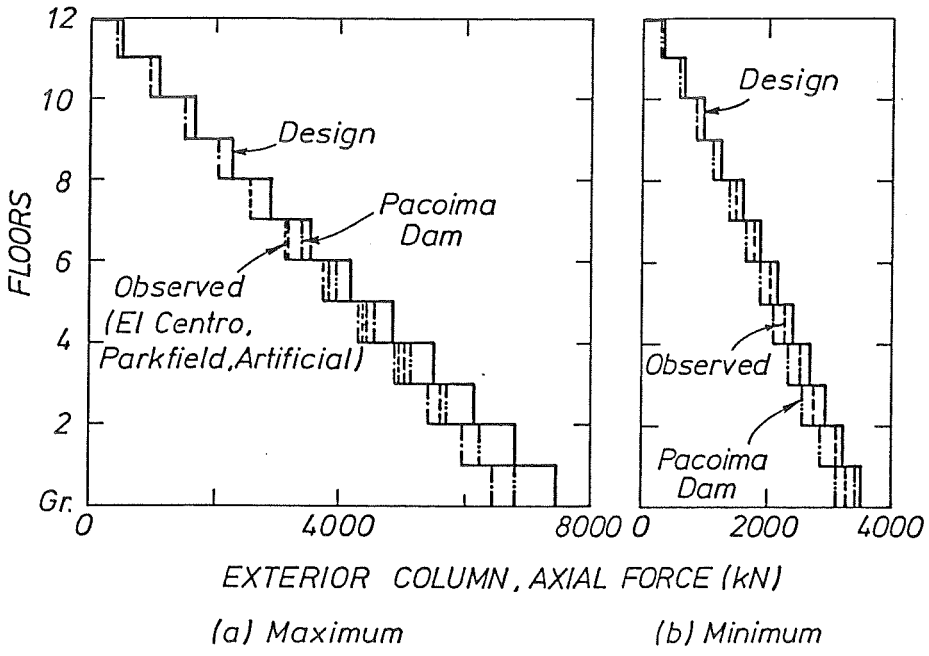

Figure 5.25: Maximum and Minimum Axial Force Envelopes for Exterior Columns in Non-Capacity Designed Twelve Storey Frame of Limited Ductility

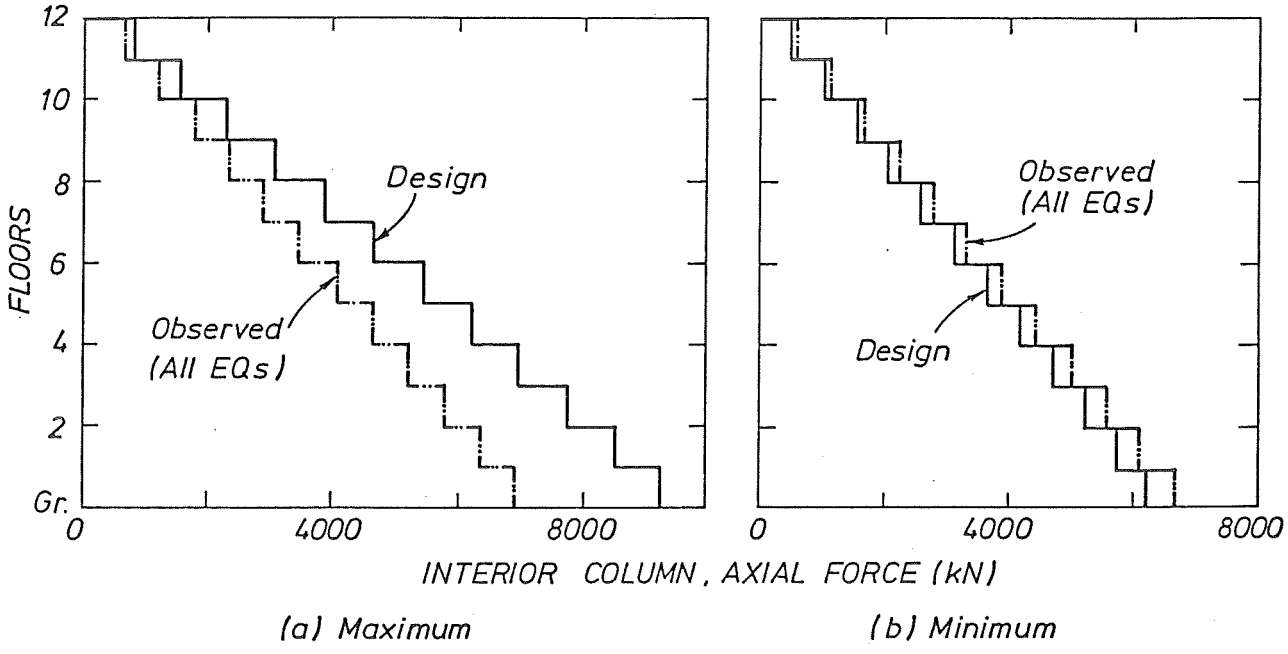

Figure 5.26: Maximum and Minimum Axial Force Envelopes for Interior Columns in Non-Capacity Designed Twelve Storey Frame of Limited Ductility

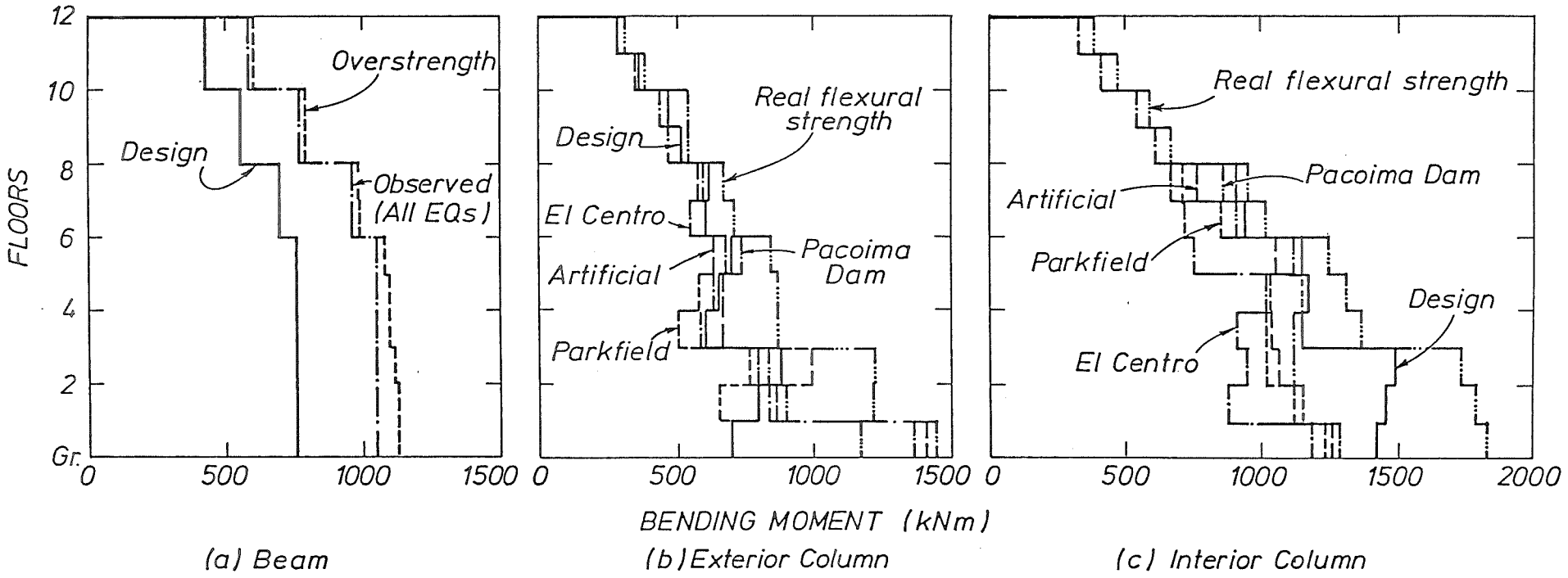

Figure 5.27: Maximum Bending Moment Envelopes for Beams and Columns in Non-Capacity Designed Twelve Storey Frame of Limited Ductility

Fig. 5.27a shows the maximum bending moment envelopes for the beams. The flexural overstrength in the beams of $1.25M_i$ were generally reached by the moments obtained from the dynamic analyses. The observed moments at the first floor during the Pacoima Dam excitation give the largest response, followed by those obtained from the Artificial New Zealand, Parkfield and El Centro records. From the sixth floor upwards, all of the excitations indicated the similar response. As expected, the dependable strengths were less than the observed values.

Due to the use of bilinear moment-curvature hysteresis loops in the analysis, which had a post-yield stiffness of r=0.02, the observed bending moments in some columns were larger than the code design flexural strengths. This was observed in the columns below the seventh level (see Figs. 5.27b and c). Except for the columns at the ground level, the real flexural strengths were never reached at the columns.

The observed bending moments in the columns at the ground level however, exceeded the code flexural strengths of $0.9M_{ACI}$ and even the real flexural strengths M_{real}. This is probably due to the smaller axial forces observed during the dynamic analyses than the maximum design axial forces, which resulted in the higher available flexural strength capacities of the columns as indicated by the axial force-bending moment interaction diagram below (see Fig. 5.28).

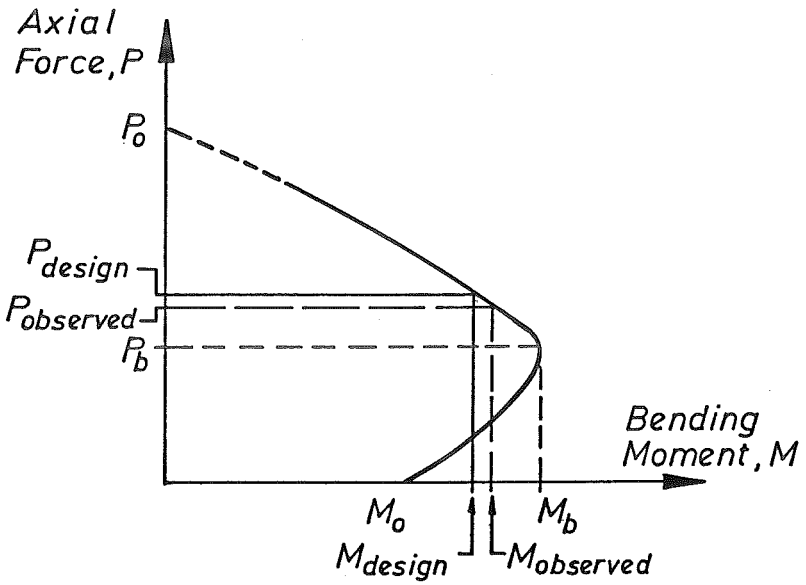

Figure 5.28: Column Axial Force-Bending Moment Interaction Diagram

The shear force envelopes for beams are illustrated in Fig. 5.29a. It is evident that the beam shear forces derived from the flexural overstrengths reached at each end of the beams simultaneously, were satisfactory.

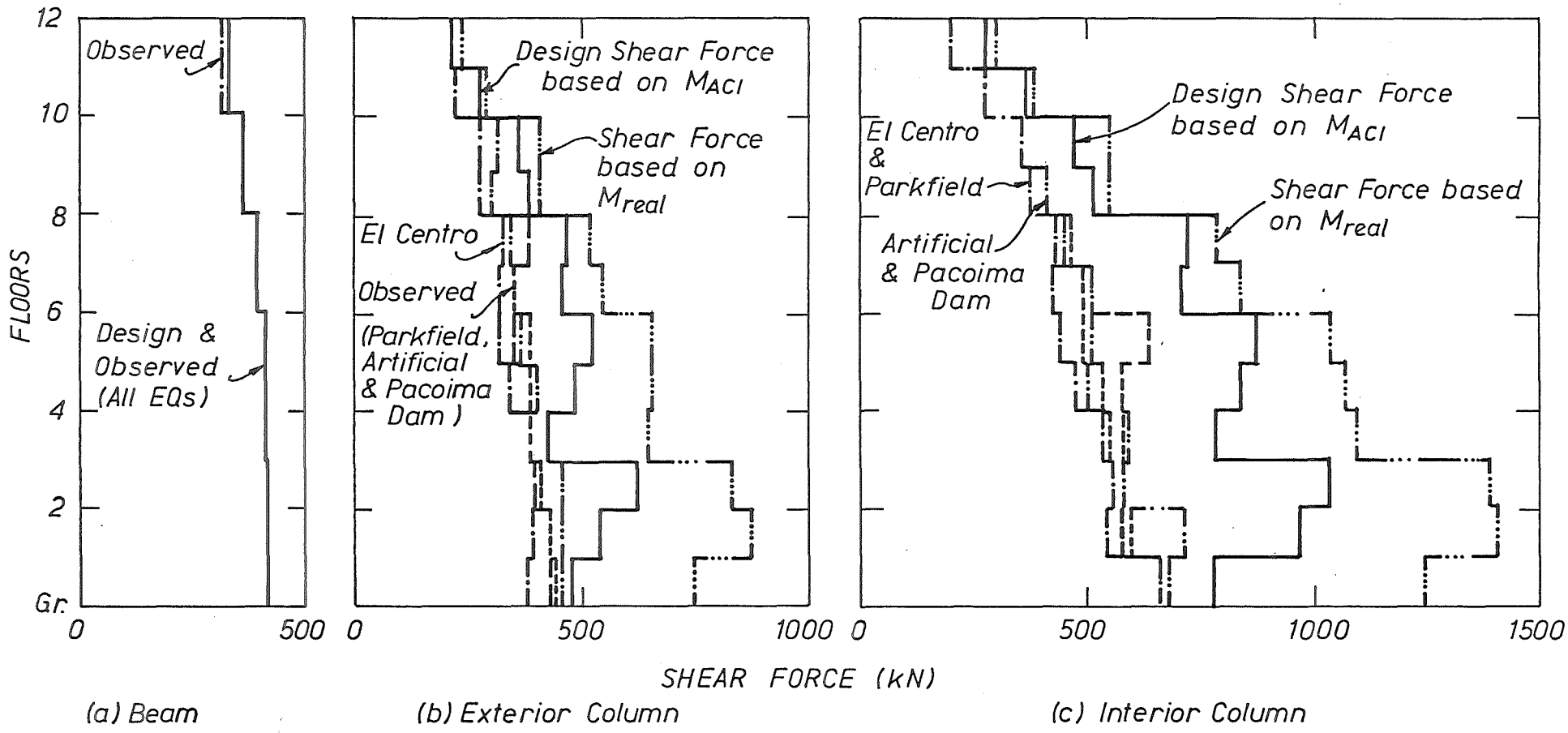

Figure 5.29: Maximum Shear Force Envelopes for Beams and Columns in Non-Capacity Designed Twelve Storey Frame of Limited Ductility

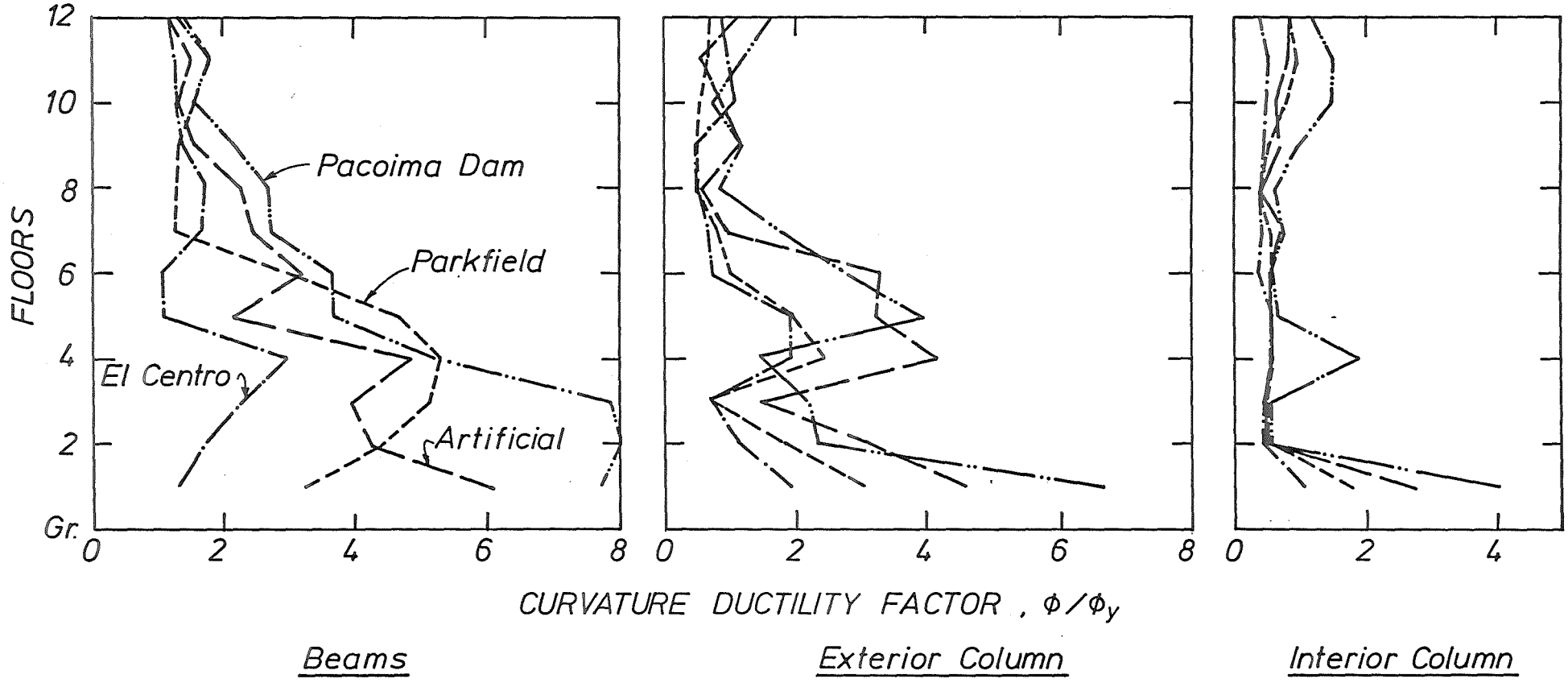

Figure 5.30: Maximum Curvature Ductility Envelopes for Beams and Columns in Non-Capacity Designed Twelve Storey Frame of Limited Ductility

The shear forces in the columns, calculated using the code flexural strength M_{ACI}, and the real flexural strength M_{real}, developed at both ends of the columns are compared with the observed shear forces in Figs. 5.29b and c. Obviously, the shear force based on the M_{ACI}, which was smaller than that based on the M_{real}, was adequate.

The curvature ductility factor envelopes for the beams and columns shown in Figs. 5.30a,b and c, indicate that the curvature ductility demands were very small. For the beams, the largest φ_u/φ_y of 8.1 was recorded during the Pacoima Dam excitation. The curvature ductility factors required at the exterior and interior columns under the El Centro ground motion, were negligible. Under the Pacoima Dam excitation, which gave the most severe response, the recorded φ_u/φ_y were 6.6 and 4.0 at the exterior and the interior columns, respectively.

As mentioned previously, because of the small plastic rotations observed, only the plastic rotations in the beams are plotted (see Fig. 5.31). The maximum plastic rotations which occurred in the columns are listed in Table 5.9. These values were much smaller than the plastic rotation generally available in a column of limited ductility, namely 0.018 radians.

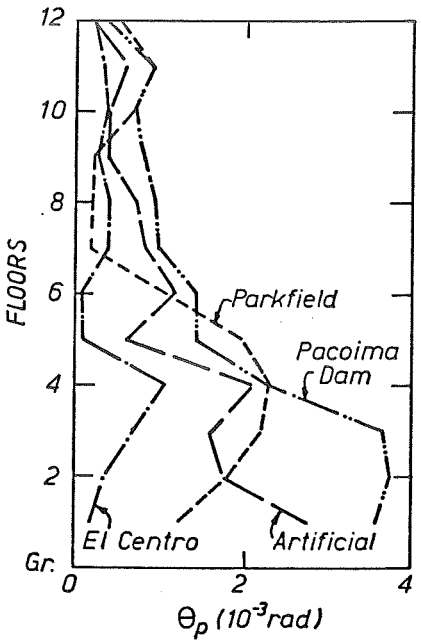

Figure 5.31: Maximum Plastic Rotation Envelopes for Beams in Non-Capacity Designed Twelve Storey Frame of Limited Ductility

Table 5.9: Maximum Plastic Rotations Occuring in Columns in the Non-Capacity Designed Twelve Storey Frame of Limited Ductility (in rad.)

	Exterior Column	Interior Column
El Centro	0.0011 (4th level)	-
Parkfield	0.0021 (ground)	0.0011 (ground)
Pacoima Dam	0.0059 (ground)	0.0044 (ground)
NZ Artificial	0.0037 (gropund)	0.0026 (ground)

Fig. 5.32 shows the instants of the development of plastic hinges during the Pacoima Dam excitation. It can be seen that most of the plastic hinges occurred in beams although at some instants, plastic hinges did occur in the columns. However, the maximum curvature ductility demand in the columns was less than 10 (see Fig. 5.30), and no column sidesway mechanisms were detected.

5.7.2 Comparison of the Inelastic Dynamic Response of Non-Capacity Designed Frames of Limited Ductility and Capacity Designed Ductile Frames

The inelastic dynamic responses of the non-capacity designed frames of limited ductility and capacity designed ductile frames are compared below and the features of both design procedures are discussed. The non-capacity designed buildings of limited ductility are denoted as *Buildings LD*, and the capacity designed ductile buildings are denoted as *Buildings D*.

As mentioned previously, the four storey ductile frame was designed according to the current code requirements [2,39], and the six and twelve storey ductile frames were designed according to the requirements of DZ3101:1978 [10] and NZS4203:1976 [29]. The design procedures described in Section 5.4.2 were adopted.

For the six storey ductile frame, three earthquake records were applied, namely the El Centro and Parkfield records with and without the $P-\Delta$ effects and the Pacoima Dam record. For the twelve storey ductile frame, two earthquake records were applied, namely the El Centro and Pacoima Dam records with and without $P-\Delta$ effects.

The seismic response of the ductile frames is compared with that of the frames of limited ductility in terms of the inter-storey drifts, column bending moments and shear forces, plastic rotation demands, and the required quantities of longitudinal and transverse reinforcement in the beams and columns.

The inelastic dynamic response of capacity designed ductile buildings (*Buildings D*) is shown in Figs. 5.33 to 5.40. It can be seen that the response is very satisfactory. The observed bending moments and shear forces in the columns were generally well within the design envelopes. The plastic hinges developed at the chosen regions, while the other regions re-

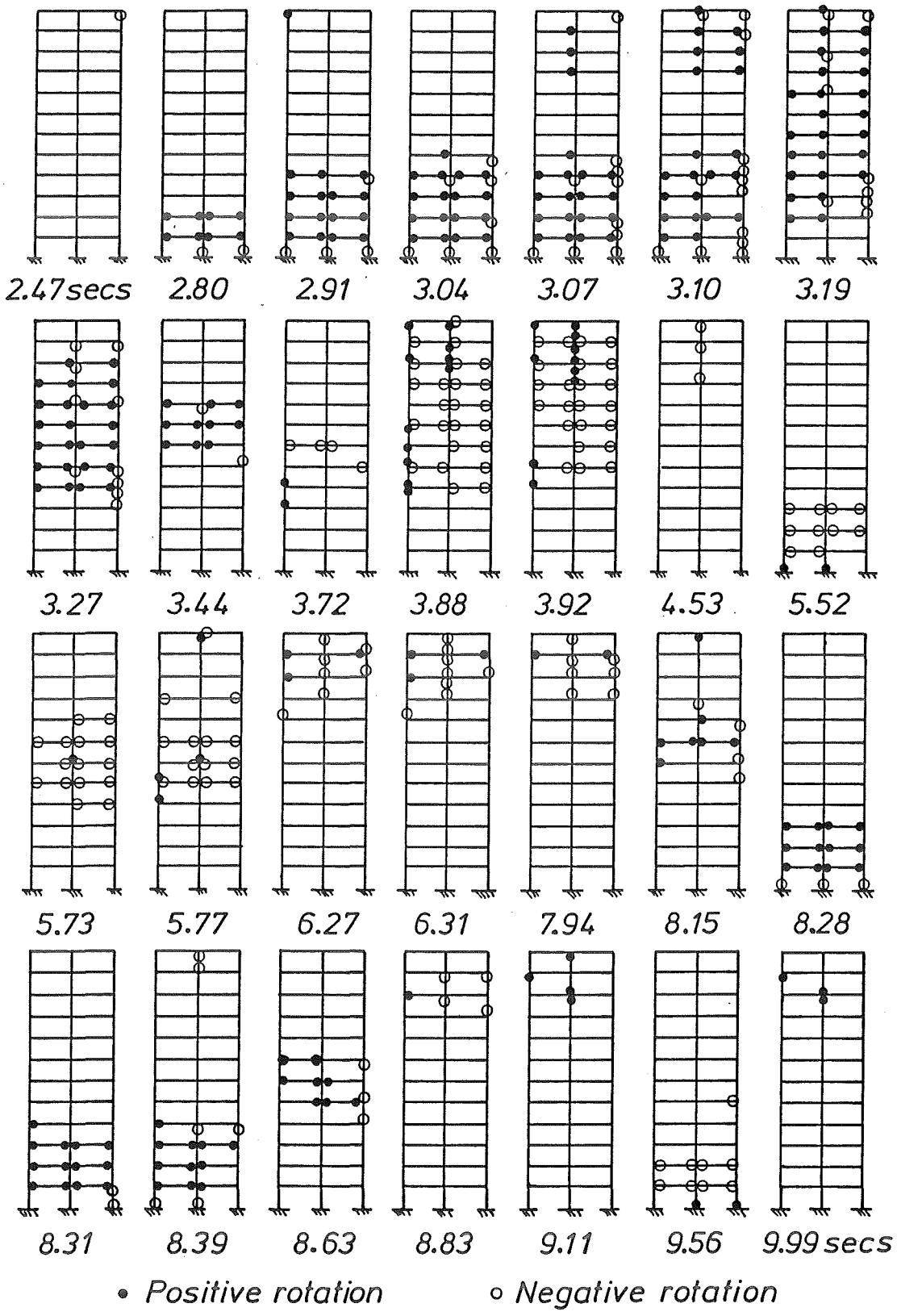

Figure 5.32: The Sequence of the Development of Plastic Hinge Formation in Non-Capacity Designed Twelve Storey Frame of Limited Ductility During the Pacoima Dam Excitation (Seconds After Start of Earthquake)

mained in the elastic range. This indicated that the behaviour of the buildings was controlled very well. The complete description of the performance of the six and twelve storey ductile frames under the simulated seismic attacks can be found in Ref. [54].

With regard to the columns, the plastic rotation envelopes for *Buildings D* indicated clearly that yielding only occurred at the base and roof levels. As shown in Tables 5.7 to 5.9, some columns up the height of the *Building LD* did develop plastic rotations during the excitations. However, the plastic rotations at the columns of *Buildings LD* were very small, although the columns were not designed to be protected from plastic hinging.

It is obvious that the behaviour of the buildings designed using the non-capacity design procedure (*Buildings LD*) was reasonably good. The plastic rotation and ductility demand in the columns were very small even under the most severe seismic event such as Pacoima Dam earthquake. The buildings satisfactorily withstood this most severe earthquake, although they were designed for less severe earthquake.

Tables 5.10 to 5.15 compare the basic dimensions of beams and columns, and the required longitudinal reinforcement contents in the beams and columns of the four, six and twelve storey capacity designed, and non-capacity designed buildings. Note that the values of ρ_t shown in Tables 5.11, 5.13 and 5.15, are for both top and bottom ends of each column.

Since the *Buildings LD* were designed for higher seismic loading, it is obvious that the longitudinal reinforcement content in the beams of the *Buildings LD* was generally larger than that of the *Buildings D*. Conversely, less quantities of longitudinal reinforcement were provided in the columns of the *Buildings LD* than that of the *Buildings D*, since the columns of the *Buildings D* were designed using the capacity design procedure.

The smaller ductility demand in the beams of the *Buildings LD* means that less stringent requirements for the quantities of transverse reinforcement are needed for beams in frames of limited ductility than for beams in ductile frames.

A quantity of transverse confining reinforcement to satisfy a required curvature ductility factor of 10 is adequate for all columns of the *Buildings LD*. Columns at the base and roof levels in the *Buildings D* need to be designed for adequate ductility (say, to satisfy a required curvature ductility of 20), while the other columns can be expected to remain in the elastic range, and the quantity of confining reinforcement needed is only one-half of that required for adequate ductility [2]. The transverse reinforcement required for concrete confinement ρ_s, calculated from Eq. 4.39 in various storeys are given in Tables 5.16 to 5.18. It is obvious, that larger quantities of confining reinforcement were required at the base of the columns of the *Buildings D*. On the other hand, larger quantities were required at the other levels of the columns of the *Buildings LD*.

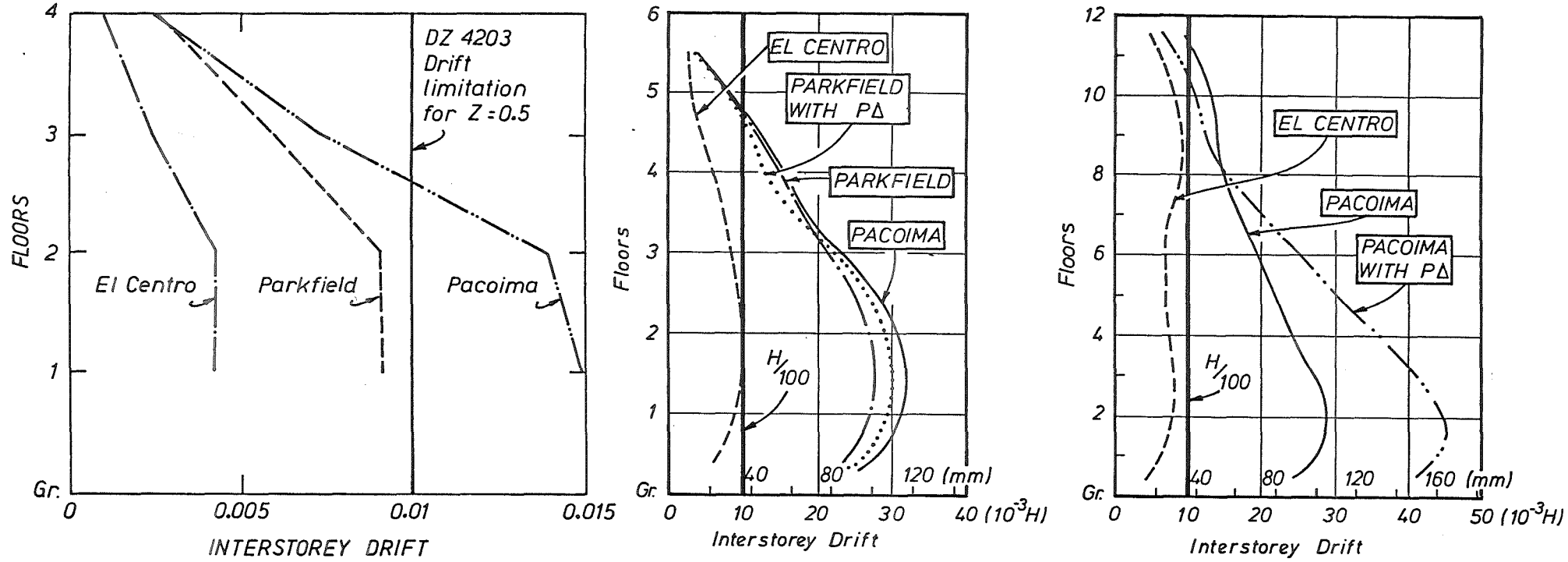

Figure 5.33: Maximum Inter-Storey Drift Envelopes for Capacity Designed Four, Six and Twelve Storey Ductile Frames

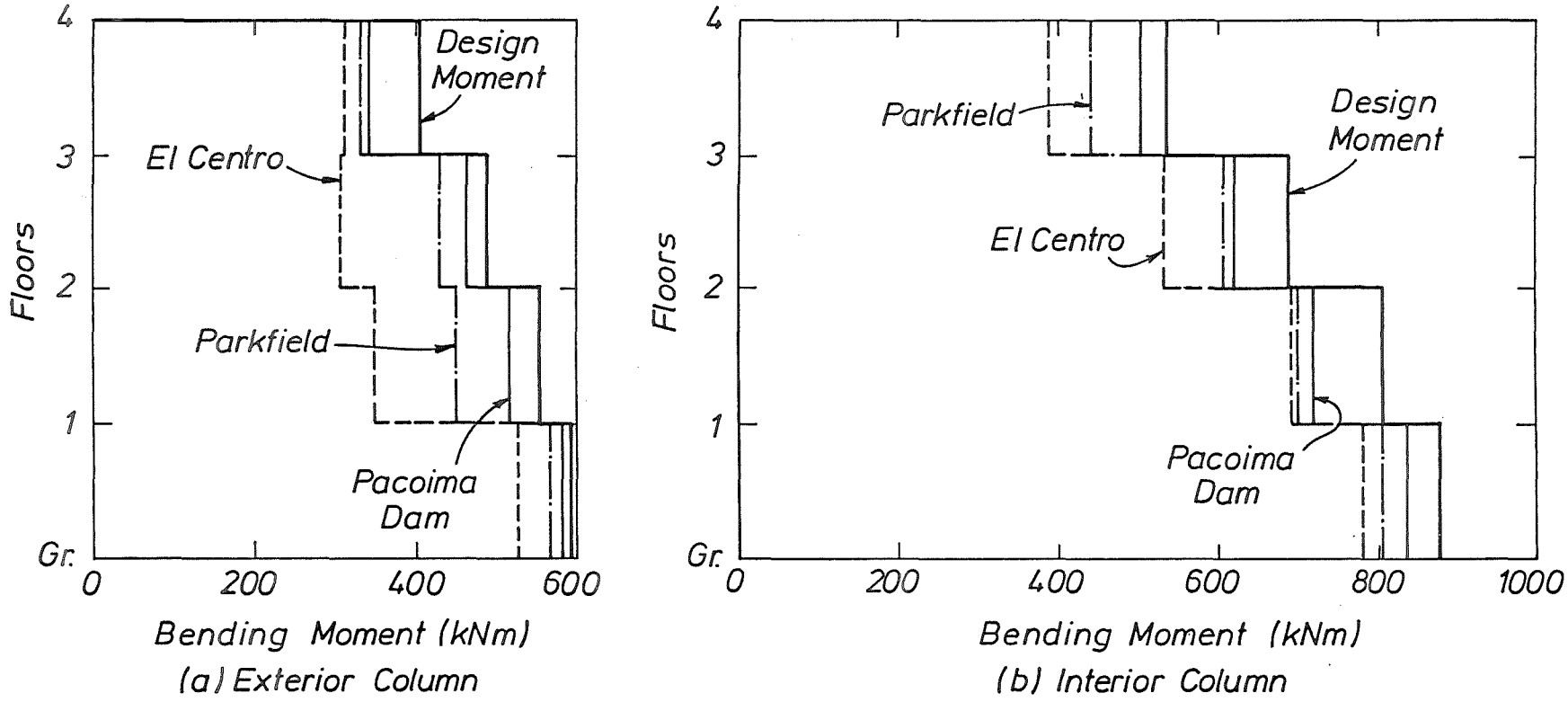

Figure 5.34: Maximum Bending Moment Envelopes for Columns in Capacity Designed Four Storey Ductile Frame

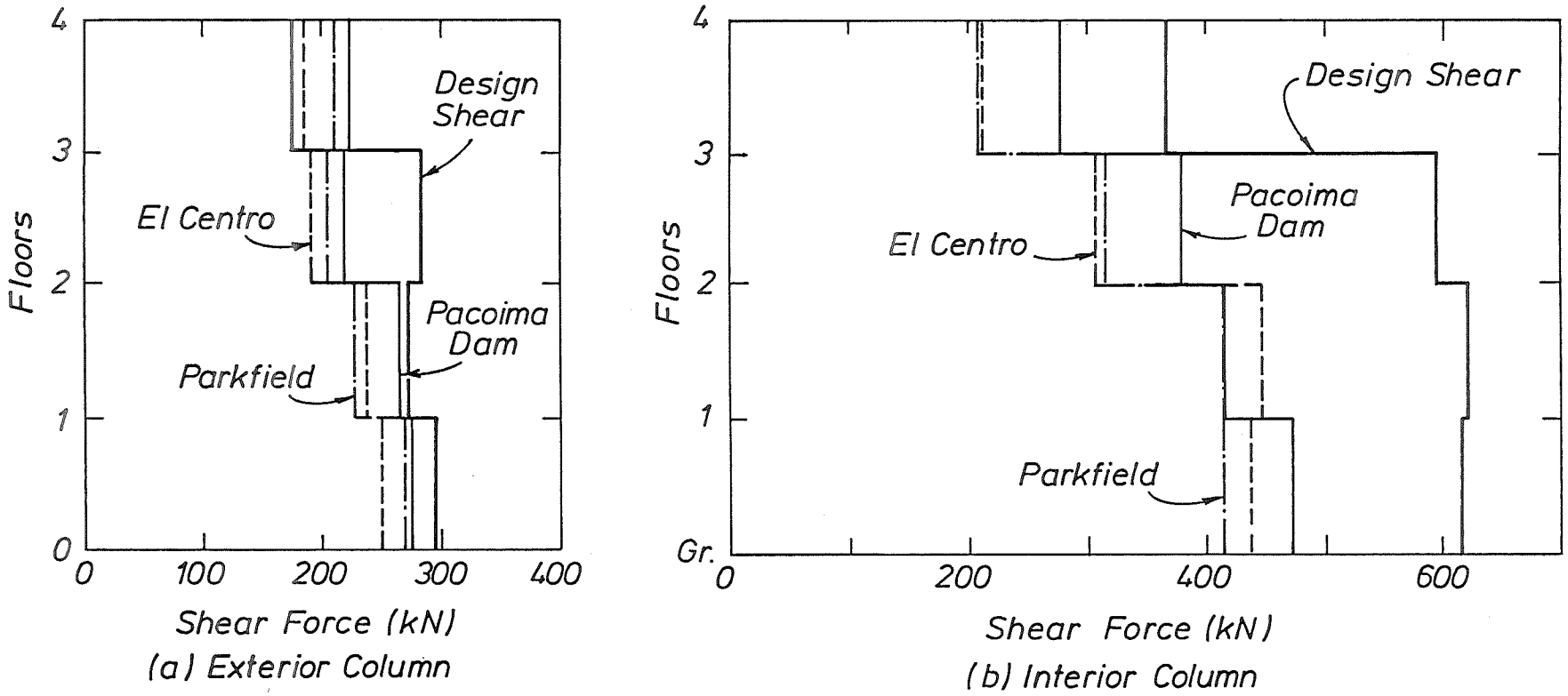

Figure 5.35: Maximum Shear Force Envelopes for Columns in Capacity Designed Four Storey Ductile Frame

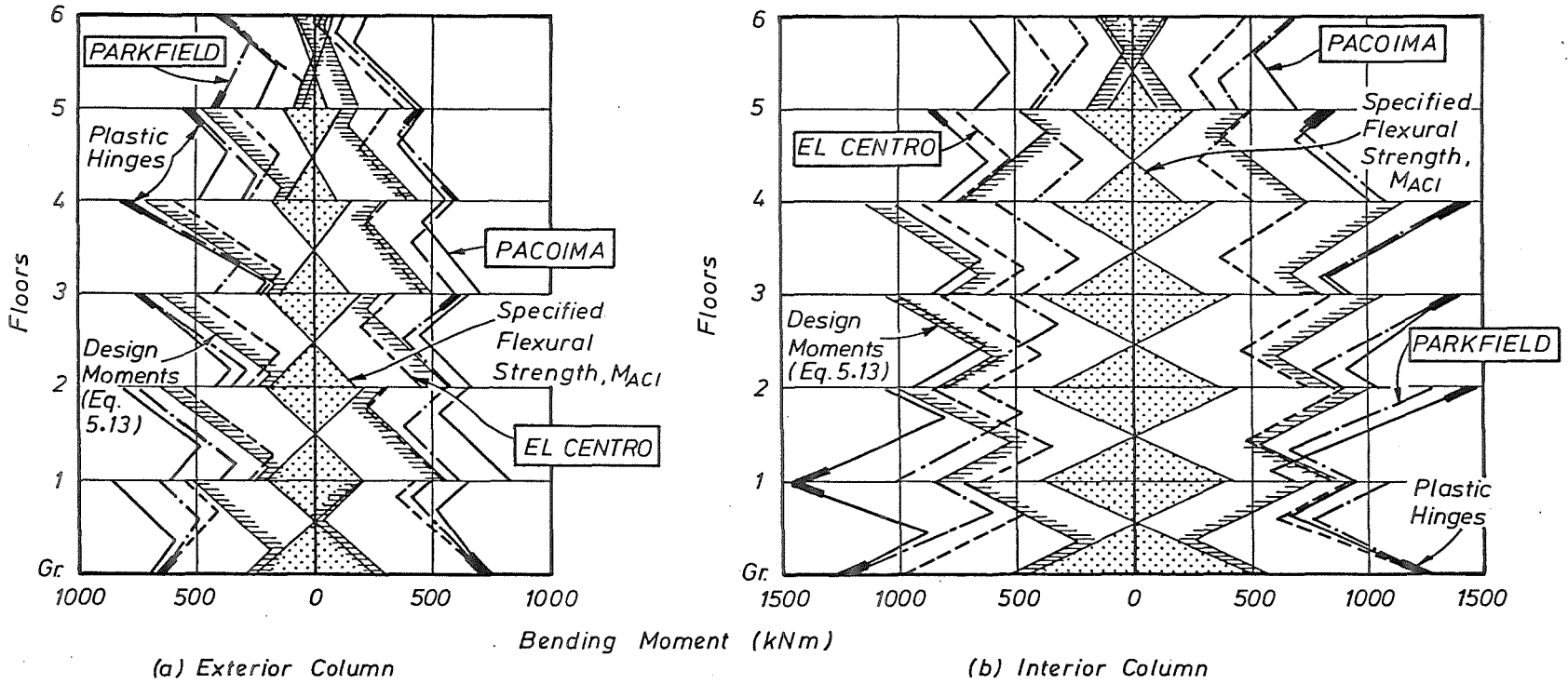

Figure 5.36: Maximum Bending Moment Envelopes for Columns in Capacity Designed Six Storey Ductile Frame

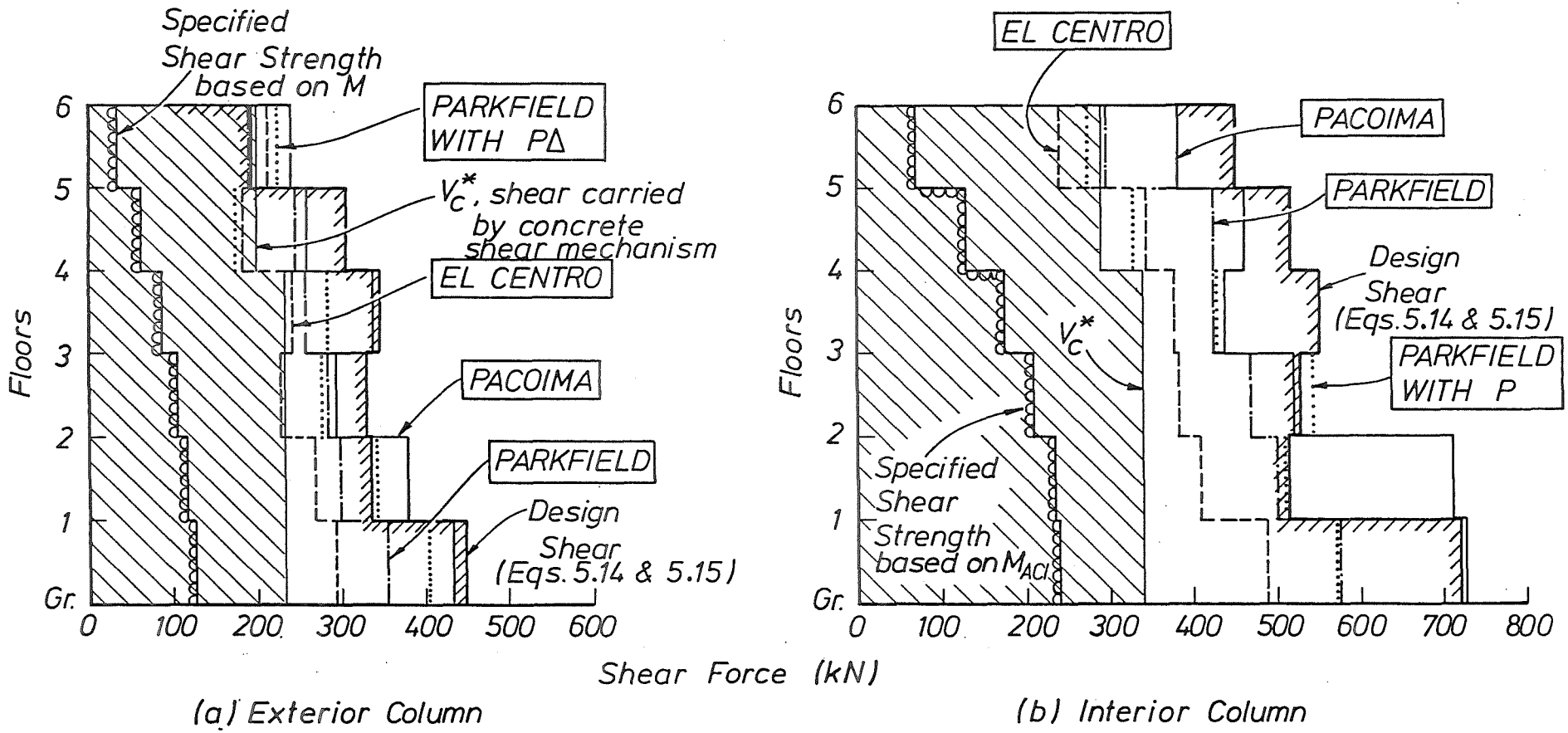

Figure 5.37: Maximum Shear Force Envelopes for Columns in Capacity Designed Six Storey Ductile Frame

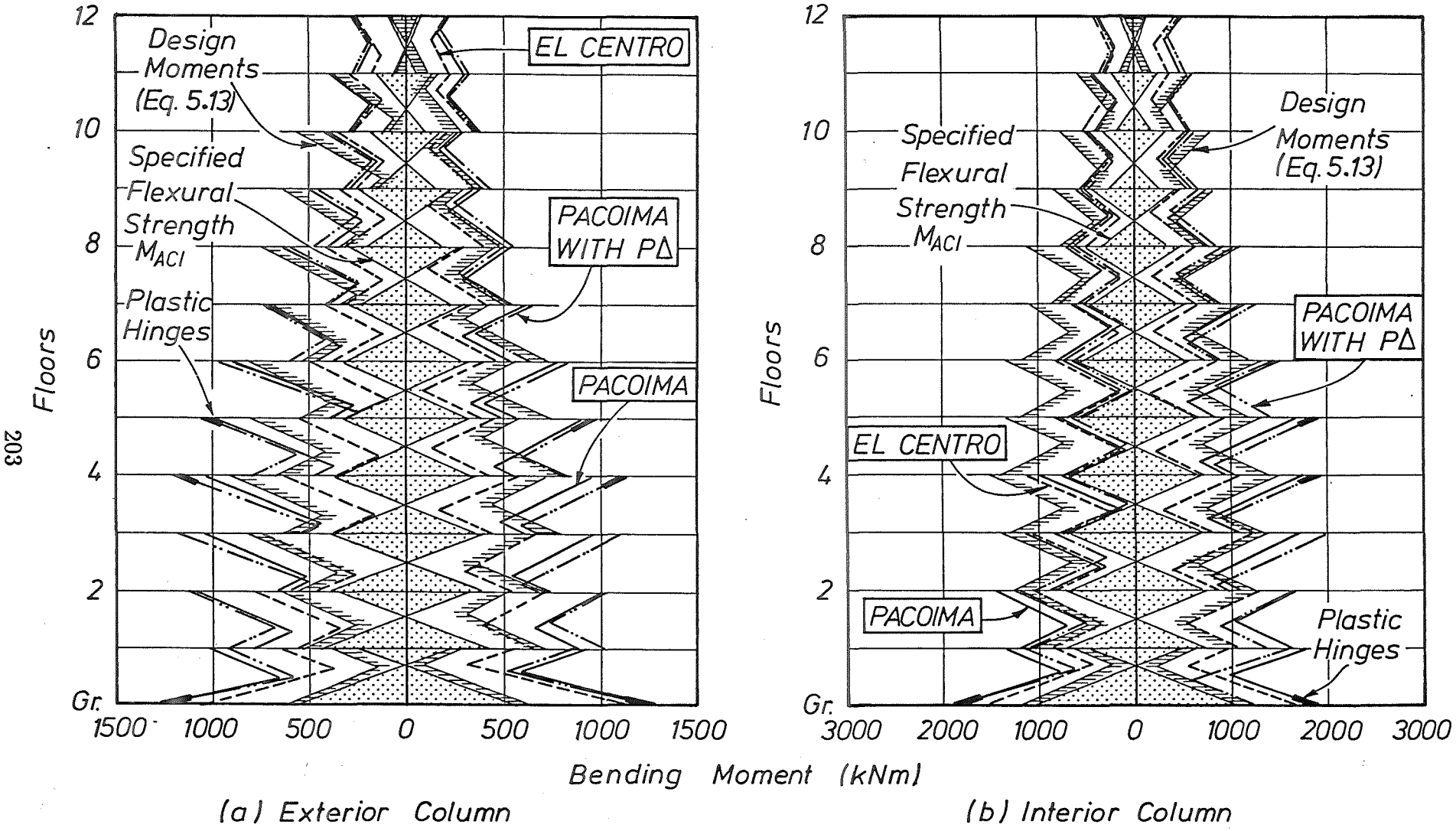

Figure 5.38: Maximum Bending Moment Envelopes for Columns in Capacity Designed Twelve Storey Ductile Frame

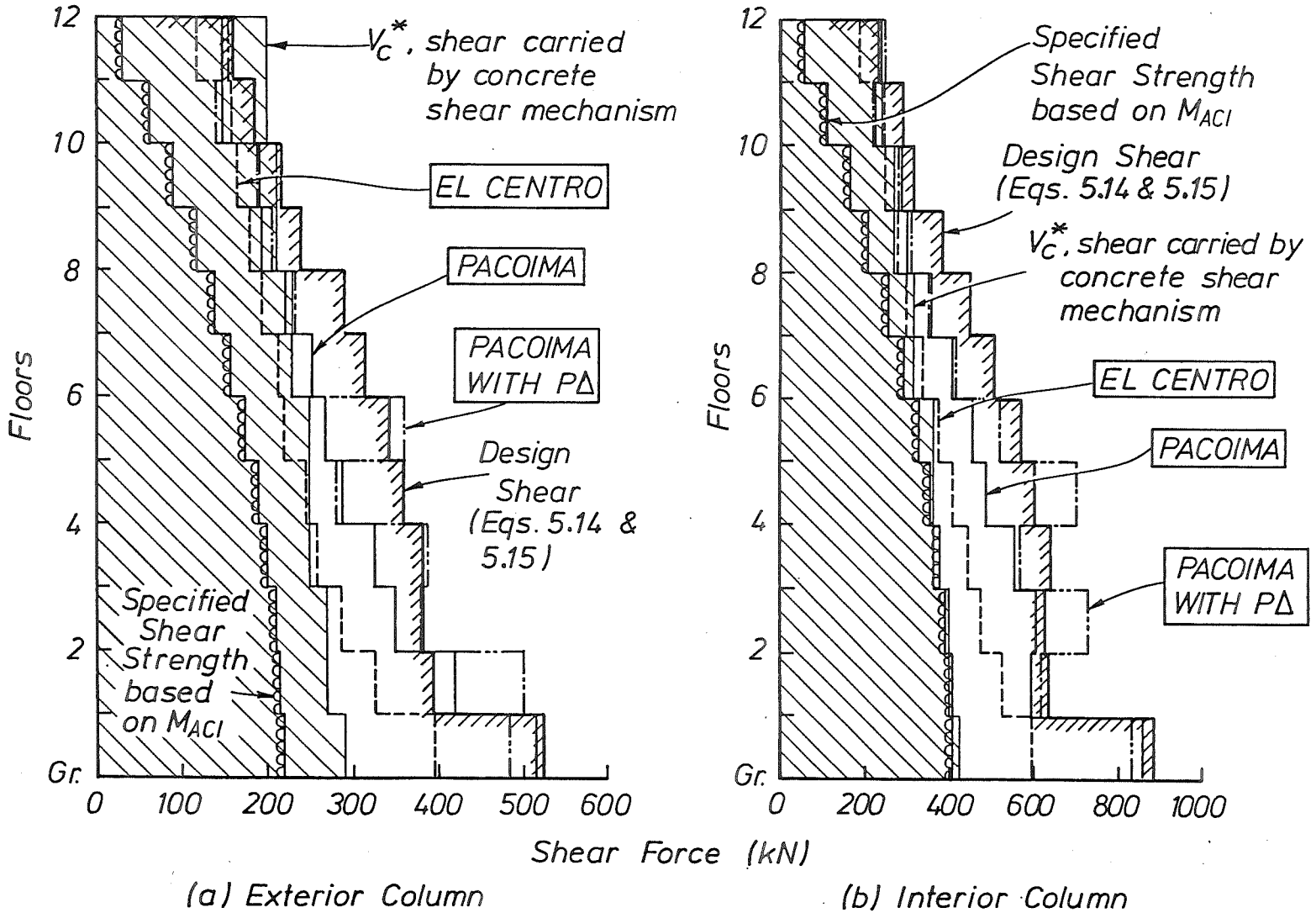

Figure 5.39: Maximum Shear Force Envelopes for Columns in Capacity Designed Twelve Storey Ductile Frame

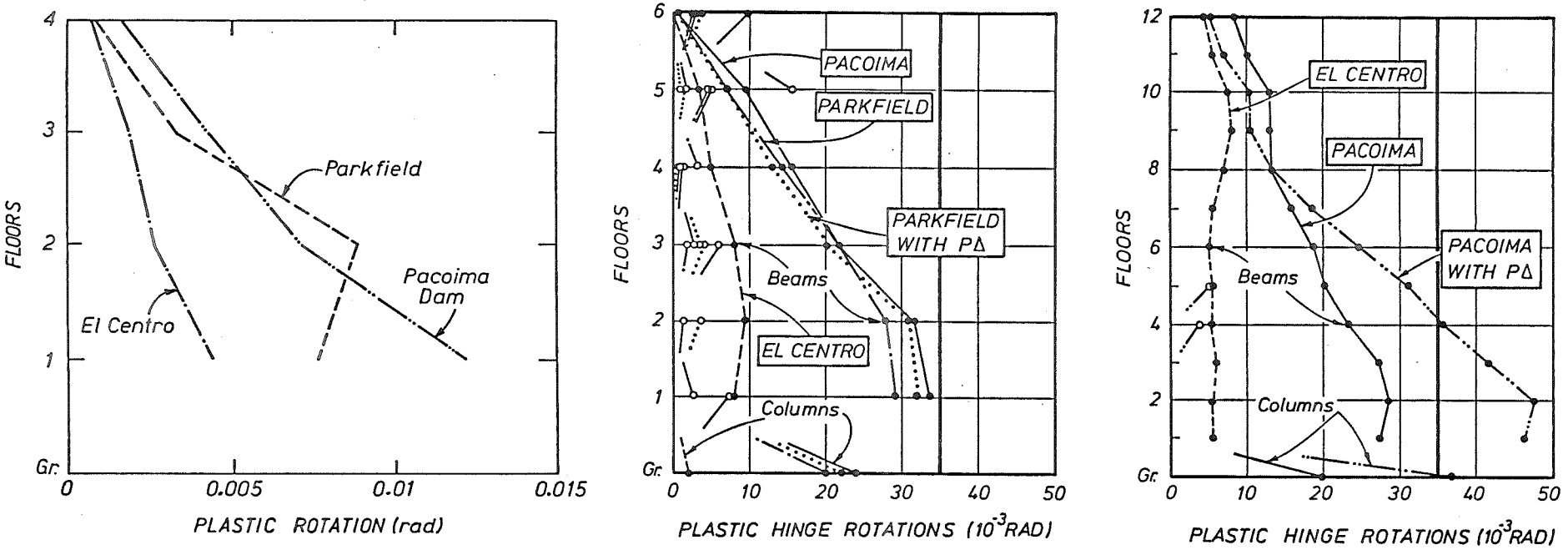

Figure 5.40: Maximum Plastic Rotation Envelopes for Beams in Capacity Designed Four, Six and Twelve Storey Ductile Frames

Table 5.10: Comparison of Dimensions and Required Longitudinal Tension Reinforcement Contents in the Beams of the Four Storey *Buildings LD* and *D*

Floor	Dimension		Longitudinal Tension Reinforcement Content ρ							
			At Face of Exterior Column				At Face of Interior Column			
	LD	D	M^-		M^+		M^-		M^+	
			LD	D	LD	D	LD	D	LD	D
4	400 × 750	400 × 750	0.66%	0.49%	0.45%	0.33%	1.11%	1.02%	0.66%	0.61%
3	400 × 750	400 × 750	1.28%	0.97%	0.78%	0.61%	1.28%	1.02%	0.78%	0.61%
2	400 × 750	400 × 750	1.40%	1.02%	0.78%	0.61%	1.35%	1.19%	0.78%	0.66%
1	400 × 750	400 × 750	1.40%	1.02%	0.78%	0.61%	1.57%	1.19%	0.90%	0.66%

- LD=Limited ductility building
- D=Ductile building
- f_y=430 MPa, f'_c=30 MPa and f_{yh}=300 MPa

Table 5.11: Comparison of Dimensions and Required Total Longitudinal Reinforcement Contents in the Columns of the Four Storey *Buildings LD* and *D*

Level	Exterior				Interior			
	Dimension		ρ_t		Dimension		ρ_t	
	LD	D	LD	D	LD	D	LD	D
4	500 × 500	500 × 500	0.96%	0.96%	600 × 600	600 × 600	0.89%	0.89%
			0.96%	1.45%			0.89%	0.89%
3	500 × 500	500 × 500	0.96%	1.45%	600 × 600	600 × 600	0.89%	0.89%
			0.96%	1.45%			0.89%	0.89%
2	500 × 500	500 × 500	0.96%	1.45%	600 × 600	600 × 600	0.89%	0.89%
			0.96%	1.45%			0.89%	0.89%
1	500 × 500	500 × 500	0.96%	1.45%	600 × 600	600 × 600	0.89%	0.89%
			0.96%	0.96%			0.89%	0.89%

- LD=Limited ductility building
- D=Ductile building
- f_y=430 MPa, f'_c=30 MPa and f_{yh}=300 MPa

Table 5.12: Comparison of Dimensions and Required Longitudinal Tension Reinforcement Contents in the Beams of the Six Storey *Buildings LD* and *D*

Floor	Dimension		Longitudinal Tension Reinforcement Content ρ							
			At Face of Exterior Column				At Face of Interior Column			
	LD	D	M^-		M^+		M^-		M^+	
			LD	D	LD	D	LD	D	LD	D
6	400 × 750	400 × 750	0.70%	0.89%	0.57%	0.48%	1.40%	1.37%	0.84%	0.74%
5	400 × 750	400 × 750	1.19%	0.89%	0.66%	0.48%	1.40%	1.37%	0.84%	0.74%
4	400 × 750	400 × 750	1.40%	1.21%	0.79%	0.64%	1.40%	1.34%	0.84%	0.72%
3	400 × 750	400 × 750	1.40%	1.21%	0.79%	0.64%	1.64%	1.34%	0.90%	0.72%
2	400 × 750	400 × 750	1.64%	1.30%	0.79%	0.69%	1.64%	1.34%	0.90%	0.72%
1	400 × 750	400 × 750	1.64%	1.30%	0.79%	0.69%	1.64%	1.34%	0.90%	0.72%

- LD=Limited ductility building
- D=Ductile building
- f_y=430 MPa, f'_c=30 MPa and f_{yh}=300 MPa

Table 5.13: Comparison of Dimensions and Required Total Longitudinal Reinforcement Contents in the Columns of the Six Storey *Buildings LD* and *D*

Level	Exterior				Interior			
	Dimension		ρ_t		Dimension		ρ_t	
	LD	D	LD	D	LD	D	LD	D
6	500 × 500	500 × 500	0.96%	1.0%	550 × 550	600 × 600	0.8%	1.0%
			0.96%	1.3%			0.8%	1.0%
5	500 × 500	500 × 500	0.96%	1.3%	550 × 550	600 × 600	0.8%	1.0%
			0.96%	1.8%			0.8%	1.9%
4	500 × 550	500 × 575	0.88%	1.6%	600 × 600	650 × 650	0.89%	1.6%
			0.88%	1.0%			0.89%	1.3%
3	500 × 550	500 × 575	0.88%	1.0%	600 × 600	650 × 650	0.89%	1.3%
			0.88%	1.0%			0.89%	1.0%
2	500 × 550	500 × 575	0.88%	1.0%	600 × 600	650 × 650	0.89%	1.0%
			0.88%	1.0%			0.89%	1.0%
1	500 × 550	500 × 575	0.88%	1.0%	600 × 600	650 × 650	0.89%	1.0%
			0.88%	1.0%			0.89%	1.0%

- LD=Limited ductility building
- D=Ductile building
- f_y=430 MPa, f'_c=30 MPa and f_{yh}=300 MPa

Table 5.14: Comparison of Dimensions and Required Longitudinal Tension Reinforcement Contents in the Beams of the Twelve Storey *Buildings LD* and *D*

Floor	Dimension		Longitudinal Tension Reinforcement Content ρ							
			At Face of Exterior Column				At Face of Interior Column			
	LD	D	M^-		M^+		M^-		M^+	
			LD	D	LD	D	LD	D	LD	D
12	400 × 600	400 × 600	1.76%	0.62%	1.05%	0.66%	2.49%	0.86%	1.34%	0.66%
11	400 × 600	400 × 600	2.42%	0.94%	1.44%	0.66%	2.12%	1.02%	1.15%	0.66%
10	400 × 650	400 × 650	1.93%	1.04%	1.05%	0.61%	1.93%	1.04%	1.05%	0.61%
9	400 × 650	400 × 650	2.21%	1.23%	1.05%	0.76%	2.21%	1.19%	1.05%	0.72%
8	400 × 700	400 × 700	2.03%	1.32%	0.97%	1.0%	2.03%	1.29%	0.97%	0.88%
7	400 × 700	400 × 700	2.03%	1.32%	0.97%	1.0%	2.03%	1.29%	0.97%	0.88%
6	400 × 750	400 × 750	1.87%	1.36%	1.15%	0.9%	1.87%	1.46%	0.92%	0.9%
5	400 × 750	400 × 750	1.87%	1.36%	1.15%	0.9%	1.87%	1.46%	0.92%	0.9%
4	400 × 750	400 × 750	1.87%	1.55%	1.41%	0.9%	1.87%	1.68%	1.03%	0.9%
3	400 × 750	400 × 750	2.11%	1.57%	1.41%	1.12%	1.87%	1.68%	1.03%	0.9%
2	400 × 750	400 × 750	2.11%	1.57%	1.41%	1.12%	1.87%	1.68%	1.03%	0.9%
1	400 × 750	400 × 750	1.87%	1.36%	1.15%	0.9%	1.87%	1.46%	0.92%	0.9%

- LD=Limited ductility building
- D=Ductile building
- f_y=430 MPa, f'_c=30 MPa and f_{yh}=300 MPa

Table 5.15: Comparison of Dimensions and Required Total Longitudinal Reinforcement Contents in the Columns of the Twelve Storey *Buildings LD* and *D*

Level	Exterior				Interior			
	Dimension		ρ_t		Dimension		ρ_t	
	LD	D	LD	D	LD	D	LD	D
12	500 × 500	500 × 500	0.96%	1.0%	550 × 550	550 × 550	0.8%	1.0%
			0.96%	1.0%			0.8%	1.0%
11	500 × 500	500 × 500	0.96%	1.0%	550 × 550	550 × 550	0.8%	1.0%
			0.96%	1.5%			0.8%	1.9%
10	500 × 525	500 × 525	0.92%	1.4%	575 × 575	575 × 575	0.73%	1.7%
			0.92%	1.4%			0.73%	1.7%
9	500 × 525	500 × 525	0.92%	1.4%	575 × 575	575 × 575	0.73%	1.7%
			0.92%	1.5%			0.73%	2.0%
8	500 × 575	500 × 575	0.84%	1.4%	625 × 625	625 × 625	0.87%	1.7%
			0.84%	1.4%			0.87%	1.7%
7	500 × 575	500 × 575	0.84%	1.4%	625 × 625	625 × 625	0.87%	1.7%
			0.84%	1.1%			0.97%	1.6%
6	500 × 625	500 × 625	0.77%	1.0%	675 × 675	675 × 675	0.83%	1.4%
			0.77%	1.0%			0.83%	1.4%
5	500 × 625	500 × 625	0.77%	1.0%	675 × 675	675 × 675	0.83%	1.4%
			0.77%	1.4%			0.83%	1.6%
4	500 × 625	500 × 625	0.77%	1.4%	675 × 675	675 × 675	0.83%	1.6%
			0.77%	1.1%			0.83%	1.1%
3	500 × 725	500 × 725	0.89%	1.0%	725 × 725	725 × 725	0.96%	1.0%
			0.89%	1.0%			0.96%	1.0%
2	500 × 725	500 × 725	0.89%	1.0%	725 × 725	725 × 725	0.96%	1.0%
			0.89%	1.0%			0.96%	1.0%
1	500 × 725	500 × 725	0.89%	1.0%	725 × 725	725 × 725	0.96%	1.0%
			0.89%	1.0%			0.96%	1.0%

- LD=Limited ductility building
- D=Ductile building
- f_y=430 MPa, f'_c=30 MPa and f_{yh}=300 MPa

Table 5.16: Comparison of Required Transverse Reinforcement for Concrete Confinement ρ_s in the Columns of the Four Storey *Buildings LD* and *D*

	Exterior Column		Interior Column	
Level	LD	D	LD	D
Ground	0.0014	0.0064	0.0023	0.0058
2nd level, bot.end	-	0.0013	-	0.0029
3rd level, bot.end	-	-	-	-

Table 5.17: Comparison of Required Transverse Reinforcement for Concrete Confinement ρ_s in the Columns of the Six Storey *Buildings LD* and *D*

	Exterior Column		Interior Column	
Level	LD	D	LD	D
Ground	0.0058	0.0110	0.0065	0.0111
2nd level, bot.end	0.0038	0.0041	0.0044	0.0042
3rd level, bot.end	0.0017	0.0027	0.0023	0.0028

Table 5.18: Comparison of Required Transverse Reinforcement for Concrete Confinement ρ_s in the Columns of the Twelve Storey *Buildings LD* and *D*

	Exterior Column		Interior Column	
Level	LD	D	LD	D
Ground	0.0162	0.0183	0.0122	0.0164
2nd level, bot.end	0.0143	0.0082	0.0107	0.0073
6th level, bot.end	0.0087	0.0050	0.0067	0.0040

- LD=Limited ductility building
- D=Ductile building
- f_y=430 MPa, f'_c=30 MPa and f_{yh}=300 MPa
- "-" indicates that transverse steel for confinement is not required

5.7.3 Comparison of Capacity Design and Non-Capacity Design Procedures

The desirable features of the capacity design approach for ductile frames have been recognized. This design procedure is capable of ensuring that a desired hierarchy of ductile failure mechanisms occurs during the inelastic response of a structure to seismic excitations. To achieve this satisfactory performance, the potential plastic hinge regions need to be determined and detailed for adequate strength and ductility, and the other regions need to be strong enough to remain in the elastic range. Therefore, the strengths of the elastic regions have to be derived from the overstrength of the regions which are expected to behave inelastically, in order to ensure that the energy dissipation occurs in the expected regions. Shear failure can be prevented by designing the shear strength as that derived from the flexural overstrength in the beams.

On the other hand, the strength design approach for frames of limited ductility is a simple design procedure. The design actions in the beams and columns can be obtained directly from an elastic analysis of two dimensional structures. It was shown in the dynamic analyses, that the observed bending moments and shear forces in the members were generally well within the suggested design values. It is considered that the conventional strength design method can be appropriately used for the design of frames of limited ductility, providing that sufficient concrete confinement and shear resistance is given to the columns.

5.7.4 Suggested Design Steps for Non Capacity Designed Frames of Limited Ductility

The suggested design steps for non-capacity designed frames of limited ductility are as follows:

1. Use a two-dimensional structural elastic analysis to determine the design actions in beams and columns due to the various combinations of loadings as given in Eq. 5.2. A displacement ductility factor of μ=3 needs to be used in determining the earthquake load E.

2. Determine the most critical combination of loadings in the beams and columns. Apply up to 30% and 20% moment redistribution to the beam and column bending moments, respectively, to determine the design actions.

3. Determine the longitudinal reinforcement content required for those design actions in the beams using the code method [2].

4. Determine the longitudinal reinforcement required for those design actions in the columns using the code [2] approach.

5. Determine the beam design shear forces by assuming that the flexural overstrengths are reached at each end of the beams simultaneously. Calculate the quantity of transverse reinforcement required for shear in the beams.

6. Determine the quantities of transverse reinforcement required in the columns for concrete confinement using the refined design equation given in Chapter 4 for a curvature ductility factor of φ_{max}/φ_y=10.

7. Determine the design shear forces of the columns, by assuming that both ends of the columns reached the code flexural strengths M_{ACI}.

8. Check the quantities of transverse reinforcement in the beams and columns to ensure that it is adequate to provide lateral restraint to the compressed longitudinal bars in potential plastic hinge regions.

5.8 Concluding Remarks

From the dynamic analysis carried out to investigate the seismic response of frames designed for ductility and limited ductility, the significant conclusions can be summarized as follows:

1. The seismic response of typical non-capacity designed frames of limited ductility, and capacity designed ductile frames, was examined under the El Centro, Parkfield, Pacoima Dam and Artificial generated earthquakes. Three frames were thoroughly investigated, namely a 3-bay 4-storey frame, a 2-bay 6-storey frame, and a 2-bay 12-storey frame. For the six and twelve storey ductile frames, the results obtained from the analysis carried out by Tompkins *et al.* [54] were used and were compared to those obtained from the current analysis. From a preliminary study of a 6-bay 6-storey frame, it was shown that the number of bays does not have significant influence on the results of the investigation. It should also be noted, that only regular frames were investigated in this study.

2. The results obtained from the dynamic analyses indicated that the response of the buildings under the El Centro excitation was the least severe, followed by that observed during the Parkfield, Artificially generated, and the Pacoima Dam excitations.

3. From the comparison of the seismic response of the frames designed for ductility and limited ductility, it was found that the ductile frames performed very well. The plastic hinges generally formed at the beams, and at the base and roof levels of the columns, while the other regions remained in the elastic range. On the other hand, some plastic hinges did develop up the height of the columns of non-capacity designed frames of limited ductility. However, the curvature ductility demand was small, and no column sidesway mechanisms were detected even under the strongest seismic event, such as the Pacoima Dam. By designing the frames for higher seismic forces, larger strengths are available in the beams and columns, which are likely to prevent the formation of the column sidesway mechanisms.

4. In general, the non-capacity designed frames of limited ductility exhibited reasonably good performance under the simulated seismic attack. Moreover, they were capable of surviving the greatest earthquake likely in New Zealand although they were designed for less severe seismic zones.

5. The conventional strength design, which is a relatively simple design procedure, can be used for the design of frames of limited ductility, providing that the columns are adequately confined and that sufficient shear resistance is available to ensure that shear failure will not occur. It is suggested that the transverse reinforcement for concrete confinement in columns be based on a curvature ductility factor demand of 10 and that the design shear forces in columns be based on shear forces calculated for the stage where the code [2] flexural strengths M_{ACI} are attained at both ends of the columns.

Chapter 6

PROPOSED SEISMIC DESIGN PROVISIONS FOR FRAMES OF LIMITED DUCTILITY

6.1 Introduction

As mentioned in Chapter 5, the capacity design of ductile structures can be a relatively complex procedure. The detailing of potential plastic hinge regions results in the presence of large quantities of transverse reinforcement, which often results in construction difficulties due to congestion of reinforcement. In some structures, where a higher seismic design load is economical, the ductility demand can be reduced, and non-capacity design of structures of limited ductility can be applied.

In this Chapter, the existing New Zealand code requirements for frames of limited ductility are given, and are compared with the requirements for ductile frames. Based on the results obtained from this study, some seismic design requirements for frames of limited ductility are proposed.

6.2 The Existing New Zealand Codes For Moment-Resisting Frames of Limited Ductility

The NZS 4203:1984 [30] states that: "Structures of limited ductility, not specifically designed to ensure ductile flexural yielding through the application of the principles of capacity design, shall be suitably designed and detailed in accordance with the appropriate materials code".

Moment resisting frames of limited ductility are assigned a structural type factor of S=2.0. This structural type factor may be compared with the value of S=0.8 assigned to ductile frames. That is, moment resisting frames of limited ductility are designed for seismic forces which are 2.0/0.8=2.5 times the seismic force used for the design of ductile moment resisting frames.

This comparison of design seismic forces is only pertinent to flexural actions in beams. The required flexural strengths of columns and shear strengths of beams and columns of ductile moment resisting frames are determined by capacity design, while for frames of limited ductility, the required flexural and shear strengths of all members are specified directly.

The commentary of the NZS 3101:1982 [2] states that for structures which are designed for only limited ductility, the complexity in the design as a result of the additional seismic requirements of the code for ductile structures may not be warranted. Therefore, the code has established simple yet not unduly conservative rules for structures of limited ductility as stated in Section 14, which is intended to be used with the "General Principles and Requirements" specified in the other sections of the code. The main features of Section 14 for moment resisting frames of limited ductility are:

1. Capacity design is not required
2. Design for concurrent earthquake effects from loadings in two principal directions is not required
3. Shear strengths provided are to have a suitable margin over the required flexural strengths (as determined by the structural type factor)
4. Flexural strengths outside the designated end regions are to have a suitable margin over the design moments (as determined by the structural type factor)
5. Lengths of designated end regions of beams and columns are equal to member depth. However, if flexural strengths outside of the region so defined do not meet the requirements of (4) above, then the end region is designated as the whole length of the beam or column
6. Transverse reinforcement in the designated end regions should have spacing not exceeding 10 longitudinal bar diameters. An equation is given for transverse reinforcement for confinement, if required.
7. In the designated end regions the contribution to shear strength provided by the concrete may be assumed to be not greater than one-half of that for gravity load design. The spacing of shear reinforcement may not exceed one-quarter of the effective depth of the members.

The design provisions for limited ductility are expected to be used as a matter of convenience for structures which are inherently strong due to structural form or material content and hence which can be economically designed for high seismic forces, and also for those structures where the designer recognizes a limitation to the ductility capacity as a result of structural complexity or irregular form.

Appropriate detailing of the designated end regions, in accordance with Section 14 [2] however, shall ensure that the reduced ductility demands can be met. This indicates that the regions must still be ductile and therefore the requirements for detailing to achieve ductility must be complied with, although they are somewhat relaxed in recognition of the lower ductility demand.

Because ductility and consequent detailing is provided, capacity design procedures can be used. Nevertheless, to simplify design procedures, the code also allows the strength design method, together with the appropriate strength reduction factors, to be used. To ensure that no premature brittle failures can occur, certain restrictions, particularly relevant to shear strength are specified. This simplified design procedure is necessarily more conservative than that of capacity design.

6.3 Comparison of New Zealand Codes for Ductile Frame and Frames of Limited Ductility

A comparison between the main design provisions of New Zealand codes for reinforced concrete ductile moment resisting frames and moment resisting frames of limited ductility, as summarized in Ref. [1] is given in Table 6.1.

6.4 Experimental Investigation of Columns and Beam-Column Joints of Limited Ductility

6.4.1 General

The need to evaluate the existing code requirements for limited ductility structures, have been recognized. Some tests of columns, and beam-column joints of limited ductility have been carried out at the University of Canterbury. The results from the column tests were given in Chapter 3, and the results of beam-column joints conducted by Dai *et al* [68] are reviewed in this section.

Table 6.1: New Zealand Seismic Design Provisions for Reinforced Concrete Moment Resisting Frames [1]

Clause	Ductile Frames	Clause	Frames of Limited Ductility
NZS 4203 3.3.3.1	1. Definition Ductile frames shall be capable of dissipating seismic energy in a flexural mode at a significant number of plastic hinges in beams except that dissipation of seismic energy at plastic hinges in columns is permitted for buildings which comply with Clause 3.3.3.5	NZS 4203 3.4.2 Table 5	1. Definition Frames of limited ductility have a maximum height of four storeys or 18 m, or if roof and wall mass are less than 150 kg/m^2 of floor area a maximum height of five storeys or 22.5 m
NZS 4203 3.4.2 Table 5 NZS 3101 3.5.1.1 and 6.5.1.4	2. Design Actions The structural type factor used for determining seismic design forces is S = 0.8 Capacity design is used and the effects of concurrent seismic forces are included	NZS 4203 3.4.2 Table 5 NZS 3101 14.4.3	2. Design Actions The structural type factor used for determining seismic design forces is S = 2.0 Capacity design and design for concurrent seismic forces are not required
NZS 3101 4.3.1 C3.A	3. Required Flexural Strengths Flexural strengths: Beams $\phi M_i \geq M_g + M_{eq}$ Columns $M_i \geq M_u$	NZS 3101 14.4.2.2	3. Required Flexural Strengths In end regions: Beams $\phi M_i \geq M_g + M_{eq}$ Columns $\phi M_i \geq M_g + M_{eq}$ Outside end regions: Beams $\phi M_i \geq M_g + 1.5M_{eq}$ Columns $\phi M_i \geq M_g + 1.5M_{eq}$
NZS 3101 7.5.1.1 7.5.1.2 9.5.2	4. Required Shear Strengths Beams $V_i \geq V_u^o$ Columns $V_i \geq V_u^o$ Joints $V_i \geq V_u^o$	NZS 3101 14.4.2.1	4. Required Shear Strengths Beams $\phi V_i \geq V_g + 2V_{eq}$ Columns $\phi V_i \geq V_g + 2V_{eq}$ Joints $\phi V_i \geq V_g + 2V_{eq}$
NZS 3101 6.5.2.1 6.5.4.1	5. Length of Potential Plastic Hinge Regions Beams: Over lengths equal to twice the beam depth at the ends of the beam and within the span where plastic hinges can form. Columns: Over end regions equal to the larger of the largest cross section dimension or where the moment exceeds 0.8 of the moment at that end of the member. This length is increase by 50% if $P_e \geq 0.3f'_c A_g \phi$.	NZS 3101 14.5.2	5. Length of End Regions Beams and columns: Over lengths equal to the depth of the member at the ends of the member, except that if Clause 14.4.2.2 is not complied with it is considered to be the whole length of the member.
NZS 3101 6.5.3.3	6. Transverse Reinforcement Within the Potential Plastic Hinge Regions Beams: If yielding of flexural steel can occur on both faces of member, the centre to centre spacing of stirrup-ties s is not to exceed the smaller of d/4 or six longitudinal bar diameters, or 150 mm.	NZS 3101 14.6.2	6. Transverse Reinforcement Within the End Regions Beams and Columns: The centre to centre spacing of stirrup-ties, or rectangular hoops or cross ties, is not to exceed ten longitudinal bar diameters. The area of transverse reinforcement for confinement is given by

Continuation of Table 6.1

Clause	Ductile Frames	Clause	Frames of Limited Ductility
6.5.3.3 7.5.2.2	The yield force of the stirrup-tie must at least equal one-sixteenth of the yield force of the longitudinal bar or bars it is to restrain multiplied by s/100. The stirrups must also satisfy shear strength requirements computed assuming $v_c = 0$.		$A_{sh} = R_C(0.02 s_h h \frac{f'_c}{f_{yh}})$ if $\gamma > 1.0$ where $\gamma = \frac{M^*_e + 0.3P_e h}{0.6\phi f'_c A^*_g h} \leq 3.0$ and $0 \leq R_C = \left[\frac{\gamma}{1 + \rho^* m} - 1\right] \leq 1.0$
6.5.4.3	Columns: The centre to centre spacing of transverse confining steel is not to exceed the smaller of one-fifth of the least lateral dimension of the cross section or six longitudinal bar diameters or 200 mm. The yield force of the transverse bar in rectangular arrangements of hoop steel must at least equal one-sixteenth of the yield force of the longitudinal bar or bars it is to restrain. The transverse reinforcement must satisfy the code equations 6-22 and 6-23 for spirals or circular hoops or equations 6-24 and 6-25 for rectangular hoops.	14.7.2 14.7.5	The transverse reinforcement provided must also satisfy the shear strength requirements computed assuming v_c is one-half of that for gravity load design. Maximum spacing of shear reinforcement is not to exceed d/4.
6.5.4.3	The transverse reinforcement must also satisfy shear strength requirements computed assuming $v_c = 0$ if $P_e/f'_c A_g \leq 0.1$ or v_c as given by equation 7-41 if $P_e/f'_c A_g > 0.1$.		
NZS 3101 9.3 and 9.5 5.5.2.1 -5,5.2.2	7. Beam-Column Joints Shear: Transverse and vertical reinforcement must satisfy the shear strength requirements for horizontal and vertical shear using equations 9-1 to 9-15. Anchorage: Longitudinal reinforcement passing through interior joint cores should have diameters not exceeding that permitted by the code. Longitudinal beam reinforcement anchored in column cores or beam strips shall have anchorage commencing either at mid-depth of the column or at $10d_b$ from the column face, unless plastic hinging is located away from the column face in which case anchorage can be considered to commence at the column face.	NZS 3101	7. Beam-Column Joints No specific design rules stated. Use design rules for non-seismic joints with the full value of v_c .

6.4.2 Results from Beam-Column Joint Tests

In 1987, four beam-column joints were tested subjected to simulated earthquake loading [68]. A brief description of the units tested is summarized as follows:

- Unit 1: The NZS 3101:1982 [2] requirements for ductile detailing were followed entirely.
- Unit 2: The code [2] requirements for ductile detailing were followed, except that the diameter of the beam longitudinal bars d_b was 72% greater than that specified by the code. The ratio of $d_b/h_c = 1/14.5$ was used (h_c=column depth), whereas the code permitted value of this ratio is 1/25 for Grade 275 deformed longitudinal reinforcement.
- Unit 3: The code [2] requirements for ductile detailing were followed, except that in the joint core, the horizontal and vertical shear reinforcement provided, was only 56% and 65% of that required by the code.
- Unit 4: The code [2] requirements for ductile detailing were followed. However, as for Unit 2, the diameter of the beam longitudinal bars d_b was 72% greater than required by the code, and the horizontal and vertical shear reinforcement provided in the joint core, was 56% and 78% of the code quantities.

From the above description, it is obvious that according to the code [2] only Unit 1 was expected to have adequate ductility, while the other units were expected to have limited ductility behaviour.

During the tests, the units were capable of completing two cycles to displacement ductility factors of at least 5, without significant strength degradation. This indicated that the units had more than limited ductility, and therefore that the existing code requirements for the quantity of shear reinforcement in beam-column joint cores of ductile structures could be made less stringent. Also, that larger diameter beam longitudinal bars passing through the joint core of ductile structures could be permitted when the concrete strength was substantially greater than 20 MPa. It is to be noted that for the four units, f'_c was approximately 40 MPa and that this high concrete strength undoubtedly enhanced the bond behaviour. Further tests on beam- column joints of limited ductility are required.

6.5 Proposed Seismic Design Requirements for Frames of Limited Ductility

6.5.1 General

As mentioned previously, the seismic design requirements for frames of limited ductility as stated in Section 14 of the existing New Zealand concrete design code [2] are aimed to provide a simple and yet conservative design procedure. In practice, it is found however, that the existing provisions are not simple to use. Also, Section 14 treats the design of all structural members in a uniform manner. The required shear and flexural strengths

specified can be overly conservative. Moreover, the equation for confinement within the end regions is a rather crude approach. By restricting the neutral axis depth, it is expected that lateral instability will not be a critical design criterion. Therefore, the existing provisions need be stated simply but with more general formulations introduced. Based on the results of column units tested (refer to Chapter 3), and the inelastic dynamic analyses carried out (refer to Chapter 5), some modifications to those existing code requirements for limited ductility structures are proposed. In the following sections, the provisions which need to be modified are discussed.

6.5.2 Design of Frames of Limited Ductility Subjected to Seismic Loadings

In determining the earthquake load E, moment resisting frames of limited ductility can be designed using a displacement ductility μ=3, as specified in the DZ4203:1986 [39]. The conventional strength design method can be used to determine the design actions in the beams and columns. The member forces are obtained from the two dimensional elastic structural analysis. Moment redistribution of up to 30% and 20% for the beam and column bending moments may be applied.

The dependable strengths in the members, that is ϕ times the ideal strengths, should exceed the design forces. The strength reduction factor ϕ is taken as:

ϕ = 0.9 for flexure
ϕ = 0.9 for flexure and axial load
ϕ = 0.85 for shear

The longitudinal reinforcement content required in the beams and columns is determined using the code [2] approach.

The design shear forces of the beams are calculated by assuming that the flexural over-strengths are developed at both ends of the beams simultaneously. The design shear forces of the columns are calculated by assuming that both ends of the columns reached the code flexural strengths M_{ACI}.

Design Forces for Beam-Column Joints of Limited Ductility

Based on the very few available test results [68], the following recommendations could be suggested for the design of beam-column joints of limited ductility:

(1) Shear carried by concrete diagonal compression strut mechanism and shear carried by shear reinforcement: For beam-interior column joints of frames of limited ductility, $V_{ch} = 0.6V_{jh}$ and $V_{sh} = 0.4V_{jh}$ may be assumed. At least one column intermediate bar should exist at each side of the column passing through the joint core.

(2) Diameter of beam longitudinal bars: For beam-interior column joints of frames of limited ductility, no restriction of d_b/h_c ratio may be necessary.

6.5.3 Transverse Reinforcement in Beams and Columns

For beams, the current code requirements for transverse reinforcement could be maintained (see Section 14.6.2.3).

For columns, the current code requirements of the quantities of transverse reinforcement for concrete confinement and for preventing premature buckling of longitudinal bars are updated as a result of the columns tested.

(1) Transverse Reinforcement for Concrete Confinement in Columns

Using the design charts for ductility [4], which were derived from the cyclic moment-curvature theory [3], and confirmed by the experiment investigation (see Ref. [5] and Chapter 3), a proposed refined design equation to replace the existing code equations for concrete confinement was derived. The equation can be used for designing transverse confining reinforcement in column sections of ductility and limited ductility depending on the specified curvature ductility factor. For a column of limited ductility, a φ_u/φ_y=10 can be specified. The required quantities for concrete confinement are then:

For square and rectangular hoops arrangement:

$$\rho_s = \frac{A_g}{A_c}\frac{(32-33\rho_t m)}{111}\frac{f'_c}{f_{yh}}\frac{P_e}{\phi f'_c A_g} - 0.006 \tag{6.1}$$

For spirals and circular hoops arrangement:

$$\rho_s = 1.4\,\frac{A_g}{A_c}\frac{(32-33\rho_t m)}{111}\frac{f'_c}{f_{yh}}\frac{P_e}{\phi f'_c A_g} - 0.008 \tag{6.2}$$

These quantities of confining reinforcement need to be provided over the potential plastic hinge regions of columns, which are defined as the end regions of the column with a length of l_c as follows:

$$\frac{l_c}{h} = 1.0 + 2.8\frac{P_e}{\phi f'_c A_g} \tag{6.3}$$

The equation gives values of $l_c = h$, and $3h$ for $P_e/(\phi f'_c A_g)$=0 and 0.7, respectively, where h=the largest lateral dimension or diameter of column.

(2) Transverse Reinforcement for Preventing Premature Buckling of Longitudinal Compression Bars

To ensure that the compression bars do not buckle when subjected to simulated cyclic loading such as earthquake excitations, the spacings of transverse reinforcement should not exceed six longitudinal bar diameters. This limit was found to give satisfactory restraint against bar buckling [5] (See also Chapter 3). Outside the potential plastic hinge regions, the spacings can be increased to twice of that in the potential plastic hinge regions.

(3) Transverse Reinforcement for Shear Resistance

The current code requirements for transverse reinforcement in column sections with limited ductility to provide adequate shear resistance are maintained.

6.5.4 Limit for Number of Storeys

It was shown in Chapter 5, even for six and twelve storey frames, the proposed design procedures for frames of limited ductility giave satisfactory results. Therefore the limitation of the number of storeys specified by the existing code of four to five storeys could be increased to at least 12 storeys.

Chapter 7

MAJOR CONCLUSIONS AND RECOMMENDATIONS FOR FUTURE RESEARCH

7.1 Conclusions

Concluding remarks regarding the results from the study undertaken have generally been given at the end of each chapter. A summary of those findings are as follows:

1. An experimental study was carried out to investigate the behaviour of columns with square and octagonal cross sections under simulated earthquake loading. The columns tested had axial compression loads of $0.5f'_cA_g$ or $0.7f'_cA_g$, and contained various quantities of transverse confining reinforcement. The tests were a continuation of the previous tests [28] where four column units (Units 1 to 4) of square cross section were subjected to axial compression loads of $0.1f'_cA_g$ or $0.3f'_cA_g$. The main conclusions from the current tests are:

   Column Units 5 and 6 with square cross section, and contained 38% and 19% of the NZS 3101 specified quantity of confining reinforcement, and column Unit 10 with octagonal cross section, and contained 44% of the NZS 3101 specified quantity of confining reinforcement were subjected to a constant axial compression load ratio of $P_e/(f'_cA_g)$=0.5 and cyclic flexure. It was found that Units 5 and 10 achieved real displacement ductility factors μ_r of at least 6. Unit 6 was only capable of reaching μ_r of approximately 5. Buckling of the longitudinal bars was observed at the end of testing of Units 5 and 6, while fracture of spirals terminated the test of Unit 10.

   Column Units 7, 8 and 9 with square cross section, and contained 48%, 34% and 93% of the NZS 3101 specified quantity of confining reinforcement, and column Unit 11 with octagonal cross section, and contained 77% of the NZS 3101 specified quantity of confining reinforcement were subjected to an axial compression load ratio of $P_e/(f'_cA_g)$=0.7 and cyclic flexure. The test results indicated that all units, except Unit 8 achieved real displacement ductility factors μ_r of at least 6. At the end of testing of Unit 7, it was observed that the buckling of the longitudinal bars occurred at the

region with nominal confining reinforcement. Unit 9 which was expected to behave in ductile manner, did not show any degradation in strength when the test was terminated after completing two cycles to a nominal displacement ductility factor of 10. Units 8 and 11 exhibited buckling of the longitudinal bars at the end of the tests.

2. An evaluation of the existing code [2] requirement for the length of confined region l_c was undertaken. The predicted l_c for a number of columns and piles tested at the University of Canterbury, which had different levels of axial compression load ratios, aspect ratios and section type were calculated. It was observed that the required l_c was strongly dependent on the level of the axial compression load. The aspect ratio and section type of the columns were found to have insignificant effects by comparison. The current code requirements of $l_c = 1.0h$ for columns with axial compression load ratio of ≤ 0.3, and of $l_c = 1.5h$ for columns with axial compression load ratio of > 0.3, providing the moment gradient did not govern, were inadequate for many columns. As a result, a greater length of confined region was suggested as follows:

$$l_c = h \left(1 + 2.8 \frac{P_e}{\phi f'_c A_g} \right)$$

where h=column section dimension. The above equation gives values of $l_c = h$, and $3h$ for $P_e/(\phi f'_c A_g)$=0 and 0.7, respectively.

3. A comparison between the experimental results of the column units and the theoretical predictions using a theory for cyclic moment-curvature analysis [3,4] was carried out. This included determination of the yield curvatures and yield displacements, the lateral load-displacement hysteresis loops, the flexural strength enhancement factors, the maximum plastic rotations and curvatures, the available curvature ductility factors, and the monotonic moment-curvature relations. The comparisons indicated that the cyclic moment-curvature theory was generally conservative.

4. An analytical investigation to determine a more appropriate design equation for the quantities of confining reinforcement in the potential plastic hinge regions of columns was conducted. The following parameters were found to have significant effects: The level of axial compression load, the mechanical reinforcing ratio, the concrete compressive strength, the cover ratio, and the curvature ductility demand. The investigation revealed that the current code [2] equations for confining reinforcement are conservative when the axial compression load ratio of columns is relatively low, and may be unconservative when the axial load ratio is large, particularly for columns with large cover thickness.

   From the design charts for ductility [4], the data points in terms of the values of $\rho_s f_{yh}/f'_c$, were obtained. Using these values, a refined design equation to determine the quantities of confining reinforcement was derived. It was found that the required quantities of confining reinforcement for circular columns were significantly different from those for square and rectangular columns for the same parameters. The equation for square and rectangular columns was modified by a section type factor of f for use for circular columns.

Using a regression analysis, the best-fit curve for a refined design equation for square and rectangular hoops arrangement based on the 95% upper-tail values of $\rho_s f_{yh}/f'_c$, was found as follows:

$$\rho_s = \frac{A_g}{A_c}\frac{(\varphi_u/\varphi_y - 33\rho_t m + 22)}{111}\frac{f'_c}{f_{yh}}\frac{P_e}{\phi f'_c A_g} - 0.006$$

where $\rho_s = A_{sh}/(s_h h_c) \geq 0$.

This equation, is applicable to curvature ductility factors between 10 and 20. For spirals and circular hoops arrangement, the right hand side of the above equation should be multiplied by a factor of $f = 1.4$.

A refined design equation was also derived using the gradient optimization methods for φ_u/φ_y=10 and 20, respectively. These equations were found to be:

For $\varphi_u/\varphi_y = 10$:

$$\rho_s = \frac{A_g}{A_c}\frac{(21 - 0.1\rho_t m)}{100}\frac{f'_c}{f_{yh}}\frac{P_e}{\phi f'_c A_g} - 0.004$$

For $\varphi_u/\varphi_y = 20$:

$$\rho_s = \frac{A_g}{A_c}\frac{(31.8 - 0.2\rho_t m)}{100}\frac{f'_c}{f_{yh}}\frac{P_e}{\phi f'_c A_g} - 0.006$$

where $\rho_s = A_{sh}/(s_h h_c) \geq 0$.

The equation based on the 95% upper-tail values of $\rho_s f_{yh}/f'_c$ was more conservative in most of the cases than the equations obtained from the optimization methods. The quantities of confining reinforcement provided in the columns tested previously at the University of Canterbury [7,8,9,4], were also checked against the theoretical quantities suggested. It was found that the equation based on the 95% upper-tail values of $\rho_s f_{yh}/f'_c$ ensured that columns are capable of achieving the specified curvature ductility factor, even for columns with large axial compression. It is suggested that this equation is suitable as a replacement for the current code [2] recommended equations for the quantities of confining reinforcement.

Note that in design the quantities of transverse reinforcement in columns have to be checked to ensure that the other requirements for transverse reinforcement, namely prevention of premature buckling of longitudinal compression bars and shear requirements, are also satisfied.

5. Inelastic dynamic analyses were carried out to examine the behaviour of frames designed for code seismic loading associated with limited ductility and ductility under seismic excitations. Four earthquake records were chosen for the dynamic analysis, namely the El Centro 1940, the Parkfield 1966, the Pacoima Dam 1971 and the Generated Artificial Earthquake. The frames of limited ductility were designed using the conventional strength design method, and the ductile frames were designed using the capacity design procedure [6].

To study the behaviour of non-capacity designed frames of limited ductility, the worst situations for the possible development of column sidesway mechanisms, and the occurence of shear failure, were examined. Two sets of dynamic analyses were conducted to investigate both the flexural and shear behaviour of columns under seismic attack. It was found that frames of limited ductility performed reasonably well. Although plastic hinges occurred in some columns, column sidesway mechanisms did not occur. Moreover, the curvature ductility demand was found to be less than 10. This order of ductility can be achieved by providing sufficient confining reinforcement in the potential plastic hinge regions of the columns. Quantities of confining reinforcement for $\varphi_u/\varphi_y = 10$ were suggested. To have adequate shear resistance, the shear forces in the columns should be designed assuming that moments at each end of the columns reached the code [2] flexural strength. The shear forces in the beams should be designed assuming that the flexural overstrengths develop at both ends of the beams simultaneously.

The ductile frames so designed exhibited very good performance. Plastic hinges developed at the expected regions, and no column sidesway mechanisms were detected.

The investigation showed that the strength design method, which is a relatively simple design procedure, can be used for the design of frames of limited ductility, providing that adequate confinement in the columns is provided, and that adequate shear resistance in the columns and beams is available.

As a result of this study, a step-by-step design procedure for frames of limited ductility is suggested (see Section 5.6.4).

6. Based on the experimental results of the column units tested, followed by the analytical investigation of the required quantities of confining reinforcement in the potential plastic hinge regions of columns, and the results of the inelastic dynamic analyses of the frames of limited ductility, some seismic design provisions to clarify the existing code [2] provisions for frames of limited ductility are also proposed (see Section 6.5).

7.2 Recommendations for Future Research

1. As mentioned in Chapter 5, only regular frames of limited ductility were investigated in this study. The behaviour of non-capacity designed irregular frames of limited ductility under seismic excitations needs to be examined.

2. In the existing code provisions, the shear carried by concrete mechanisms in members of limited ductility is simply taken as one-half of that specified for gravity loading. An experimental study is required to obtain more information on the concrete shear mechanisms in beams, columns and beam-column joints of limited ductility, in order to enable more precise design equations for the shear reinforcement in the members of limited ductility to be derived.

3. More tests are needed to investigate the behaviour of beam-column joints of limited ductility to supplement existing test results [68].

References

[1] Study Group of New Zealand National Society for Earthquake Engineering, *Structures of Limited Ductility*, Bulletin Vol. 19, No. 4, December 1986, pp. 285-336.

[2] Standards Association of New Zealand, *Code of Practice for the Design of Reinforced Concrete Structures, NZS 3101:1982*, Wellington, 1982.

[3] Mander, J.B., Priestley, M.J.N. and Park, R., *Seismic Design of Bridge Piers*, Research Report 84-2, Department of Civil Engineering, University of Canterbury, February 1984, 483 pp.

[4] Zahn, F.A., Park, R. and Priestley, M.J.N., *Design of Reinforced Concrete Bridge Column for Strength and Ductility*, Research Report 86-7, Department of Civil Engineering, University of Canterbury, Christchurch, March 1986, 330 pp. plus appendices.

[5] Soesianawati, M.T., Park, R. and Priestley, M.J.N., *Flexural Ductility of Reinforced Concrte Columns with Low Axial Load and Limited Transverse Reinforcement*, Pacific Conference on Earthquake Engineering, Wairakei, August 1987, pp. 201-212.

[6] Park, R. and Paulay, T., *Reinforced Concrete Structures*, John Wiley & Sons, New York, 1975, 769 pp.

[7] Park, R., Priestley, M.J.N. and Gill, W.G., *Ductility of Square Confined Concrete Columns*, Journal of the Structural Division, Proceedings of American Society of Civil Engineers, Vol. 97, No. ST 7, Vol. 108, No. ST 4, April 1982, pp. 929-950.

[8] Priestley, M.J.N., Park, R. and Potangaroa, R.T., *Ductility of Spirally Confined Concrete Columns*, Journal of the Structural Division, Proceedings of American Society of Civil Engineers, Vol. 107, No. ST 1, January 1981, pp. 181-202.

[9] Ang, B. G., Priestley, M.J.N. and Park, R., *Ductility of Reinforced Concrete Bridge Piers Under Seismic Loading*, Research Report 81-3, Department of Civil Engineering, University of Canterbury, February 1981, 109 pp.

[10] Standards Association of New Zealand, *Code of Practice for the Design of Reinforced Concrete Structures, First Draft DZ 3101:1978*, Wellington, 1978.

[11] Standards Association of New Zealand, *Code of Practice for the Design of Reinforced Concrete Structures, Second Draft DZ 3101:1980*, Wellington, 1980.

[12] Ministry of Works and Development, *Ductility of Bridges with Reinforced Concrete Piers, CDP 810/A*, April 1975 (plus December 1977 amendment), 109 pp.

[13] Priestley, M.J.N. and Park, R., *Strength and Ductility of Bridge Substructures*, Bulletin No. 71, Road Research Unit, National Roads Board, Wellington, November 1984, 113 pp.

[14] Priestley, M.J.N. and Park, R., *Bridge Columns under Seismic Loading*, Structural Journal, American Concrete Institute, Vol. 84 No. 1, January-February 1987, pp. 61-76.

[15] Richart, F.E., Brandtzaeg, A., and Brown, R.L., *A Study of the Failure of Concrete Under Combined Compressive Stresses*, University of Illinois Engineering Experimental Station, Bulletin No. 185, 1928, 104 pp.

[16] Richart, F.E., Brandtzaeg, A., and Brown, R.L., *The Failure of Plain and Spirally Reinforced Concrete in Compression*, University of Illinois Engineering Experimental Station, Bulletin No. 190, 1929, 74 pp.

[17] Tentative Final Report of Committee 105, *Reinforced Concrete Column Investigation*, Journal of American Concrete Institute, Proceedings Vol. 29, No. 5, February 1933, pp. 275-282.

[18] ACI Committee, *Building Code Requirements for Reinforced Concrete (ACI 318-71)*, American Concrete Institute, Detroit, 1977, 78 pp.

[19] ACI Committee, *Building Code Requirements for Reinforced Concrete (ACI 318-77)*, American Concrete Institute, Detroit, 1977, 103 pp.

[20] ACI Committee, *Building Code Requirements for Reinforced Concrete (ACI 318-83)*, American Concrete Institute, Detroit, 1983, 102 pp.

[21] Park, R. and Priestley, M.J.N., *Code Provisions for Confining Steel in Potential Plastic Hinge Regions of Columns in Seismic Design*, Bulletin of the New Zealand National Society for Earthquake Engineering Vol. 13, No. 1, March 1980, pp. 60-70.

[22] CEB-FIP, *Model Code for Seismic Design of Concrete Structures*, Bulletin d'Information No. 165, Comite Euro-International du Beton, Athens, April 1985, 58 pp.

[23] Seismology Committee, *Recommended Lateral Force Requirements and Commentary*, Structural Engineers Association of California, 1975.

[24] Park, R. and Sampson, R.A., *Ductility of Reinforced Concrete Column Sections in Seismic Design*, Journal of American Concrete Institute, Proceedings Vol. 69, No. 9, September 1972, pp. 543-555.

[25] Kent, D.C. and Park, R., *Flexural Members with Confined Concrete*, Journal of the Structural Division, Proceedings of American Society of Civil Engineers, Vol. 97, No. ST7, July 1971, pp. 1969-1990.

[26] Park, R. and Leslie, P.D. *Curvature Ductility of Circular Reinforced Concrete Columns Confined by the ACI Spiral*, 6th Australasian Conference on the Mechanics of Structures and Materials, Vol. 1, Christchurch, New Zealand, August 1977, pp. 342-349.

[27] Paulay, T., *A Critique of the Special Provisions for Seismic Design of the Building Code Requirements for Reinforced Concrete (ACI 318-83)*, Journal of American Concrete Institute, Proceedings Vol. 83, No. 2, March-April 1986, pp. 274-283.

[28] Soesianawati, M.T., Park, R. and Priestley, M.J.N., *Limited Ductility Design of Reinforced Concrete Columns*, Research Report 86-10, Department of Civil Engineering, University of Canterbury, Christchurch, March 1986, 208 pp.

[29] Standards Association of New Zealand, *Code of Practice for General Structural Design and Design Loadings for Buildings NZS 4203:1976*, Wellington, 1976.

[30] Standards Association of New Zealand, *Code of Practice for General Structural Design and Design Loadings for Buildings NZS 4203:1984*, Wellington, 1984.

[31] Johal, L.S., Azizinamini, A., Musser, D.W. and Corley, W.G., *Seismic Evaluation of Columns to Improve Design Criteria for Transverse Reinforcement*, 5th Canadian Conference Earthquake Engineering, Ottawa, 1987, pp. 799-806.

[32] Fafitis, A. and Shah, S.P., *Predictions of Ultimate Behavior of Confined Columns Subjected to Large Deformations*, ACI Journal, July-August 1985, pp. 423-433.

[33] Sheikh, S.A., Yeh, C.C. and Menzies, D., *Confined Concrete Columns*, Pacific Conference on Earthquake Engineering, Wairakei, August 1987, pp. 177-188.

[34] Yeh, C.C. and Sheikh, S.A., *Flexural Behavior of Confined Concrete Columns Subjected to High Axial Loads*, 5th Canadian Conference Earthquake Engineering, Ottawa, 1987, pp. 817-824.

[35] Pam, H. J., *Data Reduction Program*, Department of Civil Engineering, University of Canterbury, October 1985.

[36] British Standards Institute, *Methods for Tensile Testing of Metals, BS 18:1971, Part 2: Steel (General)*, London, July 1971.

[37] American Society for Testing and Materials, *Annual Book of ASTM Standards, ASTM 1973, Part 4*, Philadelphia, 1973.

[38] Standards Association of New Zealand, *Specification for Methods of Test for Concrete, NZS 3112:1980, Part 2: Test Relating to the Determination of Strength of Concrete*, Wellington, December 1980.

[39] Standards Association of New Zealand, *Draft for Comment, New Zealand Standard, General Structural Design and Design Loadings for Buildings DZ4203:1986*, Wellington, November 1986.

[40] Bertero, V.V. and Popov, E.P., *Seismic Behavior of Ductile Moment-Resisting Reinforced Concrete Frames*, ACI Special Publication No. 53, Reinforced Concrete Structures in Seismic Zones, American Concrete Institute, Detroit, 1977, pp. 247-291.

[41] Falconer, T.J. and Park, R., *Ductility of Prestressed Concrete Piles Under Seismic Loading*, Research Report 82-6, Department of Civil Engineering, University of Canterbury, February 1982, 121 pp.

[42] Pam, H. J. and Park, R., *Ductility of Prestressed Concrete Piles Subjected to Simulated Seismic Loading*, Research Report 84-4, Department of Civil Engineering, University of Canterbury, February 1984, 169 pp.

[43] Park, R. J. T., Priestley, M. J. N. and Walpole, W. R., *Seismic Performance of Steel Encased Reinforced Concrete Bridge Piles*, Research Report 82-12, Department of Civil Engineering, University of Canterbury, February 1982, 158 pp.

[44] Tanaka, H. and Park, R., *Effectiveness of Transverse Reinforcement with Alternative Anchorage Details in Reinforced Concrete Columns*, Pacific Conference on Earthquake Engineering, Wairakei, August 1987, pp. 225-235.

[45] Whittaker, D., Park, R. and Carr, A.J., *Third Progress Report on Research Project on the Seismic Performance of Offshore Concrete Gravity Platforms*, New Zealand Concrete Society 22nd Technical Conference, Christchurch, 12-14 September 1986, pp. 4-18.

[46] Andriono, T.,*Stress-Strain Properties of New Zealand Manufactured Micro-Alloy Reinforcing Steel Used in Seismic Design* (unpublished), 21 pp.

[47] Zahn, F.A., Park, R.,Priestley, M.J.N. and Chapman, H.E., *Development of Design Procedures for the Flexural Strength and Ductility of Reinforced Concrete Bridge Columns*, Bulletin of New Zealand National Society for Earthquake Engineering, Vol.19 No.3, September 1986, pp. 200-212.

[48] Willam, K.J. and Warnke, E.P.,*Constitutive Model for the Triaxial Behaviour of Concrete*, International Association for Bridge and Structural Engineering, Proceedings Vol.19, 1975.

[49] Scott, B.D., Park, R. and Priestley, M.J.N., *Stress-Strain Behaviour of Concrete Confined by Overlapping Hoops at Low and High Strain Rates*, Journal of American Concrete Institute, Proc.V.79, No.1, Jan-Feb. 1982, pp. 13-27.

[50] HARWELL, *VF04AD*, Subroutine Library Specification, April 1986.

[51] Adby, P.R. and Dempster, M.A.H., *Introduction to Optimization Methods*, Chapman and Hall, London, 1982, 204 pp.

[52] Fletcher, R., *Practical Methods of Optimization, Vol. 1: Unconstrained Optimization*, John Wiley & Sons, 1980, 120 pp.

[53] Fletcher, R., *Practical Methods of Optimization, Vol. 2: Constrained Optimization*, John Wiley & Sons, 1981, 224 pp.

[54] Tompkins, D.M., Paulay, T. and Carr, A.J., *The Seismic Response of Reinforced Concrete Multistorey Frames*, Research Report 80- 5, Department of Civil Engineering, University of Canterbury, Christchurch, February 1980, 141 pp. plus Appendices.

[55] Carr, A.J., *RUAUMOKO*, Computer Program Library, Department of Civil Engineering, University of Canterbury, Christchurch, May 1986.

[56] Standards Association of New Zealand, *News Release*, Wellington, 25 November 1987.

[57] MacRae, G.A., *Two Dimensional Elasto-Plastic Frame Analysis Program*, Department of Civil Engineering, University of Canterbury, Christchurch, August 1987.

[58] MacRae, G.A., *FORPER*, Department of Civil Engineering, University of Canterbury, Christchurch.

[59] Newmark, N.M., *A Method of Computation for Structural Dynamics*, Journal of the Engineering Mechanics Division, ASCE, Vol. 85, No. EM3, July 1959, pp. 67-94.

[60] Powell, G.H. and Kanaan, A.E., *General Purpose Computer Program for Inelastic Dynamic Response of Plane Structures*, Report No. EERC 73-6, Earthquake Engineering Research Centre, University of California, Berkeley, April 1973.

[61] Chrisp, D.J., *Damping Models for Inelastic Structures*, Master of Engineering Thesis, Department of Civil Engineering, University of Canterbury, Christchurch, February 1980, 42 pp.

[62] Archer, J.S., *Consistent Mass Matrix for Distributed Mass System*, Journal of the Structural Division, ASCE, Vol. 89, No. ST4, August 1963, pp. 161-178.

[63] New Zealand Concrete Society, *Applications of New Zealand Standard Code of Practice for the Design of Concrete Structures NZS 3101:1982*, New Zealand Concrete Society Technical Report No. 2, Section 3, August 1983.

[64] Paulay, T., *Moment Redistribution in Continuous Beams of Earthquake Resistant Multistorey Reinforced Concrete Frames*, Bulletin of the New Zealand Society of Earthquake Engineering, Vol. 9, No. 4, 1976, pp. 205-212.

[65] Carr, A.J., *SIMQKE*, Computer Program Library, Department of Civil Engineering, University of Canterbury, Christchurch.

[66] King, D.J., Priestley, M.J.N. and Park, R., *Computer Programs for Concrete Column Design*, Research Report 86-12, Department of Civil Engineering, University of Canterbury, May 1986, 72 pp. plus appendices.

[67] New Zealand Portland Cement Association, *New Zealand Reinforced Concrete Design Handbook*, 1979.

[68] Dai, R. and Park, R., *A Comparison of the Behaviour of Reinforced Concrete Beam-Column Joints Designed for Ductility and Limited Ductility*, Research Report 87-4, Department of Civil Engineering, University of Canterbury, June 1987, 65 pp.

Classn:

DESIGN OF REINFORCED CONCRETE FRAMES OF LIMITED DUCTILITY

Soesianawati Watson

ABSTRACT: A theoretical and experimental investigation leading to the derivation of a refined design equation for the quantities of transverse reinforcement required for reinforced concrete columns in order to achieve various ductility levels is presented. Design procedures for frames of limited ductility are suggested, and some provisions for seismic design requirements for this type of frame are outlined.

Department of Civil Engineering, University of Canterbury,
Doctor of Philosophy Thesis, 1989.